Étude de données et analyse de modèles intégro-différentiels en biologie cellulaire

Hugo Martin

SCIENCES SORBONNE UNIVERSITÉ

École doctorale Science Mathématique de Paris Centre

Étude de données et analyse de modèles intégro-différentiels en biologie cellulaire

THÈSE

présentée et soutenue publiquement le 15 juillet 2019

pour l'obtention du

Doctorat de Sorbonne Université

(spécialité mathématiques)

par

Hugo Martin

Composition du jury

Frédérique Clément	*Examinatrice*
Marie Doumic	*Directrice de thèse*
Pierre Gabriel	*Directeur de thèse*
Anna Marciniak-Czochra	*Rapporteuse*
Antoine Perasso	*Rapporteur*
Laurent Pujo-Menjouet	*Examinateur*
Delphine Salort	*Examinatrice*

Laboratoire Jacques-Louis Lions

Mis en page avec la classe thesul.

Remerciements

Mes premiers remerciements vont tout naturellement à mon directeur et ma directrice de thèse. Ils m'ont fait confiance lors de mon stage de Master 2 et ont fait le pari de prolonger pour trois ans en thèse. Je ne peux que leur exprimer ma profonde gratitude pour cela. J'ai énormément appris durant cette période grâce à eux, tant du point de vue mathématique qu'humain. La liberté dont j'ai rapidement disposé quant à mes sujets de recherche fut un délice. Je me souviendrai longtemps de ces longues heures à discuter et noircir des tableaux avec Pierre à Versailles. Le goût pour les applications des mathématiques à la biologie de Marie est très communicatif ! Je ne peux désormais écouter un exposé sans me demander si les modèles ont fait l'objet d'une validation par des données expérimentales. Cette question — en apparence simple — a redonné du sens à mon travail à un moment où j'en avais besoin.
I am very grateful to Anna Marciniak-Czochra for taking time to review my thesis. I am very happy that she could make it to the defense all the way from Heildelberg. Je remercie également Antoine Perasso d'avoir accepté de rapporter ma thèse. Je suis très heureux qu'une date permettant la présence des deux rapporteurs ait pu être trouvée. Mes remerciement vont également à Frédérique Clément, Laurent Pujo-Menjouet et Delphine Salort qui me font l'honneur de prendre part à mon jury de thèse.
Durant ces trois années, j'ai eu la chance de collaborer avec de remarquables scientifiques, déjà reconnus ou dont la valeur n'attend point le nombre des années. Outre Marie et Pierre, j'ai travaillé l'été dernier à Marseille avec Cristina, Frédéric, Magali et Pascal. Je souhaite bien du courage et une bonne réussite aux deux jeunes pour la thèse ! Plus proche d'ici, j'ai rencontré deux collaborateurs exceptionnels, avec qui les réunions de travail furent toujours pour moi incroyablement enrichissantes.
Une thèse, c'est également de nombreuses rencontres, au LJLL, à Versailles, à l'INRIA, au CEMRACS ou en conférence. Je vais certainement en oublier, mais citons pêle-mêle : Amaury, Christophe, Camille, Antoine, Lydie, Pierre (x2), Gabriela, Alexandre, Jules, Valentin, JF, AF, Olivier, Anouck, Jean, Idriss, Gontran, Ludovic, Alan, Po-Yi, David, Nicolas, Eugenio, Hugo, Fabien, Léa, Anna, Camila, Ilaria, Patricio, Antoine, Sybille, Harold, Marouans, Alvaro, Céline, Alexis, Samuel, Angélique, Cécile (x2), Luis, Jean, Diane, Chloé, Noémie, Nastassia... Un mot en particulier pour mes frères et soeurs de thèse Mathieu, Julia et Cécile pour qui la soutenance est encore plus ou moins loin. Courage ! Les visites régulières à Jussieu après son expatriation à Saclay de Frédérique furent toujours source de moult rires, sois en remerciée. Enfin, que serait une thèse sans collègues de bureau ? L'ambiance du deuxième étage fut sans cesse assurée, tant par les vieux déjà partis —Florian, Malik, Chen-Yu, Carlos— ou celles ceux de passage —Dany, Maria, Emilio— que les jeunes avec Lise et Igor. Je retiendrai de longues et passionnantes discussions avec chacun et chacune d'entre vous, ainsi qu'un mémorable weekend à Guidel avec la team Bretagne.
Un thésard bénéficie également de soutiens non scientifiques lors de ses années au laboratoire. Évidemment Malika, Salima et Catherine au secrétariat pour l'appui administratif impeccable, Kashayar pour les nombreuses fois où l'informatique me résistait, Nelly puis Kevin et finalement Nicole pour l'efficacité chirurgicale avec les missions. Enfin merci à Corentin Lacombe pour les éclaircissements et l'exécution de tout l'administratif relatif à la soutenance. Une forme peut-être inattendue de soutien fut le sérénité procurée la certitude dès janvier d'avoir un postdoc à la rentré, qui m'a permis de finir ma thèse avec une quiétude bienvenue sur cet aspect. Je remercie donc Annabelle.
Je ne peux m'empêcher ensuite d'avoir une pensée pour les enseignants de mathématiques qui ont marqué mon parcours, comme Valérie Farkas (qui ne m'a pas enseigné que les maths, certes), Martin Cerisier, Marie-Christine Laporte *and last but not least* Mathieu Fructus. C'est en bonne partie grâce à eux que j'en suis ici aujourd'hui.
Ma vie hors du labo fut rythmée par différentes sphères sociales, d'intersections pas toujours vides. La bise à mes anciens collocs et logueurs de tous poils, ma porte vous sera toujours ouverte. Même si cela ne se voit pas forcément, j'ai réussi à maintenir une activité physique pendant ces trois années, au Cercle Athlétique de Montrouge. La bise également aux copains du hockey ! Mon épanouissement durant ces dernières années tient aussi de la participation à l'organisation de conférences mensuelles autour de l'esprit critique lors des Skeptics in the Pub Paris. Je remercie chaleuresement les autres organisateurs pour leur accueil au sein de l'équipe, ainsi que la communauté grandissante que fédèrent ces thématiques et qui se retrouve régulièrement lors de ces réunions. L'attrait pour ces thématiques m'a donnée l'occasion de donner une conférence lors de la fête de la Science 2018. J'étais un peu « comme à la maison », car je

participais déjà à la vulgarisation des mathématiques *via* le groupe P6-P7. Merci en particulier à Frédérique et Mathilde. Enfin, je souhaite exprimer ma gratitude envers Fréd et Manu, qui m'ont accueilli à bras ouverts il y a déjà un moment.
Ensuite viennent les vieux copains et vieilles copines. Peu sont en région parisienne, les contacts sont parfois épisodiques, mais avec qui les retrouvailles sont toujours source de plaisir. Dans un ordre vaguement antéchronologique, il y a Ruben, Romain, Augustin, Thibault, Emily, Axel, Maud, Sylvain, les seniors du Cercle Paul Bert à Rennes, Christophe et Sylvie, mes copréparationnaires, Marion, Léonor, Thibault, Nono x2, Nahel, Célia, Margot, Ludovic, Cécile (qui compte un peu comme enseignante), Ronan (j'ai soutenu avant toi finalement, j'attends avec impatience ton grand moment !), Chloé... Mes excuses à celles et ceux que ma faillible mémoire a omis de mentionner.
Mes parents ont toujours su me procurer ce dont j'avais besoin pour étudier, je mesure aujourd'hui la chance que j'ai eu. Je vous remercie pour votre soutien, malgré cette idée saugrenue d'aller faire des maths. Lionel, mon bro, tu ne réalises peut-être pas à quel point ton soutien est précieux. Reste égal à toi-même.
Le mot de la fin est destiné à Solène. Je ne m'étalerai pas : merci d'être là, tout simplement. Dans les moment difficiles, dans les moments heureux. Merci.

À mes parents.

Sommaire

Introduction générale

Cette thèse rend compte de mon travail commencé en stage à l'INRIA Paris en mai 2016 puis prolongé pendant trois ans au LJLL, sous la direction de Marie Doumic et Pierre Gabriel. Dans les pages à venir seront évoqués plusieurs modèles de dynamique des populations cellulaire, avec en fil rouge la question de la pertinence du choix de modélisation.

Le premier chapitre introduit des notions de modélisationsen dynamiques des populations, puis présente deux célèbres modèles, dit de renouvellement et de croissance-fragmentation. Dans le deuxième, on présente une méthode pour comparer deux modèles qui décrivent le même organisme, que l'on appliquex aux deux modèles de populations structurées présentés dans le premier chapitre. On étudie ensuite un troisième modèle sur le même organisme, qui présente d'intéressantes propriétés qualitatives du point de vue biologique. Le chapitre suivant est dédié à la présentation du concept de solutions mesures à une équations de population structurée, qu'on applique sur deux équations. Enfin, le quatrième et dernier chapitre concerne une analyse de données expérimentales sur des lignées de levures, se prêtant plutôt à une modélisation individu-centrée, stochastique.

1 Quelques éléments de dynamique des populations

Une approche générale pour modéliser une population est présentée dans [125]. Il s'agit de réaliser un bilan démographique (ou bilan de masse). Notant N_t le nombre d'individus au temps t dans la population étudiée, alors la variation de cette population lors d'une période Δt peut s'écrire

$$N_{t+\Delta t} - N_t = \Delta N = naissances - morts + migrations,$$

avec naissances, morts et migration le nombre de ces évènements qui se produisent pendant le laps de temps Δt.

Il existe plusieurs manières d'écrire un modèle résultant de ce bilan démographique. Une description avec un modèle continu peut s'écrire sous la forme d'équations différentielles ou d'équations aux dérivées partielles. Des exemples de telles descriptions seront données dans le reste de cette section, présentée de manière chronologique. Le modèle de croissance malthusienne sera présenté en premier lieu, à la fois pour illustrer la démarche de modélisation de dynamiques de population et pour souligner les dangers d'une interprétation peu précautionneuses des résultats. Ensuite, on introduit un paramètre structurant, décrivant une caractéristique physiologique des individus composant la population étudiée. Ce type de modèle est aujourd'hui très étudié, tant du point de vue population, résultant en une formulation EDO ou EDP, qu'individu centré, *via* une écriture probabiliste. Parmi les champs d'application en biologie utilisant des modèles de ce genre, on peut citer, parmi moult autres, des interactions proie-prédateur [84, 168, 93], la pharmacocinétique-pharmacodynamique [113, 121, 8], l'interaction de gènes [101], l'effet de protocoles médicaux dans un traitement contre le VIH [172], la chimiothérapie [28, 131], l'hématopoïese [152, 37, 2, 85, 126], le chimiotactisme [25, 128, 114, 22, 155, 104], la diffusion croisée [47, 21], la prolifération cellulaire [56, 57, 33, 61, 60, 17, 59, 67], la croissance tumorale [11, 142, 140], les neurosciences [134, 135, 30, 31, 64, 77, 83] la dynamique du prion [58, 26, 145, 38, 32, 146, 80], la structuration par trait phénotypique [122, 127]

1.1 Histoire d'une équation différentielle

Pour cette courte partie historique, on s'inspire de [7]. En 1798, Robert Malthus publie de manière anonyme un essai en réaction à une proposition de loi du gouvernement britannique visant à aider financièrement les familles nombreuses les plus pauvres. Bien que ne contenant pratiquement pas de données ou de modélisation mathématique pour appuyer son hypothèse, son ouvrage connut un succès retentissant, et influença de nombreux savants tels que Charles Darwin ou Karl Marx. En substance, Malthus défend l'idée d'une croissance linéaire des ressources tandis que la croissance de la population tend à être exponentielle. Dans cette optique, apporter un soutien financier aux familles nombreuses des classes défavorisées ne peut qu'aggraver l'accroissement exponentielle de la population, résultant à terme à des situations de famine plus grave que si cette mesure n'avait pas été appliquée. Il en conclut que cette mesure serait inefficace pour améliorer les conditions de vie des plus démunis sur le long terme. Mathématiquement, son idée peut se traduire par léquation différentielle

$$\frac{\mathrm{d}N}{\mathrm{d}t} = nN - mN =: \lambda N, \tag{1}$$

où n et m désignent respectivement les taux de naissance et mort. Leur différence $\lambda = n - m$ est souvent appelée taux de croissance, ou paramètre de Malthus, ou encore paramètre malthusien, bien que l'idée de croissance exponentielle de la population semble avoir été connue de Leonhard Euler, un demi-siècle plus tôt. Selon le signe de ce paramètre, la population va soit s'éteindre (cas $\lambda < 0$), soit croître indéfiniment (cas $\lambda > 0$,) soit être constante (cas $\lambda = 0$), indépendemment de toute considération extérieure. Le recul qu'on a aujourd'hui sur la démographie nous fait bien entendu dire que ce modèle est trop limité, mais on peut également en tirer une leçon : il convient d'être prudent lorsqu'on modélise une situation, et plus encore avec les interprétations qu'on tire des simulations.

Le comportement assez « caricatural » de ce modèle ainsi que le peu de confirmations par les données démographiques réelles ont résulté, au moins pour la démographie humaine, en son abandon au profit par exemple de l'équation logistique, de modèles par compartiments ou de modèle structurés par traits physiologiques. On notera cependant avant de clore cette partie qu'une modélisation de ce type a été proposée récemment dans [165] pour étudier la dynamique de clonage de cellules cancéreuses.

1.2 Prise en compte d'un trait physiologique : modélisation par une équation aux dérivées partielles

Lorsqu'on modélise une population par une équation différentielle, on compte le nombre d'individus dans chaque catégorie qu'on définit. Par exemple en épidémiologie, le modèle SIR compte trois catégories : les individus susceptibles de contracter une maladie (classe notée S), les individus infectés par cette maladie (classe notée I) et enfin les individus remis de cette maladie (classe notée R). On considère la population comme complètement homogène à l'intérieur de chaque classe. Un ouvrage de référence sur ce type de modèle est [50] ou dans une version plus récente [49].

Il pourrait cependant être pertinent de faire l'hypothèse qu'un individu très jeune présente un système immunitaire encore immature, et est alors plus susceptible de succomber à ladite maladie. Une manière de tenir compte de l'âge avec des modèles en temps discret a été de diviser la population en classes d'âge. Cette idée fut introduite par Leslie dans les années 50 dans les articles [111, 112]. Si on souhaite un modèle en temps continu, où l'âge est donné par un réel positif a, on peut considérer des équations dites *structurées*. Dans ce type de modèle, on associe à chaque individu un ensemble de paramètres en fonction de leurs caractéristiques physiologiques, et on parle alors de *variables structurantes*. On se concentrera sur les variables structurantes *physiologiques*, qui peuvent être par exemple l'âge, la taille, la concentration d'une protéine dans le milieu intracellulaire... Une référence récente et classique sur le sujet est [139].

Au début du 20^{eme} siècle, Sharpe et Lotka proposèrent dans [156] le premier modèle structuré en âge. Ensuite, les travaux de Kermack et McKendrick [117, 105, 106] et plus tard ceux de Von Foerster aboutirent à une équation aux dérivées partielles structurée en âge, que l'on appelle aujourd'hui équation

de McKendrick–von Foerster ou équation de renouvellement, ici dans sa version conservative

$$\begin{cases} \dfrac{\partial}{\partial t}n(t,a) + \dfrac{\partial}{\partial a}n(t,a) + \mu(a)n(t,a) = 0 \qquad t>0, a>0, \\ \\ n(t,a=0) = \displaystyle\int_0^\infty B(a)n(t,a)\,\mathrm{d}a \qquad t>0, \qquad n(0,a) = n^{in}(a). \end{cases} \tag{2}$$

La terminologie « âge » et « renouvellement » est justifiée par la dynamique de l'équation. Un nouvel individu arrivant dans la population ne peut le faire que par le bord du domaine, en $a = 0$, ce qui traduit bien des naissances. Ensuite, la partie transport $(\partial_t + \partial_a)$ rend compte du vieillissement de la population, à vitesse $\frac{\mathrm{d}a}{\mathrm{d}t} = 1$. Le terme $-\mu(a)n(t,a)$ indique quant à lui un retrait d'individus de la population. On dit alors que μ est le taux de mort de la population. On peut vouloir réinitialiser l'âge d'un individu qui vient de donner naissance. Cette modélisation peut s'appliquer par exemple à une population de levures, où la division aymétrique peut s'interpréter comme un adulte donnant naissance à un jeune. Dans ce cas, on choisit une formulation conservative. Pour ce faire, on remplace $\mu(a)$ par $\mu(a) + B(a)$ et on ajoute un 2 devant l'intégrale du terme de naissance. On peut regarder la variation de la population totale. Que l'on retienne une ou deux naissances apres une division, on obtient alors

$$\frac{\mathrm{d}}{\mathrm{d}t}\int_0^\infty n(t,a)\,\mathrm{d}a = \int_0^\infty \left(B(a) - \mu(a)\right) n(t,a)\,\mathrm{d}a,$$

à comparer avec le modèle malthusien (1). Deux mécanismes sont à l'œuvre ici : le vieillissement, qui tend à déplacer la masse vers les grandes valeurs de a, et le processus de naissance qui injecte de la masse en zéro.

Le système (2) et ses variantes combinant d'autres variables structurantes sont utilisées dans de très nombreuses situations de modélisation. En adéquation avec le champ d'application de cette thèse, on peut mentionner en premier lieu la biologie cellulaire : citons parmi de nombreux exemples une description du cycle cellulaire donnée dans [33]. On peut également regarder des applications assez classique à l'étude de populations de cellules cancéreuses : leur réaction à un traitement, par exemple dans [82], des modélisations des métastases, comme dans [103, 12, 48]. Une adaptation de ce modèle permet de décrire le processus d'ovulation et est étudiée dans [66, 65]. Plus récemment, une version multitype de l'équation de renouvellement a été proposée pour étudier les dynamiques cellulaires du follicule ovarien (au cours des premiers stades de son développement) dans [35]. Un autre domaine classique d'application d'une structuration en âge est l'épidémiologie. Une description de la dynamique du VIH et SIDA est donnée dans [170]. Dans ce modèle, la population est également structurée en âge de l'infection, c'est à dire le temps écoulé depuis l'infection du sujet. Ce type de structuration se retrouve dans [116, 115]. On peut également combiner la structuration en âge à celle en charge infectieuse, rendant ainsi possible la prise en compte d'une vitesse de développement de la maladie dans l'organisme, typiquement pour modéliser une infection par le prion. On peut se référer par exemple à [136, 108] pour une modélisation et l'étude du caractère bien posé et [137] pour l'étude du comportement asymptotique et des simulations numériques. Mentionnons enfin une récente structuration en âge du classique modèle proie-prédateur, décrite dans [138].

Une autre approche de modélisation s'est dégagée dans la deuxième moitié du 20^{eme} siècle, par les travaux de Bell et Anderson [13] puis Sinko et Streifer [160]. Celle-ci consiste à structurer la population en fonction d'un trait $x > 0$ qui n'est pas réinitialisé lorsqu'un nouvel individu apparaît. On parle alors d'équation structurée en taille. On notera cependant que malgré la terminologie « taille », cette équation se retrouve dans de multiples situations de modélisation, voir les références donnés dans l'introduction de [57]. Une première version de l'équation dite de croissance-fragmentation linéaire en une dimension avait été formulée dans [160]. Sous sa forme la plus générale, elle s'écrit

$$\frac{\partial}{\partial t}n(t,x) + \frac{\partial}{\partial x}(g(x)n(t,x)) + \mu(x)n(t,x) + B(x)n(t,x) = \int_x^\infty b(y,x)n(t,y)\,\mathrm{d}y \tag{3}$$

avec la condition au bord $g(0)n(t,0) = 0$ et une condition initiale. La partie transport représente la croissance à vitesse $g(x)$ de la population. Comme précédemment, les termes en $\mu(x)n(t,x)$ et $B(x)n(t,x)$

traduisent respectivement la disparition d'individus par mort et par division. Enfin, le terme intégral code la fragmentation : les individus naissant à la taille x sont issus de la division d'individus de taille $y > x$, avec un taux $b(y, x)$. On impose que le processus de fragmentation préserve la masse, c'est à dire que lorsqu'un individu se fragmente, la somme de ses fragments soit égale à la taille de cet individu au moment de la division. Cela se traduit par la loi de conservation

$$xB(x) = \int_0^x yb(x, y)\,\mathrm{d}y. \tag{4}$$

On note également, pour les tailles telles que $B(x) \neq 0$,

$$n_0(x) := \frac{1}{B(x)} \int_0^x b(x, y)\,\mathrm{d}y$$

le nombre moyen de fragments. Muni de l'hypothèse de conservation précédente et de cette notation, on obtient alors en intégrant formellement l'équation (3) contre la mesure $x\,\mathrm{d}x$ sur $\mathbb{R}_+$

$$\frac{\mathrm{d}}{\mathrm{d}t} \int_0^\infty xn(t, x)\,\mathrm{d}x = \int_0^\infty g(x)n(t, x)\,\mathrm{d}x - \int_0^\infty x\mu(x)n(t, x)\,\mathrm{d}x. \tag{5}$$

Cette équation traduit le fait que la variation de la masse totale ne varie que par les phénomènes de croisance et de mort d'individus. À l'inverse, en intégrant cette fois contre $\mathrm{d}x$, on obtient une équation sur le nombre total d'individus qui fait intervenir la fragmentation (et toujours le nombre de morts)

$$\frac{\mathrm{d}}{\mathrm{d}t} \int_0^\infty n(t, x)\,\mathrm{d}x = \int_0^\infty B(x)\,(n_0(x) - 1)\,n(t, x)\,\mathrm{d}x - \int_0^\infty \mu(x)n(t, x)\,\mathrm{d}x. \tag{6}$$

De manière analogue à la dynamique de l'équation de renouvellement, deux mécanismes agissent sur la densité. Le processus de croissance « pousse » la densité vers le x grands, alors que la fragmentation la ramène vers 0. Parmi les exemples courants de noyaux de fragmentations étudiés, on peut citer la mitose dans lequel

$$b(y, x) = B(y)\left(\delta_{y=\sigma x} + \delta_{y=(1-\sigma)x}\right),$$

avec $0 \leqslant \sigma \leqslant 1$. Avec $\sigma = 1/2$, on se place dans le cadre de la mitose égale, dans lequel une cellule se divise en deux parties égales. Il est important de noter que le cas $\sigma = 0$ (ou son symétrique $\sigma = 1$) et avec le taux de croissance $g \equiv 1$ permet de retrouver l'équation de renouvellement.

Une différence fondamentale de ces deux équations réside dans la non localité. Pour le renouvellement, il se situe au bord du domaine. Pour obtenir la masse qui arrive en 0, il faut regarder tout ce qu'il se passe sur $\mathbb{R}_+^*$, alors que pour la mitose, pour obtenir les naissances en un point x, on se contente de regarder sur (x, ∞). En particulier pour la mitose égale, on regardement "localement plus loin", puisqu'il suffit de connaître les individus à taille $2x$ qui se divisent. Ce phénomène se produit aussi pour l'équation dite du pantographe [67], qui génralise la mitose égale dans le cas où les taux de croissance et division sont constants. Dans ce cas, la fission d'un individu de taille x donne naissance à deux nouveaux individus de tailles x/α et x/β, où

$$\frac{1}{\alpha} + \frac{1}{\beta} = 1$$

pour assurer la conservation de la masse.

2 Modèles de populations de bactéries : éléments propres, comportement en temps long, comparaison de modèles

Parmi les différentes situations que modélisent les équations de renouvellement et de croissance-fragmentation figure l'évolution de colonies de bactéries. Avant toute chose, il convient de prendre en compte un caractère fondamental des bactéries, appuyé par [129] : leur taux de mort est négligeable. On

choisit alors $\mu \equiv 0$ dans les équation précédentes.

Pour l'équation de renouvellement, on retient la version où une bactérie qui se divise est retirée de la population et crée deux nouveaux individus. On considère donc le système

$$\begin{cases} \dfrac{\partial}{\partial t}n(t,a) + \dfrac{\partial}{\partial a}n(t,a) + B(a)n(t,a) = 0 \qquad t > 0, a > 0, \\ \\ n(t,a=0) = 2\displaystyle\int_0^\infty B(a)n(t,a)\,\mathrm{d}a \qquad t > 0, \qquad n(0,a) = n^{in}(a). \end{cases} \tag{7}$$

On peut donner ici une interprétation probabiliste du taux de division B. On note A la variable aléatoire qui désigne l'âge auquel se divise une bactérie. La probabilité qu'une bactérie ne se soit pas divisée avant l'âge a est donnée par

$$\mathbb{P}(A \geqslant a) = e^{-\int_0^a B(\alpha)\,\mathrm{d}\alpha}.$$

On veut que toutes les bactéries se divisent à un moment ou à un autre, on impose donc la condition

$$\lim_{a \to +\infty} \int_0^a B(\alpha)\,\mathrm{d}\alpha = +\infty. \tag{8}$$

Sous cette hypothèse, la loi de la variable aléatoire A est connue explicitement, il s'agit de $B(a)e^{-\int_0^a B(\alpha)\,\mathrm{d}\alpha}$. On vérifie alors que sous l'hypothèse (8), cette fonction se somme bien à 1.

Pour l'équation en taille, on considère le cas de la mitose égale, c'est-à-dire $b(y,x) = 2B(y)\delta_{y=2x}$, où δ représente la masse de Dirac. On obtient alors

$$\frac{\partial}{\partial t}n(t,x) + \frac{\partial}{\partial x}(g(x)n(t,x)) + B(x)n(t,x) = 4B(2x)n(t,2x), \tag{9}$$

associée à une condition de bord en $x = 0$ et à une condition initiale.
Ces deux modèles étant intrinsèquement différents, il convient de déterminer, si possible, lequel des deux décrit le mieux l'organisme étudié. Cette question est ici reliée à une autre, issue du monde de la biologie : quels mécanismes régissent la division cellulaire ? Trancher entre ces deux modèles donnerait des indications quant à cette interrogation fondamentale de la biologie cellulaire. Mais comment faire ?

Dans un premier temps, on développera la théorie des éléments propres principaux pour les équations de population structurées, dans laquelle on cherche une solution dont le temps est une variable séparée des autres puis on montrera le lien entre ce type de solution et une autre solution quelconque du problème d'évolution.
Ensuite, on montrera comment tirer avantage de ces solutions particulières grâce à la théorie des problèmes inverses, afin de pouvoir comparer ces deux modèles. C'est à la suite de cette comparaison qu'intervient mon travail, en collaboration avec Pierre Gabriel. Dans [79], on étudie l'existence et l'unicité d'éléments propres pour un modèle de bactéries proposé récemment. Dans la dernière partie, on suggère des perspectives sur ce sujet.

2.1 Éléments propres et comportement en temps long

Dans une situation où une division donne naissance à deux nouveaux nés, le nombre d'individus croît exponentiellement au cours du temps. Cette situation rappelle la croissance malthusienne présentée précédemment. Ce constat incite à chercher une solution particulière sous la forme $(t,\alpha) \mapsto e^{\lambda t}N(\alpha)$ pour le problème direct et $(t,\alpha) \mapsto e^{-\lambda t}\phi(\alpha)$ pour le problème adjoint, où $t \geqslant 0$ désigne le temps et $\alpha \in \Omega \subset \mathbb{R}^d$ la variable structurante. Cette approche est classique lorsqu'on étudie une équation d'évolution en dynamique des populations, et trouver un triplet (λ, N, ϕ) avec $N, \phi \geqslant 0$ s'appelle résoudre le problème de Perron associé au système.

Pour l'équation de renouvellement, ce problème s'écrit donc

$$\begin{cases} \dfrac{\partial}{\partial a}N(a) + (B(a)+\lambda)N(a) = 0, \\ N(0) = 2\displaystyle\int_0^\infty B(a)N(a)\,\mathrm{d}a, \qquad N(a) > 0, \qquad \int_0^\infty N(a)\,\mathrm{d}a = 1, \\ -\dfrac{\partial}{\partial a}\phi(a) + (B(a)+\lambda)\phi(a) = 2\phi(0)B(a), \\ \phi(a) \geqslant 0, \qquad \displaystyle\int_0^\infty \phi(a)N(a)\,\mathrm{d}a = 1. \end{cases}$$

Il s'agit donc d'équations différentielles non locales à paramètre. L'hypothèse (8) assure l'existence et l'unicité d'un triplet propre (λ, N, ϕ) avec $\lambda > 0$, et les deux fonctions propres N et ϕ strictement positives.

Le problème de Perron associé l'équation (9) s'écrit

$$\begin{cases} \dfrac{\partial}{\partial x}(\tau(x)N(x)) + (B(x)+\lambda)\,N(x) = 4B(2x)N(2x), \\ \tau N(0) = 0, \qquad N(x) \geqslant 0, \qquad \displaystyle\int_0^\infty N(x)\,\mathrm{d}x = 1, \\ -\tau(x)\dfrac{\partial}{\partial x}\phi(x) + (B(x)+\lambda)\,\phi(x) = \displaystyle\int_0^x b(x,y)\phi(y)\,\mathrm{d}y, \\ \phi(x) \geqslant 0, \qquad \displaystyle\int_0^\infty \phi(x)N(x)\,\mathrm{d}x = 1. \end{cases}$$

Dans [57], Doumic et Gabriel ont montré, sous des hypothèses très générales sur le taux de croissance, le noyau et le taux de fragmentation, l'existence d'un unique triplet propre (λ, N, ϕ), avec en plus des résultats de positivité.

Une fois ces solutions particulières obtenues, on s'emploie à comparer le comportement en temps long d'une solution en temps quelconque avec ces solutions. Pour ce faire, un outil fondamental et désormais classique est l'entropie relative généralisée, introduite par Michel, Mischler et Perthame dans [119, 120]. Il s'agit d'obtenir une quantité positive et décroissance au cours du temps, qui indiquerait à quel point une solution de l'équation (7) ou de l'équation (9) est différente de la solution de la forme $(t, \alpha) \mapsto e^{\lambda t}N(\alpha)$.

Théorème 1 (Michel, Mischler et Perthame 2004)**.** *Soit une fonction $H : \mathbb{R} \to \mathbb{R}$ suffisamment régulière. Sous réserve d'existence d'un triplet propre (λ, N, ϕ) pour* (7) *ou* (9)*, on a pour toute solution n de ces équations*

$$\frac{\mathrm{d}}{\mathrm{d}t}\mathcal{H}[n(t,\cdot)e^{-\lambda t}] = -\mathcal{D}^H[n(t,\cdot)e^{-\lambda t}], \tag{10}$$

où

$$\mathcal{H}[u] = \int_0^\infty \phi(\alpha)N(\alpha)H\left(\frac{u(t,\alpha)}{N(\alpha)}\right)\,\mathrm{d}\alpha$$

et

$$\mathcal{D}^H_{age}[u] = \phi(0)N(0)\left[\int_0^\infty H\left(\frac{u(a)}{N(a)}\right)\,\mathrm{d}\mu(a) - H\left(\int_0^\infty \frac{u(a)}{N(a)}\,\mathrm{d}\mu(a)\right)\right]$$

où $\mathrm{d}\mu(a) = 2B(a)\frac{N(a)}{N(0)}\,\mathrm{d}a$ *pour le renouvellement et*

$$\mathcal{D}^H_{taille}[u] = 4\int_0^\infty \phi(x)N(2x)B(2x)\left[H'\left(\frac{u(x)}{N(x)}\right)\left(\frac{u(2x)}{N(2x)} - \frac{u(x)}{N(x)}\right) - H\left(\frac{u(x)}{N(x)}\right) + H\left(\frac{u(2x)}{N(2x)}\right)\right]\,\mathrm{d}x$$

pour la croissance-fragmentation. Si de plus H *est convexe, alors* $\mathcal{D}^H \geqslant 0$.

On applique alors ce résultat à la fonction convexe $H(x) = |\rho - x|^p$ où $\rho = \int_0^\infty n^0(\alpha)\phi(\alpha)\,\mathrm{d}\alpha$ pour obtenir (avec quelques hypothèses en plus sur le taux de division) une convergence en temps long de $n(t,\cdot)e^{-\lambda t}$ vers ρN, comme énoncé dans le théorème suivant.

Théorème 2 (Michel, Mischler et Perthame 2005)**.** *Sous certaines hypothèses sur le taux de division, on a*

$$\forall p \in [1,\infty), \quad \lim_{t\to\infty} \|n(t,\cdot)e^{-\lambda t} - \rho N\|_{\mathrm{L}^p(N^{1-p}\phi\,\mathrm{d}x} = 0.$$

2.2 Problème inverse et comparaison de modèles

Maintenant que l'on connaît le comportement en temps long d'une solution du problème d'évolution, on peut comparer le modèle en âge au modèle en taille en s'appuyant sur les données expérimentales. Ce travail est l'objet de [149]. Dans cet article, les auteurs font l'hypothèse que la population a atteint l'état stable du système afin de construire une approximation de la fonction *continue* N à partir de n observations *discrètes* $(x_1, \cdots, x_n)$, tirées au hasard dans la population. On suppose alors que ces observations sont des réalisations de variables aléatoires indépendantes de loi N, solution du système (7) ou (9). On régularise alors la mesure empirique $\frac{1}{n}\sum_{i=1}^n \delta_{x_i}$ avec une suite régularisante $K_h = \frac{1}{h}K\left(\frac{\cdot}{h}\right)$, où K est une fonction de classe $\mathcal{C}^\infty$ à support compact, positive, d'intégrale 1 et h un paramètre réel positif. On obtient alors l'estimateur

$$\hat{N}_h(x) = \frac{1}{n}\sum_{i=1}^n K_h(x - X_i).$$

Le choix de la bonne valeur pour le paramètre h est une question difficile, qui a fait l'objet de nombreux travaux, par exemple [87, 86]. On reconstruit de manière similaire $\frac{\partial}{\partial x}N$, puis on estime λ et τ, et on obtient enfin une estimation du taux de division B pour chacun de ces modèles. Une fois ces fonctions reconstruites, on simule des données *via* les modèles correspondants, puis on les compare aux données expérimentales, *via* une mesure d'erreur. Il apparaît que les prédictions du modèle en taille présentent une meilleure adéquation avec les données réelles que le modèle en âge. De plus, ces prédictions sont robustes par rapport à l'hypothèse que les auteurs formulent quant à la forme du taux de croissance, contrairement à celles produites par le modèle en âge.

2.3 Au-delà des modèles en âge et taille : le modèle incrémental

Le travail présenté dans cette partie a été réalisé en collaboration avec Pierre Gabriel, de l'Université Versailles Saint-Quentin-en-Yvelines. Il fait l'objet du premier chapitre de chapitre de ce manuscrit et a été publié dans une édition spéciale de *Networks & Heterogeneous Media* dédiée aux méthodes mathématiques en biologie.

Si les prédictions de l'équation (3) montrent une meilleure adéquation avec la distribution en âge-taille que l'équation (2), ces deux modèles ne sont pas les seuls en lices pour décrire des populations de bactéries. Parmi les modèles concurrents, celui dit *incrémental* a fait l'objet de nombreux travaux. Dans [173] puis [3] est évoquée l'idée qu'un modèle approprié serait non pas de se diviser après avoir atteint une taille critique, mais plutôt après avoir grandi d'une quantité fixée (ceci est appelé en anglais *adder principle*). Plus tard, dans [27], les auteurs ont montré que ce mécanisme permettait chez deux types de bactéries assez éloignées évolutivement d'assurer l'homéostasie cellulaire chez certaines bactéries. De plus, dans [161], il a été montré que ce mécanisme de régulation s'appliquait aussi à *Saccharomyces cerevisiae*. Une revue de littérature sur l'évolution de l'état des connaissances sur un modèle adapté à

une population de bactéries est produite dans [153]. Cet article montre que le modèle en taille échoue à prédire la taille au moment de la division, et confirme que le modèle en âge est inadapté pour ce type d'organismes, car ne parvient pas à prédire correctement le temps entre deux divisions, alors que le modèle incrémental prédit ces deux quantités de manière satisfaisante. De plus, ce modèle prédit correctement à la fois la quantité ajoutée entre la naissance et la division et le taux de croissance.

La formalisation sous forme d'équation aux dérivées partielles proposée dans [167] appelait donc une analyse mathématique. Une des hypothèses de ce modèle est que le taux de croissance est gouverné uniquement par la taille courante, alors que le taux de division n'est fonction que de l'incrément, c'est à dire la quantité dont la bactérie a grandi depuis son apparition. Si on note respectivement g et B les taux de croissance et division et $n = n(t, a, x)$ la densité de population de taille x et d'incrément de taille a au temps t, le système s'écrit

$$\begin{cases} \dfrac{\partial}{\partial t} n(t,a,x) + \dfrac{\partial}{\partial a}(g(x)n(t,a,x)) + \dfrac{\partial}{\partial x}(g(x)n(t,a,x)) + B(a)g(x)n(t,a,x) = 0, \qquad t \geqslant 0,\ x > a > 0, \\ g(x)n(t,0,x) = 4g(2x)\displaystyle\int_0^\infty B(a)n(t,a,2x)\,\mathrm{d}a, \qquad t \geqslant 0,\ x > 0, \end{cases} \tag{11}$$

complété par une condition initiale $n(0, a, x) = n^{in}(a, x)$. Pas plusieurs aspects, cette équation présente des similarités avec les deux modèles précédents. Tout d'abord, le fait que la non-localité dans l'équation (11) soit uniquement portée par le terme de bord relève du modèle en âge, tandis que le terme de transport $\partial_t n(t, a, x) + \partial_a(g(x)n(t, a, x)) + \partial_x(g(x)n(t, a, x))$ traduit l'augmentation avec le temps de la taille et l'incrément de taille à même vitesse $g(x)$, à la manière du modèle en taille. Pus précisément au suje de ce terme de bord, on note que les naissances sont modélisées par un terme intégral, traduisant le fait que les individus naissant à taille x sont issus de la division des individus de taille $2x$ qui se sont divisés pour tout incrément $a \geqslant 0$. On peut immédiatement remarquer que pour compter tous les nouveaux nés, le terme de bord en $a = 0$ ne requiert pas d'intégrer jusqu'à l'infini. En effet, il ne peut pas y avoir de bactéries de taille plus petite que leur incrément courant, on peut donc sans perte de généraliser se restreindre à intégrer de 0 à $2x$. Enfin, le terme $B(a)g(x)n(t, a, x)$ désigne les bactéries de trait (a, x) qui se divisent à l'instant t.
À l'instar des deux modèles précédents, on peut formellement intégrer la premère ligne de (11) et intervertir les intégrales grâce au théorème de Fubini pour obtenir des informations sur la variation de la population totale et de la masse totale. On remarque que la population n'augmente que par la division de bactéries en deux nouveaux individus, comme le montre la relation

$$\frac{\mathrm{d}}{\mathrm{d}t}\int_0^\infty \int_0^x n(t,a,x)\,\mathrm{d}a\,\mathrm{d}x = \int_0^\infty \int_0^x g(x)B(a)n(t,a,x)\,\mathrm{d}a\,\mathrm{d}x.$$

L'expression de la variation de la masse totale

$$\frac{\mathrm{d}}{\mathrm{d}t}\int_0^\infty \int_0^x xn(t,a,x)\,\mathrm{d}a\,\mathrm{d}x = \int_0^\infty \int_0^x g(x)n(t,a,x)\,\mathrm{d}a\,\mathrm{d}x$$

suggère l'équation de croissance-fragmentation. Le modèle incrémental emprunte-il à l'un ou l'autre de ces modèles, ou alors fait-il montre d'un tout autre comportement ?

Pour une première approche de ce modèle, nous avons décidé de résoudre le problème de Perron dans le cas particulier d'une croissance linéaire, soit $g(x) = x$, et d'une fragmentation autosimilaire, c'est-à-dire qu'une bactérie de taille x se divise en plusieurs fragments, avec une probabilité pour obtenir une combinaison de fragments donnée indépendante de la taille x de la mère. Ce cas généralise celui de la mitose égale, et est motivé biologiquement, voir [167]. On note alors μ la mesure de fragmentation, à laquelle on impose pour assurer la conservation de la masse

$$\int_0^1 z\,\mathrm{d}\mu(z) = 1.$$

Un autre intérêt de ce cas est qu'à la fois la valeur propre dominante et le vecteur propre adjoints sont connus et explicitement donnés, à savoir $\lambda = 1$ et $\phi(x) = x$. Notre problème se formule donc

$$\begin{cases} \dfrac{\partial}{\partial a}(xN(a,x)) + \dfrac{\partial}{\partial x}(xN(a,x)) + (1 + xB(a))N(a,x) = 0, \qquad x > a > 0, & \text{(12a)} \\ N(0,x) = \displaystyle\int_0^1 \int_0^\infty B(a)N(a,\frac{x}{z})\,\mathrm{d}a\ \frac{\mathrm{d}\mu(z)}{z^2}, \qquad x > 0, & \text{(12b)} \\ N(a,x) \geqslant 0, \qquad x \geqslant a \geqslant 0, & \text{(12c)} \\ \displaystyle\int_0^\infty \int_0^x N(a,x)\,\mathrm{d}a\,\mathrm{d}x = 1. & \text{(12d)} \end{cases}$$

Nous avons obtenu le résultat d'existence et d'unicité suivant, formulé en donnant les interprétations des hypothèses plutôt que leurs expressions exactes.

Théorème 3 (Gabriel et M. 2019)**.** *Si la fragmentation satisfait une hypothèse de conservation de la masse et ne produit pas des nouveaux nés trop petits, et si le taux de division est localement intégrable et ne décroit pas trop vite à l'infini, alors il existe une unique solution N dans un espace L^1 à poids au problème de Perron* (12a)–(12d) *telle que*

$$N(a,x) = \frac{1}{x^2}B(a)e^{-\int_0^a B(\alpha)\,\mathrm{d}\alpha} f(x-a) \tag{13}$$

où f est une fonction positive donnée par le point fixe d'un opérateur et appartient à un espace L^1 à poids.

Rappelons que $B(a)e^{-\int_0^a B(\alpha)\,\mathrm{d}\alpha}$ s'interprète comme la loi de la variable aléatoire qui prend pour valeur la quantité dont un individu grandit avant de se diviser. Ainsi, la fonction f dans (13) s'interprète comme la distribution des tailles à la naissance des nouveaux individus. En effet, la différence $x - a$ désigne la taille actuelle moins la taille dont on a grandi depuis la naissance, il s'agit donc de la taille à la naissance, que nous noterons s. Une illustration est donnée à la figure 1. L'opérateur

$$Tf(s) = \int_\theta^\eta \int_0^{\frac{s}{z}} B(\frac{s}{z} - a)e^{-\int_0^{\frac{s}{z}-a} B(\alpha)\,\mathrm{d}\alpha} f(a)\,\mathrm{d}a\ \ \mathrm{d}\mu(z) \tag{14}$$

qui donne ce point fixe renforce cette interprétation. Si f est un point fixe, la relation (14) indique que les bactéries qui naissent à taille s sont issues de celles qui sont nées à taille a, ont grandi de $\frac{s}{z} - a$, puis en se fragmentant a donnée une bactérie plus petite d'un facteur z. Pour obtenir l'opérateur T, on commence par réécrire (12a)–(12d) avec les variables incrément de taille et taille à la naissance. Puisque cette dernière quantité ne varie pas au cours de la vie de la bactérie, on donc pour l'équivalent de (12a) une équation différentielle ordinaire dans laquelle on peut voir s comme un paramètre. On injecte ensuite l'expression obtenue dans le terme de naissance et on obtient une équation de point fixe, que l'on résoud grâce à des résultats issus de la théorie des opérateurs dans les treillis de Banach. En particulier le théorème suivant, qui est une combinaison des théorèmes de Krein-Rutman et de Pagter, est fondamental dans notre démonstration.

Théorème 4. *Soit $A : \mathrm{L}^1(\Omega,\nu) \to \mathrm{L}^1(\Omega,\nu)$ un opérateur non nul positif compact irréductible. Alors son rayon spectral est une valeur propre strictement positive associée à un vecteur propre non nul positif.*

Tel qu'il est écrit, l'opérateur T, qui agit sur des fonctions définies sur $\mathbb{R}_+$, est bien irréductible. En revenche, il n'est pas compact, c'est pourquoi on tronque le domaine de définition des fonctions sur lesquelles il agit. On obtient alors une famille d'opérateurs $(T_\Sigma)_{\Sigma>0}$, qui héritent par ailleurs de la propriété d'irréductibilité de l'opérateur initial. On applique donc le théorème 4 à chaque T_Σ pour obtenir l'existence d'un couple propre (ρ_Σ, f_Σ). Il s'agit ensuite de montrer que lorsque Σ tend vers l'infini, la valeur propre ρ_Σ tend vers 1 et (à une sous-suite près) f_Σ converge dans une norme L^1 à poids vers une fonction f, dont on vérifie que c'est un point fixe de l'opérateur T. Pour prouver l'unicité du point fixe, on remarque tout d'abord que $Tf(s)$ peut s'écrire comme l'intégrale d'un produit de convolution contre une mesure de probabilité. On exploite ensuite des propriétés de la transformée de Laplace : linéarité,

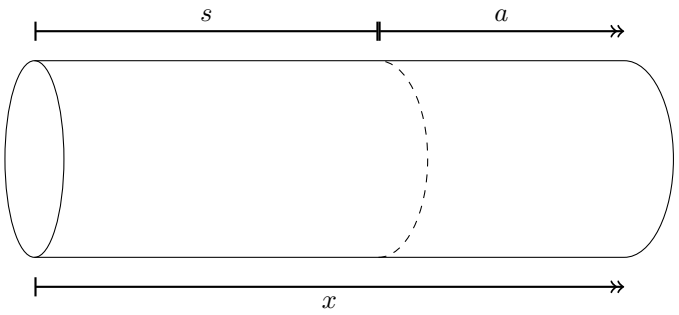

FIGURE 1 – Représentation des variables x, a et s sur un schéma de la bactérie *E. coli*. Les barres verticales indiquent une quantité qui ne varie pas au cours de la vie de la bactérie, des flèches une quantité qui grandit.

comportement vis à vis d'une mesure de probabilité, injectivité. L'unicité du point fixe est obtenue après quelques manipulations. La dernière étape est de montrer que l'unicité du point fixe induit celle du vecteur propre solution de (12a)–(12d). Il est à noter qu'une description similaire à celle du modèle incrémental avait été formulée en 1991 par Hall, Wake et Gandar dans [95] pour modéliser la croissance de cellules végétales rectilignes. Dans cet articles, les auteurs ont employé les variables taille x et taille à la naissance s. Leur méthode n'a cependant permi d'obtenir des résultats que sur un compact, restriction à laquelle n'est pas soumise notre approche.

On peut ensuite se demander si une convergence vers le vecteur propre se produit, comme pour les modèles précédents. On écrit alors une inégalité d'entropie.

Proposition 1. *Soit n une solution du problème d'évolution* (11) *vérifiant $|n(t,a,x)| \leqslant Ce^t N(a,x)$, alors*

$$\frac{\mathrm{d}}{\mathrm{d}t}\mathcal{H}[n(t,\cdot,\cdot)e^{-t}] = -\mathcal{D}^H[n(t,\cdot,\cdot)e^{-t}],$$

avec

$$\mathcal{D}^H[n] = \int x^2 N(0,x)\left[\int\int H\left(\frac{n(a,\frac{x}{z})}{N(a,\frac{x}{z})}\right)\,\mathrm{d}\nu_x(a,z) - H\left(\int\int \frac{n(a,\frac{x}{z})}{N(a,\frac{x}{z})}\,\mathrm{d}\nu_x(a,z)\right)\right]\,\mathrm{d}x$$

où $\mathrm{d}\nu_x(a,z) = \frac{B(a)N(a,\frac{x}{z})}{N(0,x)z^2}\,\mathrm{d}a\,\mathrm{d}\mu(z)$ *est une mesure de probabilité. De plus, si H est convexe, alors $\mathcal{D} \geqslant 0$.*

Choisissant $H(x) = |1-x|$ dans cette inégalité, on obtient la décroissance de la quantité

$$\|N - n(t,\cdot)e^{-t}\|_{\mathrm{L}^1}.$$

Si le noyau de fragmentation admet une densité par rapport à la mesure de Lebesgue, on conjecture que cette quantité converge vers 0. En revanche, dans le cas de la mitose égale, c'est à dire si $\mu(z) = \delta_{z=\frac{1}{2}}$, on s'attend à ce que cette quantité ne tende pas vers 0. En effet, il existe en fait une famille de triplets propres (λ_j, N_j, ϕ_j) indexés par $\mathbb{Z}$ définis par

$$\lambda_j = 1 + \frac{2ij\pi}{\mathrm{Log}\ 2}, \qquad N_j(a,x) = x^{1-\lambda_j}N(a,x), \qquad \phi_j(a,x) = x^{\lambda_j}.$$

Une situation similaire a déjà été mise en évidence pour l'équation de croissance-fragmentation linéaire, dans le cas de croissance linéaire et de la mitose égale, comme montré dans [14]. Les auteurs ont également montré que, si on note n la solution du problème d'évolution, alors la fonction $n(t,\cdot)e^{-t}$ converge dans un espace L^2 à poids vers une série de Fourier dans laquelle intervient la famille $(\lambda_j, N_j, \phi_j))_{j\in\mathbb{Z}}$. Ce comportement est aussi à la base de l'étude menée dans la partie suivante.

2.4 Perspectives sur le modèle incrémental

On peut poursuivre ce travail dans plusieurs directions. Du point de vue mathématique, on peut appliquer au modèle incrémental le même programme de démonstration que pour les modèles en âge et en taille. On pourra s'employer à démontrer l'existence d'un triplet propre dans des cas moins pathologiques, en particuliers dans une situation où on s'attend à une convergence vers un profil stationnaire plutôt que vers un profil oscillant. Les cas de cette gamme présente une difficulté supplémentaire par rapport à celui qu'on a élucidé, puisqu'il faut en plus en plus démontrer l'existence d'une valeur propre dominante positive et d'un vecteur propre adjoint positif. On pourra également prouver l'existence et l'unicité de solution du problème d'évolution, puis en utilisant des inégalités d'entropie, montrer leur comportement asymptotique. Dans notre travail, nous avons supposé disposer d'une telle solution pour écrire l'inégalité (10). Dans une autre optique, on pourrait ajouter à ce modèle de la variabilité, à la manière d'Olivier dans [130].
Comme évoqué précédemment, la question de la pertinence du modèle choisi se pose très rapidement. Pour cela, on pourra comparer le moddèle incrémental au modèle en taille, dans la même démarche que celle décrite dans la section 2.2. Une autre question difficile se pose, reliée aux dispositifs expérimentaux utilisés. En effet, une manière d'acquérir des données expérimentales consiste faire passer les bactéries une par une dans un dispositif permettant de mesurer leur taille, par exemple un compteur Coulter ou un dispositif de cytométrie en flux. Cette méthode permet d'obtenir en peu de temps une distribution de tailles, mais ne renseigne pas sur les incréments de tailles. En somme, on mesure les marginales

$$\mathcal{N}(x) = \int_0^x N(a,x)\,\mathrm{d}x.$$

Pour obtenir des informations sur la distribution en taille-incrément de taille, on peut alors filmer (ou prendre des photos à intervalle régulier) la colonie de bactéries suffisamment longtemps pour atteindre la distribution stable. L'analyse de données consécutive est alors considérablement plus longue qu'avec le dispositif précédent. Un défi consiste alors à arriver à estimer une fonction dépendant uniquement de l'incrément de taille, $B(a)$ à partir de mesures des marginales précédentes.

3 Solutions mesures pour des équations de populations structurées

Les solutions mesures offrent un cadre nouveau pour résoudre des équations différentielles et aux dérivées partielles. Cette idée a été introduite en 1984 dans un célèbre article de DiPerna [53], dans lequel est développé le concept de solution à valeur mesure admissible pour des lois de conservation scalaires. Dans [44], cette idée est associée celle de *mesures de Young généralisée* (introduite dans [54]) pour étudier le comportement asymptotique de (3) and le cas $\mu \equiv 0$. Ce concept très général de solution permet dans de nombreux cas d'obtenir l'existence de solution, mais l'unicité fait parfois défaut (voir l'exemple donné [44]).
On se tourne alors plutôt vers des solution mesures, qui jouissent plus souvent d'unicité de la solution. De plus, ce type de solution permet une interprétation assez immédiate en terme de densité. C'est l'objet des deux sous-sections suivantes, dans lesquelles on applique deux théories de solutions mesures successivement à un cas particulier de (3) dans lequel on s'attend à observer un comportement cyclic en temps long puis à une modélisation de populations par compartiments.

3.1 Construction par semigroupe dual

Le travail présenté dans cette section est également issu d'une collaboration avec Pierre Gabriel et constitue le sujet du deuxième chapitre du manuscrit. Un article regroupant nos résultat est en cours d'écriture et sera sous peu soumis pour publication.

Tous les résultats d'existence, unicité et comportement asymptotique précédents ont été énoncés dans un cadre L^p. Depuis plusieurs années, un autre type de solution aux équations de populations structurées

émerge : les solutions mesures. Une solution mesure permet de considérer comme condition initiale une masse de Dirac, ce qui s'interprète biologiquement comme une situation dans laquelle le trait étudié est connu précisément, par exemple lorsqu'une culture de bactéries est initialisée avec une unique cellule. Des résultats d'existence et d'unicité de solution mesure, ainsi que de stabilité par rapport aux paramètres du modèle ont été montré dans [29, 89, 90, 81] par exemple. On donne dans un premier temps des résultats assez formels, le cadre sera précisé plus bas.

Pour étudier le comportement en temps long de solutions mesures d'équations aux dérivées partielles structurées, plusieurs approches ont été développées. Dans [91] puis dans [44], les auteurs ont étendu aux mesures les inégalités d'entropie fournies par le théorème 1, d'abord pour l'équation de renouvellement, puis pour l'équation de croissance-fragmentation. Une autre possibilité consiste à faire appel à la méthode de Doeblin. C'est la stratégie utilisée dans [81] pour l'équation de renouvellement conservative, également dans [9] pour le renouvellement non conservatif, et enfin dans [10] pour la fragmentation. Enfin, la dernière approche déjà existente qu'on citera est issue de [75]. Dans cet article, les auteurs montrent comment on peut, sous certaines hypothèses, appliquer la théorie des semigroupes positifs fortement continus à des solutions mesures, et ainsi obtenir une convergence asymptotique vers un attracteur global.

Dans [81], la solution mesure $(\mu_t)_{t\geqslant 0}$ converge vers une mesure $C(\mu^{in})\mu_\infty$. La constante s'exprime comme

$$C(\mu^{in}) = \int_0^\infty \mathrm{d}\mu^{in}(x)$$

tandis que la mesure μ_∞ admet une densité par rapport à la mesure de Lebesque sur $\mathbb{R}_+$, notée $\Lambda_{\mathbb{R}_+}$. Cette densité vaut $N(a)$, où $N(a)$ est le vecteur propre dominant de l'équation de renouvellement (2), dans le cas $\mu = B$. De manière analogue, dans [91], les auteurs ont montré que dans beaucoup de cas, la solution mesure $(\mu_t)_{t\geqslant 0}$ converge en variation totale. Précisément, ils ont montré la convergence

$$\lim_{t\to\infty} \int_{\mathbb{R}_+} \phi(x)\, \mathrm{d}\left|\mu_t(x)e^{-\lambda t} - C(\mu^{in})\Lambda_{\mathbb{R}_+}(x)\right| = 0,$$

où

$$C(\mu^{in}) = \int_0^\infty \phi(x)\, \mathrm{d}\mu^{in}(x).$$

Dans les deux cas évoqués, la constante $C(\mu^{in})$ est le vecteur propre principal adjoint testé contre la mesure initiale.

Parmi les cas non pris en compte par les hypothèses de [91], figure celui de la mitose égale avec taux de croissance linéaire. Ce cas représente une situation idéalisée pour lequel on connait explicitement la valeur propre dominante $\lambda = 1$ et le vecteur propre adjoint dominant $\phi(x) = x$, et il a été montré dans [14] que dans un cadre L^2 se produit une convergence vers une solution périodique de l'équation. Plus précisément, sous l'hypothèse sur le taux de division B

$$\begin{cases} B : (0,\infty) \to (0,\infty) \text{ est localement intégrable,} \\ \\ \exists b > 0,\ \operatorname{supp} B = [b,\infty), \\ \\ \exists z_0, \gamma_0, K_0 > 0,\ \forall x < z_0, \quad B(x) \leqslant K_0 x^{\gamma_0}, \\ \\ \exists z_1, \gamma_1, \gamma_2, K_1, K_2 > 0\ \forall x > z_1 \quad K_1 x^{\gamma_1} \leqslant B(x) \leqslant K_2 x^{\gamma_2}, \end{cases} \tag{15}$$

si l'on note $n(t,x)$ la solution de

$$\frac{\partial}{\partial t} n(t,x) + \frac{\partial}{\partial x}(x n(t,x)) + B(x) n(t,x) = 4B(2x) n(t,2x) \tag{16}$$

avec condition initiale n^{in} et

$$\lambda_j = 1 + \frac{2ij\pi}{\text{Log } 2}, \qquad N_j(x) = x^{1-\lambda_j} N(x), \qquad \phi_j(x) = x^{\lambda_j} \tag{17}$$

les éléments propres indexés par $\mathbb{Z}$ de cette équation, alors on a la convergence

$$\lim_{t\to\infty} \left\| n(t,\cdot)e^{-t} - \sum_{j\in\mathbb{Z}} (n^{in}, N_j) e^{\frac{2ij\pi}{\text{Log } 2}t} N_j \right\|_{\mathrm{L}^2\left(\mathbb{R}_+, \frac{x}{N(x)}\,\mathrm{d}x\right)} = 0.$$

On s'attend alors à une convergence de la solution mesure vers une mesure oscillante de période Log 2, bâtie à partir des éléments propres précédents. Avant d'énoncer le résultat, on précise le cadre fonctionnel, en suivant l'exposition de [81], adapté au cas étudié.

On rappelle ici quelques résultats sur les mesures complexes qui nous serviront par la suite. Ce qui suit est tiré de [151]). On munit $\mathbb{R}_+^*$ de sa topologie usuelle et de la tribu de Borel associée. On commence par une définition.

Définition 1 (Mesure portée par un ensemble, mesures mutuellement singulières)**.** *Une mesure μ est dite portée par le mesurable A si pour tout mesurable E disjoint de A on a $\mu(E) = 0$. Deux mesures μ et ν portée par des ensembles A et B respectivement sont dites mutuellement singulières si $A \cap B = \emptyset$.*

On note $\dot{\mathcal{M}}$ l'ensemble des applications d'ensemble μ des mesurables de $\mathbb{R}_+^*$ dans les réelles telles que la mesure $\phi\mu$ qui à un mesurable A associe

$$\phi\mu(A) = \int_{\mathbb{R}_+^*} \phi \mathbb{1}_A \,\mathrm{d}\mu,$$

avec $\phi(x) = \phi_0(x) = x$, est une mesure signée. On notera en particulier que la définition de mesures signées implique la finitude de la mesure. On a alors le théorème de décomposition suivant.

Théorème 5 (Décomposition de Jordan)**.** *Toute mesure signée μ sur $\mathbb{R}_+^*$ admet une unique décomposition de la forme $\mu = \mu_+ - \mu_-$, où μ_+ et μ_- sont des mesures positives finie qui sont mutuellement singulières. La mesure notée $|\mu| = \mu_+ + \mu_-$ est appelé la mesure en variation totale de la mesure μ, et c'est une mesure finie.*

On dispose alors d'une norme sur l'espace $\dot{\mathcal{M}}$

$$\|\mu\|_{\dot{\mathcal{M}}} := |\phi\mu|(\mathbb{R}_+^*) = (\phi\mu)_+(\mathbb{R}_+^*) + (\phi\mu)_-(\mathbb{R}_+^*).$$

On définit maintenant l'espace vectoriel

$$E = \left\{ f : \mathbb{R}_+^* \to \mathbb{R}, \quad \|f\|_E = \sup_{x>0} \frac{|f(x)|}{x} < \infty \right\},$$

à partir duquel on obtient l'espace de Banach $(E, \|\cdot\|_E)$. On note ensuite E_0 le sous-espace vectoriel fermé des fonctions continues de E telles que

$$\lim_{x\to 0,\ x\to\infty} \frac{f(x)}{x} = 0.$$

Pour toute mesure $\mu \in \dot{\mathcal{M}}$, on peut définir la forme linéaire

$$T_\mu : \begin{cases} E_0 \longrightarrow \mathbb{R}, \\ \\ f \mapsto \displaystyle\int_{\mathbb{R}_+^+} f \,\mathrm{d}\mu, \end{cases}$$

dont la continuitée est assurée par l'inégalité

$$|T_\mu f| \leqslant \int_{\mathbb{R}_+^+} \frac{|f|}{\phi} \phi \, \mathrm{d}\mu \leqslant \|f\|_E \|\mu\|_{\dot{\mathcal{M}}}.$$

Contrairement à la situation présentée dans [81], on ne peut pas ici appliquer directement le théorème de représentation de Riesz, cependant l'existence d'une isométrie entre $\mathcal{C}_b(0,\infty)$ et E d'une part, et entre $\mathcal{C}_0(0,\infty)$ et E_0 d'autre part, permet d'obtenir le résultat similaire suivant.

Lemma 2. *Pour toute forme linéaire $T \in E_0'$, il existe une unique mesure $\mu \in \dot{\mathcal{M}}$ telle que $T = T_\mu$. De plus, on a $\|T\|_{E_0'} = \|\mu\|_{\dot{\mathcal{M}}}$.*

Une fois ce cadre fonctionnel posé, on peut donner la définition de solution mesure que l'on retient, qui s'énonce par dualité.

Définition 2. *On dit que la famille $(\mu_t)_{t\geqslant 0}$ est une solution mesure de* (16) *si pour toute fonction $f \in E$ l'application $t \mapsto \mu_t f$ est continue et si pour toute fonction $f \in \mathcal{C}_c^1(\mathbb{R}_+^*)$ on a*

$$\mu_t f = \mu^{in} f + \int_0^t \mu_s \left(\mathcal{A} f\right) \, \mathrm{d}s,$$

où

$$\mathcal{A} f(x) = x \frac{\partial}{\partial x} f(x) + B(x) \left[2 f(\frac{x}{2}) - f(x) \right].$$

Dans le cadre mesure, plusieurs modes de convergence coexistent. Nous évoquons ici la convergence faible et la convergence forte, qui implique la précédente. La convergence faible correspond à la convergence étroite. La convergence forte, ou convergence en variation totale, est une convergence en norme : on dit que $(\mu_n)_{n\in\mathbb{N}} \in \mathcal{M}$ converge en variation totale vers $\mu \in \mathcal{M}$ si

$$\lim_{n\to\infty} \|\mu_n - \mu\|_{TV} = 0.$$

On obtient le résultat d'existence, d'unicité et de comportement asymptotique suivant.

Théorème 6 (Gabriel et M.)**.** *Si le taux de division est une fonction continue, alors il existe une unique solution mesure à* (16) *avec condition initiale μ^{in}, donnée par un semigroupe $t \mapsto \mu^{in} M_t$. S'il satisfait de plus l'hypothèse* (15)*, alors la solution converge faiblement vers une mesure* Log $2-$*périodique.*

Pour démontrer la partie existence et unicité, on suit les étapes de [81]. Tout d'abord, on commence par montrer que le problème d'évolution adjoint admet une unique solution, que l'on exprime sous forme de semigroupe agissant sur une condition initiale. Si $f = f(x)$ est la condition initiale, alors $(t,x) \mapsto M_t f(x)$ est l'unique solution de ce problème, où l'on a bien pris soin de définir le semigroupe $(M_t)_{t\geqslant 0}$ sur un espace assez grand pour contenir les indicatrices de $\mathbb{R}_+^*$. Ensuite, pout $\mu \in \mathcal{M}$ et $t \geqslant 0$, on définit l'application μM_t qui à un mesurable A de $\mathbb{R}_+^*$ associe la quantité

$$\mu M_t(A) := \int_{\mathbb{R}_+^*} M_t \mathbb{1}_A \, \mathrm{d}\mu.$$

On montre que cette application vérifie les axiomes pour d'une mesure, et de plus est un semigroupe. L'étape suivante consiste à montrer que cette mesure est bien solution de l'équation (16) au sens de la définition 2.

La méthode de [44] ne s'applique pas dans notre cas, car le noyau de division qu'on considère est singulier. Ici, on s'inspire de la preuve donnée dans [14], couplée à l'idée d'exploiter le comportement en temps longs de $M_t f$, *via* la relation

$$(\mu M_t) f = \mu (M_t f).$$

En effet, comme la fonction $M_t f$ est solution de l'équation

$$\frac{\partial}{\partial t} f(t,x) - x\frac{\partial}{\partial x} f(t,x) + B(x) f(t,x) = 2B(x) f(t,\frac{x}{2}), \quad t \geqslant 0,\ x > 0,$$

à laquelle s'ajoute une condition finitiale $f(0,x) = f^{in}(x)$, on peut appliquer les résulats de [120] afin d'obtenir une inégalité d'entropie sur le problème adjoint. Avec les notations précédentes, on parvient à la proposition 1 ci-dessous, pour laquelle on introduit d'abord quelques notations. Il nous faut une adaptation des triplets propres (17). Les valeurs propres et vecteurs propres adjoints restent les mêmes. Pour la version mesure des vecteurs propres primaux, on définit la famille de mesures $\nu_j \in \mathcal{M}$ ayant pour densité par rapport à la mesure de Lebesgue

$$\mathrm{d}\nu_j = x^{-\frac{2ij\pi}{\mathrm{Log}\ 2}} N(x)\, \mathrm{d}\Lambda_{\mathbb{R}_+^*}.$$

On aura donc besoin de travailler avec des fonctions à valeurs complexes. On définit alors l'espace

$$E^{\mathbb{C}} := \{f : \mathbb{R} \to \mathbb{C}, \Re(f), \Im(f) \in E\}.$$

De manière analogue aux éléments propres considérés dans [14], on a bien $\nu_j \phi_k = \delta_{j,k}$, où $\delta_{j,k}$ est le symbole de Kronecker. On définit par analogie avec la preuve de cet article l'espace

$$X = \overline{\mathrm{vect}}\,\{\phi_k,\ k \in \mathbb{Z}\}$$

et on montre l'égalité d'ensembles

$$X = \left\{f \in E^{\mathbb{C}},\ \forall x > 0,\ f(2x) = 2f(x)\right\},$$

qui, encore comme dans [14], est l'ensemble des fonctions qui annulent la dissipation d'entropie.

Proposition 1. *Pour toute fonction $f \in \mathcal{C}_c^1(\mathbb{R}_+^*)$, la somme de Fejèr*

$$\sum_{n=-N}^{N} \Big(1 - \frac{|n|}{N}\Big)(\nu_n f) e^{\frac{2i\pi n}{\mathrm{Log}\ 2} t} \phi_n$$

converge dans E, et sa limite notée $R_t f$ définit une famille Log $2-$*périodique d'opérateurs linéaires bornés. On peut étendre par densité R_t en un opérateur $E_0 \to X$ tel que pour tout $f \in E_0$, la fonction $e^{-t} M_t f - R_t f$ converge localement uniformément vers* 0 *sur $\mathbb{R}_+^*$. De plus, on peut étendre R_t par linéarité pour obtenir un projecteur $R_t : X \oplus E_0 \to X$.*

La preuve repose sur le fait qu'une une sous-suite près, la suite $h_k(t,\cdot) = e^{-t-k\mathrm{Log}\ 2} M_{t+k\mathrm{Log}\ 2} f$ converge localement uniformément sur $[0,\infty) \times (0,\infty)$ vers une fonction $g(t,\cdot)$ dont on montre qu'elle appartient à l'ensemble X. On a alors convergence uniforme de la somme de Fejèr de $g(t,\cdot)$ vers $g(t,\cdot)$, et on note $R_t f$ cette limite.

3.2 Construction par le poussé en avant de la mesure initiale

Les résultats présentés ici ont fait l'objet d'un travail en groupe lors du CEMRACS 2018 et sont détaillés dans le troisième chapitre de ce manuscrit. L'article qui en a résulté est soumis pour publication dans *ESAIM : Proceedings and Surveys.*

Dans cette section, on présente une autre construction de solution mesure d'une équation de population structurée, due à Poupaud et Rascle en 1997 dans [144], qui permet de traiter le cas d'un champs de vitesse discontinu. Leur construction se base sur l'existence et l'unicité de caractéristiques d'une équation différentielle dans ce cas, prouvée par Filippov, voir [78]. On présente quelques résultats issus de cet ouvrage permettant d'obtenir existence et unicité des caractéristiques. Puisqu'on ne considère que des application en dimension un, les résultats seront formulés dans cette dismension, bien qu'ils soient valides

en dimension finie quelconque.
On s'intéresse au problème de transport avec condition initiale

$$\begin{cases} \dfrac{\partial}{\partial t}u(t,x) + \dfrac{\partial}{\partial x}(a(t,x)u(t,x)) = 0, \qquad t>0,\ x\in\mathbb{R} & \text{(18a)} \\ \\ u(0,x) = u_0(x), \qquad x\in\mathbb{R}. & \text{(18b)} \end{cases}$$

La résolution d'une équation de transport telle que (18a)–(18b) avec champ de vitesse continu est aujourd'hui très classique. Pour ce faire, on emploie le flot associé *i.e.* la solution notée $X(t;s,x)$ de l'équation

$$\begin{cases} \frac{\mathrm{d}}{\mathrm{d}t}y(t) = a(t,y(t)), \\ \\ y(s) = x, \end{cases}$$

pour $t > s$. L'idée de Poupaud et Rascle est alors de généraliser cette notion, pour pouvoir définir le poussé en avant de la mesure initiale via les caractéristiques au sens de Filippov, que l'on définit plus bas. Cette idée était déjà en germe pour un système hyperbolique de lois de conservation dans [41] D'abord, on introduit l'*enveloppe convexe essentielle* de a.
On note $\mathcal{N}$ l'ensemble des measurables de $\mathbb{R}$ de mesure nulle, $Conv(E)$ l'enveloppe convexe de l'ensemble E, soit le plus petit ensemble convexe fermé contenant E et $B(x,r)$ la boule de centre x et de rayon r. Alors on définit

$$\{Convess(a(t,\cdot))\}(x) := \bigcap_{r>0}\bigcap_{N\in\mathcal{N}} Conv(a(t,B(x,r)\backslash N)).$$

On peut alors définir des caractéristiques généralisées au sens de Filippov.

Définition 3. *Une caractéristique de Filippov $X(t;s,x)$ issue de $x\in\mathbb{R}$ au temps $s\in\mathbb{R}$ est une fonction continue $X(\cdot;s,x)\in\mathcal{C}(\mathbb{R};\mathbb{R})$ qui satisfait*

$$\begin{cases} \frac{\partial}{\partial t}X(t;s,x)) \in \{Convess(a(t,\cdot))\}(X(t;x,s)) \quad p.p. \quad t\in\mathbb{R}, \\ \\ X(s;s,x) = x, \end{cases}$$

On énonce alors un théorème d'uncité pour les caractéristiques au sens de Filippov. Soit $L = L(t,u) \in \mathrm{L}^1(\mathbb{R};\mathrm{L}^\infty(\mathbb{R}))$ fonction telle que l'unique solution de

$$\frac{\partial}{\partial t}u(t) = L(t,u(t)) \text{ p.p. } t>s,\ u(s)=0$$

est identiquement égale à la fonction nulle. On dira qu'une fonction remplissant une telle condition satisfait l'hypothèse (U). On a alors le théorème d'unicité suivant.

Théorème 7. *Si le champ de vitesse a satisfait*

$$(a(t,x)-a(t,y))\cdot(x-y) \leqslant |x-y|L(t,|x-y|) \text{ p.p. } t>s,\ x,y\in\mathbb{R}, \tag{19}$$

avec L satisfaisant l'hypothèse (U) *précédente, alors les caractéristiques sont uniques pour $t \geqslant s$.*

On appelle (19) *condition de Lipschitz unilatérale*, et cette condition permet les discontinuités de type compressif, c'est à dire dont le flot associé réduit les volumes. Autrement dit, la divergence du champs de vitesses est inférieure ou égale à 0. On obtient alors le théorème suivant, on conservant les notations définies à la section précédente.

Théorème 8. *Supposons que le champ de vitesse vérifie la condition d'unicité* (19) *et*

$$a\in \mathrm{L}^1_{loc}(\mathbb{R};\mathrm{L}^\infty(\mathbb{R})). \tag{20}$$

Alors pour toute mesure initiale $\mu\in\mathcal{M}(\mathbb{R})$, il existe une unique solution au sens des distributions de (18a)–(18b). *Cette solution appartient à $\mathcal{C}([0,\infty);\mathcal{M}(\mathbb{R})-w)$ et est donnée par*

$$\mu_t = X(t)(\mu). \tag{21}$$

L'équatin (21) signifie simplement que μ_t est le poussé en avant de la mesure μ par le caractéristique $X(t)$, *i.e.* pour tout borélien B, on a $\mu_t(B) = \mu(X(t)^{-1}(B))$, ou encore pour toute fonction $\varphi \in \mathcal{C}_0(\mathbb{R})$, on a $\mu_t\varphi = \mu(\varphi(X(t;\cdot)))$ avec les notations de dualité précédentes. Poupaud et Rascle étendent ensuite ce résulat à des équations de transport plus générales, à savoir

$$\begin{cases} \dfrac{\partial}{\partial t}u(t,x) + \dfrac{\partial}{\partial x}(a(t,x)u(t,x)) + b(t,x)u(t,x) = f(t,x), \qquad t>0,\ x\in\mathbb{R} & \text{(22a)} \\ \\ u(0,x) = u_0(x), \qquad x\in\mathbb{R}. & \text{(22b)} \end{cases}$$

avec

$$b \in \mathrm{L}^1(0,\infty;\mathcal{C}_b(\mathbb{R})) \tag{23}$$

et

$$f \in \mathrm{L}^1([0,\infty);\mathcal{M}(\mathbb{R})). \tag{24}$$

Grâce à un argument de point fixe, les auteurs montrent le résutlat suivant.

Théorème 9. *Sous les mêmes hypothèses que dans le théorème 8 et les hypothèses* (23) *et* (24)*, pour toute condition initiale $\mu \in \mathcal{M}((0,\infty))$, le problème* (22a)–(22b) *admet une unique solution mesure $\mu_t \in \mathcal{C}([0,\infty);\mathcal{M}(\mathbb{R})-w)$ qui satisfait la formule de Duhamel*

$$\mu_t = X(t)(\mu) + \int_0^t X(t-s)(f_s - b(s,\cdot)\mu_s\,\mathrm{d}s.$$

Pour illustrer la puissance de cette théorie, on l'applique à une équation modélisant des adipocytes, qui sont les cellules chez les animaux en charge de stocker l'excédent de gras et ont la particularité de pouvoir énormément augmenter leur volume, jusqu'à atteindre un rayon critique noté r_c. On structure alors cette population en rayon, avec une vitesse V qu'on détaille plus bas, te un taux de mort γ''. Une distribution de taille pour les adipocytes avait déjà été obtenue dans les modèles déjà existants [164, 163]. Une des originalités du modèle que l'on propose ici réside dans la modélisation de deux populations intéragissant avec les adipocytes. La première est composée de cellules mésenchymateuses, qui sont des cellules souches présentes dans le mésenchyme de l'embryon. Elles sont capables de se différencier en de nombreux types cellulaires, dont des préadipocytes, qui constituent la deuxième population modélisée. Ces cellules peuvent ensuite se différencier en adipocytes. On fait des hypothèses sur ces population. De manière assez classique, on modélise un phénomène prolifération, à taux α et α' respectivement, et un phénomène de mort, à taux γ et γ' respectivement. À cela, on ajoute des rétrocontrôles, qui stimulent ou inhibent la différenciation, de cellule mésenchymateuse en préadipocyte d'une part, et de préadipocyte d'autre part. Ces contrôles sont donnés respectivement par les fonctions β et β', qu'on explicitera plus bas et dont on fait l'hypothèse qu'elles ne dépendent que du rayon moyen des adipocytes. De plus, on considère que ces deux populations sont composées de cellules de rayon constant, noté r_*, hypothèse issue des données expérimentales. Toutes ces intéractions sont résumées sur la figure 2. On adjoint donc à l'équation aux dérivées partielles sur les adipocytes deux équations différentielles. Ainsi le modèle s'écrit

$$\begin{cases} \dfrac{\mathrm{d}m}{\mathrm{d}t}(t) = -\gamma m(t) + \alpha m(t) - \beta(\bar{r}(t))m(t), \\ \\ \dfrac{\mathrm{d}p}{\mathrm{d}t}(t) = -\gamma' p(t) + \alpha' p(t) - \beta'(\bar{r}(t))p(t) + \beta(\bar{r}(t))m(t), \\ \\ \dfrac{\partial a}{\partial t}(t,r) + \partial_r\left(Va\right)(t,r) = -\gamma'' a(t,r), \end{cases}$$

où

$$\bar{r}(t) = \frac{\displaystyle\int_{r_\star}^{r_c} s\ a(t,s)\,\mathrm{d}s}{\displaystyle\int_{r_\star}^{r_c} a(t,s)\,\mathrm{d}s}$$

donne le rayon moyen des adipocytes. On complète ce système de conditions initiales

$$m(0) = m_0 \geqslant 0, \qquad p(0) = p_0 \geqslant 0, \qquad a(0,r) = a_0(r) \geqslant 0.$$

On choisit ensuite pour les taux de différenciation deux sigmoïdes, que l'on choisit de la forme

$$\bar{r} \mapsto \beta_m + \frac{\beta_M - \beta_m}{1 + e^{-\frac{\bar{r} - r_\beta}{R_\beta}}},$$

avec des paramètres $\beta_M \geqslant \beta_m$ et $r_\beta,\ R_\beta$ à spécifier pour β et β'. La vitesse est obtenue grâce au raisonnement suivant. Tout d'abord, la dynamique d'un adipocyte $t \mapsto R(t)$ est donnée par

$$\frac{\mathrm{d}}{\mathrm{d}t} R(t) = V(t, R(t)),$$

et on suppose que les adipocyte captent toutes les lipides qui ne sont pas utilisées pour le fonctionnement courant du métabolisme. Ces lipides en goutelettes traversent la paroi des adipocytes, donc le flux de nourriture excédentaire, supposé constant, entrant dans ceux de rayon $r_\star < R < r_c$ est donnée par

$$k \frac{R^2}{\int_{r_\star}^{r_c} s^2\ a(t,s)\,\mathrm{d}s},$$

où $k >$ est la nourriture à stocker. Le volume de ces adipocytes n'augmentant que par incorporations de goutelettes de lipides, on a alors

$$\mathscr{V}(t + \ \mathrm{d}t) = \mathscr{V}(t) + k \frac{R(t)^2}{\displaystyle\int_{r_\star}^{r_c} s^2 a(t,s)\,\mathrm{d}s} \times\ \mathrm{d}t,$$

dont on déduit que le volume satisfait l'équation différentielle

$$\frac{\mathrm{d}V}{\mathrm{d}t} = k \frac{R(t)^2}{\displaystyle\int_{r_\star}^{r_c} s^2 a(t,s)\,\mathrm{d}s}.$$

Ensuite, on relie le rayon d'un adipocyte à son volume *via* la formule $\mathscr{V}(t) = 4/3\pi R(t)^2$ pour obtenir une expression pour la vitesse de croissance pour les adipocytes de rayon compris entre $r_\star$ et r_c

$$V(t,r) = \frac{k}{4\pi \displaystyle\int_{r_\star}^{r_c} s^2 a(t,s)\,\mathrm{d}s} =: \frac{k}{S(t)}.$$

Afin d'avoir une définition de la vitesse pour tout $r \geqslant r_\star$, on définit

$$V(t,r) = \frac{k}{S(t)} \mathbb{1}_{[r_\star, r_c)}(r), \tag{25}$$

et on vérifie qu'elle vérifie bien la condition (19). Comme $V(t, r_\star)$ est strictement positive, on doit imposer une condition de bord en $r_\star$ pour a. Pour prendre en compte la déifférencation des préadipocytes en adipocytes, on impose donc

$$V(t, r_\star) a(t, r_\star) = \beta'(\bar{r}(t)) p(t).$$

On peut alors donner une définition d'une solution mesure de notre équation aux dérivées partielles. On considère d'abord la famille de caractéristiques de Filippov continues, en changeant légèrement la notation précédente, pour plus de clarté

$$X_t : ([0,t] \times \{r_\star\}) \cup (\{0\} \times [r_\star, +\infty)) \to [r_\star, +\infty),$$

satisfaisant $X_s(s, r_\star) = r_\star$ pour tout $s \in [0, t]$, $X_0(0, r) = r$ pour tout $r \in [r_\star, +\infty)$. Dans notre cas particulier, on peut spécifier les caractéristiques associées à une surface totale des adipocytes S

$$X_t^S(0, r) = \min\left(r + \int_0^t \frac{k}{S(u)}\,\mathrm{d}u, r_c\right),\ t \geqslant 0, \quad X_t^S(s, r_\star) = \min\left(r_\star + \int_s^t \frac{k}{S(u)}\,\mathrm{d}u, r_c\right),\ t \geqslant s \geqslant 0.$$

Ainsi, pour obtenir les caractéristiques, il faut connaitre la fonction S, qui se calcule grâce à la solution mesure a_t, que l'on obtient en poussant en avant la mesure initiale a_0 par les caractéristiques. Cette situation est donc typiquement une situation dans laquelle on souhaite appliquer un théorème de point fixe. On définit donc un annexe

$$\begin{cases} \partial_t a(t, r) + \partial_r(Va)(t, r) = -\gamma'' a(t, r), & t > 0,\ r > r_\star, \\ V(t, r_\star)a(t, r_\star) = f(t), & t > 0, \\ a(0, r) = a_0(r), & r > r_\star, \end{cases} \tag{26}$$

et on définit une solution mesure du système (26) tout fonction $a : [0, \infty) \to \mathcal{M}$ faiblement continue telle que pour toute fonction $\varphi \in \mathcal{C}_b([r_\star, \infty))$ et tout $t \in [0, T)$,

$$\int_{r_\star}^{+\infty} \phi(r)\,\mathrm{d}a_t(r) = \int_0^t e^{-\gamma''(t-s)}\phi\left(X_t^S(s, r_\star)\right) f(s)\,\mathrm{d}s + \int_{r_\star}^{+\infty} e^{-\gamma'' t}\phi\left(X_t^S(0, r)\right)\,\mathrm{d}a_0(r) \tag{27}$$

avec $T = \inf\{t : S(t) = 0\}$. La solution a obtenue dépend du terme source f. Le reste de la preuve consiste à montrer que l'on peut appliquer le théorème de point de fixe de Banach-Picard pour obtenir une unique solution mesure de (26), avec le terme source est donné par

$$f(t) = \beta'(\bar{r}(t))p(t),$$

où le rayon moyen est donné par

$$\bar{r}(t) = \frac{\int_{r_\star}^{r_c} s\,\mathrm{d}a_t(s)}{\int_{r_\star}^{r_c} \mathrm{d}a_t(s)}.$$

On a ensuite démontré des résultats asymptotiques, dont les détails sont donnés dans le chapitre 3. On a montré l'existence d'états stationnaires pour les équations différentielles, puis sous certaines conditions sur les coefficients du système, la convergence faible de la solution mesure a_t vers une masse de Dirac en le rayon critique r_c. Ce comportement était attendu, étant donné la forme de la vitesse $V(t, r)$ et a justifié l'usage de ce cadre théorique. De plus, cette concentration de la masse vers le bord droit du domaine a été retrouvé numériquement. On a également montré, sous d'autres conditions, que le rayon moyen $\bar{r}(t)$ tendait vers le rayon d'apprition des adipocyte $r_\star$, ce qui traduit une convergence de a_t vers une masse de Dirac en $r_\star$, ce qui justifie à nouveau le choix de solutions mesure, cette fois-ci *a posteriori*.
Dans le reste de ce travail, on propose une spcialisation du modèle, à laquelle on adjoint un champ de vitesse sur le domaine physique, afin de mimer certaines contraintes mécaniques auxquelles sont soumis les trois populations modélisées.

3.3 Perspectives sur les solutions mesures

De multiples continuations sont possibles pour de futurs travaux. Concernant l'équation (16), il apparait de manière évidente qu'obtenir une convergence forte dans le théorème 6 est un objectif à court terme. On peut aussi vouloir généraliser notre résultat pour des taux de divisions discontinus. Cela permettrait de prendre en compte des situations dans lesquelles un individus ne peut pas se diviser avant d'avoir atteint une certaine taille, et pour lesquelles le taux de division présente un saut de 0 à une valeur strictement positive. Par ailleurs, on peut se demander si l'opérateur R_t construit dans la proposition 1 peut s'étendre en un opérateur sur l'espace E tout entier. On peut également s'employer à obtenir une expressino explicite pour la mesure μR_t. Du point de vue numérique, des solutions mesures appellent à des schémas adaptés. Dans [14], une grille non uniforme était proposée pour tenir compte du caractère

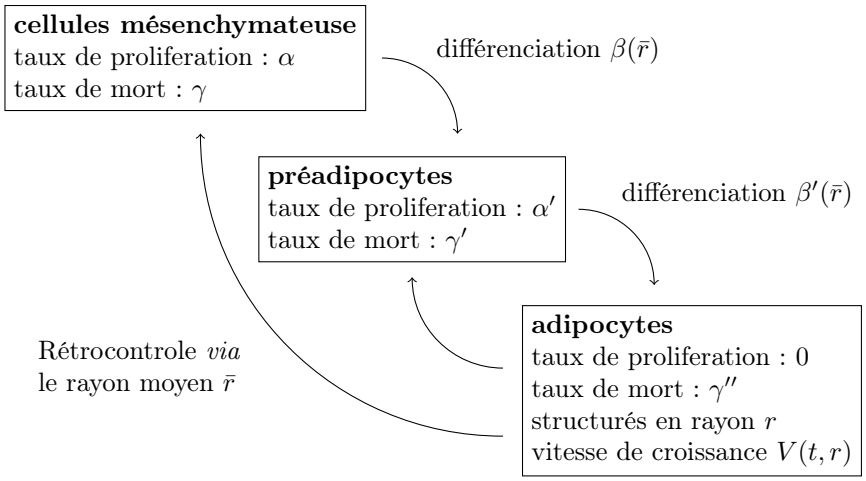

FIGURE 2 – Représentation schématique des intéractions entre les trois populations.

non dissipatif exigé pour le schéma pour observer des oscillations. Une autre approche serait d'adapter le schéma *Escalator Boxcar Train* proposé dans [43], dans lequel après division la masse est envoyée à un bord du domaine, ce qui n'est pas le cas avec une équation de croissance-fragmentation.
Sur le modèle d'adipocytes, une continuation serait de mettre en oeuvre un schéma numérique adapté à une vitesse discontinue, et en prouver la convergence. Toujours sur des aspects numériques, il serait intéressant de regarder précisément pourquoi on n'observe pas de mouvement des adipocytes, malgré une spacilisation et l'ajout d'un champ de vitesse sur le domaine physique. On pourra également faire dépendre du temps le flux de nourriture excédentaire, afin de prendre en compte les cycles circadiens. On peut pour cela penser à des fonctions périodiques et discontinues, pour lesquelles le cadre théorique qu'on a développé jusque là est compatible.

4 Étude des cycles anormaux dans un processus de racourcissement de télomères

Dans cette section, on présente les fruits d'une collaboration avec les biologistes Teresa Teixeira du Laboratoire de biologie moléculaires et cellulaires des eucaryotes, à Paris, Zhou Xu du Laboratoire de biologie computationelle et quantitative, et Marie Doumic. Le quatrième chapitre de ce manuscrit décrit les analyses de données que nous avons menées. Un article regroupant nos résultats est en cours d'écriture.

La prolifération cellulaire permet le renouvellement des tissus, et est soumise à de nombreux mécanismes de régulation, visant notamment à éviter une prolifération non contrôlée, autrement appelé cancer. Pour étudier ces mécanismes de contrôle, on peut par exemple étudier la vieillissement cellulaire en suivant des lignées de cellules et relever la durée de chaque cycle cellulaire. En effet, un cycle cellulaire anormalement long — une durée *normale* devant être définie au cas par cas — est le signe que la cellule prend son temps pour (tenter de) réparer un « problème ». Si on arrive à contrôler la cause du problème, on peut alors obtenir des informations sur les effets de cette source sur les cellules.
Pour ce faire, on retient comme organisme modèle *Saccharomyces cerevisiae*, dont certains mélanges de ses différentes souches sont appelées « levure de boulanger » et « levure de bière ». Un dispositif expérimental de microfluidie est alors employé, dont une description est donné dans [180]. Notre travail consiste en une analyse des données produites par cette méthode (décrite à la section 4.2), afin d'en tirer des informations sur la survenue de cycles anormalement longs.

On donnera d'abord quelques notions de biologie cellulaire en rapport avec la sénescence réplicative, puis on reviendra sur les protocoles expérimentaux et les modèles existants avant de présenter les résultats

de nos analyses. Enfin, on mentionne quelques perspecteives sur ce sujet.

4.1 Élements de biologie de la sénesence réplicative

Un chromosome est un élément microscopique constitué de molécules d'ADN et de protéines. Il porte les gènes, supports de l'information génétique, transmis des cellules mères aux cellules filles lors des divisions cellulaires. Dans les cellules eucaryotes, les chromosomes se trouvent dans le noyau cellulaire, et se trouve à leurs extrémités une région hautement répétitive, riche en bases guanine-cytosine et non codante de la double hélice d'acide désoxyribonucléique (ADN) appelée télomère. La présence de télomères permet une protection des terminaisons chromosomiques. En effet, le mécanisme de réplication par l'ADN polymérase nécessite une amorce sur laquelle ajouter de nouveaux désoxyribonucléotides, c'est pourquoi l'intégralité de la chaine d'ADN n'est pas dupliquée. La présence de cet ADN non codant permet donc d'éviter la perte d'information génétique qui résulterait de l'attrition de la partie codante de la molécule d'ADN [24].
Les télomères peuvent être rallongés par l'action d'une holoenzyme appelée télomérase, mise en évidence en 1985 par Greider et Blackburn [88]. Présente chez la plupart des eukaryotes [18], il s'agit d'une enzyme transcriptase inverse, c'est à dire une enzyme qui synthétise un brin simple d'ADN à partir d'un brin simpl d'ARN [5], qui est active notamment chez les cellules destinées à se diviser de nombreuses fois, comme par exemples les cellules-souches. Dans [169], les auteurs ont montré que la télomérase tendait à rallonger les télomères les plus courts. Lorsque celle-ci est exprimée, un équilibre dynamique de la longueur des télomères résulte des mécanismes d'élongation par la télomère et la raccourcissement par la réplication incomplète de la chaine d'ADN.
Lorsque les télomères deviennent trop courts, la réplication de l'ADN ne peut plus s'enclencher. Ce phénomène est désigné en anglais par *end-replication problem*, voir [175, 132]. La cellule ne peut alors plus se diviser et entre dans un état appelé sénescence réplicative. Le caractère inéluctable, en l'absence d'activité de la télomérase, de la survenue de cet état a amené à la comparaisonen avec une horloge, résultant en l'usage du terme d'horloge moléculaire. En effet, il a été montré que des cellules humaines diploïdes en culture ne survivent qu'à une cinquantaine de divisions [99, 98]. Plusieurs articles [100, 1, 179, 19] suggèrent qu'un seul télomère suffisemment court déclenche l'entrée en sénescence réplicative.
Du point de vue médical, de très nombreux travaux portent sur le lien entre les télomères et la survenue de certaines pathologies. On ne donnera que quelques exemples. Dans [102], il est montré qu'hors des conditions expérimentales, des maladies infectieuses peuvent causer le racourcissement des télomères. Ce racourcissement peut consituter un important facteur de mutation dans la carcinogenèse [76]. Des perspectives sur les traitements de cancers sont données dans [147] tandis que des liens entre cancer et sénescence sont explicités dans [157]. Une récente méta-analyse [174] examine les liens entre le raccourcissement des télomères et la survenue de diverses pathologies.

4.2 Dispositifs expérimentaux, données expérimentales et modèles existants

Le dispositif décrit dans cette section a été développé par Teresa Teixeira et Zhou Xu au Laboratoire de biologie moléculaires et cellulaires des eucaryotes. Des lignées de *Saccharomyces cerevisiae* exprimant la télomérase sont prélevées et placées dans un dispositif de microfluidie. La population croit jusqu'à occuper tout l'espace, puis un flux de liquide traverse le dispositif pour évacuer les levures qu'on n'observe pas. Des photos sont prises à intervalle régulier pour suivre l'évolution les individus qui sont situés le plus au fond de chaque microcavité. À chaque division, celle des deux cellules (mère ou fille) qui prend cette position est conservée et devient le nouvel individu suivi dans la microcavité concernée. Le temps zéro est alors donné par le moment où l'on désactive la télomérase en injectant de la doxycycline dans le dispositif de microfluidie, et l'on suit les lignées soit jusqu'à leur extinction soit jusqu'à la fin de l'expérience. On constitue ainsi une lignée, pour laquelle on reporte par exemple la durée du cycle cellulaire de chacun de ses représentants.
L'emploi de ce dispositif expérimental a permi de mettre en évidence dans [180] l'existence de deux phénotypes distincts, désignés par les lettres A et B. Dans cet article, les auteurs commencent par déterminer la distribution des durées des cycles sur une population dite *wild type*, pour laquelle on n'a pas désactivé la télomérase. Notant μ et σ respectivement la moyenne et l'écart-type de cette distribution, ils définissent

un cycle anormalement comme durant au moins $\mu + 3\sigma$. Ensuite, ils déterminent la phase de sénescence, c'est à dire une succession cycles anormalement à la fin de la lignée, en tolérant un éventuel cycle court accidentel. La dernière étape consiste à compte le nombre de cycles longs se produisant avant la sénescence. Avec aucun ou un seul (pour inclure un certain nombre d'accidents), on classe la lignée parmi les type A, et avec plus, on la range dans les type B. L'idée sous-jacente à ce classement est de quantifier la proportion de cellule qui ne correspond pas au schéma classique d'attrition progressive des télomères jusqu'à atteindre un *check point* et déclencher la sénescence réplicative. Une proportion inattendue de 40% de type B a été trouvée, suggérant ici l'existence que des mécanismes pour échapper à la sénescence existent. Cette capacité de certaines lignées à perdurer malgré la survenue d'un nombre parfois conséquent de cycles anormalement longs est à relier avec la prolifération incontrôlée que l'on observe dans les cas de cancer. On cherche alors à comprendre l'origine de ladite capacité chez cette souche de levure.
On se base alors sur deux modèles, issus de précédentes collaborations entre nos deux équipes. On désigne dans la suite la longueur des télomères à la n^{eme} génération par un vecteur $L^n = (L_1^n, \cdots, L_{32}^n)$. La sénescence réplicative est donc déclenchée lorsque une certaine quantité construite sur ces télomères devient plus petite qu'un certain seuil. Tout d'abord, une longueur intiale est tirée pour chacun des télomères, suivant une loi de probabilité proposée dans [179], décrivant l'équilibre dynamique évoqué plus haut lorsque la télomérase est active. Ensuite, dans la phase dans laquelle la télomérase est désactivée, on réduit la longueur des télomères à chaque étapes. Il est suggéré dans [162] qu'un télomère est raccourcit de 5 à 10 nucléotides lorsqu'il l'est. Partant de ce constat, les auteurs de [19] ont proposé de tirer au hasard 16 télomères parmi 32, puis de réduire chacun d'une certaine quantité, à chaque fois tirée selon une loi uniforme sur $\{5, 6, 7, 8, 9, 10\}$. Dans cet article, les auteurs testent l'hypothèse selon laquelle le télomère le plus court déclenche à lui seul l'entrée dans l'état de sénescence réplicatve. Pour ce faire, ils se donnent deux paramètres $a \in [0, 1]$ et $L_{\min} \in \mathbb{N}$ et posent que la sénescence est atteinte à la première génération n telle que

$$L^{1,n} + aL^{2,n} < L_{\min},$$

où $L^{1,n}$ et $L^{2,n}$ désignent les deux télomères les plus courts. Les auteurs disposaient de 24 lignées réelles auxquelles comparer leur modèle, et donc d'une suite $G_1, \cdots, G_{24}$ triée par ordre croissant de générations d'entrée en sénescence. Ils ont donc simulé N fois 24 générations d'entrée en sénescence selon leur modèle. Pour la l^{eme} simulation, on note $g_1^l, \cdots g_{24}^l$ les prédictions, rangées par ordre croissant. Au couple $(a, L_{\min})$ est associée fonctionnelle d'erreur

$$(a, L_{\min}) \mapsto \frac{1}{N}\left[\sum_{l=1}^{N}\sum_{i=1}^{24}(g_i^l - G_i)^2\right]^{1/2} \tag{28}$$

que l'on cherche à minimiser par le choix de a et $L_{\min}$. Il apparait dans [19] que le couple $(a = 0, L_{\min} = 19)$ donne l'erreur minimale. De plus, la valeur $a = 0$ pour le premier paramètre se révèle très robuste par rapport à la condition initiale. On retiendra donc cette valeur pour les extensions d'application de ce modèle qu'on propose dans la suite.
Peu après, un autre modèle pour la prédiction de l'apparition de la sénescence a été proposé dans . La nouveauté par rapport au précédent résidence dans un couplage des télomères. En effet, lors d'une réplication par l'ADN polymérase, uniquement l'une des deux extrémités du filament d'ADN subit un raccourcissement. Contrairement au modèle précédent, on ne va pas choisir 16 télomères parmi 32 à réduire, mais tirer à pile ou face pour chacune des paires. Cela revient donc à effectuer 16 fois une expérience de Bernoulli de paramètre 1/2, puis comme précédemment réduire chacun des télomères désignés d'une quantité tirée selon une loi uniforme sur $\{5, 6, 7, 8, 9, 10\}$.

4.3 Analyse des données

Depuis les articles [180, 19], on dispose de beaucoup plus de données. Un premier travail consiste donc à revisiter la classification obtenue dans [180] avec ces nouvelles données. Tout d'abord, on a, en accord avec nos collègues biologistes, construit une nouvelle définition de la sénescence, que l'on retiendra dans la suite. Une lignée est dite sénescente si elle remplit deux critères :

1. la lignée doit s'être terminée par une mort cellulaire pendant l'expérience ;

2. le dernier cycle doit être long.

Le premier critère permet d'éviter de considérer comme sénescente une lignée qui serait juste en train de vivre une succession de cycles longs, dont elle parviendrait éventuellement à s'échapper. Le second permet d'écarter ce que l'on interprétera comme des morts accidntelles si l'ultime cycle de la lignée est plus court que le seuil qu'on se fixe pour départager long et court. Il convient ici de souligner que le choix de la formule $\mu + 3\sigma$ de la distribution de durées des lignées *wild type* pour déterminer à partir de quelle durée un cycle est long comprend un dose non négligeable d'arbitraire. On essaiera aussi souvent que possible de vérifier la robustesse de nos résultats par rapport à la valeur du seuil départageant cycles longs et cycles courts. Notre premier travail consiste donc à reprendre la classification en lignées de type A et type B pour en tester la robustesse. On a pour cela essayé plusieurs approches. L'une fut de regarder l'évolution de la proportion de lignées de type A dans la population à mesure que le seuil augmente. L'observation d'un plateau indiquerait une région pour laquelle la classification est stable, désignant alors des valeurs toutes désignées pour le seuil. Malheureusement, ce phénomène ne se produit pas, la proportion de type A dans la population évolue de façon monotone et non stationnaire à mesure que le seuil augmente, pour les valeurs raisonnables (au sens de l'intuition biologique) de ce que pourrait être un cycle long.
Une question qui nous est immédiatement venue était de déterminer si le modèle du télomère le plus court permettait de prédire les données expérimentale, avec bien entendu un couple $(a, L_{\min})$ différent de la situation de prédiction du début de la sénescence. Par soucis d'exhaustivité, on a d'abord essayé un modèle plus simple, à savoir prédire la génération d'apparition du premier cycle long *via* une loi géométrique, dont le paramètre est estimé grâce à estimateur de maximum de vraissemblance. Il appraît que ce modèle n'est pas approprié pour prédire le nombre de générations avant le début de la sénescence. En effet, on constate une trop grande présence de petite valeurs par rapport aux données. Maintenant, on essaie le modèle du télomère le plus court avec couplage des télomère pour le premier cycle longs. On adapte donc la fonctionnelle d'erreur (28) pour prendre en compte un jeu de données spécifique, en définissant

$$e(a, L_{\min}) = \sqrt{\frac{\sum_{l=1}^{N} \sum_{i=1}^{K} \left(g_i^l - G_i\right)^2}{N \sum_{i=1}^{K} G_i^2}},$$

en conservant les notations précédentes. Des tests doivent encore être conduits pour trancher la question. On s'est ensuite pose la question suivante : lorsqu'une cellule d'une lignée vit un cycle long et y survit, c'est à dire parvient à se diviser, a-t-on tendance à observer un cycle long pour la cellule suivante ? Autrement dit, si l'on désigne par séquence une succession de cycles d'un même type (long ou court), précédée et suivie par des cycles de l'autre type, quelle est la distribution des séquences de cycles longs ? On a alors proposé l'hypothèse d'une loi géométrique. Une telle distribution s'interprète biologiquement ainsi : à la survenue d'un « accident », la levure prend du temps pour tenter de se réparer. Si elle n'y parvient pas, elle peut toutefois se diviser malgré tout, en laissant à sa fille le soin de réparer le problème. On estime alors le paramètre de la loi géométrique en question *via* un estimateur de maximum de vraissemblance, puis on procède à des tests du χ^2 d'adéquation. Le test ne rejette pas l'hypothèse de distribution géométrique pour les séquences de cycles longs qui sont strictement avant la sénescence. Au contaire, le test rejette cette hypothèse pour les séquences de cycles longs qui sont les sénescences de lignées. On vérifie ensuite que ce résultat est robuste, car valide pour une large région des valeurs qu'on a testées pour le seuil.

4.4 Perspectives sur l'étude des hétérogénéités télomériques

De nombreuses suites peuvent être données à ce travail. On pourra par exemple construire un modèle permettant de prédire l'apparition de premier cycle long. On peut pour cela envisager une chaîne de Markov à temps discret et à espace d'état $\{court, long\}$, ou alors à un espace d'état continu, auquel cas, on prédit la durée du cycle et non uniquement son type. On peut aussi penser à créer un modèle décrivant la survenue de la sénescence réplicative chez les lignée de comportement similaire aux type B. Idéalement, on cherchera un modèle recouvrant à la fois les type A et les type B, et mécaniciste, c'et à dire basé sur des mécasnismes biologiques des télomères, à la manière du modèle du télomère le plus court.
Une autre approche consiste à adopter une vision « population centrée » plutôt que celles employées jusque là, plutôt « individu centrée ». On cherchera alors à prédire l'évolution de la population entière au

lieu de regarder lignée par lignée, afin de prendre en compte le caractère asynchrone des divisions. Cela permettrait une modélisation de populations de cellules sénescentes, et éventuellement l'émergeance de cancers.

Chapitre 1

Éléments propres principaux pour un modèle de prolifération de bactéries

---

Ce chapitre reporte un article [79] paru dans un numéro spécial de *Network and Heterogeneous Media* portant sur les méthodes mathématiques en biologie, sous le titre *Steady distribution of the incremental model for bacteria proliferation.* Ce travail commun avec Pierre Gabriel fait suite à mon stage de Master 2. Son objet est l'établissement de l'existence et l'unicité d'un vecteur propre principal positif pour le modèle de dynamique de population de bactéries dit *incrémental*, introduit dans [167], dans le cas particulier d'une croissance exponentielle et d'une fragmentation autosimilaire. Nous obtenons l'existence dudit vecteur propre sous des hypothèses très faible sur le comportement asymptotique du taux de division, en le construisant à partir du point fixe d'un opérateur idoine.

1.1 Introduction

In structured population dynamics, finding the structuring variable(s) which best describes a phenomenon is a crucial question. For a population of proliferating cells or bacteria the variables usually considered are age, size (see [176, 52, 139]) or a combination of both (see [13, 160, 95] for modeling and [177, 52, 95, 56] for mathematical analysis). Recent experimental work highlighted the limits of these models to describe bacteria, and a new variable to trigger division emerged : the *size-increment*, namely the size gained since the birth of the cell (see [153] and references therein for a review of the genesis of the related model). This so called 'adder principle' ensures homeostasis with no feedback from the bacteria and explains many experimental data. In this model, bacteria are described by two parameters : their size-increment and their size, respectively denoted by a and x in the following (the choice of letter a is reminiscent from the age variable, since as for the age, the size increment is reset to zero after division). This choice of variables is motivated by the main assumption of the model, which is that the control of the cellular reproduction is provided by the division rate B which is supposed to depend only on a, and the growth rate g which is assumed to depend only on x. With the variables we introduced, the model formulated in [167] reads

$$\begin{cases} \partial_t n(t,a,x) + \partial_a(g(x)n(t,a,x)) + \partial_x(g(x)n(t,a,x)) + B(a)g(x)n(t,a,x) = 0, \\ \qquad\qquad t \geqslant 0,\ x > a > 0, \\ g(x)n(t,0,x) = 4g(2x)\displaystyle\int_0^\infty B(a)n(t,a,2x)\,\mathrm{d}a, \qquad t \geqslant 0,\ x > 0. \end{cases}$$

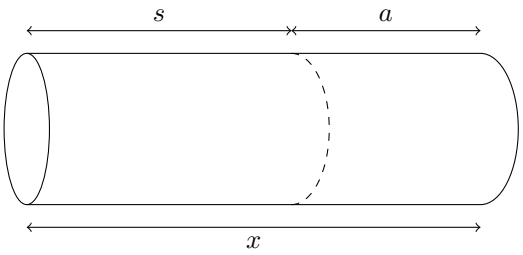

FIGURE 1.1 – schematic representation of the variables on an *E. coli* bacterium.

The function $n(t, a, x)$ represents the number of cells at time t of size x that have grown of an increment a since their birth. The boundary term denotes an equal mitosis, meaning that after division, a mother cell gives birth to two daughters of equal size. However, if this special case of equal mitosis is appropriate to describe the division of some bacterium (*e.g.* E. Coli), it is inadequate for asymetric division (like yeast for instance) or for a fragmentation involving more than two daughters (as in the original model formulated for plant growth in [95]). In the current paper, we propose to consider more general division kernels. We assume that when a cell of size x divides, it gives birth to a daughter of size zx with a certain probability which depends on $z \in (0, 1)$ but is independent of x. Such fragmentation process is usually called self-similar. More precisely the number of daughters with a size between zx and $(z + \mathrm{d}z)x$ is given by $\mu([z, z + \mathrm{d}z])$, where μ is a positive measure on $[0, 1]$. The model we consider is then formulated as

$$\partial_t n(t,a,x) + \partial_a(g(x)n(t,a,x)) + \partial_x(g(x)n(t,a,x)) + B(a)g(x)n(t,a,x) = 0, \qquad t \geqslant 0,\ x > a > 0, \tag{1.1a}$$

$$g(x)n(t,0,x) = \int_0^1 g(\frac{x}{z}) \int_0^\infty B(a)n(t,a,\frac{x}{z})\,\mathrm{d}a\ \frac{\mathrm{d}\mu(z)}{z}, \qquad t \geqslant 0,\ x > 0. \tag{1.1b}$$

It appears that this model is a particular case of the one proposed in the pioneer work [95] for plants growing in a single dimension, mixing age and size control. Indeed, in this paper the authors noticed that in the case of a deterministic and positive growth rate, a size/age model is equivalent to a size/birth-size through the relation $a = x - s$, where s denotes the birth-size (see Figure 1.1). They preferred working with the size/birth-size description since in this framework the transport term acts only in the x direction. In the case when g is independent of x and B is bounded from above and below by positive constants, it is proved in [177] for μ a uniform measure on $[0, 1]$, and in [52, Chapter V] for the equal mitosis, that the solutions to the system (1.1) converge to a stable distribution as time goes to infinity. In the present paper we propose to study the model (1.1) in the case of a linear growth rate (see [13] for a discussion on this hypothesis). More precisely we are interested in populations which evolve with a stable size and size-increment distribution, *i.e.* solutions of the form $n(t, a, x) = h(t)N(a, x)$. The existence of such separable solutions when g is linear was already the topic of [95], but their proof required the equation to be set on a bounded domain and they had to impose *a priori* the existence of a maximal size for the population. In our case no maximal size is prescribed and it brings additional difficulties due to a lack of compactness. To address this problem, we will make the following assumptions.

First, we want the sum of the daughters' sizes to be equal to the size of the mother. This rule, called mass conservation, prescribes

$$\int_0^1 z\,\mathrm{d}\mu(z) = 1. \tag{1.2}$$

We also assume that the division does not produce any arbitrarily small daughter by imposing that the support of μ is a compact subset of $(0, 1)$, which ensures that

$$\theta := \inf \operatorname{supp} \mu > 0 \qquad \text{and} \qquad \exists \eta \in (\theta, 1),\ \operatorname{supp} \mu \subset [\theta, \eta]. \tag{1.3}$$

In particular, these assumptions imply that the mean number of daughters $\mu([0, 1])$ is finite. The division

rate B is assumed to be a nonnegative and locally integrable function on $\mathbb{R}_+$ such that

$$\exists\, b \geqslant 0, \quad \operatorname{supp} B = [b, \infty), \tag{1.4}$$

see [57] for instance. It will be useful in our study to define the associated *survivor function* Ψ by

$$\Psi(a) = \mathrm{e}^{-\int_0^a B(z)\ \mathrm{d}z}.$$

For a given increment a, $\Psi(a)$ represents the probability that a cell did not divide before having grown of at least a since its birth. We assume that the function B is chosen in such a way that Ψ tends to zero at infinity, meaning that all the cells divide at some time. More precisely we make the following quantitative assumption

$$\exists\, k_0 > 0, \quad \Psi(a) \underset{+\infty}{=} \mathcal{O}(a^{-k_0}). \tag{1.5}$$

This assumption on the decay at infinity of the survivor function enables a wide variety of division rates. For instance, it is satisfied if there exists $A > 0$ such that

$$\forall\, a \geqslant A, \quad B(a) \geqslant \frac{k_0}{a}.$$

The function B being locally integrable, the function Ψ belongs to $W^{1,1}_{loc}(\mathbb{R}_+)$ and (1.5) ensures that its derivative belongs to $\mathrm{L}^1(\mathbb{R}_+)$. We can introduce the useful function Φ defined by

$$\Phi = B\Psi = -\Psi' \tag{1.6}$$

which is the probability distribution that a cell divides at increment a. Recall that, as in [95], we consider the special case of a linear growth rate, namely $g(x) = x$. In this case, multiplying by the size x and integrating, we obtain $\frac{\mathrm{d}}{\mathrm{d}t}\iint xn(t,a,x)\,\mathrm{d}a\,\mathrm{d}x = \iint xn(t,a,x)\,\mathrm{d}a\,\mathrm{d}x$, and so

$$\iint xn(t,a,x)\,\mathrm{d}a\,\mathrm{d}x = \mathrm{e}^t \iint xn^0(a,x)\,\mathrm{d}a\,\mathrm{d}x. \tag{1.7}$$

This implies that if we look for a solution with separated variables $n(t,a,x) = h(t)N(a,x)$, necessarily $h(t) = h(0)\mathrm{e}^t$. In other words, the Malthus parameter of the population is 1. This motivates the Perron problem which consists in finding $N = N(a,x)$, which is solution to the system

$$\partial_a(xN(a,x)) + \partial_x(xN(a,x)) + (1 + xB(a))N(a,x) = 0, \qquad x > a > 0,\ x > a > 0, \tag{1.8a}$$

$$N(0,x) = \int_0^1 \int_0^\infty B(a)N(a,\frac{x}{z})\,\mathrm{d}a\ \frac{\mathrm{d}\mu(z)}{z^2}, \qquad x > 0, \tag{1.8b}$$

$$N(a,x) \geqslant 0, \qquad x \geqslant a \geqslant 0, \tag{1.8c}$$

$$\int_0^\infty \int_0^x N(a,x)\,\mathrm{d}a\,\mathrm{d}x = 1. \tag{1.8d}$$

It is convenient to define the set $X := \{(a,x) \in \mathbb{R}^2,\ 0 \leqslant a \leqslant x\}$, and we are now ready to state the main result of the paper.

Theorem 3. *Let μ be a positive measure on $[0,1]$ satisfying (1.2) and (1.3), and B be a nonnegative and locally integrable function on $\mathbb{R}_+$ satisfying (1.4) such that the associated survivor function Ψ satisfies (1.5). Then, there exists a unique solution $N \in \mathrm{L}^1(X, (1+(x-a)^2)\,\mathrm{d}a\,\mathrm{d}x)$ to the eigenproblem (1.8). This solution is expressed as*

$$N : (a,x) \in X \mapsto \frac{\Psi(a)}{x^2} f(x-a) \tag{1.9}$$

where f is a nonnegative function which satisfies

$$f \in \mathrm{L}^1(\mathbb{R}_+, x^l\,\mathrm{d}x)$$

for all $l < k_0$, k_0 being the positive number given in hypothesis (1.5), and

$$\operatorname{supp} f = [b_\theta, \infty)$$

with $b_\theta = \frac{\theta}{1-\theta}b$, where θ and b are defined in (1.3) and (1.4) respectively.

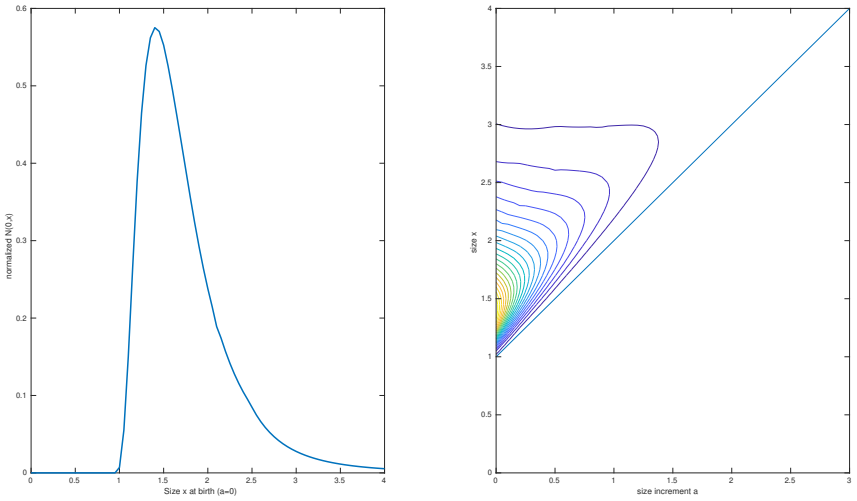

FIGURE 1.2 – Left : simulation of the function f by the power method with $B(a) = \frac{2}{1+a}\mathbb{1}_{\{1\leqslant a\}}$ and $\mu(z) = 2\delta_{\frac{1}{2}}(z)$. Right : level set of the density $N(a,x)$ obtained from this function f. Straight line : the set $\{x = a+1\}$.

The fast decay of the function f near zero is a consequence of the form of the support of the fragmentation kernel μ. Furthermore, this decay is consistent with the decay near zero of the eigenvector for the size equation (see [57]). Remark that for any nonnegative and appropriately normalized function $f \in \mathrm{L}^1(\mathbb{R}_+)$, the expression given in (1.9) satisfies (1.8a), (1.8c), and (1.8d). The proof of Theorem 3 consists in finding the appropriate function f such that (1.8b) is also satisfied. This function is obtained as the fixed point of a conservative operator, and this allows us to compute it numerically by using the power iteration (see [148]). We obtain the function on the left on Figure 1.2. On the right is the related density $N(a,x)$.

Notice also that for the function N given by (1.9), the function $s \mapsto N(a+s, x+s)$ is continuous for any $a \leqslant x$. It corresponds to the trajectories along the characteristics.

The article is organised as follows. In Section 1.2 we reduce the Perron eigenvalue problem with two variables to a fixed point problem for an integral operator in dimension one. Section 1.3 is dedicated to proving the existence and uniqueness of the fixed point by using functional analysis and Laplace transform methods. In Section 1.4 we go through the usefulness of knowing N to develop entropy methods. Finally in Section 1.5 we discuss some interesting perspectives.

1.2 Transformation into an integral equation

Our study consists in constructing a solution to the eigenproblem (1.8) from the solution of a fixed point problem. First, we notice that the size x of a cell and its size increment a grow at the same speed $g(x)$, so the quantity $x - a$ remains constant : it corresponds to the birth-size of the cell, denoted by s. To simplify the equation and obtain horizontal straight lines as characteristics (see Figure 1.3), we give a description of the population with size increment a and birth-size s, namely we set

$$M(a,s) := N(a, a+s). \tag{1.10}$$

Thanks to this relation, it is equivalent to prove the existence of an eigenvector for the increment-size system or for the increment/birth-size system. To determine the equation verified by M, we compute the partial derivatives of $xN(a,x) = (a+s)M(a,s)$, which leads to the equation

$$\partial_a((a+s)M(a,s)) + (1 + (a+s)B(a))\, M(a,s) = 0.$$

Writing the non-local boundary condition (1.8b) with the new variables takes less calculation and more interpretation. In (1.8b) the number of cells born at size s resulted of the division of cells at size $\frac{s}{z}$. Then

the equivalent of (1.8b) in the new variables with a linear growth rate is given by

$$M(0,s) = \int_\theta^\eta \int_0^{\frac{s}{z}} B(a)M(a, \frac{s}{z} - a)\,\mathrm{d}a\ \frac{\mathrm{d}\mu(z)}{z^2}$$

since there is no mass for $a \geqslant \frac{s}{z}$. With the relation (1.10), it is equivalent to solve (1.8) and to solve

$$\partial_a((a+s)M(a,s)) + (1 + (a+s)B(a))M(a,s) = 0, \qquad a, s > 0, \tag{1.11a}$$

$$M(0,s) = \int_\theta^\eta \int_0^{\frac{s}{z}} B(a)M(a, \frac{s}{z} - a)\,\mathrm{d}a\ \frac{\mathrm{d}\mu(z)}{z^2}, \qquad s > 0, \tag{1.11b}$$

$$M(a,s) \geqslant 0, \qquad a, s \geqslant 0, \tag{1.11c}$$

$$\int_{\mathbb{R}_+^2} M(a,s)\,\mathrm{d}a\,\mathrm{d}s = 1. \tag{1.11d}$$

Considering the variable s as a parameter in (1.11a), we see this equation as an ODE in the variable a. A formal solution is given by

$$M(a,s) = \frac{\Psi(a)}{(a+s)^2} s^2 M(0,s).$$

Having this expression in mind, we note that for any nonnegative function $f \in \mathrm{L}^1(\mathbb{R}_+, \mathrm{d}s)$, the function M_f defined on $\mathbb{R}_+^2$ by

$$M_f : (a,s) \mapsto \frac{\Psi(a)}{(a+s)^2} f(s)$$

is a solution of (1.11a) and satisfies (1.11c). Then it remains to choose the appropriate function f and normalize the related function M_f to solve the whole system (1.11). It turns out that this appropriate function f is a fixed point of the operator $T : \mathrm{L}^1(\mathbb{R}_+) \to \mathrm{L}^1(\mathbb{R}_+)$ defined by

$$Tf(s) = \int_\theta^\eta \int_0^{\frac{s}{z}} \Phi(\frac{s}{z} - a) f(a)\,\mathrm{d}a\,\mathrm{d}\mu(z), \tag{1.12}$$

where $\Phi = B\Psi$, as stated in the following lemma.

Lemma 4. *The function M_f satisfies* (1.11b) *if and only if f is a fixed point of the operator T.*

Démonstration.

$$\begin{aligned}
M_f \ \text{ satisfies } \ (1.11b) &\iff \frac{f(s)}{s^2} = \int_\theta^\eta \int_0^{\frac{s}{z}} B(a) \frac{\Psi(a)}{(\frac{s}{z})^2} f(\frac{s}{z} - a)\,\mathrm{d}a\ \frac{\mathrm{d}\mu(z)}{z^2} \\
&\iff f(s) = \int_\theta^\eta \int_0^{\frac{s}{z}} \Phi(a) f(\frac{s}{z} - a)\,\mathrm{d}a\ \ \mathrm{d}\mu(z) \\
&\iff f(s) = \int_\theta^\eta \int_0^{\frac{s}{z}} \Phi(\frac{s}{z} - a) f(a)\,\mathrm{d}a\ \ \mathrm{d}\mu(z) \\
&\iff f(s) = Tf(s)
\end{aligned}$$

□

The operator T can be seen as some kind of *transition operator* : it links the laws of birth size of two successive generations. If f is the law of the parents, then Tf is the law of the birth size of the newborn cells. Indeed, Equation (1.12) can be understood in words as 'the number of cells born at size s come from the ones that were born at size $a \in [b_\theta, \frac{s}{z}]$ and elongated of $\frac{s}{z} - a$ for all $z \in [\theta, \eta]$ and all a before dividing into new cells'. See [59] for a probabilistic viewpoint on the conservative size equation. It is easy to check that T is a continuous linear operator on $\mathrm{L}^1(\mathbb{R}_+)$ and that $\|T\|_{\mathcal{L}(\mathrm{L}^1(\mathbb{R}_+))} \leqslant \|\Phi\|_{\mathrm{L}^1(\mathbb{R}_+)} = 1$ using (1.2) and (1.6). The following lemma provides a slightly stronger result.

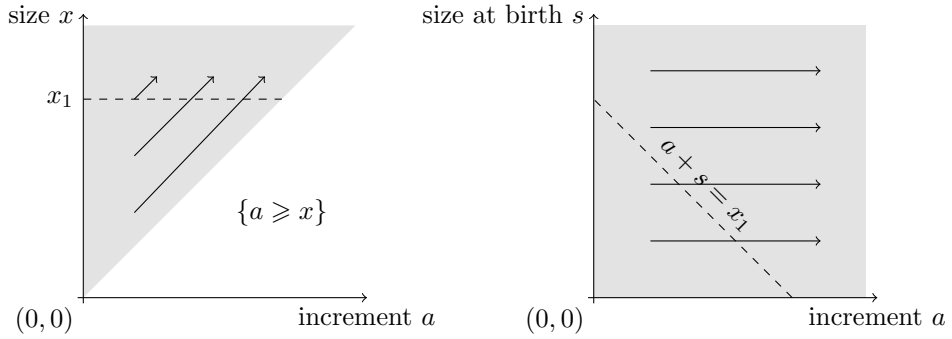

FIGURE 1.3 – Domain of the model, with respect to the choice of variables to describe the bacterium. Grey : domain where the bacteria densities may be positive. Arrows : transport. Left : size increment/size. Right : size increment/birth size. Dashed : location of cells of size x_1.

Lemma 5. *For all $l \leqslant 0$, the operator T maps continuously $\mathrm{L}^1(\mathbb{R}_+, s^l\,\mathrm{d}s)$ into itself. Additionally, if (1.5) holds true, then T maps continuously $\mathrm{L}^1(\mathbb{R}_+, (s^k + s^l)\,\mathrm{d}s)$ into itself for any $l \leqslant 0$ and $k \in [0, k_0)$.*

Démonstration. We start with $\mathrm{L}^1(\mathbb{R}_+, s^l\,\mathrm{d}s)$ where $l \leqslant 0$. For $f \in \mathrm{L}^1(\mathbb{R}_+, s^l\,\mathrm{d}s)$ and $\beta > \alpha > 0$ one has

$$\begin{aligned}
\int_\alpha^\beta |Tf(s)| s^l\,\mathrm{d}s &\leqslant \int_\theta^\eta \int_\alpha^\beta s^l \int_0^{\frac{s}{z}} \Phi(\frac{s}{z} - a)|f(a)|\,\mathrm{d}a\,\mathrm{d}s\,\mathrm{d}\mu(z) \\
&\leqslant \int_\theta^\eta \int_0^{\frac{\alpha}{z}} |f(a)| \int_\alpha^\beta \Phi(\frac{s}{z} - a) s^l\,\mathrm{d}s\,\mathrm{d}a\,\mathrm{d}\mu(z) \\
&\quad + \int_\theta^\eta \int_{\frac{\alpha}{z}}^{\frac{\beta}{z}} |f(a)| \int_{za}^\beta \Phi(\frac{s}{z} - a) s^l\,\mathrm{d}s\,\mathrm{d}a\,\mathrm{d}\mu(z) \\
&\leqslant \int_\theta^\eta \int_0^{\frac{\alpha}{z}} |f(a)| \int_{\frac{\alpha}{z}-a}^{\frac{\beta}{z}-a} \Phi(\sigma)(a+\sigma)^l z^{l+1}\,\mathrm{d}\sigma\,\mathrm{d}a\,\mathrm{d}\mu(z) \\
&\quad + \int_\theta^\eta \int_{\frac{\alpha}{z}}^{\frac{\beta}{z}} |f(a)| \int_0^{\frac{\beta}{z}-a} \Phi(\sigma)(a+\sigma)^l z^{l+1}\,\mathrm{d}\sigma\,\mathrm{d}a\,\mathrm{d}\mu(z) \\
&\leqslant \int_\theta^\eta z^{l+1} \int_0^{\frac{\alpha}{z}} |f(a)| a^l\,\mathrm{d}a\,\mathrm{d}\mu(z) + \int_\theta^\eta z^{l+1} \int_{\frac{\alpha}{z}}^\infty |f(a)| a^l\,\mathrm{d}a\,\mathrm{d}\mu(z) \\
&\leqslant \theta^l \|f\|_{\mathrm{L}^1(\mathbb{R}_+, s^l\,\mathrm{d}s)},
\end{aligned}$$

which gives the conclusion by passing to the limits $\alpha \to 0$ and $\beta \to +\infty$.

For the second part we begin with the proof that under condition (1.5), for any $k \in [0, k_0)$ one has

$$\int_0^\infty \Phi(a) a^k\,\mathrm{d}a < \infty.$$

First, recall that $\int_0^\infty \Phi(a)\,\mathrm{d}a = 1$ and $\Phi = -\Psi'$. Integrating by parts for $\beta \geqslant 1$, one has

$$\int_0^\beta \Phi(a) a^k\,\mathrm{d}a \leqslant \int_0^1 \Phi(a)\,\mathrm{d}a + \int_1^\beta \Phi(a) a^k\,\mathrm{d}a \leqslant 1 + k \int_1^\beta \Psi(a) a^{k-1}\,\mathrm{d}a$$

and the last integral converges when $\beta \to +\infty$ under Assumption (1.5) because $k < k_0$. Now let $l \leqslant 0$ and $k \in [0, k_0)$, and let $f \in \mathrm{L}^1(\mathbb{R}_+, (s^k + s^l)\,\mathrm{d}s)$. Due to the first part of the proof, we only have to estimate $\int_0^\beta |Tf(s)| s^k\,\mathrm{d}s$ for $\beta > 0$. Since the function $x \mapsto \frac{(1+x)^k}{1+x^k}$ is uniformly bounded on $\mathbb{R}_+$, there exists of a

constant $C > 0$ such that $(a+\sigma)^k \leqslant C(a^k + \sigma^k)$ for all $a, \sigma \geqslant 0$, and it allows us to write for any $\beta > 0$

$$\begin{aligned}
\int_0^\beta |Tf(s)| s^k \,\mathrm{d}s &\leqslant \int_\theta^\eta \int_0^\beta s^k \int_0^{\frac{s}{z}} \Phi(\frac{s}{z} - a)|f(a)| \,\mathrm{d}a \,\mathrm{d}s \,\mathrm{d}\mu(z) \\
&= \int_\theta^\eta \int_0^{\frac{\beta}{z}} |f(a)| \int_0^{\frac{\beta}{z}-a} \Phi(\sigma)(a+\sigma)^k z^{k+1} \,\mathrm{d}\sigma \,\mathrm{d}a \,\mathrm{d}\mu(z) \\
&\leqslant C \int_\theta^\eta z^{k+1} \int_0^{\frac{\beta}{z}} |f(a)| a^k \int_0^{\frac{\beta}{z}-a} \Phi(\sigma) \,\mathrm{d}\sigma \,\mathrm{d}a \,\mathrm{d}\mu(z) \\
&\quad + C \int_\theta^\eta z^{k+1} \int_0^{\frac{\beta}{z}} |f(a)| \int_0^{\frac{\beta}{z}-a} \Phi(\sigma)\sigma^k \,\mathrm{d}\sigma \,\mathrm{d}a \,\mathrm{d}\mu(z) \\
&\leqslant C\eta^k \left(\|f\|_{\mathrm{L}^1(\mathbb{R}_+, s^k \,\mathrm{d}s)} + \|\Phi\|_{\mathrm{L}^1(\mathbb{R}_+, s^k \,\mathrm{d}s)} \|f\|_{\mathrm{L}^1(\mathbb{R}_+)} \right).
\end{aligned}$$

□

1.3 The fixed point problem

In this section we prove the existence of a unique nonnegative and normalized fixed point of the operator T.

Let us first recall some definitions from the Banach lattices theory (for more details, see [63, 154]). Let Ω be a subset of $\mathbb{R}_+$ and ν be a positive measure on Ω. The space $\mathrm{L}^1(\Omega, \nu)$ is an ordered set with the partial order defined by

$$f \geqslant 0 \text{ if and only if } f(s) \geqslant 0 \ \nu\text{-a.e. on } \Omega.$$

Furthermore, endowed with its standard norm, the space $\mathrm{L}^1(\Omega, \nu)$ is a Banach lattice, *i.e.* a real Banach space endowed with an ordering $\geqslant$ compatible with the vector structure such that, if $f, g \in \mathrm{L}^1(\Omega, \nu)$ and $|f| \geqslant |g|$, then $\|f\|_{\mathrm{L}^1(\Omega,\nu)} \geqslant \|g\|_{\mathrm{L}^1(\Omega,\nu)}$. A vector subspace $I \subset \mathrm{L}^1(\Omega, \nu)$ is called an ideal if $f \in I, g \in \mathrm{L}^1(\Omega, \nu)$ and $|g| \leqslant |f|$ implies $g \in I$. For a given operator A defined on $\mathrm{L}^1(\Omega, \nu)$, a closed ideal I is *A-invariant* if $A(I) \subset I$, and A is irreducible if the only A-invariant ideals are $\{0\}$ and $\mathrm{L}^1(\Omega, \nu)$. To each closed ideal I in the Banach lattice $\mathrm{L}^1(\Omega, \nu)$ corresponds a subset $\omega \subset \Omega$ such that $I = \{f \in \mathrm{L}^1(\Omega, \nu), \operatorname{supp} f \subset \omega\}$. We also define the *positive cone* $\mathrm{L}^1_+(\Omega, \nu) := \{f \in \mathrm{L}^1(\Omega, \nu) \mid f \geqslant 0 \ \nu\text{-a.e. on } \Omega\}$. An operator $A : \mathrm{L}^1(\Omega, \nu) \to \mathrm{L}^1(\Omega, \nu)$ is said to be positive if $A(\mathrm{L}^1_+(\Omega, \nu)) \subset \mathrm{L}^1_+(\Omega, \nu)$. To prove the existence of an eigenvector associated to the eigenvalue 1, we will use the following theorem, easily deduced from Krein-Rutman's theorem (see [63] for instance) and De Pagter's [42].

Theorem 6. *Let $A : \mathrm{L}^1(\Omega, \nu) \to \mathrm{L}^1(\Omega, \nu)$ be a non-zero positive compact irreducible operator. Then its spectral radius $\rho(A)$ is a nonnegative eigenvalue associated to a nonzero eigenvector belonging to the positive cone $\mathrm{L}^1_+(\Omega, \nu)$.*

Due to a lack of compactness of the operator T, which is due to the lack of compactness of $\mathbb{R}_+$, we truncate the operator T into a family of operators $(T_\Sigma)_\Sigma$. Let $b_\theta = \frac{\theta}{1-\theta} b$ and for $\Sigma > b_\theta$ define the operator T_Σ on $\mathrm{L}^1((b_\theta, \Sigma))$ by

$$T_\Sigma f(s) = \int_\theta^\eta \int_{b_\theta}^{\min(\frac{s}{z}, \Sigma)} \Phi(\frac{s}{z} - a) f(a) \,\mathrm{d}a \,\mathrm{d}\mu(z) \tag{1.13}$$

$$= \begin{cases}
\displaystyle\int_\theta^\eta \int_{b_\theta}^{\frac{s}{z}} \Phi(\frac{s}{z} - a) f(a) \,\mathrm{d}a \,\mathrm{d}\mu(z), & b_\theta \leqslant s < \theta\Sigma, \\
\displaystyle\int_\theta^{\frac{s}{\Sigma}} \int_{b_\theta}^{\Sigma} \Phi(\frac{s}{z} - a) f(a) \,\mathrm{d}a \,\mathrm{d}\mu(z) + \int_{\frac{s}{\Sigma}}^\eta \int_{b_\theta}^{\frac{s}{z}} \Phi(\frac{s}{z} - a) f(a) \,\mathrm{d}a \,\mathrm{d}\mu(z), & \\
\qquad\qquad \theta\Sigma \leqslant s \leqslant \eta\Sigma, & \\
\displaystyle\int_\theta^\eta \int_{b_\theta}^{\Sigma} \Phi(\frac{s}{z} - a) f(a) \,\mathrm{d}a \,\mathrm{d}\mu(z), & \eta\Sigma < s \leqslant \Sigma.
\end{cases}$$

Defining the lower bound of the domain as b_θ will ensure the irreducibility of T_Σ. We will apply Theorem 6 to the operator T_Σ for Σ large enough to prove the existence of a pair (ρ_Σ, f_Σ) such that $T_\Sigma f_\Sigma = \rho_\Sigma f_\Sigma$. Then, we will prove that there exists a unique f in a suitable space such that $\rho_\Sigma \to 1$ and $f_\Sigma \to f$ as $\Sigma \to \infty$, with f satisfying $Tf = f$. The following lemma ensures that the truncated operator T_Σ is well defined.

Lemma 7. *If $f \in \mathrm{L}^1(\mathbb{R}_+)$ and $\operatorname{supp} f \subset [b_\theta, \Sigma]$, then*

$$(Tf)_{|[b_\theta,\Sigma]} = T_\Sigma(f_{|[b_\theta,\Sigma]}).$$

Lemma 7 is a straightforward consequence of the definition of operator T_Σ by (1.13). From Lemmas 5 and 7, we deduce that T_Σ has the same stability mapping properties as T. To prove the compactness of the operator T_Σ for a fixed Σ and later on that the family $(T_\Sigma)_\Sigma$ is also compact, we use a particular case of a corollary of the Riesz-Fréchet-Kolmogorov theorem. First, we define two properties for a bounded subset $\mathcal{F}$ of $\mathrm{L}^1(\Omega, \nu)$ with Ω an open subset of $\mathbb{R}_+$, and ν a positive measure, the first on translations and the second on the absence of mass on the boundary of the domain

$$\begin{cases} \forall \varepsilon > 0,\ \forall \omega \subset\subset \Omega,\ \exists \delta \in (0, \operatorname{dist}(\omega, {}^c\Omega)) \text{ such that} \\ \|\tau_h f - f\|_{\mathrm{L}^1(\omega,\nu)} < \varepsilon,\ \forall h \in (-\delta, \delta),\ \forall f \in \mathcal{F} \end{cases} \tag{1.14}$$

$$\begin{cases} \forall \varepsilon > 0,\ \exists \omega \subset\subset \Omega, \text{ such that} \\ \|f\|_{\mathrm{L}^1(\Omega\setminus\omega,\nu)} < \varepsilon,\ \forall f \in \mathcal{F} \end{cases} \tag{1.15}$$

where ${}^c\Omega$ is understood as the complement of this set in $\mathbb{R}_+$.

Theorem 8 (from [20], corollary 4.27)**.** *If $\mathcal{F}$ is a bounded set of $\mathrm{L}^1(\Omega, \nu)$ such that (1.14) and (1.15) hold true, then $\mathcal{F}$ is relatively compact in $\mathrm{L}^1(\Omega, \nu)$.*

1.3.1 Existence of a principal eigenfunction for T_Σ

Using Theorem 6, we prove the existence of an eigenpair (ρ_Σ, f_Σ) for the operator T_Σ.

Proposition 9. *Let l be a nonpositive number. Under the hypotheses (1.2), (1.3) and (1.4), there exists a unique normalized eigenvector $f_\Sigma \in \mathrm{L}^1_+((b_\theta, \Sigma), s^l\,\mathrm{d}s)$ of the operator T_Σ in $\mathrm{L}^1((b_\theta, \Sigma), s^l\,\mathrm{d}s)$ associated to the spectral radius ρ_Σ for every $\Sigma > \max(\frac{1}{1-\theta}b, 1)$.*

Applying Theorem 8, to $\Omega = (b_\theta, \Sigma)$ and the family

$$\mathcal{F} = \{T_\Sigma f, f \in \mathrm{L}^1((b_\theta, \Sigma), s^l\,\mathrm{d}s), \|f\|_{\mathrm{L}^1((b_\theta,\Sigma),s^l\,\mathrm{d}s)} \leqslant 1\},$$

which is bounded in $\mathrm{L}^1((b_\theta, \Sigma), s^l\,\mathrm{d}s)$, as already shown in the proof of Lemma 5, we prove the following Lemma.

Lemma 10. *Let l be a nonpositive number. Under the hypotheses of Proposition 9, for all*

$$\Sigma > \max(\frac{b}{1-\theta}, 1),$$

the set $\mathcal{F}$ is relatively compact.

Proof of Lemma 10. The set $\mathcal{F}$ is bounded due to the continuity of T proven in Lemma 5. First, we show that (1.14) is satisfied. Any compact set in (b_θ, Σ) is included in a segment $[\alpha, \beta]$. Without loss of generality, we take $b_\theta < \alpha < \theta\Sigma,\ \eta\Sigma < \beta < \Sigma$. It is sufficient to treat the case h positive, so let $0 \leqslant h < \min(\theta\Sigma - \alpha, \Sigma - \beta, \Sigma(\eta - \theta))$. Since $T_\Sigma f$ is piecewise defined, we have to separate the integral

on $[\alpha,\beta]$ into several parts, depending on the interval s and $s+h$ belong to, and we obtain

$$\begin{aligned}
&\int_\alpha^\beta |T_\Sigma f(s+h)-T_\Sigma f(s)|\, s^l\,\mathrm{d}s\\
&\leqslant \int_\alpha^{\theta\Sigma-h} |T_\Sigma f(s+h)-T_\Sigma f(s)|\, s^l\,\mathrm{d}s =: (A)\\
&\quad+\int_{\theta\Sigma-h}^{\theta\Sigma} |T_\Sigma f(s+h)-T_\Sigma f(s)|\, s^l\,\mathrm{d}s =: (B)\\
&\quad\quad+\int_{\theta\Sigma}^{\eta\Sigma-h} |T_\Sigma f(s+h)-T_\Sigma f(s)|\, s^l\,\mathrm{d}s =: (C)\\
&\quad\quad\quad+\int_{\eta\Sigma-h}^{\eta\Sigma} |T_\Sigma f(s+h)-T_\Sigma f(s)|\, s^l\,\mathrm{d}s =: (D)\\
&\quad\quad\quad\quad+\int_{\eta\Sigma}^{\beta} |T_\Sigma f(s+h)-T_\Sigma f(s)|\, s^l\,\mathrm{d}s =: (E).
\end{aligned}$$

since for (A), (C) and (E), $T_\Sigma f$ and $\tau_h T_\Sigma f$ have the same expression, the same kind of calculations apply, so we only treat (C), which has the most complicated expression.

$$\begin{aligned}
(C) &= \int_{\theta\Sigma}^{\eta\Sigma-h} |T_\Sigma f(s+h)-T_\Sigma f(s)|\, s^l\,\mathrm{d}s\\
&\leqslant \int_{\theta\Sigma}^{\eta\Sigma-h} \left| \int_\theta^{\frac{s+h}{\Sigma}} \int_{b_\theta}^{\Sigma} \Phi(\frac{s+h}{z}-a) f(a)\,\mathrm{d}a\,\mathrm{d}\mu(z) \right.\\
&\qquad\qquad \left. - \int_\theta^{\frac{s}{\Sigma}} \int_{b_\theta}^{\Sigma} \Phi(\frac{s}{z}-a) f(a)\,\mathrm{d}a\,\mathrm{d}\mu(z) \right| s^l\,\mathrm{d}s\\
&\quad+\int_{\theta\Sigma}^{\eta\Sigma-h} \left| \int_{\frac{s+h}{\Sigma}}^{\eta} \int_{b_\theta}^{\frac{s+h}{z}} \Phi(\frac{s+h}{z}-a) f(a)\,\mathrm{d}a\,\mathrm{d}\mu(z) \right.\\
&\qquad\qquad \left. - \int_{\frac{s}{\Sigma}}^{\eta} \int_{b_\theta}^{\frac{s}{z}} \Phi(\frac{s}{z}-a) f(a)\,\mathrm{d}a\,\mathrm{d}\mu(z) \right| s^l\,\mathrm{d}s\\
&\leqslant \int_{\theta\Sigma}^{\eta\Sigma-h} s^l \int_\theta^{\frac{s}{\Sigma}} \int_{b_\theta}^{\Sigma} \left| \Phi(\frac{s+h}{z}-a) - \Phi(\frac{s}{z}-a) \right| |f(a)|\,\mathrm{d}a\,\mathrm{d}\mu(z)\,\mathrm{d}s =: (C1)\\
&\quad+\int_{\theta\Sigma}^{\eta\Sigma-h} s^l \int_{\frac{s}{\Sigma}}^{\frac{s+h}{\Sigma}} \int_{b_\theta}^{\Sigma} \Phi(\frac{s+h}{z}-a) |f(a)|\,\mathrm{d}a\,\mathrm{d}\mu(z)\,\mathrm{d}s =: (C2)\\
&\quad\quad+\int_{\theta\Sigma}^{\eta\Sigma-h} s^l \int_{\frac{s+h}{\Sigma}}^{\eta} \int_{b_\theta}^{\frac{s}{z}} \left| \Phi(\frac{s+h}{z}-a) - \Phi(\frac{s}{z}-a) \right| |f(a)|\,\mathrm{d}a\,\mathrm{d}\mu(z)\,\mathrm{d}s =: (C3)\\
&\quad\quad\quad+\int_{\theta\Sigma}^{\eta\Sigma-h} s^l \int_{\frac{s+h}{\Sigma}}^{\eta} \int_{\frac{s}{z}}^{\frac{s+h}{z}} \Phi(\frac{s+h}{z}-a) |f(a)|\,\mathrm{d}a\,\mathrm{d}\mu(z)\,\mathrm{d}s =: (C4)\\
&\quad\quad\quad\quad+\int_{\theta\Sigma}^{\eta\Sigma-h} s^l \int_{\frac{s}{\Sigma}}^{\frac{s+h}{\Sigma}} \int_{b_\theta}^{\frac{s}{z}} \Phi(\frac{s+h}{z}-a) |f(a)|\,\mathrm{d}a\,\mathrm{d}\mu(z)\,\mathrm{d}s =: (C5)
\end{aligned}$$

The integrals $(C1)$ and $(C3)$ are dealt with in the same way, and we have the following estimate

$$
\begin{aligned}
(C1) &= \int_{\theta\Sigma}^{\eta\Sigma-h} s^l \int_{\theta}^{\frac{s}{\Sigma}} \int_{b_\theta}^{\Sigma} \left|\Phi(\frac{s+h}{z}-a)-\Phi(\frac{s}{z}-a)\right| |f(a)|\,\mathrm{d}a\,\mathrm{d}\mu(z)\,\mathrm{d}s \\
&= \int_{\theta}^{\eta-\frac{h}{\Sigma}} \int_{b_\theta}^{\Sigma} |f(a)| \int_{z\Sigma}^{\eta\Sigma-h} \left|\Phi(\frac{s+h}{z}-a)-\Phi(\frac{s}{z}-a)\right| s^l\,\mathrm{d}s\,\mathrm{d}a\,\mathrm{d}\mu(z) \\
&= \int_{\theta}^{\eta-\frac{h}{\Sigma}} z^{l+1} \int_{b_\theta}^{\Sigma} |f(a)| \int_{\Sigma-a}^{\frac{\eta\Sigma-h}{z}-a} |\tau_{\frac{h}{z}}\Phi(\sigma)-\Phi(\sigma)|(a+\sigma)^l\,\mathrm{d}\sigma\,\mathrm{d}a\,\mathrm{d}\mu(z) \\
&= \int_{\theta}^{\eta-\frac{h}{\Sigma}} z^{l+1} \int_{b_\theta}^{\Sigma} |f(a)|a^l \int_{\Sigma-a}^{\frac{\eta\Sigma-h}{z}-a} |\tau_{\frac{h}{z}}\Phi(\sigma)-\Phi(\sigma)|\,\mathrm{d}\sigma\,\mathrm{d}a\,\mathrm{d}\mu(z) \\
&\leqslant \theta^l \sup_{\varepsilon\in[\theta,\eta]} \|\tau_{\frac{h}{\varepsilon}}\Phi-\Phi\|_{\mathrm{L}^1(\mathbb{R}_+)}.
\end{aligned}
$$

These integrals are as small as needed when h is small enough, due to the continuity of the translation in $\mathrm{L}^1(\mathbb{R}_+)$. For $(C2)$ one has

$$
\begin{aligned}
(C2) &= \int_{\theta\Sigma}^{\eta\Sigma-h} s^l \int_{\frac{s}{\Sigma}}^{\frac{s+h}{\Sigma}} \int_{b_\theta}^{\Sigma} \Phi(\frac{s+h}{z}-a)|f(a)|\,\mathrm{d}a\,\mathrm{d}\mu(z)\,\mathrm{d}s \\
&= \int_{\theta}^{\theta+\frac{h}{\Sigma}} \int_{b_\theta}^{\Sigma} |f(a)| \int_{\theta\Sigma}^{z\Sigma} \Phi(\frac{s+h}{z}-a)s^l\,\mathrm{d}s\,\mathrm{d}a\,\mathrm{d}\mu(z) \\
&\quad + \int_{\theta+\frac{h}{\Sigma}}^{\eta-\frac{h}{\Sigma}} \int_{b_\theta}^{\Sigma} |f(a)| \int_{z\Sigma-h}^{z\Sigma} \Phi(\frac{s+h}{z}-a)s^l\,\mathrm{d}s\,\mathrm{d}a\,\mathrm{d}\mu(z) \\
&\quad\quad + \int_{\eta-\frac{h}{\Sigma}}^{\eta} \int_{b_\theta}^{\Sigma} |f(a)| \int_{z\Sigma-h}^{\eta\Sigma-h} \Phi(\frac{s+h}{z}-a)s^l\,\mathrm{d}s\,\mathrm{d}a\,\mathrm{d}\mu(z) \\
&\leqslant \int_{\theta}^{\eta} \int_{b_\theta}^{\Sigma} |f(a)| \int_{z\Sigma-h}^{z\Sigma} \Phi(\frac{s+h}{z}-a)s^l\,\mathrm{d}s\,\mathrm{d}a\,\mathrm{d}\mu(z) \\
&= \int_{\theta}^{\eta} z^{l+1} \int_{b_\theta}^{\Sigma} |f(a)| \int_{\Sigma-\frac{h}{z}-a}^{\Sigma-a} \Phi(\sigma+\frac{h}{z})(a+\sigma)^l\,\mathrm{d}\sigma\,\mathrm{d}a\,\mathrm{d}\mu(z) \\
&\leqslant \int_{\theta}^{\eta} z^{l+1} \int_{b_\theta}^{\Sigma} |f(a)|a^l \int_{\Sigma-\frac{h}{z}-a}^{\Sigma-a} \Phi(\sigma+\frac{h}{z})\,\mathrm{d}\sigma\,\mathrm{d}a\,\mathrm{d}\mu(z) \\
&\leqslant \theta^l \sup_{|I|=\frac{h}{\theta}} \int_I \Phi(a)\,\mathrm{d}a
\end{aligned}
$$

which is small when h is small since Φ is a probability density. To deal with $(C4)$, we use Fubini's theorem

and some changes of variables to obtain

$$
\begin{aligned}
(C4) &= \int_{\theta\Sigma}^{\eta\Sigma-h} s^l \int_{\frac{s+h}{\Sigma}}^{\eta} \int_{\frac{s}{z}}^{\frac{s+h}{z}} \Phi(\frac{s+h}{z}-a)|f(a)|\,\mathrm{d}a\,\mathrm{d}\mu(z)\,\mathrm{d}s \\
&= \int_{\theta+\frac{h}{\Sigma}}^{\eta} \int_{\theta\Sigma}^{z\Sigma-h} s^l \int_{\frac{s}{z}}^{\frac{s+h}{z}} \Phi(\frac{s+h}{z}-a)|f(a)|\,\mathrm{d}a\,\mathrm{d}s\,\mathrm{d}\mu(z) \\
&= \int_{\theta+\frac{h}{\Sigma}}^{\eta} \int_{\theta\Sigma}^{z\Sigma-h} s^l \int_{-\frac{h}{z}}^{0} \Phi(\frac{h}{z}+a')|f(\frac{s}{z}-a')|\,\mathrm{d}a'\,\mathrm{d}s\,\mathrm{d}\mu(z) \\
&= \int_{\theta+\frac{h}{\Sigma}}^{\eta} \int_{-\frac{h}{z}}^{0} \Phi(\frac{h}{z}+a') \int_{\theta\Sigma}^{z\Sigma-h} |f(\frac{s}{z}-a')|s^l\,\mathrm{d}s\,\mathrm{d}a'\,\mathrm{d}\mu(z) \\
&= \int_{\theta+\frac{h}{\Sigma}}^{\eta} z^{l+1} \int_{-\frac{h}{z}}^{0} \Phi(\frac{h}{z}+a') \int_{\frac{\theta\Sigma}{z}-a'}^{\Sigma-\frac{h}{z}-a'} |f(\sigma)|(\sigma+a')^l\,\mathrm{d}\sigma\,\mathrm{d}a'\,\mathrm{d}\mu(z) \\
&\leqslant \int_{\theta+\frac{h}{\Sigma}}^{\eta} z^{l+1} \int_{-\frac{h}{z}}^{0} \Phi(\frac{h}{z}+a')\,\mathrm{d}a'\,\mathrm{d}\mu(z) \\
&\leqslant \theta^l \left(1-\Psi(\frac{h}{\theta})\right),
\end{aligned}
$$

and the continuity of Ψ at 0 provides the wanted property. Finally, noticing that $(C5) \leqslant (C2)$ because the integrand are nonnegative, we obtain the desired control on the integral (C). Now for the integral (B), which is dealt with as would be (D), we write

$$
\begin{aligned}
(B) &= \int_{\theta\Sigma-h}^{\theta\Sigma} \Bigg| \int_{\theta}^{\frac{s+h}{\Sigma}} \int_{b_\theta}^{\Sigma} \Phi(\frac{s+h}{z}-a) f(a)\,\mathrm{d}a\,\mathrm{d}\mu(z) \\
&\quad + \int_{\frac{s+h}{\Sigma}}^{\eta} \int_{b_\theta}^{\frac{s+h}{z}} \Phi(\frac{s+h}{z}-a) f(a)\,\mathrm{d}a\,\mathrm{d}\mu(z) \\
&\quad - \int_{\theta}^{\eta} \int_{b_\theta}^{\frac{s}{z}} \Phi(\frac{s}{z}-a) f(a)\,\mathrm{d}a\,\mathrm{d}\mu(z) \Bigg| s^l\,\mathrm{d}s \\
&\leqslant \int_{\theta}^{\eta} \int_{b_\theta}^{\Sigma} |f(a)| \int_{\theta\Sigma-h}^{\theta\Sigma} \left[\Phi(\frac{s+h}{z}-a) + \Phi(\frac{s}{z}-a)\right] s^l\,\mathrm{d}s\,\mathrm{d}a\,\mathrm{d}\mu(z) \\
&\leqslant \int_{\theta}^{\eta} z^{l+1} \int_{b_\theta}^{\Sigma} |f(a)| a^l \int_{\frac{\theta\Sigma-h}{z}-a}^{\frac{\theta\Sigma}{z}-a} \left[\Phi(\sigma+\frac{h}{z}) + \Phi(\sigma)\right] \mathrm{d}\sigma\,\mathrm{d}a\,\mathrm{d}\mu(z) \\
&\leqslant 2\,\theta^l \sup_{|I|=\frac{h}{\theta}} \int_I \Phi(a)\,\mathrm{d}a
\end{aligned}
$$

and again the last term vanishes as h vanishes. We now show that there is no mass accumulation at the boundary of the domain (b_θ, Σ), *i.e.* that (1.15) holds true. For $\Sigma > \frac{1}{1-\theta} b$, we haves $b_\theta < \theta\Sigma$ and we can

choose $\alpha < \theta\Sigma$, so that for all $s \in (b_\theta, \alpha)$, $\frac{s}{\Sigma} < \theta$. With the expression of $T_\Sigma f(s)$, we have

$$\begin{aligned}
&\int_{b_\theta}^{\alpha} |T_\Sigma f(s)| s^l \,\mathrm{d}s \\
&\leqslant \int_{b_\theta}^{\alpha} s^l \int_\theta^\eta \int_{b_\theta}^{\frac{s}{z}} \Phi(\frac{s}{z} - a)|f(a)| \,\mathrm{d}a \,\mathrm{d}\mu(z) \,\mathrm{d}s \\
&\leqslant \int_\theta^\eta \int_{b_\theta}^{\frac{b_\theta}{z}} |f(a)| \int_{b_\theta}^{\alpha} \Phi(\frac{s}{z} - a) s^l \,\mathrm{d}s \,\mathrm{d}a \,\mathrm{d}\mu(z) \\
&\quad + \int_\theta^\eta \int_{\frac{b_\theta}{z}}^{\frac{\alpha}{z}} |f(a)| \int_{za}^{\alpha} \Phi(\frac{s}{z} - a) s^l \,\mathrm{d}s \,\mathrm{d}a \,\mathrm{d}\mu(z) \\
&\leqslant \int_\theta^\eta z^{l+1} \int_{b_\theta}^{\frac{b_\theta}{z}} \left(\Psi(\frac{b_\theta}{z} - a) - \Psi(\frac{\alpha}{z} - a)\right) |f(a)| a^l \,\mathrm{d}a z \,\mathrm{d}\mu(z) \\
&\quad + \int_\theta^\eta \int_{\frac{b_\theta}{z}}^{\frac{\alpha}{z}} \left(1 - \Psi(\frac{\alpha}{z} - a)\right) |f(a)| a^l \,\mathrm{d}a z \,\mathrm{d}\mu(z) \\
&\leqslant \theta^l \left(1 - \Psi(\frac{\alpha - b_\theta}{\theta})\right),
\end{aligned} \tag{1.16}$$

since for $b_\theta < s \leqslant \frac{b_\theta}{z}$ we have $\frac{b_\theta}{z} - a \leqslant b$ and so $\Psi(\frac{b_\theta}{z} - a) = 1$. Taking α as closed to b_θ as needed, we obtain the first estimate of (1.15).

As done before, we choose a β to obtain a simpler expression of T_Σ, namely $\beta > \eta\Sigma$. Then, one has

$$\begin{aligned}
\int_\beta^\Sigma |T_\Sigma f(s)| s^l \,\mathrm{d}s &\leqslant \int_\theta^\eta \int_{b_\theta}^{\Sigma} |f(a)| \int_\beta^\Sigma \Phi(\frac{s}{z} - a) s^l \,\mathrm{d}s \,\mathrm{d}a \,\mathrm{d}\mu(z) \\
&\leqslant \int_\theta^\eta z^{l+1} \int_{b_\theta}^{\Sigma} |f(a)| a^l \int_{\frac{\beta}{z} - a}^{\frac{\Sigma}{z} - a} \Phi(\sigma) \,\mathrm{d}\sigma \,\mathrm{d}a \,\mathrm{d}\mu(z) \\
&\leqslant \theta^l \sup_{|I| = \frac{\Sigma - \beta}{\theta}} \int_I \Phi(a) \,\mathrm{d}a,
\end{aligned} \tag{1.17}$$

which is small when $\Sigma - \beta$ is small.

We have checked the assumptions of Theorem 8 for the family $\mathcal{F}$, so it is relatively compact. □

To prove the irreducibility of the operator T_Σ, it is useful to notice that T_Σ can be expressed differently after switching the two integrals. One has

$$T_\Sigma f(s) = \begin{cases}
\displaystyle\int_{b_\theta}^{\frac{s}{\eta}} f(a) \int_\theta^\eta \Phi(\frac{s}{z} - a) \,\mathrm{d}\mu(z) \,\mathrm{d}a + \int_{\frac{s}{\eta}}^{\frac{s}{\theta}} f(a) \int_\theta^{\frac{s}{a}} \Phi(\frac{s}{z} - a) \,\mathrm{d}\mu(z) \,\mathrm{d}a, \\
\qquad b_\theta \leqslant s < \theta\Sigma, \\
\displaystyle\int_{b_\theta}^{\frac{s}{\eta}} f(a) \int_\theta^\eta \Phi(\frac{s}{z} - a) \,\mathrm{d}\mu(z) \,\mathrm{d}a + \int_{\frac{s}{\eta}}^{\Sigma} f(a) \int_\theta^{\frac{s}{a}} \Phi(\frac{s}{z} - a) \,\mathrm{d}\mu(z) \,\mathrm{d}a, \\
\qquad \theta\Sigma \leqslant s \leqslant \eta\Sigma, \\
\displaystyle\int_{b_\theta}^{\Sigma} f(a) \int_\theta^\eta \Phi(\frac{s}{z} - a) \,\mathrm{d}\mu(z) \,\mathrm{d}a, \qquad \eta\Sigma < s \leqslant \Sigma.
\end{cases}$$

Lemma 11. *Let l be a nonpositive number. Under the hypotheses of Proposition 9, for all $\Sigma > \frac{1}{1-\theta} b$, the operator $T_\Sigma : \mathrm{L}^1((b_\theta, \Sigma), s^l \,\mathrm{d}s) \to \mathrm{L}^1((b_\theta, \Sigma), s^l \,\mathrm{d}s)$ is irreducible.*

Démonstration. Let $J \neq \{0\}$ be a T_Σ-invariant ideal in $\mathrm{L}^1((b_\theta,\Sigma), s^l\,\mathrm{d}s)$. There exists a subset $\omega \subset (b_\theta,\Sigma)$ such that $J = \{f \in \mathrm{L}^1((b_\theta,\Sigma), s^l\,\mathrm{d}s) \mid \operatorname{supp} f \subset \omega\}$. Let $f_\omega := s^{-l}\mathbb{1}_\omega$ and $s_0 := \inf \operatorname{supp} f_\omega \geqslant b_\theta$. Since $J \neq \{0\}$ (so $s_0 < \Sigma$) and $\theta < \eta$, one can find ζ and ξ both positive such that

$$T_\Sigma f_\omega(s) \geqslant \int_{s_0}^{s_0+\zeta}\int_\theta^{\theta+\xi} \Phi(\frac{s}{z}-a)\,\mathrm{d}\mu(z) f_\omega(a)\,\mathrm{d}a.$$

For $s \geqslant s_0$, the functions $z \mapsto \frac{s}{z} - a$ and $a \mapsto \frac{s}{z} - a$ are continuous decreasing functions. So, if s is such that $\frac{s}{\theta} - s_0 > b$, then one can choose ζ and ξ such that for all $(a,z) \in [s_0, s_0+\zeta] \times [\theta, \theta+\xi]$, $\frac{s}{z} - a \in \operatorname{supp}\Phi$. Additionally, for each $\zeta > 0$, the integral $\int_{s_0}^{s_0+\zeta} f_\omega(a)\,\mathrm{d}a$ is positive. We deduce that $[\theta(b+s_0),\Sigma] \subset \operatorname{supp} T_\Sigma f_\omega \subset [s_0,\Sigma]$, so $s_0 \leqslant \theta(b+s_0)$, which is equivalent to $s_0 \leqslant b_\theta$. Finally $b_\theta = s_0$, so $J = \mathrm{L}^1((b_\theta,\Sigma), s^l\,\mathrm{d}s)$ and T_Σ is irreducible. □

Proof of Proposition 9. Lemma 10 shows that the set $\mathcal{F}$ is relatively compact in $\mathrm{L}^1((b_\theta,\Sigma), s^l\,\mathrm{d}s)$, which is exactly saying that T_Σ is a compact operator of the Lebesgue space $\mathrm{L}^1((b_\theta,\Sigma), s^l\,\mathrm{d}s)$. With Lemma 11 in addition, we can apply Theorem 6 to the operator T_Σ for $\Sigma > \frac{1}{1-\theta}b$ to obtain the existence of a nonnegative function $f_\Sigma \in \mathrm{L}^1((b_\theta,\Sigma), s^l\,\mathrm{d}s)$ which is an eigenvector of T_Σ associated to the eigenvalue ρ_Σ. Since this function is defined on a compact subset of $\mathbb{R}_+$, it also belongs to $\mathrm{L}^1((b_\theta,\Sigma), (s^k+s^l)\,\mathrm{d}s)$ for $k < k_0$.

□

1.3.2 Passing to the limit $\Sigma \to \infty$

We now want to show that up to a subsequence, $(f_\Sigma)_\Sigma$ converges to a fixed point of T. To that end, in the rest of the article we extend the functions defined on (b_θ,Σ) to $\mathbb{R}_+$ by 0 out of (b_θ,Σ). Then we obtain the following proposition

Proposition 12. *Under hypotheses* (1.2)-(1.5) *there exists a nonnegative and normalized fixed point*

$$f \in \mathrm{L}^1(\mathbb{R}_+, (s^k+s^l)\,\mathrm{d}s)$$

for all $l \leqslant 0$ and $k < k_0$, of the operator T. Additionally, f is unique in $\mathrm{L}^1(\mathbb{R}_+)$ and its support is $[b_\theta,\infty)$.

First, we will show that the sequence $(\rho_\Sigma)_\Sigma$ converges to 1 as $\Sigma \to \infty$.

Lemma 13. *If (ρ_Σ, f_Σ) is an eigenpair of the operator T_Σ, then the following inequality holds true*

$$1 - \Psi\left((\frac{1}{\eta}-1)\Sigma\right) \leqslant \rho_\Sigma \leqslant 1 - \Psi\left(\frac{\Sigma}{\theta} - b_\theta\right). \tag{1.18}$$

Démonstration. Integrating the equality $\rho_\Sigma f_\Sigma = T_\Sigma f_\Sigma$ over (b_θ,Σ), one has

$$\begin{aligned}
\rho_\Sigma \int_{b_\theta}^{\Sigma} f_\Sigma(s)\,\mathrm{d}s = &\int_{b_\theta}^{\theta\Sigma}\int_\theta^\eta\int_{b_\theta}^{\frac{s}{z}} \Phi(\frac{s}{z}-a) f(a)\,\mathrm{d}a\,\mathrm{d}\mu(z)\,\mathrm{d}s =: (A)\\
&+ \int_{\theta\Sigma}^{\eta\Sigma}\int_\theta^{\frac{s}{\Sigma}}\int_{b_\theta}^{\Sigma} \Phi(\frac{s}{z}-a) f(a)\,\mathrm{d}a\,\mathrm{d}\mu(z)\,\mathrm{d}s =: (B)\\
&+ \int_{\theta\Sigma}^{\eta\Sigma}\int_{\frac{s}{\Sigma}}^{\eta}\int_{b_\theta}^{\frac{s}{z}} \Phi(\frac{s}{z}-a) f(a)\,\mathrm{d}a\,\mathrm{d}\mu(z)\,\mathrm{d}s =: (C)\\
&+ \int_{\eta\Sigma}^{\Sigma}\int_\theta^\eta\int_{b_\theta}^{\Sigma} \Phi(\frac{s}{z}-a) f(a)\,\mathrm{d}a\,\mathrm{d}\mu(z)\,\mathrm{d}s =: (D)
\end{aligned}$$

$$
\begin{aligned}
(A) &= \int_\theta^\eta \int_{b_\theta}^{\frac{b_\theta}{z}} f_\Sigma(a) \int_{\frac{b_\theta}{z}}^{\theta\Sigma} \Phi(\frac{s}{z}-a)\,\mathrm{d}s\,\mathrm{d}a\,\mathrm{d}\mu(z) \\
&\quad + \int_\theta^\eta \int_{\frac{b_\theta}{z}}^{\frac{\theta\Sigma}{z}} f_\Sigma(a) \int_{za}^{\theta\Sigma} \Phi(\frac{s}{z}-a)\,\mathrm{d}s\,\mathrm{d}a\,\mathrm{d}\mu(z) \\
&= \int_\theta^\eta z \int_{b_\theta}^{\frac{b_\theta}{z}} f_\Sigma(a) \left[\Psi(\frac{b_\theta}{z}-a) - \Psi(\frac{\theta\Sigma}{z}-a)\right] \mathrm{d}a\,\mathrm{d}\mu(z) \\
&\quad + \int_\theta^\eta z \int_{\frac{b_\theta}{z}}^{\frac{\theta\Sigma}{z}} f_\Sigma(a) \left[1 - \Psi(\frac{\theta\Sigma}{z}-a)\right] \mathrm{d}a\,\mathrm{d}\mu(z) \\
(B) &= \int_\theta^\eta f_\Sigma(a) \int_{b_\theta}^{\Sigma} \int_{z\Sigma}^{\eta\Sigma} \Phi(\frac{s}{z}-a)\,\mathrm{d}s\,\mathrm{d}a\,\mathrm{d}\mu(z) \\
&= \int_\theta^\eta z \int_{b_\theta}^{\Sigma} f_\Sigma(a) \left[\Psi(\Sigma-a) - \Psi(\frac{\eta\Sigma}{z}-a)\right] \mathrm{d}a\,\mathrm{d}\mu(z)
\end{aligned}
$$

$$
\begin{aligned}
(C) &= \int_\theta^\eta \int_{b_\theta}^{\frac{\theta\Sigma}{z}} f_\Sigma(a) \int_{\theta\Sigma}^{z\Sigma} \Phi(\frac{s}{z}-a)\,\mathrm{d}s\,\mathrm{d}a\,\mathrm{d}\mu(z) \\
&\quad + \int_\theta^\eta \int_{\frac{\theta\Sigma}{z}}^{\Sigma} f_\Sigma(a) \int_{za}^{z\Sigma} \Phi(\frac{s}{z}-a)\,\mathrm{d}s\,\mathrm{d}a\,\mathrm{d}\mu(z) \\
&= \int_\theta^\eta z \int_{b_\theta}^{\frac{\theta\Sigma}{z}} f_\Sigma(a) \left[\Psi(\frac{\theta\Sigma}{z}-a) - \Psi(\Sigma-a)\right] \mathrm{d}a\,\mathrm{d}\mu(z) \\
&\quad + \int_\theta^\eta z \int_{\frac{\theta\Sigma}{z}}^{\Sigma} f_\Sigma(a) \left[1 - \Psi(\Sigma-a)\right] \mathrm{d}a\,\mathrm{d}\mu(z) \\
(D) &= \int_\theta^\eta \int_{b_\theta}^{\Sigma} f_\Sigma(a) \int_{\eta\Sigma}^{\Sigma} \Phi(\frac{s}{z}-a)\,\mathrm{d}s\,\mathrm{d}a\,\mathrm{d}\mu(z) \\
&= \int_\theta^\eta z \int_{b_\theta}^{\Sigma} f_\Sigma(a) \left[\Psi(\frac{\eta\Sigma}{z}-a) - \Psi(\frac{\Sigma}{z}-a)\right] \mathrm{d}a\,\mathrm{d}\mu(z)
\end{aligned}
$$

Then notice that for $a \in (b_\theta, \Sigma)$ and $z \in (\theta, \eta)$ one has

$$
\frac{b_\theta}{z} - a \leqslant \frac{b_\theta}{z} - b_\theta = b_\theta\left(\frac{1}{z}-1\right) \leqslant b_\theta\left(\frac{1}{\theta}-1\right) = b,
$$

so as in the computations leading to (1.16), $\Psi(\frac{b_\theta}{z}-a) = 1$. Combining these different expressions, we deduce

$$
\rho_\Sigma \int_{b_\theta}^{\Sigma} f_\Sigma(s)\,\mathrm{d}s = \int_{b_\theta}^{\Sigma} f_\Sigma(s)\,\mathrm{d}s - \int_\theta^\eta z \int_{b_\theta}^{\Sigma} \Psi(\frac{\Sigma}{z}-a) f_\Sigma(a)\,\mathrm{d}a\,\mathrm{d}\mu(z). \tag{1.19}
$$

Using the fact that the function Ψ is nonincreasing, we obtain the wanted inequality. □

Now we show that up to a subsequence, $(f_\Sigma)_\Sigma$ converges to a fixed point of T denoted by f. Thanks to (1.18) and the properties of Ψ, we can define

$$
\Sigma_0 := \inf\left\{\Sigma > \max(\frac{1}{1-\theta}b, 1) \text{ such that } \rho_\Sigma > \frac{1}{2}\right\}.
$$

Lemma 14. *Under hypotheses* (1.2), (1.3), (1.4) *and* (1.5), *the set of eigenfunctions* $\{f_\Sigma, \Sigma \geqslant \Sigma_0, \|f_\Sigma\|_{\mathrm{L}^1(\mathbb{R}_+,(s^k+s^l)\,\mathrm{d}s)} = 1\}$ *has a compact closure in* $\mathrm{L}^1(\mathbb{R}_+,(s^k+s^l)\,\mathrm{d}s)$, *for any* $l \leqslant 0$ *and* $k < k_0$, k_0 *being the real number given in* (1.5).

Démonstration. Let $l \leqslant 0$ and $k \in [0, k_0)$. Once again, we apply Theorem 8 to show the desired result. First, we show that (1.14) hold true with $\Omega = (b_\theta, \infty)$ and $\mathcal{F} = \{f_\Sigma, \Sigma \geqslant \Sigma_0 \| f_\Sigma \|_{\mathrm{L}^1(\mathbb{R}_+, (s^k + s^l)\, \mathrm{d}s)} = 1\}$. Let ω be a compact subset of (b_θ, ∞) and $b_\theta < \alpha < \beta$ such that $\omega \subset [\alpha, \beta]$. We use the following inequality

$$\begin{aligned}
\|\tau_h f_\Sigma - f_\Sigma\|_{\mathrm{L}^1(\omega,(s^k+s^l)ds)} &\leqslant 2\|\tau_h T_\Sigma f_\Sigma - T_\Sigma f_\Sigma\|_{\mathrm{L}^1(\omega,(s^k+s^l)ds)} \\
&\leqslant 2\left(\beta^k + \alpha^l\right) \|\tau_h T_\Sigma f_\Sigma - T_\Sigma f_\Sigma\|_{\mathrm{L}^1([\alpha,\beta])} \\
&\leqslant 2\left(\beta^k + \alpha^l\right) \|\tau_h T_\Sigma f_\Sigma - T_\Sigma f_\Sigma\|_{\mathrm{L}^1([\alpha,\Sigma])}.
\end{aligned}$$

The last quantity is small when h is small uniformly with respect to Σ since in the proof of Lemma 10, the estimates do not depend on the value of Σ. To prove that (1.15) holds true, we use the estimate (1.16) twice to write

$$\begin{aligned}
\|f_\Sigma\|_{\mathrm{L}^1((b_\theta,\alpha),(s^k+s^l)ds)} &= \frac{1}{\rho_\Sigma} \int_{b_\theta}^{\alpha} T_\Sigma f_\Sigma(s)(s^k + s^l) ds \\
&\leqslant 2 \int_{b_\theta}^{\alpha} T_\Sigma f_\Sigma(s) s^l ds + 2\alpha^k \int_{b_\theta}^{\alpha} T_\Sigma f_\Sigma(s) ds \\
&\leqslant 2\theta^l \left(1 - \Psi(\frac{\alpha - b_\theta}{\theta})\right) + 2\alpha^k \left(1 - \Psi(\frac{\alpha - b_\theta}{\theta})\right) \\
&\leqslant 2(\theta^l + \alpha^k) \left(1 - \Psi(\frac{\alpha - b_\theta}{\theta})\right)
\end{aligned}$$

which is again independent of Σ. The estimate (1.17) though depends on Σ, so we write for Σ larger than β

$$\rho_\Sigma \int_\beta^\Sigma f_\Sigma(a)\, \mathrm{d}a = \int_\beta^{\theta\Sigma} T_\Sigma f_\Sigma(a)\, \mathrm{d}a + \int_{\theta\Sigma}^{\eta\Sigma} T_\Sigma f_\Sigma(a)\, \mathrm{d}a + \int_{\eta\Sigma}^{\Sigma} T_\Sigma f_\Sigma(a)\, \mathrm{d}a.$$

For the first integral, we compute

$$\begin{aligned}
&\int_\beta^{\theta\Sigma} T_\Sigma f_\Sigma(a)\, \mathrm{d}a \\
&= \int_\theta^\eta z \int_{b_\theta}^{\frac{\beta}{z}} \left[\Psi(\frac{\beta}{z} - a) - \Psi(\frac{\theta\Sigma}{z} - a)\right] f_\Sigma(a)\, \mathrm{d}a\, \mathrm{d}\mu(z) \\
&\quad + \int_\theta^\eta z \int_{\frac{\beta}{z}}^{\frac{\theta\Sigma}{z}} \left[1 - \Psi(\frac{\theta\Sigma}{z} - a)\right] f_\Sigma(a)\, \mathrm{d}a\, \mathrm{d}\mu(z).
\end{aligned}$$

The two other integrals correspond to the integrals (B), (C) and (D) from the previous proof. Combining the integrals, we obtain

$$\begin{aligned}
&\rho_\Sigma \int_\beta^\Sigma f_\Sigma(a)\, \mathrm{d}a \\
&= \int_\theta^\eta z \int_{b\theta}^{\frac{\beta}{z}} \Psi(\frac{\beta}{z} - a) f_\Sigma(a)\, \mathrm{d}a\, \mathrm{d}\mu(z) + \int_\theta^\eta z \int_{\frac{\beta}{z}}^{\Sigma} f_\Sigma(a)\, \mathrm{d}a\, \mathrm{d}\mu(z) \\
&\quad - \int_\theta^\eta z \int_{b\theta}^{\Sigma} \Psi(\frac{\Sigma}{z} - a) f_\Sigma(a)\, \mathrm{d}a\, \mathrm{d}\mu(z).
\end{aligned}$$

We deal with the last integral using (1.19) and obtain after interverting integrals

$$\begin{aligned}
\rho_\Sigma \int_\beta^\Sigma f_\Sigma(a)\,\mathrm{d}a &= \int_{b_\theta}^{\frac{\beta}{\eta}} f_\Sigma(a) \int_\theta^\eta z\Psi(\frac{\beta}{z}-a)\,\mathrm{d}\mu(z)\,\mathrm{d}a \\
&\quad + \int_{\frac{\beta}{\eta}}^{\frac{\beta}{\theta}} f_\Sigma(a) \int_\theta^{\frac{\beta}{a}} z\Psi(\frac{\beta}{z}-a)\,\mathrm{d}\mu(z)\,\mathrm{d}a + \int_{\frac{\beta}{\eta}}^{\frac{\beta}{\theta}} f_\Sigma(a) \int_{\frac{\beta}{a}}^\eta z\,\mathrm{d}\mu(z)\,\mathrm{d}a \\
&\quad + \int_{\frac{\beta}{\theta}}^\Sigma f_\Sigma(a)\,\mathrm{d}a + \rho_\Sigma \int_{b_\theta}^\Sigma f_\Sigma(a)\,\mathrm{d}a - \int_{b_\theta}^\Sigma f_\Sigma(a)\,\mathrm{d}a \\
\iff \int_{b_\theta}^{\frac{\beta}{\eta}} f_\Sigma(a)\,\mathrm{d}a &= \int_{b_\theta}^{\frac{\beta}{\eta}} f_\Sigma(a) \int_\theta^\eta z\Psi(\frac{\beta}{z}-a)\,\mathrm{d}\mu(z)\,\mathrm{d}a \\
&\quad + \int_{\frac{\beta}{\eta}}^{\frac{\beta}{\theta}} f_\Sigma(a) \int_\theta^{\frac{\beta}{a}} z\Psi(\frac{\beta}{z}-a)\,\mathrm{d}\mu(z)\,\mathrm{d}a + \rho_\Sigma \int_{b_\theta}^\beta f_\Sigma(a)\,\mathrm{d}a \\
&\quad - \int_{\frac{\beta}{\eta}}^{\frac{\beta}{\theta}} f_\Sigma(a) \int_\theta^{\frac{\beta}{a}} z\,\mathrm{d}\mu(z)\,\mathrm{d}a \\
\iff \int_\beta^{\frac{\beta}{\eta}} f_\Sigma(a) \int_\theta^\eta z\left[1-\Psi(\frac{\beta}{z}-a)\right]\,\mathrm{d}\mu(z)\,\mathrm{d}a &+ (1-\rho_\Sigma)\int_{b_\theta}^\beta f_\Sigma(a)\,\mathrm{d}a \\
&+ \int_{\frac{\beta}{\eta}}^{\frac{\beta}{\theta}} f_\Sigma(a) \int_\theta^{\frac{\beta}{a}} z\left[1-\Psi(\frac{\beta}{z}-a)\right]\,\mathrm{d}\mu(z)\,\mathrm{d}a \\
&= \int_{b_\theta}^\beta f_\Sigma(a) \int_\theta^\eta z\Psi(\frac{\beta}{z}-a)\,\mathrm{d}\mu(z)\,\mathrm{d}a
\end{aligned}$$

Since $0<\theta<\eta<1$, we can choose $\beta > \frac{\eta}{1-\eta}b \geqslant b_\theta$. In that case, $\frac{1}{\eta}-\frac{b}{\beta}>1$, and we can pick $r \in]1, \frac{1}{\eta}-\frac{b}{\beta}[$ such that $\left(\frac{1}{\eta}-r\right)\beta > b$. Noticing that $1-\Psi(\frac{\beta}{z}-a)$ and $1-\rho_\Sigma$ are nonnegative, we obtain

$$\int_\beta^{r\beta} f_\Sigma(a) \int_\theta^\eta z\left[1-\Psi(\frac{\beta}{z}-a)\right]\,\mathrm{d}\mu(z)\,\mathrm{d}a \leqslant \int_{b_\theta}^\beta f_\Sigma(a) \int_\theta^\eta z\Psi(\frac{\beta}{z}-a)\,\mathrm{d}\mu(z)\,\mathrm{d}a,$$

then

$$\left(1-\Psi((\frac{1}{\eta}-r)\beta)\right)\int_\beta^{r\beta} f_\Sigma(a)\,\mathrm{d}a \leqslant \Psi((\frac{1}{\eta}-1)\beta),$$

and finally

$$\int_\beta^{r\beta} f_\Sigma(a)(a^l+a^k)\,\mathrm{d}a \leqslant (\beta^l+(r\beta)^k)\frac{\Psi((\frac{1}{\eta}-1)\beta)}{\left(1-\Psi((\frac{1}{\eta}-r)\beta)\right)} \leqslant 4(r\beta)^k\Psi((\frac{1}{\eta}-1)\beta)$$

for β large enough. We use this estimate to get

$$\begin{aligned}
\int_\beta^\infty f_\Sigma(s)(s^k+s^l)\,\mathrm{d}s &= \sum_{j=0}^\infty \int_{r^j\beta}^{r^{j+1}\beta} f_S(s)(s^k+s^l)\,\mathrm{d}s \\
&\leqslant 4r^k \sum_{j=0}^\infty \left(r^j\beta\right)^k \Psi((\frac{1}{\eta}-1)r^j\beta) \\
&\leqslant 4Cr^k \sum_{j=0}^\infty \left(r^j\beta\right)^k \left((\frac{1}{\eta}-1)r^j\beta\right)^{-k_0} \\
&\leqslant \frac{C_{k,k_0,\eta,r}}{\beta^{k_0-k}}
\end{aligned}$$

due to hypothesis (1.5), for β large enough.

□

We are now ready to prove the existence and uniqueness of a fixed point for the operator T.

Proof of Proposition 12. We have proved in Lemma 14 that the set of eigenfunctions $\{f_\Sigma,\ \|f_\Sigma\|_{\mathrm{L}^1(\mathbb{R}_+,(s^l+s^k)\,\mathrm{d}s)} = 1\}$ has a compact closure in $\mathrm{L}^1(\mathbb{R}_+,(s^k+s^l)\,\mathrm{d}s)$. We deduce the existence of $f \in \mathrm{L}^1(\mathbb{R}_+,(s^k+s^l)\,\mathrm{d}s)$ such that, up to a subsequence still denoted by $(f_\Sigma)_\Sigma$, $f_\Sigma \to f$ strongly as $\Sigma \to +\infty$. Now we prove that the function f is a fixed point of the operator T. We use the following inequality

$$\begin{aligned}\|f - Tf\|_{\mathrm{L}^1(\mathbb{R}_+,(s^k+s^l)\,\mathrm{d}s)} \leqslant &\|f - f_\Sigma\|_{\mathrm{L}^1(\mathbb{R}_+,(s^k+s^l)\,\mathrm{d}s)} \\ &+ (1-\rho_\Sigma) + \|T_\Sigma f_\Sigma - Tf\|_{\mathrm{L}^1(\mathbb{R}_+,(s^k+s^l)\,\mathrm{d}s)}.\end{aligned}$$

The first term of the right-hand side tends to zero as Σ tends to ∞ by definition of f, and the second one is smaller than $\Psi\big((\frac{1}{\eta}-1)\Sigma\big)$ according to (1.18). For the last one, we write

$$\begin{aligned}&\|T_\Sigma f_\Sigma - Tf\|_{\mathrm{L}^1(\mathbb{R}_+,(s^k+s^l)\,\mathrm{d}s)} \\ &\leqslant \underbrace{\|T_\Sigma f_\Sigma - Tf_\Sigma\|_{\mathrm{L}^1(\mathbb{R}_+,(s^k+s^l)\,\mathrm{d}s)}}_{=0} + \|T(f-f_\Sigma)\|_{\mathrm{L}^1(\mathbb{R}_+,(s^k+s^l)\,\mathrm{d}s)} \\ &\leqslant \|f - f_\Sigma\|_{\mathrm{L}^1(\mathbb{R}_+,(s^k+s^l)\,\mathrm{d}s)}\end{aligned}$$

due to Lemma 7 and to the continuity of T, which is proved in Lemma 5.

To prove uniqueness of the fixed point, we consider f_1 another nonnegative fixed point of T in $\mathrm{L}^1(\mathbb{R}_+)$ satisfying $\int_0^\infty f_1(s)\,\mathrm{d}s = \int_0^\infty f(s)\,\mathrm{d}s$. Recalling the definition (1.12) of the operator T, the functions f and f_1 satisfy the integral convolution equation

$$f(s) = \int_\theta^\eta \Phi * f(\frac{s}{z})\,\mathrm{d}\mu(z). \tag{1.20}$$

Since $f,\ f_1$ and Φ are in $\mathrm{L}^1(\mathbb{R}_+)$, their Laplace transforms exist on $\mathbb{R}_+$ and are continuous decreasing functions. Taking the Laplace transform of $f - f_1$ and switching integrals thanks to Fubini's theorem, one has for every $y \geqslant 0$

$$\mathcal{L}[f-f_1](y) = \int_\theta^\eta \mathcal{L}[f-f_1](zy)\mathcal{L}[\Phi](zy)z\,\mathrm{d}\mu(z). \tag{1.21}$$

The Laplace transform $\mathcal{L}[f-f_1]$ is continuous on $\mathbb{R}_+$ and vanishes at the origin

$$\mathcal{L}[f-f_1](0) = \int_0^\infty f(s)\,\mathrm{d}s - \int_0^\infty f_1(s)\,\mathrm{d}s = 0.$$

We now define the functions

$$\overline{\mathrm{L}}(y) = \sup_{x\in[0,y]} \mathcal{L}[f-f_1](x) \quad \text{and} \quad \underline{\mathrm{L}}(y) = \inf_{x\in[0,y]} \mathcal{L}[f-f_1](x).$$

By continuity in 0 of $\mathcal{L}[f-f_1]$ and because $\mathcal{L}[f-f_1](0) = 0$, one has

$$\forall y \geqslant 0, \qquad \overline{\mathrm{L}}(y) \geqslant 0,\ \underline{\mathrm{L}}(y) \leqslant 0.$$

From (1.21), we obtain the inequality

$$\mathcal{L}[f-f_1](y) \leqslant \overline{\mathrm{L}}(\eta y)\int_\theta^\eta \mathcal{L}[\Phi](zy)z\,\mathrm{d}\mu(z) \leqslant \overline{\mathrm{L}}(\eta y),$$

since Φ is a probability measure. $\overline{L}$ is a continuous increasing function, so for all $x \leqslant y$, one has

$$\mathcal{L}[f-f_1](x) \leqslant \overline{\mathrm{L}}(\eta x) \leqslant \overline{\mathrm{L}}(\eta y),$$

from which we deduce

$$\overline{\mathrm{L}}(y) \leqslant \overline{\mathrm{L}}(\eta y). \tag{1.22}$$

Iterating (1.22), we obtain for all $y \geqslant 0$ and all positive integer j

$$\overline{\mathrm{L}}(y) \leqslant \overline{\mathrm{L}}(\eta^j y).$$

Letting $j \to \infty$ in this inequality and using the continuity of the function $\overline{\mathrm{L}}$ we obtain $\overline{\mathrm{L}}(y) = 0$ for all nonnegative y. With the same method, we show that $\underline{\mathrm{L}}(y) = 0$ for all nonnegative y, and finally $\mathcal{L}[f - f_1]$ is the null function. By the injectivity of the Laplace transform (Lerch's theorem [110]), one has $f = f_1$.

It remains to prove that $\operatorname{supp} f = [b_\theta, \infty)$. With the same kind of proof than the one we used for T_Σ, we can prove that T is irreducible on $\mathrm{L}^1(b_\theta, \infty)$, and since f is not the zero function we get the result. □

1.3.3 Proof of the main theorem

We are now ready to prove the main theorem of the paper.

Proof of Theorem 3. Combining Lemma 4 and Proposition 12, we construct a solution to (1.11) using

$$M(a,s) := \frac{\psi(a)}{(a+s)^2} f(s).$$

It remains to prove uniqueness of the solution in the appropriate space. This solution belongs to $\mathrm{L}^1(\mathbb{R}_+^2, (1+s^2)\,\mathrm{d}a\,\mathrm{d}s)$ thanks to the following calculation

$$\begin{aligned}
&\int_{b_\theta}^\infty \int_0^\infty M(a,s)(1+s^2)\,\mathrm{d}a\,\mathrm{d}s \\
&= \int_{b_\theta}^\infty \int_0^\infty \frac{1}{(a+s)^2} f(s)\Psi(a)\,\mathrm{d}a\,\mathrm{d}s + \int_{b_\theta}^\infty \int_0^\infty \frac{s^2}{(a+s)^2} f(s)\Psi(a)\,\mathrm{d}a\,\mathrm{d}s \\
&\leqslant \int_{b_\theta}^\infty f(s) s^{-2} \int_0^\infty \Psi(a)\,\mathrm{d}a\,\mathrm{d}s + \int_{b_\theta}^\infty f(s) \int_0^\infty \Psi(a)\,\mathrm{d}a\,\mathrm{d}s \\
&= \|f\|_{\mathrm{L}^1((b_\theta,\infty),(1+s^{-2})\,\mathrm{d}s)} < \infty
\end{aligned}$$

because $f \in \mathrm{L}^1((b_\theta, \infty), s^l\,\mathrm{d}s)$ for all nonpositive number l. To prove the uniqueness of the solution $M \in \mathrm{L}^1(\mathbb{R}_+^2, (1+s^2)\,\mathrm{d}a\,\mathrm{d}s)$, consider another solution $M_1 \in \mathrm{L}^1(\mathbb{R}_+^2, (1+s^2)\,\mathrm{d}a\,\mathrm{d}s)$. Necessarily, as for M, there exists a measurable function f_1 such that for almost all $s \geqslant a \geqslant 0$

$$M_1(a,s) = \frac{\Psi(a)}{(a+s)^2} f_1(s).$$

For $0 < \alpha < \beta < \infty$, we can write

$$\begin{aligned}
\int_0^\infty f_1(s)\,\mathrm{d}s &= \frac{1}{\beta-\alpha} \int_0^\infty \int_\alpha^\beta \frac{(a+s)^2}{\Psi(a)} M_1(a,s)\,\mathrm{d}a\,\mathrm{d}s \\
&\leqslant \frac{2(\beta^2+1)}{(\beta-\alpha)\Psi(\beta)} \|M_1\|_{\mathrm{L}^1(\mathbb{R}_+,(1+s^2)\,\mathrm{d}s)},
\end{aligned}$$

and this ensures that $f_1 \in \mathrm{L}^1(\mathbb{R}_+)$. Additionally we easily check as in Lemma 4 that f_1 has to be a fixed point of T. Then the uniqueness result in Proposition 12 ensures that $f_1 = f$, and so $M_1 = M$. The existence and uniqueness of a solution to the initial problem (1.8) follows from the relation (1.10). □

1.4 Entropy and long time behaviour

Now that we have solved the eigenvalue problem, we would like to characterize the asymptotic behaviour of a solution n of (1.1), as in [139]. The General Relative Entropy principle provides informations about the evolution of the distance in L^1 norm between a solution $n(t,\cdot,\cdot)$ and $\mathrm{e}^t N$. To establish such useful inequalities, we use the formalism introduced in [119] and [120]. Strictly speaking, to use this method, we should prove some properties on a time-dependent solution n, in particular its existence and uniqueness for any reasonable initial condition. Let us here assume the existence of such a solution, which moreover satisfies the common estimate (see [139])

$$|n(t,a,x)| \leqslant Ce^t N(a,x), \qquad t,x>0. \tag{1.23}$$

It is usually ensured by the hypothesis $|n^0(a,x)| \leqslant CN(a,x)$ and a maximum principle. For H a function defined on all $\mathbb{R}$, we define, for $n \in \mathrm{L}^1(\mathbb{R}_+^2)$

$$\mathcal{H}[n] = \int_{b_\theta}^{\infty} \int_0^{x-b_\theta} xN(a,x) H\left(\frac{n(a,x)}{N(a,x)}\right) \mathrm{d}a\,\mathrm{d}x$$

which satisfies the following entropy property.

Proposition 15. *If n is a solution of (1.1) satisfying (1.23), then*

$$\frac{d}{dt}\mathcal{H}[n(t,\cdot,\cdot)\mathrm{e}^{-t}] = -\mathcal{D}[n(t,\cdot,\cdot)\mathrm{e}^{-t}], \tag{1.24}$$

with

$$\mathcal{D}[n] = \int_{b_\theta}^{\infty} x^2 N(0,x) \left[\int_\theta^\eta \int_0^{\frac{x}{z}-b_\theta} H\left(\frac{n(a,\frac{x}{z})}{N(a,\frac{x}{z})}\right) \mathrm{d}\nu_x(a,z) - H\left(\int_\theta^\eta \int_0^{\frac{x}{z}-b_\theta} \frac{n(a,\frac{x}{z})}{N(a,\frac{x}{z})}\,\mathrm{d}\nu_x(a,z)\right)\right] \mathrm{d}x$$

where $\mathrm{d}\nu_x(a,z) = \frac{B(a)N(a,\frac{x}{z})}{N(0,x)z^2}\,\mathrm{d}a\,\mathrm{d}\mu(z)$ is a probability measure. Furthermore if H is convex, then $\mathcal{D} \geqslant 0$.

Before proving this proposition, we make a remark about the conservative problem (*i.e.* when only one daughter out of two is kept after division). In this case, the dominant eigenvalue is 0 instead of 1, and $xN(a,x)$ is an eigenvector associated with the eigenvalue 0, since the total mass is preserved. Then we obtain the equation

$$\frac{\partial}{\partial a}(x^2N) + \frac{\partial}{\partial x}(x^2N) = -x^2BN, \tag{1.25}$$

which might also be obtained multiplying (1.8a) by x.

Démonstration. Easy computations lead to

$$\frac{\partial}{\partial t}\frac{n\mathrm{e}^{-t}}{N} + x\frac{\partial}{\partial a}\frac{n\mathrm{e}^{-t}}{N} + x\frac{\partial}{\partial x}\frac{n\mathrm{e}^{-t}}{N} = 0,$$

where $N(a,x)>0$, *i.e.* on the domain $\Omega := \{x-a>b_\theta\}$. From this equality and (1.25), we deduce

$$\frac{\partial}{\partial t}\left(xNH\left(\frac{n\mathrm{e}^{-t}}{N}\right)\right) + \frac{\partial}{\partial a}\left(x^2NH\left(\frac{n\mathrm{e}^{-t}}{N}\right)\right) + \frac{\partial}{\partial x}\left(x^2NH\left(\frac{n\mathrm{e}^{-t}}{N}\right)\right) = -x^2BNH\left(\frac{n\mathrm{e}^{-t}}{N}\right), \tag{1.26}$$

and integrating (1.26) over Ω, we obtain

$$
\begin{aligned}
&\frac{d}{dt}\iint_{(b_\theta,\infty)\times(0,x-b_\theta)} xNH\left(\frac{n\mathrm{e}^{-t}}{N}\right)\\
&=\int_{b_\theta}^{\infty} x^2N(0,x)H\left(\frac{n(t,0,x)\mathrm{e}^{-t}}{N(0,x)}\right)\,\mathrm{d}x\\
&\quad-\int_{b_\theta}^{\infty} x^2N(x-b_\theta,x)H\left(\frac{n(t,x-b_\theta,x)e^{-t}}{N(x-b_\theta,x)}\right)\,\mathrm{d}x\\
&\qquad+\int_0^{\infty}(a+b_\theta)^2N(a,a+b_\theta)H\left(\frac{n(t,a,a+b_\theta)\mathrm{e}^{-t}}{N(a,a+b_\theta)}\right)\,\mathrm{d}a\\
&\qquad\quad-\int_{b_\theta}^{\infty}\int_0^{x-b_\theta} x^2BNH\left(\frac{n\mathrm{e}^{-t}}{N}\right)\,\mathrm{d}a\,\mathrm{d}x\\
&=\int_{b_\theta}^{\infty} x^2N\left(0,x\right)H\left(\frac{\mathrm{e}^{-t}}{N(0,x)}\int_\theta^\eta\int_0^{\frac{x}{z}-b_\theta} B(a)n(t,a,\frac{x}{z})\,\mathrm{d}a\frac{\mathrm{d}\mu(z)}{z^2}\right)\,\mathrm{d}x\\
&\quad-2\int_\theta^\eta\int_{b_\theta}^{\infty}\int_0^{x-b_\theta} x^2BNH\left(\frac{n\mathrm{e}^{-t}}{N}\right)\,\mathrm{d}a\,\mathrm{d}x z\,\mathrm{d}\mu(z)\\
&=\int_{b_\theta}^{\infty} x^2N\left(0,x\right)H\left(\int_\theta^\eta\int_0^{\frac{x}{z}-b_\theta}\frac{n(t,a,\frac{x}{z})\mathrm{e}^{-t}}{N(a,\frac{x}{z})}\,\mathrm{d}\nu_x(a,z)\right)\,\mathrm{d}x\\
&\quad-2\int_\theta^\eta\int_{zb_\theta}^{b_\theta}\int_0^{\frac{x}{z}-b_\theta} x^2B(a)N(a,\frac{x}{z})H\left(\frac{n(t,a,\frac{x}{z})\mathrm{e}^{-t}}{N(a,\frac{x}{z})}\right)\,\mathrm{d}a\,\mathrm{d}x\frac{\mathrm{d}\mu(z)}{z^2}\\
&\qquad-2\int_\theta^\eta\int_{b_\theta}^{\infty}\int_0^{\frac{x}{z}-b_\theta} x^2B(a)N(a,\frac{x}{z})H\left(\frac{n(t,a,\frac{x}{z})\mathrm{e}^{-t}}{N(a,\frac{x}{z})}\right)\,\mathrm{d}a\,\mathrm{d}x\frac{\mathrm{d}\mu(z)}{z^2}\\
&=\int_{b_\theta}^{\infty} x^2N(0,x)\left[H\left(\int_\theta^\eta\int_0^{\frac{x}{z}-b_\theta}\frac{n(t,a,\frac{x}{z})\mathrm{e}^{-t}}{N(a,\frac{x}{z})}\,\mathrm{d}\nu_x(a,z)\right)\right.\\
&\quad\left.-\int_\theta^\eta\int_0^{\frac{x}{z}-b_\theta} H\left(\frac{n(t,a,\frac{x}{z})\mathrm{e}^{-t}}{N(a,\frac{x}{z})}\right)\,\mathrm{d}\nu_x(a,z)\right]\,\mathrm{d}x,
\end{aligned}
$$

since for $x\in[zb_\theta,b_\theta]$ and $z\in[\theta,\eta]$, $\frac{x}{z}-b_\theta\leqslant b$, and we conclude using Jensen's inequality.

□

Appropriate choices of the function H in (1.24) lead to interesting results. With $H(x)=x$, we recover the conservation law (1.7). Then taking $H(x)=|1-x|$, we obtain the decay of $\|N-ne^{-t}\|_{\mathrm{L}^1(\mathbb{R}_+,x\,\mathrm{d}x\,\mathrm{d}a)}$ as t tends to infinity. In the case where the fragmentation kernel μ has a density with respect to the Lebesgue measure on $[0,1]$, we expect that this quantity will vanish, as in [120, 139]. In contrast, in the case of the equal mitosis, there is not hope for this distance to vanish. Indeed, one has an infinite number of eigentriplets (λ_j,N_j,ϕ_j) with $j\in\mathbb{Z}$ defined by

$$
\lambda_j=1+\frac{2ij\pi}{\mathrm{Log}\ 2},\qquad N_j(a,x)=x^{1-\lambda_j}N(a,x),\qquad \phi_j(a,x)=x^{\lambda_j},
$$

so we expect a behaviour as in [14], *i.e.* the convergence of $n(t,a,x)\mathrm{e}^{-t}$ to the periodic solution

$$
\sum_{j\in\mathbb{Z}}\langle n^0,\phi_j\rangle\,\mathrm{e}^{\frac{2ij\pi t}{\mathrm{Log}\ 2}}N_j(a,x),
$$

where $\langle n,\phi\rangle=\int\int n(a,x)\phi(a,x)\,\mathrm{d}a\,\mathrm{d}x$.

1.5 Discussion and perspectives

We have proved the existence and uniqueness of a solution of the eigenproblem (1.8) in the special yet biologically relevant case of linear growth rate with a self-similar fragmentation kernel. Hypotheses on both this kernel and the division rate are fairly general.

As possible future work we can imagine to extend the result to general growth rates. In this case the Perron eigenvalue is not explicit and it has to be determined in the same time as the eigenfunction, as in [177, 52, 56]. If we denote by λ the eigenvalue, the equivalent of Equation (1.20) is

$$P_\lambda(s) = \int_0^1 e^{-\lambda \int_s^{\frac{s}{z}} \frac{\mathrm{d}u}{g(u)}} (\Phi * P_\lambda)(\frac{s}{z}) \frac{\mathrm{d}\mu(z)}{z}$$

with $P_\lambda(y) = e^{\lambda \int_1^s \frac{\mathrm{d}u}{g(u)}} M(0,s)$ and the equivalent of the solution given in (1.9) is

$$N : (a,x) \mapsto \frac{\Psi(a)}{g(x)} e^{-\lambda \int_0^x \frac{\mathrm{d}\alpha}{g(\alpha)}} P_\lambda(x-a).$$

Additionally for nonlinear growth rates, the function $(a,x) \mapsto x$ does not provide a conservation law as in (1.7), and it has to be replaced by a solution to the dual Perron eigenproblem. Such a dual eigenfunction appears in the definition of the General Relative Entropy [119, 120], and for proving its existence one could follow the method in [141, 57] for the size-structured model. Another possible generalization of the growth rate is adding variability, in the spirit of [150, 123, 130]. One might also consider a more general fragmentation kernel than in the case of self-similar fragmentation, or/and with a support which is not a compact subset of $(0,1)$.

The other natural continuation of the present work is the proof of the well-posedness and the long-time behaviour of the evolution equation, as in [177, 52]. To do so one can take advantage of the General Relative Entropy as in [120, 23, 14] or use general spectral methods [178, 124].

Acknowledgments

The authors are very grateful to Marie Doumic for having suggested them the problem treated in this paper, and for the many fruitful discussions.

Chapitre 2

Solutions mesures pour l'équation de la mitose avec vitesse de croissance linéaire

---

Dans ce chapitre, nous empruntons à plusieurs articles de dynamique des populations. En effet, on s'intéresse au comportement asymptotique oscillant pour l'équation de croissance-fragmentation dans le cas critique étudié dans [14], mais énoncé pour des solutions mesures. Après avoir prouvé l'existence et l'unicité d'une solution mesure à cette équation, on obtient sa convergence faible vers une mesure périodique. Un article est en cours d'écriture et sera soumis cette année.

2.1 Introdution

Structured population models aim at describing and predicting the evolution of a population over time. The first size-structured models go back to the second half of the 20^{th} century with the works of Bell and Anderson [13] and Sinko and Streifer [160]. Then, a lot of refinements have been made by many authors, see for example [51, 52] or [139] for a recent but classical reference. In its most general form, this model is formulated as

$$\frac{\partial}{\partial t}n(t,x) + \frac{\partial}{\partial x}(g(x)n(t,x)) + \mu(x)n(t,x) + B(x)n(t,x) = \int_x^\infty b(y,x)n(t,y)\,\mathrm{d}y, \tag{2.1}$$

where $n(t,x)$ represents the number of individuals of size $x \geqslant 0$ at time t, $g \geqslant 0$ and $B \geqslant 0$ their growth and division rate, respectively, and $b(y,x) \geqslant 0$ is the quantity of indivduals born at size x from the division of individuals of size y. Variants of this equation model several situations such as internet protocol, protein polymerization or cell division (see the references given in the introduction of [57]), thus numerous studies already exist on this equation.
In the L^p framework, wellposedness and large time asymptotic of this equation were extensively studied, see for example [139] and references therein. Two antagonistic mecanisms are at work in this equation, giving it its name : the growth of the individuals, symbolized by the transport part, that tends to 'move' the mass to the large values of x, and the fragmentation process, that in contrast brings back the mass to smaller values of the size through division. Intuitively, if the growth phenomenon prevails, it will lead to the appearance of individuals of infinite size, a phenomenon know as gelation, see [71, 72], whereas if the fragmentation is 'the strongest', then dusts, *i.e.* individuals of infinitely small size, will be produced, see [6, 92] for references on shattering. When a balance does exist between these two phenomena, we

expect an equilibrium to occur. Such an equilibrium is related to the solution of the Perron problem related to Equation (2.1), namely finding a triplet $(\lambda,\mathcal{U},\phi)$ with λ a nonnegative number and N and ϕ nonnegative functions such that $t,x \mapsto e^{\lambda t}\mathcal{U}(x)$ is solution to (2.1) and $t,x \mapsto e^{-\lambda t}\phi(x)$ is solution to its adjoint equation. When such functions are obtained, one can use the Generalized Relative Entropy, introduced by Michel, Mishler and Perthame in [119, 120], see also [109], which in a way quantifies how different are two nonnegative solutions of an hyperbolic equation. In most cases, this theorem allows to prove the convergence

$$\forall p \in [1,\infty), \quad \lim_{t\to\infty} \|n(t,\cdot)e^{-\lambda t} - \rho N\|_{\mathrm{L}^p(N^{1-p}\phi\,\mathrm{d}x)} = 0, \tag{2.2}$$

where $u = u(t,x)$ is a solution of (2.1) and $\rho = \int_0^\infty u^{in}(x)\phi(x)\,\mathrm{d}x$. However, in some critical case, some unusual behaviours can occur, see for example [70, 16, 69, 62].
In this paper, we focus on a particular case of Equation (2.1) for which the convergence (2.2) does not hold. We consider the critical case of a growth rate $g(x) = x$ and equal mitosis, on the complete genealogical tree, for which the death rate is neglected (see [129] for a biological justification for bacteria), that is to say we take $\mu \equiv 0$. The equation we study then reads

$$\frac{\partial}{\partial t}u(t,x) + \frac{\partial}{\partial x}(xu(t,x)) + B(x)u(t,x) = 4B(2x)u(t,2x) \tag{2.3}$$

complemented with an initial condition $u(0,x) = u^{in}(x)$. This equation is important both for modeling — it represents the idealized case of fission into two equal parts — and mathematical point of view. The term 'critical' is justifed by the fact that in this precise case, the interplay between exponential growth and equal mitosis results in a *dynamic* equilibrium, in contrast with the previous situation the convergence (2.2). A particular feature of Equation (2.3) is the exponential growth of the total mass. Indeed, a formal integration against the measure $x\,\mathrm{d}x$ over $(0,\infty)$ leads to the balance law

$$\int_0^\infty xu(t,x)\,\mathrm{d}x = e^t \int_0^\infty xu^{in}(x)\,\mathrm{d}x. \tag{2.4}$$

This relation also provides that the principal eigenvalue is $\lambda = 1$ and the adjoint eigenvector ϕ is the identity function over $(0,\infty)$. To grasp the phenomenon at play there, it is useful to give explicitly the generalized entropy inequality, where one of the solutions is obtained from the Perron problem. First, the Perron problem associated to Equation (2.3) reads

$$\begin{cases} \dfrac{\partial}{\partial x}(x\mathcal{U}(x)) + (B(x)+\lambda)\mathcal{U}(x) = 4B(2x)N(2x), \\ \\ \mathcal{U}(x) \geqslant 0, \qquad \displaystyle\int_0^\infty \mathcal{U}(x)\,\mathrm{d}x = 1, \\ \\ -x\dfrac{\partial}{\partial x}\phi(x) + (B(x)+\lambda)\,\phi(x) = 2B(x)\phi(x/2), \\ \\ \phi(x) \geqslant 0, \qquad \displaystyle\int_0^\infty \phi(x)\mathcal{U}(x)\,\mathrm{d}x = 1, \end{cases} \tag{2.5}$$

and was the subject of many investigations, among which we can mention [52, 94, 141, 118, 57, 181]. The normalization

$$\int_0^\infty x\mathcal{U}(x)\,\mathrm{d}x = 1$$

might seem unusual, but is actually pretty natural once we consider the balance law (2.4) with a particular solution $(t,x) \mapsto e^t\mathcal{U}(x)$. System (2.5) is a particular case of the problem studied in [57], and their

hypotheses specialized to our case read

$$\begin{cases} B : (0,\infty) \to (0,\infty) \text{ is locally integrable,} \\ \exists b > 0,\ \operatorname{supp} B = [b,\infty) \\ \exists z_0, \gamma_0, K_0 > 0,\ \forall x < z_0, \quad B(x) \leqslant K_0 x^{\gamma_0} \\ \exists z, \gamma_1, \gamma_2, K_1, K_2 > 0\ \forall x > z \quad K_1 x^{\gamma} \leqslant B(x) \leqslant K_2 x^{\gamma_2}. \end{cases} \tag{A1}$$

Applied to our specific case, the main result from [57] results in the following theorem.

Theorem 16 (Doumic and Gabriel, 2010)**.** *Under assumption* (A1)*, their exists a unique solution* (λ, N, ϕ) *of the Perron problem* (2.5)*. Additionally, the eigenvalue* λ *is positive and*

$$\forall k \in \mathbb{R}, \qquad x^k N \in \mathrm{L}^1(0,\infty) \cap \mathrm{L}^\infty(0,\infty).$$

The entropy inequality is then in this case

Theorem 17 (Michel, Mischler and Perthame 2004)**.** *Let* $H : \mathbb{R} \to \mathbb{R}$ *and suppose the existence of a solution of the Perron problem* (λ, N, ϕ)*. Then, for all solution* n *of* (2.3)*, one has*

$$\frac{\mathrm{d}}{\mathrm{d}t}\mathcal{H}[n(t,\cdot)e^{-t}] = -\mathcal{D}^H[n(t,\cdot)e^{-t}],$$

with

$$\mathcal{H}[u] = \int_0^\infty x\mathcal{U}(x) H\left(\frac{u(t,x)}{\mathcal{U}(x)}\right) \mathrm{d}x$$

and

$$\mathcal{D}^H[u] = 4\int_0^\infty xN(2x)B(2x)\left[H'\left(\frac{u(x)}{\mathcal{U}(x)}\right)\left(\frac{u(2x)}{N(2x)} - \frac{u(x)}{\mathcal{U}(x)}\right) - H\left(\frac{u(x)}{\mathcal{U}(x)}\right) + H\left(\frac{u(2x)}{N(2x)}\right)\right] \mathrm{d}x.$$

If additionally H *is convex, then* $\mathcal{D}^H[u] \geqslant 0$ *for every function* $u : [0,\infty) \to \mathbb{R}$*.*

In [14], the authors exhibited the existence of complex eigentriplets indexed by $\mathbb{Z}$ built on the solution of the Perron problem (λ, N, ϕ), given by

$$\lambda_k = 1 + \frac{2ik\pi}{\operatorname{Log} 2}, \qquad N_k = x^{-\frac{2ik\pi}{\operatorname{Log} 2}}\mathcal{U}(x), \qquad \phi_k(x) = x^{1+\frac{2ik\pi}{\operatorname{Log} 2}}. \tag{2.6}$$

For every $k \in \mathbb{Z}$, the functions N_k has the special property $\mathcal{D}^H[N_k] = 0$ for every $k \in \mathbb{Z}$, which contrasts with the usual behaviour observed, as proved by Theorem 17. Later in this article, the authors proved a convergence of a rescaled solution to a Fourier series, namely

$$\lim_{t\to\infty} \left\| n(t,\cdot)e^{-t} - \sum_{j\in\mathbb{Z}} (u^{in}, \mathcal{U}_j) e^{\frac{2ij\pi}{\operatorname{Log} 2}t}\mathcal{U}_j \right\|_{\mathrm{L}^2\left(\mathbb{R}_+, \frac{x}{\mathcal{U}(x)}\,\mathrm{d}x\right)} = 0.$$

Our work in this paper consists in investigating how this cyclic asymptotic behaviour transpose in the case of measure solutions. Indeed, beside the L^p framework mentionned previously, another kind of solution of structured population models has drawn attention for some years, involving measures. Those are measure and measure-valued solutions. This framework allows for a Dirac mass as initial condition, which accounts, for example, for a cell culture starting with only one cell, so that the physiological variables are precisely known. Results on wellposedness for these equations can be found for example in [89, 90, 29, 81]. Asymptotic behaviour was also a concern about this kind of solutions. Strinkingly, it was possible to extend the Generalized Relative Entropy inequalities to a measure setting, see [91, 44].

Another approach to obtain large time asymptotics consists in using the Doeblin method, see [81, 9, 10]. In each case evoked, the behaviour of the measure solution μ_t in the long run matches the one of the L^p solution, in the sense that it converges (in a certain sense) to $\rho\mathcal{U}(x)\,\mathrm{d}x$, where $\rho = \int_{\mathbb{R}_+} \phi\,\mathrm{d}\mu^{in}$ and $\mathrm{d}x$ is the Lebesgue measure on $\mathbb{R}_+$. In the same fashion, we conjectured the convergence of a measure solution of (2.3) to a periodic measure, and indeed is the result we obtain, see Theorem 19 below.

The outline of the paper is as follows. The next section is dedicated to prove the wellposedness of Equation (2.3) in view of Definition 1. To do so, we take the steps from [81] to construct a measure solution by duality. Then in section 2.3 we prove the weak convergence of the measure solution we constructed to an oscillating measure, drawing inspiration from [14]. Finally, we highlight some possible continuations of the present work in section 2.4.

2.2 Wellposedness of the size equation in the measure setting

Following the steps proposed in [81], we construct a solution to Equation (2.3) by duality. In the first subsection, we explicit the functional framework that suits the study of our problem. In subsection 2.2.2 we solve the backward adjoint problem of (2.3), from which we construct by duality a measure satisfying Definition 1 below of a solution of (2.3) in the sense of measures.

2.2.1 Functional framework, definition of a measure solution and statement of the main theorem

In this subsection, we recall some facts of measure theory, particularly from its functional viewpoint, adapted to our problem and taken from [151]. We endow $(0,\infty)$ with its standard topology and the associated Borel $\sigma-$algebra. Using classical notations, we denote by $(\mathcal{M}, \|\cdot\|_{\mathcal{M}})$ the normed space of signed Borel measures on $(0,\infty)$ (note in particular that the definition from [151] implies that these measures are finite) endowed with the total variation norm

$$\forall \mu \in \mathcal{M}, \qquad \|\mu\|_{\mathcal{M}} = \mu_+(0,\infty) + \mu_-(0,\infty),$$

with $\mu = \mu_+ - \mu_-$ being the classical Hahn-Jordan decomposition of μ. We also denote $\mathcal{C}_0(0,\infty)$ the set of continuous functions on $(0,\infty)$ that vanish at infinity, which is a Banach space when endowed with the supremum norm.
In view of the condition

$$\int_0^\infty \phi(x)\mathcal{U}(x)\,\mathrm{d}x = 1$$

satisfied in the L^p framework, where N and ϕ are the solutions of the Perron problem (2.5), we want to consider measures μ taking real values such that

$$\int_0^\infty \phi\,\mathrm{d}\mu < \infty. \tag{2.7}$$

However, we do not particularly require for such a measure to be finite, so we will not consider the subspace of $\mathcal{M}$ such that (2.7) holds, but instead construct an appropriate space through an equivalence relation. To define such an object, we first denote $\dot{\mathcal{M}}_+$ the subset of positive measures on $(0,\infty)$ such that (2.7) holds. Now, we define the quotient space

$$\dot{\mathcal{M}} = \dot{\mathcal{M}}_+ \times \dot{\mathcal{M}}_+ /_\sim,$$

where $(\mu_1,\mu_2) \sim (\nu_1,\nu_2)$ if $\mu_1 + \nu_2 = \nu_1 + \mu_2$. We emphasize that $\dot{\mathcal{M}}$ is larger than the subspace of measures of $\mathcal{M}$ such that (2.7) holds, since the maesure μ such that

$$\mu(\mathrm{d}x) = \frac{e^{-x}}{x}\,\mathrm{d}x$$

belongs to $\dot{\mathcal{M}}$ but not to $\mathcal{M}$. Next, we denote $\dot{\mathcal{B}}$ the set of measurable functions $f : (0,\infty) \to \mathbb{R}$ such that the quantiy

$$\|f\| = \sup_{x>0} \frac{|f(x)|}{\phi(x)}$$

is finite. Note that no space is mentionned in index of the norm $\|\cdot\|$. The reason is that the same expression will be used also for continuous fonctions dominated by ϕ, the context making clear which norm precisely we use. A straightforward computation ensures that the action of any measure $(\mu_1,\mu_2) \in \dot{\mathcal{M}}$ on $\dot{\mathcal{B}}$ through the formula

$$(\mu_1,\mu_2)(f) = \int_0^\infty f \,\mathrm{d}\mu_1 - \int_0^\infty f \,\mathrm{d}\mu_2,$$

where (μ_1,μ_2) is any representative of the equivalence class of this pair, is well-defined. This motivates the notation $\mu = \mu_1 - \mu_2$ to refer to this equivalence class.
In order to a more informative structure on $\dot{\mathcal{M}}$, we prove a Riesz type result. First, we define E the space of continuous functions f on $(0,\infty)$ such that $\|f\| < \infty$, which is a Banach space. Then we set E_0 the closed vector subspace of E of the functions such that the ratio $|f(x)|/x$ vanish at 0 and infinity.
For a measure μ belonging to $\mathcal{M}$ (respetively $\dot{\mathcal{M}}$), let us denote in the sequel T_μ the real-valued linear form on $\mathcal{C}_0(0,\infty)$ (respetively E_0)

$$T_\mu : f \mapsto \int_0^\infty f \,\mathrm{d}\mu.$$

The Riesz representation theorem then ensures that for each linear form $T \in (\mathcal{C}_0(0,\infty))'$ there exists a unique measure $\mu \in \mathcal{M}$ such that $T = T_\mu$, and moreover that $\|T\|_{(\mathcal{C}_0(0,\infty))'} = \|\mu\|_{\mathcal{M}}$. Thanks to this last property, the operator $\mu \mapsto T_\mu$ is an isometry from $(\mathcal{M}, \|\cdot\|_{\mathcal{M}})$ onto $\left(\mathcal{C}_0(0,\infty))', \|\cdot\|_{(\mathcal{C}_0(0,\infty))'}\right)$, with

$$\|T\|_{(\mathcal{C}_0(0,\infty))'} := \sup_{\|f\|_\infty \leqslant 1} |T(f)|,$$

which provides that $(\mathcal{M}, \|\cdot\|_{\mathcal{M}})$ is a Banach space. We would like to have such a result for E_0 and $\dot{\mathcal{M}}$, however this theorem is not directly applicable, but we prove in the following lemma that similar properies hold.

Lemma 18. *For every $\mu \in \dot{\mathcal{M}}$, there exists a Hahn-Jordan type decomposition, i.e. a unique couple of measures $(\mu_+,\mu_-) \in \dot{\mathcal{M}}_+ \times \dot{\mathcal{M}}_+$ that are mutually singular such that $\mu = \mu_+ - \mu_-$. The quantity*

$$\|\mu\|_{\dot{\mathcal{M}}} := |\mu|(\phi) = \mu_+(\phi) + \mu_-(\phi)$$

thus defines a norm on $\dot{\mathcal{M}}$. Additionally, for any $T \in E_0'$, there exists a unique measure $\mu \in \dot{\mathcal{M}}$ such that $T = T_\mu$, and one has $\|T\|_{E_0'} = \|\mu\|_{\dot{\mathcal{M}}}$.

Démonstration. Let $G : \mathcal{M} \to \dot{\mathcal{M}}, \nu \mapsto G\nu$, with for all $f \in \dot{\mathcal{B}}, (G\nu)f = \nu(f/\phi)$. G is clearly an isomorphism, so denoting $\nu = \nu_+ - \nu_-$, the Hahn-Jordan decomposition of a measure $\nu \in \mathcal{M}$, one has the unique decomposition $G\nu = G\nu_+ - G\nu_-$ in $\dot{\mathcal{M}}$. Let $\gamma : E_0 \to \mathcal{C}_0(0,\infty) f \mapsto f/\phi$ and $\mathcal{F} : (\mathcal{C}_0(0,\infty))' \to E_0'$, $\tau \mapsto \tau \circ \gamma$. Clearly, G, γ and $\mathcal{F}$ are isometries. Let $\tau \in (\mathcal{C}_0(0,\infty))'$. Let $T \in E_0'$ and $\tau \in (\mathcal{C}_0(0,\infty))'$ such that $T = \mathcal{F}(\tau)$. Thanks to the Riesz theorem, there exists a unique measure $\nu \in \mathcal{M}$ such that $\tau = T_\nu$. Let us denote $\mu = G\nu$. Then one has for $f \in E_0$

$$Tf = (\mathcal{F}\tau)(f) = (\mathcal{F}T_\nu)f = T_\nu(\gamma f) = \int_0^\infty \frac{f}{\phi} \,\mathrm{d}\nu = (G\nu)f = \mu f = T_\mu f.$$

These computations show that there exists a unique measure $\mu \in \dot{\mathcal{M}}$ such that $T = T_\mu$. The proof of the claims on the norms are straightforward. □

This lemma ensures in particular that $(\dot{\mathcal{M}}, \|\cdot\|_{\dot{\mathcal{M}}})$ is a Banach space. Additionally, one clearly has

$$\|\mu\|_{\dot{\mathcal{M}}} = \sup_{\|f\| \leqslant 1} |\mu f|.$$

Now we give the intuition that leads to the definition of a measure solution to (2.3). Suppose we have a smooth solution $n = n(t,x)$ to this equation. Then for a test function $f = f(x)$, we obtain after integrating by parts

$$\int_0^\infty f(x)n(t,x)\,\mathrm{d}x = \int_0^\infty f(x)n(0,x)\,\mathrm{d}x + \int_0^t \left(\int_0^\infty [xf'(x) - B(x)(f(x) - 2f(\frac{x}{2}))]n(s,x)\,\mathrm{d}x\right)\,\mathrm{d}s.$$

A measure solution μ_t would then mimic $n(t,x)\,\mathrm{d}x$. This intuition leads to the following definition of a measure solution for Equation (2.3).

Definition 1. *A family $(\mu_t)_{t\geqslant 0} \subset \dot{\mathcal{M}}$ is called a measure solution to Equation* (2.3) *with initial data $\mu^{\mathrm{in}} \in \dot{\mathcal{M}}$ if for all $f \in E$, the mapping $t \mapsto \mu_t f$ is continuous in time and for all $t \geqslant 0$ and $f \in \mathcal{C}^1_c(0,\infty)$,*

$$\int_0^\infty f(x)\,\mathrm{d}\mu_t(x) = \int_0^\infty f(x)\,\mathrm{d}\mu^{\mathrm{in}}(x) + \int_0^t \left(\int_0^\infty [xf'(x) - B(x)(f(x) - 2f(\frac{x}{2}))]\,\mathrm{d}\mu_s(x)\right)\,\mathrm{d}s. \tag{2.8}$$

To prove the existence and uniqueness of a solution in the sense of Definition 1, we make the following assumption on the division rate B.

$$\text{The division rate } B \text{ is a continuous function on } (0,\infty), \text{ bounded around } 0. \tag{A2}$$

With the notations and definitions introduced in this section, we can now state the main theorem of this paper.

Theorem 19. *Under the hypothesis* (A2)*, for any $\mu^{in} \in \dot{\mathcal{M}}$, there exists a unique measure solution $(\mu_t)_{t\geqslant 0}$ of* (2.3) *in the sense of Definition 1. If additionally B satisfies hypothesis* (A1)*, then there exists a unique* Log 2*−periodic family of measures $(\pi_t)_{t\geqslant 0} \subset \dot{\mathcal{M}}$ such that*

$$\forall f \in E_0, \quad \lim_{t\to\infty} \int_0^\infty f\,\mathrm{d}(\mu_t - \pi_t) = 0.$$

2.2.2 Existence and uniqueness of a solution to the adjoint problem

The first step in [81] consists in solving the adjoint problem

$$\frac{\partial}{\partial t}f(t,x) - x\frac{\partial}{\partial x}f(t,x) + B(x)f(t,x) = 2B(x)f(t,\frac{x}{2}), \quad t \geqslant 0,\ x > 0 \tag{2.9}$$

complemented with the initial condition $f(0,x) = f_0(x)$ for $x > 0$. It will be usefull in the sequel to rewrite Equation (2.9) as a generic evolution equation

$$\frac{\partial}{\partial t}f(t,x) = \mathcal{A}f(t,\cdot)(x).$$

With this notation, Equation (2.8) becomes simply

$$\mu_t f = \mu^{\mathrm{in}} f + \int_0^t \mu_s \mathcal{A} f\,\mathrm{d}s.$$

We solve Equation (2.9) throught the method of characteristics, thus defining a weak solution. Let $\Psi(t) = f(t, xe^{-t})$, with f a solution to (2.9) in the classical sense. Then Ψ is differentiable and satisties

$$\begin{aligned}
\Psi'(t) &= \frac{\partial f}{\partial t}(t,xe^{-t}) - xe^{-t}\frac{\partial f}{\partial x}(t,xe^{-t}) \\
&= 2B(xe^{-t})f(t,\frac{xe^{-t}}{2}) - B(xe^{-t})f(t,xe^{-t}) \\
&= 2B(xe^{-t})f(t,\frac{xe^{-t}}{2}) - B(xe^{-t})\Psi(t),
\end{aligned}$$

so in turn f satisfies

$$f(t,xe^{-t}) = f_0(x)e^{-\int_0^t B(xe^{-s})\,\mathrm{d}s} + 2\int_0^t B(xe^{-\tau})e^{-\int_\tau^t B(xe^{-s})\,\mathrm{d}s} f(\tau, \frac{xe^{-\tau}}{2})\,\mathrm{d}\tau.$$

And finally the changes of variable $x \leftarrow xe^t$ and then $\tau \leftarrow t-\tau$ in the integral lead to the following definition.

Definition 2. *We say that $f : \Omega \subset [0,\infty)\times(0,\infty) \to \mathbb{R}$ is a solution to (2.9) in weak sense when, for all $t,x \in \Omega$,*

$$f(t,x) = f_0(xe^t)e^{-\int_0^t B(xe^s)\,\mathrm{d}s} + 2\int_0^t B(xe^\tau)e^{-\int_0^\tau B(xe^s)\,\mathrm{d}s} f(t-\tau, \frac{xe^\tau}{2})\,\mathrm{d}\tau \tag{2.10}$$

We will prove existence and uniqueness of a solution to Equation (2.10) in different spaces, depending on the regularity of the initial condition f_0 and the set Ω of the variables.
We now introduce some functional spaces. For any subset $\Omega \subset \mathbb{R}^d$ ($d \geqslant 1$), define $\mathcal{B}_{loc}(\Omega)$ the space of locally bounded Borel functions $f : \Omega \to \mathbb{R}$ and and $\mathcal{B}(\Omega)$ the (Banach) subspace of bounded Borel functions. In particular, we define $\mathcal{B}^0_{loc}(0,\infty)$ the subset of functions of $\mathcal{B}_{loc}$ that are bounded around 0. For a given $f \in \mathcal{B}_{loc}(0,\infty)$, we want to prove existence and uniqueness of a fixed point for the operator $\Gamma : \mathcal{B}_{loc}([0,\infty)\times(0,\infty)) \to \mathcal{B}_{loc}([0,\infty)\times(0,\infty))$ defined by

$$\begin{aligned}\Gamma g(t,x) &= f(xe^t)e^{-\int_0^t B(xe^s)\,\mathrm{d}s} + 2\int_0^t B(xe^\tau)e^{-\int_0^\tau B(xe^s)\,\mathrm{d}s} g(t-\tau, \frac{xe^\tau}{2})\,\mathrm{d}\tau \\ &= f(xe^t)e^{-\int_x^{xe^t} B(\tau)\frac{\mathrm{d}\tau}{\tau}} + 2\int_x^{xe^t} B(\tau)e^{-\int_x^\tau B(s)\frac{\mathrm{d}s}{s}} g(t-\mathrm{Log}\,(\frac{\tau}{x}), \frac{\tau}{2})\frac{\mathrm{d}\tau}{\tau}.\end{aligned} \tag{2.11}$$

To do so, we use a fixed point method on truncated spaces to construct locally a fixed point of the operator Γ.

Lemma 20. *Under the hypothesis (A2), for all $f \in \mathcal{B}^0_{loc}(0,\infty)$, there exists a unique fixed point of Γ lying in $\mathcal{B}_{loc}([0,\infty)\times(0,\infty))$ denoted $\bar{g}$. If f additionally is nonnegative / continuous / continuously differentiable, then so is $\bar{g}$. Additionally when f is continuously differentiable $\bar{g}$ satisfies*

$$\partial_t \bar{g} = \mathcal{A}\,\bar{g}.$$

Démonstration. Let $(T,K) \in [0,\infty)\times(0,\infty)$, and define the set $\Omega_{T,K} = \{(t,x) \in [0,T]\times(0,\infty),\ xe^t < K\}$ and the Banach space

$$\mathcal{B}_{T,K} = \Big\{ g : \Omega_{T,K} \to \mathbb{R} \text{ measurable},\ \|g\|_{\mathcal{B}_{T,K}} := \sup_{t,x\in\Omega_{T,K}} |g(t,x)| < +\infty \Big\}.$$

Clearly $\Gamma : \mathcal{B}_{T,K} \to \mathcal{B}_{T,K}$, since $f \in \mathcal{B}_{loc}((0,\infty))$. We prove below the existence of a unique fixed point $g_{T,K}$ in $\mathcal{B}_{T,K}$ using the Banach fixed point theorem. Let $g_1, g_2 \in \mathcal{B}_{T,K}$. For $0 \leqslant t \leqslant t_0 \leqslant T$, one has the estimate

$$\begin{aligned}|(\Gamma g_1 - \Gamma g_2)(t,x)| &\leqslant 2\int_0^t B(xe^\tau)e^{-\int_0^\tau B(xe^s)\,\mathrm{d}s} \left| (g_1-g_2)\left(t-\tau, \frac{xe^\tau}{2}\right)\right| \mathrm{d}\tau \\ &\leqslant 2\left(1 - e^{-\int_0^t B(xe^s)\,\mathrm{d}s}\right)\|g_1-g_2\|_{\mathcal{B}_{T,K}} \\ &\leqslant 2\left(1 - e^{-t_0 \sup_{(0,K)}|B|}\right)\|g_1-g_2\|_{\mathcal{B}_{T,K}}\end{aligned}$$

If t_0 is such that $\mathrm{Log}\,2 > t_0 \sup_{(0,K)}|B|$, the operator Γ is a contraction over the space of the functions of $\mathcal{B}_{t_0,K}$ restricted to $\Omega_{t_0,K} \subset \Omega_{T,K}$ into itself, for the norm $\|\cdot\|_{\mathcal{B}_{t_0,K}}$. Let us denote $g_{t_0,K}$ the unique fixed point provided by the Banach-Picard theorem. We define $g_{T,K}$ on $\Omega_{t_0,K}$ by $g_{T,K|\Omega_{t_0,K}} = g_{t_0,K}$. Then, we can use this function as the initial condition instead of f and apply the same argument on the space of the

functions of $\mathcal{B}_{T,K}$ restricted to $\Omega_{t_0,Ke^{-t_0}} \subset \Omega_{2t_0,K}$, endowed with the norm $\|\cdot\|_{\mathcal{B}_{t_0,Ke^{-t_0}}}$, in order to obtain a fixed point denoted $g^1_{t_0,Ke^{-t_0}}$ in this space. For $(t,x) \in \Omega_{t_0,Ke^{-t_0}}$, we set $g_{T,K}(t+t_0,x) = g^1_{t_0,Ke^{-t_0}}(t,x)$, and then get that $g_{T,K}$ is continous on $\Omega_{2t_0,K}$. Repeating the argument leads to the existence of a fixed point $g_{T,K}$ defined on $\Omega_{T,K}$. The uniqueness provided at each step by the Banach-Picard theorem ensures that the fixed point in $\mathcal{B}_{T,K}$ obtained is unique.
If the initial data f is nonnegative on $(0,K)$, then $g_{T,K}$ is nonnegative on $\Omega_{T,K}$, since Γ preserves this property. Similarly, the fixed point inherits continuity from the initial condition, because the set of continuous nonnegative functions on $\Omega_{T,K}$ endowed with the norm $\|\cdot\|_{\mathcal{B}_{T,K}}$ is a Banach space. For $T' > T > 0$ and $K' > K > 0$, we have $g_{T',K'|\Omega_{T,K}} = g_{T,K}$, by uniqueness of the fixed point. This allows to define $\bar{g} \in \mathcal{B}_{loc}([0,\infty)\times(0,\infty))$ by setting $\bar{g}_{|\Omega_{T,K}} = g_{T,K}$ for any $T,K > 0$. Clearly $\bar{g}$ is the unique fixed point of Γ in $\mathcal{B}_{loc}([0,\infty)\times(0,\infty))$, and is nonnegative / continuous when f is so.
Unlike continuity and nonnegativity, differentiability is not propagated from the initial condition to the fixed point straightforwardly, due to the fact that endowed with the norm $\|\cdot\|_{\mathcal{B}_{T,K}}$, the subspace of differentiable functions is not a Banach subspace of $\mathcal{B}_{T,K}$. To obtain a similar result, we treat this case separately. We can perform the fixed point method in the $\Gamma-$invariant subset $\mathcal{B}_{T,K} \cap C^1(\Omega_{T,K}) \cap \{g,\ g(0,\cdot) = f\}$, endowed with the norm

$$\|g\|_{\mathcal{C}^1_{T,K}} = \|g\|_{\mathcal{B}_{T,K}} + \|\partial_t g\|_{\mathcal{B}_{T,K}} + \|x\partial_x g\|_{\mathcal{B}_{T,K}}.$$

First of all, we derive (2.11) with respect to t, and after changing variables again obtain

$$\begin{aligned}
\partial_t(\Gamma g)(t,x) &= \left[xe^t f'(xe^t) - B(xe^t)f(xe^t)\right] e^{-\int_0^t B(xe^s)\,\mathrm{d}s} \\
&\quad + 2B(xe^t)e^{-\int_0^t B(xe^s)\,\mathrm{d}s} g(0,\frac{xe^t}{2}) + 2\int_0^t B(xe^\tau)e^{-\int_0^\tau B(xe^s)\,\mathrm{d}s}\partial_t g(t-\tau,\frac{xe^\tau}{2})\,\mathrm{d}\tau \\
&= \mathcal{A}f(xe^t)e^{-\int_0^t B(xe^s)\,\mathrm{d}s} + 2\int_0^t B(xe^\tau)e^{-\int_0^\tau B(xe^s)\,\mathrm{d}s}\partial_t g(t-\tau,\frac{xe^\tau}{2})\,\mathrm{d}\tau \qquad (2.12)
\end{aligned}$$

since $g(0,\cdot) = f$. To obtain a useful expression for the derivative of Γg with respect to x, we use an integration by parts. Deriving (2.11) with respect to x and then changing variables, we obtain

$$\begin{aligned}
&x\partial_x(\Gamma g)(t,x) \\
&= \left[xe^t f'(xe^t) - \left(B(xe^t) - B(x)\right) f(xe^t)\right] e^{-\int_0^t B(xe^s)\,\mathrm{d}s} \\
&\quad + 2B(x)\int_0^t B(xe^\tau)e^{-\int_0^\tau B(xe^s)\,\mathrm{d}s} g(t-\tau,\frac{xe^\tau}{2})\,\mathrm{d}\tau \\
&\qquad + 2\int_0^t B(xe^\tau)e^{-\int_0^\tau B(xe^s)\,\mathrm{d}s}\partial_t g(t-\tau,\frac{xe^\tau}{2})\,\mathrm{d}\tau \\
&\qquad\quad + 2\left(B(xe^t)e^{-\int_0^t B(xe^s)\,\mathrm{d}s} g(0,\frac{xe^t}{2}) - B(x)g(t,\frac{x}{2})\right) \\
&= \left[xe^t f'(xe^t) - \left(B(xe^t) - B(x)\right) f(xe^t)\right] e^{-\int_0^t B(xe^s)\,\mathrm{d}s} \\
&\quad + 2B(x)\left(g(t,\frac{x}{2}) - e^{-\int_0^t B(xe^s)\,\mathrm{d}s} g(0,\frac{xe^t}{2})\right. \\
&\qquad \left. - \int_0^t e^{-\int_0^\tau B(xe^s)\,\mathrm{d}s}\left[\partial_t g(t-\tau,\frac{xe^\tau}{2}) - \frac{xe^\tau}{2}\partial_x g(t-\tau,\frac{xe^\tau}{2})\right]\,\mathrm{d}\tau\right) \\
&\qquad + 2\int_0^t B(xe^\tau)e^{-\int_0^\tau B(xe^s)\,\mathrm{d}s}\partial_t g(t-\tau,\frac{xe^\tau}{2})\,\mathrm{d}\tau \\
&\qquad\quad + 2\left(B(xe^t)e^{-\int_0^t B(xe^s)\,\mathrm{d}s} g(0,\frac{xe^t}{2}) - B(x)g(t,\frac{x}{2})\right)
\end{aligned}$$

$$= \mathcal{A}f(xe^t)e^{-\int_0^t B(xe^s)\,\mathrm{d}s} + B(x)\left(e^{-\int_0^t B_n(xe^s)\,\mathrm{d}s}\left[f(xe^t) - 2f(\frac{xe^t}{2})\right]\right.$$
$$\left. + 2\int_0^t e^{-\int_0^\tau B(xe^s)\,\mathrm{d}s}\left[\partial_t g(t-\tau, \frac{xe^\tau}{2}) - \frac{xe^\tau}{2}\partial_x g(t-\tau, \frac{xe^\tau}{2})\right]\,\mathrm{d}\tau\right)$$
$$+ 2\int_0^t B(xe^\tau)e^{-\int_0^\tau B(xe^s)\,\mathrm{d}s}\partial_t g(t-\tau, \frac{xe^\tau}{2})\,\mathrm{d}\tau,$$

using again the fact that $g(0,\cdot) = f$. Finally, for $0 \leqslant t \leqslant t_0 \leqslant T$, we obtain

$$\|\Gamma g_1 - \Gamma g_2\|_{\mathcal{C}^1_{t_0,K}} \leqslant \underbrace{\left(2\left(1 - e^{t_0 \sup_{(0,K)} B(x)}\right) + t_0 \sup_{(0,K)} B(x)\right)}_{<1 \text{ when } t_0 \text{ is small enough}} \|g_1 - g_2\|_{\mathcal{C}^1_{t_0,K}},$$

so we proved the existence of a unique $\mathcal{C}^1$ fixed point in the space of functions of $\mathcal{B}_{T,K}$ restricted to $\Omega_{t_0,K}$, for t_0 small enough. The $\mathcal{C}^1$ regularity, first on $\Omega_{T,K}$ and then on $[0,\infty)\times(0,\infty)$, is proved with the same argument we used to propagate continuity, so when f is continuously differentiable, so is the fixed point $\bar{g} \in \mathcal{B}_{loc}([0,\infty)\times(0,\infty))$. Finally, $\bar{g}$ is the unique solution to (**??**) in the classical sense, *i.e.* satisfies $\partial_t \bar{g} = \mathcal{A}\,\bar{g}$. □

Now, we define a family of linear operators $(M_t)_{t\geqslant 0}$ in order to express the fixed point $\bar{g}$ as a semigroup acting on the initial condition, and collect some properties satisfied by this semigroup, straightforwardly deduced from this lemma.

Proposition 21. *Under assumption* (A2)*, the family of operators* $(M_t)_{t\geqslant 0}$ *defined on* $\mathcal{B}^0_{loc}((0,\infty))$ / $\mathcal{B}^0_{loc}((0,\infty)) \cap \mathcal{C}(0,\infty)$ / $\mathcal{B}^0_{loc}((0,\infty)) \cap \mathcal{C}^1(0,\infty)$ *by* $M_t f = \bar{g}(t,\cdot)$ *is a positive semigroup. Additionally, if* $f \in \mathcal{B}^0_{loc} \cap \mathcal{C}^1(0,\infty)$*, then for all* $t > 0$*, one has*

$$\partial_t M_t f = \mathcal{A}M_t f = M_t \mathcal{A}f.$$

Finally, the rescaled semigroup $(e^{-t}M_t)_{t\geqslant 0}$ *is a contraction in* E*.*

Démonstration. For technical details, adapt the proof of the equivalent result from [81]. Using again the uniqueness of the fixed point we readily verify that M_t is a linear operator, and that the family $(M_t)_{t\geqslant 0}$ has the semigroup property. The subspaces $\mathcal{B}^0_{loc}$, $\mathcal{B}^0_{loc} \cap \mathcal{C}(0,\infty)$ and $\mathcal{B}^0_{loc} \cap \mathcal{C}^1(0,\infty)$ are invariant under M_t, and if $f \in \mathcal{B}^0_{loc} \cap \mathcal{C}^1$ then $\partial_t M_t f = \mathcal{A}M_t f$. Additionally if $f \in \mathcal{B}^0_{loc} \cap \mathcal{C}^1(0,\infty)$ then $\mathcal{A}f \in \mathcal{B}^0_{loc} \cap \mathcal{C}(0,\infty)$ and we have, still by uniqueness of the fixed point, $\partial_t M_t f = M_t \mathcal{A}f$. The Lemma above also provides that M_t is positive, and since we easily check that $M_t x = xe^t$ we deduce that if $|f(x)| \leqslant Cx$, *i.e.* if $f \in E$, then $|M_t f(x)| \leqslant M_t|f|(x) \leqslant Cxe^t$. In other words we have for all $t \geqslant 0$

$$\|M_t f\| \leqslant e^t \|f\|.$$

□

We now give another useful property of the semigroup, about how it behaves with respect to an increasing sequence of nonnegative Borel functions.

Lemma 22. *Assume assumption* (A2) *is satisfied. Let* $(f_n)_{n\in\mathbb{N}}$ *be an increasing sequence of nonnegative functions of* $\mathcal{B}^0_{loc}(0,\infty)$*. Denote*

$$f(x) = \lim_{n\to\infty} \uparrow f_n(x)$$

its pointwise increasing limit in $\overline{\mathbb{R}}$*. If the limit* f *lies in* $\mathcal{B}^0_{loc}(0,\infty)$*, then*

$$\forall t \geqslant 0, \quad \lim_{n\to\infty} M_t f_n = M_t \lim_{n\to\infty} f_n.$$

In other words, the semigroup preserves the increasing limit.

Démonstration. Let $(f_n)_{n\in\mathbb{N}}$ be an increasing sequence of nonnegative functions in $\mathcal{B}^0_{loc}(0,\infty)$. By the properties collected in the previous propositon, $(M_t f_n)_{n\in\mathbb{N}}$ is also an increasing sequence of functions $\mathcal{B}^0_{loc}(0,\infty)$. Thanks to the monotonous convergence theorem, both $(f_n)_{n\in\mathbb{N}}$ and $(M_t f_n)_{n\in\mathbb{N}}$ have increasing limits, respectively denoted f and g_t. If $f \in \mathcal{B}^0_{loc}(0,\infty)$, then the positivity of the semigroup and another use of the monotonous convergence theorem provide that

$$g_t(x) = f(xe^t)e^{-\int_0^t B(xe^s)\,\mathrm{d}s} + 2\int_0^t B(xe^\tau)e^{-\int_0^\tau B(xe^s)\,\mathrm{d}s} g_{t-\tau}(\frac{xe^\tau}{2})\,\mathrm{d}\tau$$

Finally, the uniqueness of the fixed point of Γ provides that $g_t(x) = M_t f(x)$ for all $(t,x) \in \mathbb{R}^2_+$, which is the claimed result. □

2.2.3 Construction of a measure solution

In this section, we construct a measure solution to (2.3). The first step consists in defining a left semigroup, still denoted $(M_t)_{t\geqslant 0}$, acting on $\dot{\mathcal{M}}$. To do so, we start by defining a left semigroup on $\dot{\mathcal{M}}_+$ and prove some properties on it.
For $t \geqslant 0$ and $\mu \in \dot{\mathcal{M}}_+$, we define a function from the measurable sets of $(0,\infty)$ onto $[0,\infty)$ by

$$\mu M_t : A \mapsto \int_0^\infty M_t(\mathbb{1}_A)\,\mathrm{d}\mu. \tag{2.13}$$

For every measurable set A, the resulting indicator function $\mathbb{1}_A$ is a bounded Borel function, so $M_t(\mathbb{1}_A)$ is too, thanks to Lemma 20, so the function defined by (2.13) is well-defined. Now, we prove some properties satisfied by this function.

Lemma 23. *Under hypothesis* (A2)*, for all $\mu \in \dot{\mathcal{M}}_+$ and all $t \geqslant 0$, μM_t defines a positive measure.*

Démonstration. Clearly $\mu M_t(\emptyset) = \int_0^\infty M_t\mathbf{0}\,\mathrm{d}\mu = 0$ since the null function is a fixed point of Γ for a null initial value.
Let $(A_n)_{n\in\mathbb{N}}$ be a countable sequence of pairwise disjoint measurable sets of $(0,\infty)$ and define $f_n = \sum_{k=0}^n \mathbb{1}_{A_k} = \mathbb{1}_{\bigsqcup_{k=0}^n A_k}$. For every measure $\mu \in \dot{\mathcal{M}}_+$ and integer n, one has the equality

$$(\mu M_t)\left(\bigsqcup_{k=0}^n A_k\right) = \int_0^\infty M_t(\mathbb{1}_{\bigsqcup_{k=0}^n A_k})\,\mathrm{d}\mu = \sum_{k=0}^n \int_0^\infty M_t(\mathbb{1}_{A_k})\,\mathrm{d}\mu = \sum_{k=0}^n (\mu M_t)(A_k).$$

thanks to the linearity of the operator M_t and Fubini's theorem. The sequence f_n is increasing and has the limit $f = \sum_{k=0}^\infty \mathbb{1}_{A_k}$, and thanks to lemma 22 the sequence $(M_t f_n)_{n\in\mathbb{N}}$ has the same properties, so the monotnous convergence theorem ensures that

$$\lim_{n\to\infty} \int_0^\infty M_t(\mathbb{1}_{\bigsqcup_{k=0}^n A_k})\,\mathrm{d}\mu = \int_0^\infty M_t(\mathbb{1}_{\bigsqcup_{k=0}^\infty A_k}).$$

Since all terms of the sum

$$\sum_{k=0}^n (\mu M_t)(A_k)$$

are nonnegative, this last quantity tends to

$$\sum_{k=0}^\infty (\mu M_t)(A_k) \in \overline{\mathbb{R}}$$

as n tends toward infinity. □

Now we prove a duality relation between the left and right semigroups for $\mu \in \dot{\mathcal{M}}_+$. Since μM_t is a positive measure, one has by definition, for every Borel set $A \subset (0,\infty)$

$$\int_0^\infty \mathbb{1}_A\,\mathrm{d}(\mu M_t) = \mu M_t(A),$$

which leads to the following lemma.

Lemma 24. *Under hypothesis* (A2)*, for all* $\mu \in \dot{\mathcal{M}}_+$ *and all* $t \geqslant 0$*, the measure* μM_t *lies in* $\dot{\mathcal{M}}_+$ *and*

$$\forall f \in \dot{\mathcal{B}}, \qquad (\mu M_t)f = \mu(M_t f), \qquad i.e. \qquad \int_0^\infty f \,\mathrm{d}(\mu M_t) = \int_0^\infty M_t f \,\mathrm{d}\mu. \tag{2.14}$$

Démonstration. To start, we show this equality for nonnegative simple functions. Let $g = \sum_{k=0}^n \alpha_k \mathbb{1}_{A_k}$, with $\alpha_k \geqslant 0$ for all $0 \leqslant k \leqslant n$. By definition of the integral of simple functions, and thanks to Fubini's theorem, one has

$$\begin{aligned}
\int_{(0,\infty)} g \,\mathrm{d}(\mu M_t) &= \sum_{k=0}^n \alpha_k (\mu M_t)(A_k) \\
&= \sum_{k=0}^n \alpha_k \int_{(0,\infty)} M_t \mathbb{1}_{A_k} \,\mathrm{d}\mu \\
&= \int_{(0,\infty)} M_t \left(\sum_{k=0}^n \alpha_k \mathbb{1}_{A_k} \right) \mathrm{d}\mu \\
&= \int_{(0,\infty)} M_t g \,\mathrm{d}\mu.
\end{aligned}$$

Now let $f \in \dot{\mathcal{B}}$ being nonnegative, g a simple function and $C > 0$ a constant such that $0 \leqslant g \leqslant f \leqslant C\phi$. By positivity of the semigroup, one has $0 \leqslant M_t g \leqslant M_t f \leqslant C\phi$, and since μ is a positive measure, we obtain

$$\int_0^\infty M_t g \,\mathrm{d}\mu \leqslant \int_0^\infty M_t f \,\mathrm{d}\mu \leqslant C \int_0^\infty M_t \phi \,\mathrm{d}\mu,$$

and then

$$\int_0^\infty g \,\mathrm{d}(\mu M_t) \leqslant \int_0^\infty M_t f \,\mathrm{d}\mu \leqslant C e^t \mu\phi < \infty.$$

Taking the supremum over nonnegative simple functions g lower that f, we deduce

$$\int_0^\infty f \,\mathrm{d}(\mu M_t) \leqslant \int_0^\infty M_t f \,\mathrm{d}\mu < \infty,$$

and this inequality with $f = \phi$ ensures that $\mu M_t \in \dot{\mathcal{M}}_+$.
To obtain the converse inequality, let $f \in \dot{\mathcal{B}}$, g a simple function and $\varepsilon > 0$ such that $0 \leqslant f \leqslant g + \varepsilon\phi$. The same kind of computations than previously used provide

$$\int_{(0,\infty)} M_t f \,\mathrm{d}\mu \leqslant \int_{(0,\infty)} f \,\mathrm{d}(\mu M_t) + \varepsilon e^t \mu\phi.$$

The positive number ε being arbitrary, the claimed result is proved for nonnegative functions. The general case is obtain using the decomposition of a function $f \in \dot{\mathcal{B}}$ in a nonnegative and a nonpositive part, and the linearity of the semigroup and of the integral. □

A straightforward corollary is that the operator $\mu \mapsto \mu M_t$ we defined is left semigroup on $\dot{\mathcal{M}}_+$. Now, we define an operator on $\dot{\mathcal{M}}$ by $\mu \mapsto \mu M_t = \mu_1 M_t - \mu_2 M_t$, with $\mu = \mu_1 - \mu_2$ any representant of the equivalence class of μ. This operator is compatible with the equivalence relation defined on $\dot{\mathcal{M}}_+ \times \dot{\mathcal{M}}_+$ and defines a left semigroup on the space of weighted signed measures, for which relation (2.14) holds true.

Proposition 25. *The left semigroup* M_t *is positive, and satisfies*
— $\mu \geqslant 0 \qquad \Rightarrow \qquad \|\mu M_t\|_{\dot{\mathcal{M}}} = e^t \|\mu\|_{\dot{\mathcal{M}}}$,
— $\forall \mu \in \dot{\mathcal{M}}, \qquad \|\mu M_t\|_{\dot{\mathcal{M}}} \leqslant e^t \|\mu\|_{\dot{\mathcal{M}}}$.

Démonstration. It is a consequence of Lemma 20. Let $\mu \geqslant 0$. For any $f \geqslant 0$, one has $(\mu M_t)f = \mu(M_t f) \geqslant 0$. Additionally,

$$\|\mu M_t\|_{\dot{\mathcal{M}}} = \int_0^\infty \phi \, \mathrm{d}(\mu M_t) = \int_0^\infty M_t\phi \, \mathrm{d}\mu = e^t \int_0^\infty \phi \, \mathrm{d}\mu = e^t \|\mu\|_{\dot{\mathcal{M}}}.$$

Now let $\mu \in \dot{\mathcal{M}}$ and consider the rescaled semigroup $(e^{-t}M_t)_{t\geqslant 0}$, which is a contraction. One has

$$\|\mu(e^{-t}M_t)\|_{\dot{\mathcal{M}}} = \sup_{\|f\|\leqslant 1} |\mu(e^{-t}M_t)f| \leqslant \sup_{\|g\|\leqslant 1} |\mu g| = \|\mu\|_{TV_\phi}.$$

□

We are now ready to state and prove the result of existence et uniqueness of a measure solution, in term of left semigroup. The proof is an adaptation of the one provided in [81].

Theorem 26. *Under hypothesis* (A2)*, for any $\mu^{in} \in \dot{\mathcal{M}}$, the orbit map $t \mapsto \mu^{in}M_t$ is the unique measure solution to Equation* (2.3)*.*

Démonstration. Narrow continuity : let $\mu \in \dot{\mathcal{M}}$. First, we check that $t \mapsto \mu M_t$ is narrowly continuous. Let $f \in E$.

$$|\mu M_t f - \mu f| \leqslant \left| \int_0^\infty f(xe^t)e^{-\int_0^t B(xe^s)\,\mathrm{d}s} \, \mathrm{d}\mu(x) - \mu f \right| + \left| \mu\left(2\int_0^t B(xe^\tau)e^{-\int_0^\tau B(xe^s)\,\mathrm{d}s} M_{t-\tau} f(\frac{xe^\tau}{2}) \, \mathrm{d}\tau \right) \right|$$

the first term of the righthand side vanishes as t tends toward 0 by dominated convergence. For the second, we have the estimate

$$\left| \mu\left(2\int_0^t B(xe^\tau)e^{-\int_0^\tau B(xe^s)\,\mathrm{d}s} M_{t-\tau} f(\frac{xe^\tau}{2}) \, \mathrm{d}\tau \right) \right| \leqslant e^t \|f\| |\mu| \left(x(1 - e^{-\int_0^t B(xe^s)\,\mathrm{d}s}) \right).$$

Since the integrand vanishes ponctualy as t tends toward 0 and is bounded in absolute value by ϕ, which is $\mu-$integrable, the dominated convergence theorem states that $\mu\left(x(1 - e^{-\int_0^t B(xe^s)\,\mathrm{d}s}) \right)$ vanishes.
Solution : for $f \in \mathcal{C}_c^1(0,\infty)$, one has

$$M_t f = f + \int_0^t \partial_s M_s f \, \mathrm{d}s = f + \int_0^t M_s \mathcal{A} f \, \mathrm{d}s.$$

Since f is continuously differentiable and compactly supported, the function $\mathcal{A}f$ is continuous and compactly supported, and thus is bounded in norm $\|\cdot\|$. Then the estimate $|M_s(\mathcal{A}f)| \leqslant e^s \|\mathcal{A}f\| \phi$ holds for every nonnegative real number s, and we can apply Fubini's theorem to obtain

$$\mu\left(\int_0^t M_s \mathcal{A} f \, \mathrm{d}s \right) = \int_0^t (\mu M_s)\mathcal{A} f \, \mathrm{d}s,$$

from which we easily deduce that $t \mapsto \mu M_t$ satisfies (2.8).
Uniqueness : we want to check that if $t \mapsto \mu_t$ is a measure solution to Equation (2.3), then $\mu_t = \mu^{\mathrm{in}} M_t$ for all $t \geqslant 0$. We follow the framework of [64]. For $t > 0$ fixed and $f \in C_c^1(0,\infty)$ consider the mapping

$$s \mapsto \int_0^s \mu_\tau M_{t-s} f \, \mathrm{d}\tau$$

defined on $[0,t]$ and compute its derivative. For $0 < s < s+h < t$ we have

$$\frac{1}{h}\left[\int_0^{s+h} \mu_\tau \; M_{t-s-h} f \, \mathrm{d}\tau - \int_0^s \mu_\tau M_{t-s} f \, \mathrm{d}\tau \right] =$$
$$\frac{1}{h}\int_s^{s+h} \mu_\tau M_{t-s} f \, \mathrm{d}\tau + \int_s^{s+h} \mu_\tau \frac{M_{t-s-h} f - M_{t-s} f}{h} \, \mathrm{d}\tau + \int_0^s \mu_\tau \frac{M_{t-s-h} f - M_{t-s} f}{h} \, \mathrm{d}\tau.$$

The convergence of the first term is a consequence of the narrow continuity of $t \mapsto \mu_t$

$$\frac{1}{h}\int_s^{s+h} \mu_\tau M_{t-s} f \, \mathrm{d}\tau \xrightarrow[h\to 0]{} \mu_s M_{t-s} f.$$

To deal ith the second term, we begin with the computation

$$\frac{M_{t-s-h}f - M_{t-s}f}{h} = -M_{t-s-h}\frac{M_h f - f}{h} = -M_{t-s-h}\frac{1}{h}\int_0^h \partial_\tau M_\tau f \, \mathrm{d}\tau = -M_{t-s-h}\frac{1}{h}\int_0^h M_\tau \mathcal{A} f \, \mathrm{d}\tau,$$

thus

$$\left\| \frac{M_{t-s-h}f - M_{t-s}f}{h} \right\| \leqslant e^{t-s-h}\|\mathcal{A}f\|\frac{1}{h}\int_0^h e^\tau \, \mathrm{d}\tau = e^{t-s-h}\|\mathcal{A}f\|\frac{e^h - 1}{h} \leqslant e^{t-s}\|\mathcal{A}f\|.$$

Since for all $f \in E$ with $\|f\| \leqslant 1$ and all $\tau \in [0,t]$ one has $|\mu_\tau f| < \infty$, the narrow continuity of $t \mapsto \mu_t$ implies

$$\forall f \in E \text{ with } \|f\| \leqslant 1, \qquad \sup_{\tau\in[0,t]} |\mu_\tau f| < \infty,$$

so the uniform boundness principle states that $\sup_{\tau\in[0,t]} \|\mu_\tau\| < \infty$, so we obtain

$$\left| \int_s^{s+h} \mu_\tau \frac{M_{t-s-h}f - M_{t-s}f}{h} \, \mathrm{d}\tau \right| \leqslant h \sup_{\tau\in[0,t]} \|\mu_\tau\|_{\dot{\mathcal{M}}} e^{t-s}\|\mathcal{A}f\| \xrightarrow[h\to 0]{} 0.$$

For the last term we have by dominated convergence, using that $\partial_t M_t f = \mathcal{A} M_t f$,

$$\int_0^s \mu_\tau \frac{M_{t-s-h}f - M_{t-s}f}{h} \, \mathrm{d}\tau \xrightarrow[h\to 0]{} -\int_0^s \mu_\tau \mathcal{A} M_{t-s} f \, \mathrm{d}\tau.$$

Finally we get

$$\frac{\mathrm{d}}{\mathrm{d}s}\int_0^s \mu_\tau M_{t-s} f \, \mathrm{d}\tau = \mu_s M_{t-s} f - \int_0^s \mu_\tau \mathcal{A} M_{t-s} f \, \mathrm{d}\tau = \mu^{\mathrm{in}} M_{t-s} f$$

Integrating between $s = 0$ and $s = t$ we obtain

$$\int_0^t \mu_\tau f \, \mathrm{d}\tau = \int_0^t \mu^{\mathrm{in}} M_{t-s} f \, \mathrm{d}s = \int_0^t \mu^{\mathrm{in}} M_\tau f \, \mathrm{d}\tau$$

and then by differentiation with respect to t

$$\mu_t f = \mu^{\mathrm{in}} M_t f.$$

□

2.3 Long time asymptotics

To obtain the long time asymptotic behaviour of the measure solution to Equation (2.8), we first study this behaviour for the adjoint Equation. To do so, we will need to consider complex functions. Let $E^{\mathbb{C}} := \{f : \mathbb{R} \to \mathbb{C} \mid \Re(f),\ \Im(f) \in E\}$. By linearity, we extend the right semigroup to this space. We endow $E^{\mathbb{C}}$ with the norm

$$f \in E^{\mathbb{C}} \mapsto \sup_{x>0} \frac{|f(x)|}{x}$$

where $|\cdot|$ now denotes the module instead of the absolute value. We will still denote this norm $\|\cdot\|$. To adapt the eigentriplets (2.6) fro our case, we need to define weighted complex measures. A natural way do it *repose sur* the linearity of the left semigroup $(M_t)_{t\geqslant 0}$, as we did for the right semigroup to extend it to complex-valued functions. Thus we define the set $\dot{\mathcal{M}}^{\mathbb{C}} := \dot{\mathcal{M}} + i\dot{\mathcal{M}}$ of weighted complex-valued measures such that both their real and imaginary parts belong to $\dot{\mathcal{M}}$. From Theorem 16, we obtain that

for every $k \in \mathbb{Z}$, both $\cos(2k\pi\frac{\text{Log } x}{\text{Log } 2})\mathcal{U}(x)\,\mathrm{d}x$ and $\sin(2k\pi\frac{\text{Log } x}{\text{Log } 2})\mathcal{U}(x)\,\mathrm{d}x$ are measures lying in $\dot{\mathcal{M}}$, so the complex-valued function ν_k defined on Borel sets of $(0,\infty)$ by

$$\nu_k(\mathrm{d}x) = x^{-\frac{2ik\pi}{\text{Log } 2}}\mathcal{U}(x)\,\mathrm{d}x$$

defines an element of $\dot{\mathcal{M}}^{\mathbb{C}}$. Additionally, we denote for all integers

$$\lambda_k = 1 + \frac{2ik\pi}{\text{Log } 2}, \qquad \phi_k(x) = x^{1+\frac{2ik\pi}{\text{Log } 2}}.$$

Straightforward computations lead to the fact that ϕ_k and ν_k are invariant under the rescaled semigroup $e^{-\lambda_k t}M_t$, for all $k \in \mathbb{Z}$. This corresponds to the conservation laws stated in [14]. Contrary to this article, the framework here is not a L^2 space, thus not allowing us to make use of the Fourier theory. Instead, our method relies crucially on the duality relation (2.14), since the large time asymptotic is obtained on solutions of (2.9) which initial condition lies in a subset of E, and then transposed to solutions of (2.8). Indeed, since functions belonging to E are continuous, we can apply a generalized entropy inequality to get long time behaviour for solutions of the adjoint problem.
In the first subsection, apply this strategy to obtain the asymptotic behaviour mentionned above. The subsequent subsection is dedicated to the transposition of this behaviour from functions in $\mathcal{C}^1_c(0,\infty)$ to measures.

2.3.1 Asymptotic behaviour of solutions of the adjoint problem

Unlike the situation described in [14], our framework is not a Hilbert space, so the theory of Fourier series is not useable in the present context. To deal with this difficuly, we call upon the theory of Fejèr sums (*i.e. :* Cesàro means of the Fourier series).

We introduce the subset $X := \overline{\text{span}}\,\{\phi_l, l \in \mathbb{Z}\}$. This vector subspace can be expressed through a homogeneity relation, as stated in the lemma 27.

Lemma 27. *We have*

$$X = \left\{f \in E^{\mathbb{C}}, \quad \forall x > 0,\ f(2x) = 2f(x)\right\}.$$

Démonstration. The vector subspace

$$\left\{f \in E^{\mathbb{C}}, \quad \forall x \in (0,\infty),\ f(2x) = 2f(x)\right\}$$

is closed for the norm $\|\cdot\|$ and contains every functions ϕ_k, so X is included in this set. To obtain the converse inclusion, consider an element f of this set. We can write

$$f(x) = \frac{f}{\phi}(x)\phi(x) =: \theta(\text{Log } x)\phi(x),$$

with θ a continuous Log $2-$periodic function. The Fejér theroem ensures that the Fejér sum

$$y \in \mathbb{R} \mapsto \sigma_N(f)(y) := \sum_{n=-N}^{N}\left(1 - \frac{|n|}{N}\right)\hat{\theta}(n)e^{\frac{2in\pi}{\text{Log } 2}y},$$

where

$$\hat{\theta}(n) = \frac{1}{\text{Log } 2}\int_0^{\text{Log } 2}\theta(y)e^{-\frac{2in\pi}{\text{Log } 2}y}\,\mathrm{d}y$$

is bounded for all N and converges uniformly on $[0, \text{Log } 2]$ to θ. We deduce that the sequence indexed by N

$$F_N(f) : x \in (0,\infty) \mapsto \phi(x)\sigma_N(\theta)(\text{Log } x) = \sum_{n=-N}^{N}\left(1 - \frac{|n|}{N}\right)\hat{\theta}(n)\phi_n(x) \in \text{span}\,\{\phi_l, l \in \mathbb{Z}\}$$

belongs to $E^{\mathbb{C}}$ and converges to f in norm $\|\cdot\|$. □

Remark : another expression of the space X is possible, closer to the one given in [14], which is

$$X = \left\{ f \in E^{\mathbb{C}}, \quad \forall x \in (0,\infty),\ \frac{f(2x)}{\phi(2x)} = \frac{f(x)}{\phi(x)} \right\}.$$

The sum given by the linear operator $F_N : X \to \operatorname{span}\{\phi_k, |k| \leqslant N\}$ is not strictly speaking a Fejèr sum, yet we will keep this designation in the sequel. For further results, we will need a slightly different expression of F_N, which is provided by the following lemma.

Lemma 28. *Let $f \in X$ and θ a* Log $2-$*periodic function such that $f = \phi \times (\theta \circ log)$. For all $l \in \mathbb{Z}$, one has $\nu_l f = \hat{\theta}(l)$.*

Démonstration. Let $l \in \mathbb{Z}$. For all positive integer N, one has

$$\nu_l F_N(f) = \begin{cases} 0 \text{ if } N < |l|, \\ \left(1 - \frac{|l|}{N}\right) \hat{\theta}(l) \text{ otherwise.} \end{cases}$$

For N large enough, we obtain the estimate $\left|\nu_l f - \hat{\theta}(l)\right| \leqslant \|f - F_N(f)\| + \frac{|l|}{N}\|f\|$, so letting $N \to \infty$ provides the claimed result. □

Thanks to this lemma, we can extend the definition of the operator F_N to the whole space E with the expression

$$F_N(f) = \sum_{n=-N}^{N} \left(1 - \frac{|n|}{N}\right) (\nu_n f)\phi_n$$

We will now relate the space X to the set of the functions that are in the kernel of the entropy dissipation associated to Equation (2.9).

Lemma 29 (Generalized Relative Entropy)**.** *Let $f \in \mathcal{C}_c^1(0,\infty)$ and $H : \mathbb{R} \to (0,\infty)$ a positive, differentiable and convex function. Then we have*

$$\frac{\mathrm{d}}{\mathrm{d}t} \int_0^\infty \phi N H\left(\frac{e^{-t}M_t f}{\phi}\right) \mathrm{d}x = -D^H[e^{-t}M_t f] \leqslant 0,$$

with D^H defined on $\dot{\mathcal{B}}$ by

$$D^H[f] = \int_0^\infty \phi(x) B(x) \mathcal{U}(x) \underbrace{\left[H'\left(\frac{f}{\phi}(x)\right)\left(\frac{f}{\phi}(x) - \frac{f}{\phi}(x/2)\right) + H\left(\frac{f}{\phi}(x/2)\right) - H\left(\frac{f}{\phi}(x)\right)\right]}_{\geqslant 0} \mathrm{d}x.$$

Although the inequality is here obtained from the dual equation (2.9) instead the classical size equation (2.3), the computations are completely similar to the usual case.

Démonstration. Let $f \in \mathcal{C}_c^1(0,\infty)$. A straightforward computation show that

$$\left(\frac{\partial}{\partial t} - x\frac{\partial}{\partial x}\right)\left(\frac{e^{-t}M_t f}{\phi}\right)(x) = B(x)\left(\frac{M_t f(x/2)}{\phi(x/2)} - \frac{M_t f(x)}{\phi(x)}\right),$$

from which we deduce

$$\left(\frac{\partial}{\partial t} - x\frac{\partial}{\partial x}\right) H\left(\frac{e^{-t}M_t f}{\phi}\right)(x) = B(x) H'\left(\frac{e^{-t}M_t f}{\phi}\right)(x) \times \left(\frac{M_t f(x/2)}{\phi(x/2)} - \frac{M_t f(x)}{\phi(x)}\right).$$

In addition, one has

$$\frac{\partial}{\partial x}(\phi\mathcal{U}) = \frac{\partial}{\partial x}(x\mathcal{U}) = 4B(2x)\mathcal{U}(2x) - B(x)\mathcal{U}(x) - \mathcal{U}(x),$$

since in this particular case the adjoint eigenvector is equal to the growth rate. Finally, we integrate

$$\begin{aligned}
&\left(\frac{\partial}{\partial t} - x\frac{\partial}{\partial x}\right)\left(\phi\mathcal{U}H\left(\frac{e^{-t}M_t f}{\phi}\right)(x)\right)\\
=&\phi(x)\mathcal{U}(x)\left(\frac{\partial}{\partial t} - x\frac{\partial}{\partial x}\right)H\left(\frac{e^{-t}M_t f}{\phi}\right) - H\left(\frac{e^{-t}M_t f}{\phi}\right)\phi(x)\frac{\partial}{\partial x}(\phi\mathcal{U})\\
=&\phi(x)\mathcal{U}(x)B(x)H'\left(\frac{e^{-t}M_t f}{\phi}\right)(x)\times\left(\frac{M_t f(x/2)}{\phi(x/2)} - \frac{M_t f(x)}{\phi(x)}\right)\\
&- H\left(\frac{e^{-t}M_t f}{\phi}\right)\phi(x)\left(4B(2x)\mathcal{U}(2x) - B(x)\mathcal{U}(x) - \mathcal{U}(x)\right)
\end{aligned}$$

to obtain the claimed result, after integrating by parts and the change of variable $x \leftarrow x/2$. □

Simple computations show that for every $k \in \mathbb{Z}$, one has $D^H[\Re(\phi_k)] = D^H[\Im(\phi_k)] = 0$.
Thanks to Lemma 29, we will prove that the Fejèr sum previously mentionned actually converges for any $f \in \mathcal{C}^1_c(0,\infty)$, and extend this convergence to any $f \in E_0$.

Theorem 30. *Under the hypotheses* (A1)*and* (A2)*. Then for any $f \in \mathcal{C}^1_c(0,\infty)$ and any $t \geqslant 0$ the sum*

$$\sum_{n=-N}^{N}\left(1 - \frac{|n|}{N}\right)(\nu_n f)e^{\frac{2i\pi n}{\mathrm{Log}\ 2}t}\phi_n$$

converges in E and the limit $R_t f$ defines a Log 2*-periodic family of bounded linear operators $R_t : E_0 \to X$.*

Additionally for all $f \in E_0$

$$e^{-t}M_t f - R_t f \xrightarrow[t\to\infty]{} 0$$

locally uniformly on $(0,\infty)$.

Notice that R_t is actually a projector from $E_0 \oplus X$ onto X, but we are not able to prove whether it defines or not a projector on the whole space E.

Démonstration. We know that $e^{-t}M_t$ is a contraction for $\|\cdot\|$. Let $f \in \mathcal{C}^1_c(0,\infty)$. We have $\mathcal{A}f \in E$ and so $\partial_t(e^{-t}M_t f) = M_t(\mathcal{A}f - f)$ is bounded in E. Since $\partial_t M_t f = \mathcal{A}M_t f = x\partial_x M_t f(x) + B(x)(2M_t f(x/2) - M_t f(x))$ and B is locally bounded we deduce that $e^{-t}\partial_x M_t f$ is locally bounded on $(0,\infty)$. So the Arzela-Ascoli theorem ensures that there exists a subsequence of $(e^{-t-k\mathrm{Log}\ 2}M_{t+k\mathrm{Log}\ 2}f(x))_{k\geqslant 0}$ which converges locally uniformly on $[0,\infty)\times(0,\infty)$. The dissipation of entropy for the convex function $H(x) = x^2$, denoted D^2, reads

$$D^2[f] = \int_0^\infty \phi(x)B(x)\mathcal{U}(x)\left|\frac{f}{\phi}(x/2) - \frac{f}{\phi}(x)\right|^2 \mathrm{d}x. \tag{2.15}$$

Thanks to Lemma 29, the quantity

$$\int_0^\infty D^2[e^{-t}M_t f]\,\mathrm{d}t$$

is nonnegative and bounded, and one has

$$\int_0^T D^2[e^{-t-k\mathrm{Log}\ 2}M_{t+k\mathrm{Log}\ 2}f]\,\mathrm{d}t = \int_{k\mathrm{Log}\ 2}^{T+k\mathrm{Log}\ 2} D^2[e^{-t}M_t f]\,\mathrm{d}t \to 0$$

as k tends to infinity. With the form of the entropy dissipation (2.15), we deduce that

$$\frac{e^{-t-k\mathrm{Log}\ 2}M_{t+k\mathrm{Log}\ 2}f}{\phi}(x/2) - \frac{e^{-t-k\mathrm{Log}\ 2}M_{t+k\mathrm{Log}\ 2}f}{\phi}(x) \to 0$$

in the distributional sense. Since $e^{-t-k\mathrm{Log}\ 2}M_{t+k\mathrm{Log}\ 2}f$ converges locally uniformly to $h(t,\cdot)$, we deduce that

$$\frac{h(t,\cdot)}{\phi}(x/2) - \frac{h(t,\cdot)}{\phi}(x) = 0$$

for all t and x, *i.e.* the limit $h(t,\cdot)$ satisfies $h(t,2x)=2h(t,x)$, so it lies in X for all time and

$$h(t,x)=\lim_{N\to\infty}\sum_{n=-N}^{N}\Big(1-\frac{|n|}{N}\Big)(\nu_n h(t,\cdot))\phi_n(x).$$

But the conservation laws

$$\nu_n M_t = e^{(1+\frac{2in\pi}{\mathrm{Log}\ 2})t}\nu_n$$

and the dominated convergence ensure that

$$\nu_n h(t,\cdot)=\lim_{k\to\infty} e^{-t-k\mathrm{Log}\ 2}\nu_n M_{t+k\mathrm{Log}\ 2}f = e^{\frac{2in\pi}{\mathrm{Log}\ 2}t}\nu_n f \tag{2.16}$$

and so

$$h(t,x)=\lim_{N\to\infty}\sum_{n=-N}^{N}\Big(1-\frac{|n|}{N}\Big)(\nu_n f)e^{\frac{2in\pi}{\mathrm{Log}\ 2}t}\phi_n(x).$$

This guarantees that the sum on the right-hand-side is convergent in E and we denote by $R_t f$ its limit. The operator $R_t:\mathcal{C}^1_c(0,\infty)\to X$ thus defined is clearly linear. Moreover by local uniform convergence of $e^{-t-k\mathrm{Log}\ 2}M_{t+k\mathrm{Log}\ 2}f$ to $R_t f$ we get that $\|R_t f\|\leqslant \lim_{k\to\infty}\|e^{-t-k\mathrm{Log}\ 2}M_{t+k\mathrm{Log}\ 2}f\|\leqslant\|f\|$. Thus R_t is bounded and extends uniquely to a bounded linear operator $E_0\to X$. The local uniform convergence of $e^{-t-k\mathrm{Log}\ 2}M_{t+k\mathrm{Log}\ 2}f$ to $R_t f$ for $f\in\mathcal{C}^1_c(0,\infty)$ also guarantees the local uniform convergence of $e^{-t}M_t f - R_t f$ to zero when $t\to+\infty$. Indeed, let K be a compact set of $(0,\infty)$, $k=\lfloor\frac{t}{k\mathrm{Log}\ 2}\rfloor$, $t'=t-k\mathrm{Log}\ 2\in[0,\mathrm{Log}\ 2]$. One has

$$\begin{aligned}\sup_{x\in K}|e^{-t}M_t f(x)-R_t f(x)| &= \sup_{x\in K}|e^{-(k\mathrm{Log}\ 2+t')}M_{k\mathrm{Log}\ 2+t'}f(x)-R_{t'}f(x)|\\ &\leqslant \sup_{x\in K}\sup_{s\in[0,\mathrm{Log}\ 2]}|e^{-(k\mathrm{Log}\ 2+s)}M_{k\mathrm{Log}\ 2+s}f(x)-R_s f(x)|\end{aligned}$$

This convergence extends to any $f\in E_0$ by density. □

Corollary 31. *Let $f\in E_0\oplus X$. Then*

$$I_t:=\frac{1}{\mathrm{Log}\ 2}\int_t^{t+\mathrm{Log}\ 2} e^{-s}M_s f\,\mathrm{d}s \qquad \textit{and} \qquad \frac{1}{t}\int_0^t e^{-s}M_s f\,\mathrm{d}s$$

converge locally uniformly to $(\nu_0 f)\phi$.

Démonstration. Let $f\in E_0\oplus X$, so $R_t f$ lies in the set X for all $t\geqslant 0$. A straithforward computation, associated to the identity (2.16), leads to the equality

$$\frac{1}{\mathrm{Log}\ 2}\int_t^{t+\mathrm{Log}\ 2} F_N(R_s f)\,\mathrm{d}s=(\nu_0(R_t f))\phi=(\nu_0 f)\phi$$

for all positive integer N. We deduce

$$\left\|\frac{1}{\mathrm{Log}\ 2}\int_t^{t+\mathrm{Log}\ 2} R_s f\,\mathrm{d}s-(\nu_0 f)\phi\right\|\leqslant\frac{1}{\mathrm{Log}\ 2}\int_t^{t+\mathrm{Log}\ 2}\|R_s f-F_N(R_s f)\|\,\mathrm{d}s\leqslant\sup_{s\in[0,\mathrm{Log}\ 2]}\|R_s f-F_N(R_s f)\|$$

since the family of operators $(R_t)_{t\geqslant 0}$ is Log 2−periodic. This later term vanishes as N goes to infinity since $R_s f\in X$. The locally uniform convergence of I_t is then ensured by the equality

$$I_t-(\nu_0 f)\phi=I_t-\frac{1}{\mathrm{Log}\ 2}\int_t^{t+\mathrm{Log}\ 2} R_s f\,\mathrm{d}s,$$

the last term converges locally uniformly to zero when $t \to +\infty$. To prove the last convergence, first notice that it is enough to prove the convergence of

$$\frac{1}{N\text{Log } 2}\int_0^{N\text{Log } 2} e^{-s}M_s f \,\mathrm{d}s = \frac{1}{N}\sum_{n=0}^{N-1} I_{n\text{Log } 2}$$

when N tends to infinity. Let $x \in (0,\infty)$, and $V_x \subset (0,\infty)$ a neighborhood of x to have the uniform convergence of $(I_{n\text{Log } 2})_{n\geqslant 0}$ toward $(\nu_0 f)\phi$. Let $\varepsilon > 0$, there exists N_0 such that the inequality $\|I_{n\text{Log } 2} - (\nu_0 f)\phi\|_{V_x} < \varepsilon$ holds for all $n \geqslant N_0$. Then for all N larger than N_0, one has

$$\begin{aligned}\sup_{y\in V_x} \frac{\left|\frac{1}{N}\sum_{n=0}^{N-1}\left(I_{n\text{Log } 2}(y) - (\nu_0 f)\phi(y)\right)\right|}{y} &\leqslant \frac{1}{N}\sum_{n=0}^{N_0-1}\sup_{y\in V_x}\frac{|I_{n\text{Log } 2}(y) - (\nu_0 f)\phi(y)|}{y} + \frac{N-N_0}{N}\varepsilon \\ &\leqslant \frac{C(N_0)}{N} + \varepsilon\end{aligned}$$

so the locally uniform convergence is proved, for N large enough.

□

2.3.2 Weak convergence to a cyclic family of measures

Theorem 32. *Assume that B satisfies* (A1) *and* (A2). *Then there exists a unique periodic family of projectors R_t acting on $\dot{\mathcal{M}}$ such that for any initial condition $\mu \in \dot{\mathcal{M}}$, the measure solution μM_t of* (2.8) *satisfiez*

$$\mu M_t - \mu R_t \underset{t\to\infty}{\overset{*}{\rightharpoonup}} 0.$$

Démonstration. Let $f \in \mathcal{C}_c^1(0,\infty)$. Thanks to Theorem 30, $e^{-t}M_t f - R_t f$ converges uniformly to 0 on the support of f, with R_t is the operator defined in this Theorem. Now let $\mu \in \dot{\mathcal{M}}$. Then $\mu\left(e^{-t}M_t f - R_t f\right)$ vanishes as t tends to infinity. Thanks to relation 2.14, one has $\mu(e^{-t}M_t f) = (e^{-t}\mu M_t)f$. For the other term, define $T^t : f \in E_0 \to \mu(R_t f)$. We invoke Lemma 18 applied to the linear form T^t to obtain, for all $t \geqslant 0$, existence and uniqueness of measure, denoted π_t, such that $T^t f = \pi_t f$ for all $f \in E_0$ and $t \geqslant 0$. Denoting $\mu R_t := \pi_t$, we obtain the claimed result for functions in $\mathcal{C}_c^1(0,\infty)$. We extend this result to functions in E_0 by density.

□

As in the previous subsection, we prove a mean ergodic behaviour corollary.

Corollary 33. *Let $\mu \in \dot{\mathcal{M}}$. Then*

$$J_t := \frac{1}{\text{Log } 2}\int_t^{t+\text{Log } 2} e^{-s}\mu M_s \,\mathrm{d}s \qquad \textit{and} \qquad \frac{1}{t}\int_0^t e^{-s}\mu M_s \,\mathrm{d}s$$

converge weakly to $(\mu\phi)\nu_0$.

The proof is a straightforward adaptation of the previous one, combined with Corollary 31 with functions in E_0.

2.4 Conclusion and future work

In this work, we investigated how the cyclic asymptotic behaviour of rescaled solutions of the growth-fragmentation equation in the critical case of linear growth rate and equal mitosis exhibited in [14] transpose to measure solutions. After defining and suited functional framework, we constructed a solution to the reverse in time adjoint evolution problem (2.9), expressed as a semigroup acting on the initial condition. From this object, we built a measure solution to Equation (2.3) by duality with elementary computations, in particular without invoking the adaptation of Riesz representation theorem proved

in Lemma 18. The proof of the asymptotic behaviour raised some technical difficulties, related to the different notions of convergence in a space of measures. The first step of our method to study the large time asymptotic involves a *log* $2-$ periodic projection $R_t : E_0 \oplus X \to X$. Wether or not this operator can be extended to the whole space E is a question yet to be adressed. From this operator and Lemma 18, we proved a weak convergence of the measure solution to a periodic function/solution. Unfortunately, we are not able to obtain a strong convergence to this periodic solution. This is a natural fit for a continuation of this work. A numerical concern would be to adapt the scheme proposed in [43] to this problem, since after division, the masse is not sent to a boundary of the domain, and prove its convergence.

Chapitre 3

Modélisation et analyse de la dynamique des adipocytes avec un processuss de différenciation

---

Ce travail a été réalisé lors du CEMRACS 2018 dont le thème portait sur la modélisation mathématique appliquée à la biologie et la médecine. En collaboration avec Jérôme Gilleron, Thierry Goudon, Frédéric Lagoutière, Benjamin Mauroy, Pascal Millet, Magali Ribot et Cristina Vaghi, nous proposons un modèle décrivant la dynamique d'un ensemble d'adipocytes structurés en taille. Ce modèle tient compte de la différentiation d'une population de cellules mésenchymales en préadipocytes et des préadipocytes en adipocytes ; les taux de différentiation dépendent du rayon moyen des adipocytes. Les équations considérées sont, par conséquence, des équations différentielles ordinaires, couplées avec une équation d'advection, dont le taux de croissance dépend de la nourriture disponible et de la surface totale des adipocytes. Comme la vitesse est discontinue, nous introduisons une notion appropriée des solutions, provenant de la théorie de Filippov. Nous sommes alors en mesure de déterminer les solutions stationnaires du système, de prouver l'existence et l'unicité de solutions et de décrire le comportement asymptotique des solutions dans certains cas simples. Finalement, les paramètres du modèles sont estimés grâce à des données expérimentales et des simulations numériques sont présentées ; une extension spatiale du modèles est étudiée numériquement. Un article est soumis pour publication à *ESAIM : Proceedings and Surveys* sous le titre *Modeling and analysis of adipocytes dynamic with a differentiation process.*

3.1 Introduction

Obesity is a worldwide major public health issue that doubled since 1980 and affects nowadays almost two billions of adults considered as overweight and 600 millions considered as obese [133]. Strikingly, obesity is the most prevalent cause for the development of cardio-metabolic diseases (cardiovascular diseases, type 2 diabetes, and liver diseases) as well as cancer, increasing mortality and morbidity and justifying the need for intensive research and intervention policy.

Obesity is characterized by an increase in adipose tissue (AT) mass. This expansion of AT is a complex process which requires succeeding steps of proliferation, differentiation and maturation of the cells from the adipocytes lineage [15]. Indeed, within AT, vascular-resident adipose progenitor cells (APCs) proli-

ferate and, under specific signals, differentiate into pre-adipocytes. Pre-adipocytes also expand through proliferation before to differentiate into small mature adipocytes. Mature adipocytes have an impressive capacity of expanding their volume by more than 30-fold through triglyceride accumulation in lipid droplets [55, 159]. Ultimately, one single large lipid droplet occupies most of the cytoplasm and stiffens locally the AT [166]. The mechanical forces generated by hypertrophic stiff adipocytes may both limit their size and stimulate the differentiation of APCs and pre-adipocytes to recruit new adipocytes [158]. Mature adipocyte size is not only critical for adipogenesis initiation but also for adipocyte functions. Indeed, hypertrophic adipocytes have less ability to properly store lipids, resulting in spillover of lipids and excessive fat deposition in other tissues, both favorizing cardio-metabolic diseases. Although there is growing evidence that impaired AT expandability plays a pivotal role in obesity-related cardio-metabolic diseases, the molecular and cellular basis of this phenomenon is complex and far from being understood. Indeed, the expansion of AT depends on a large number of parameters including the rate of APCs and pre-adipocytes proliferation/differentiation/death, the mechanical feedback loop of adipogenesis stimulation, the size of the adipocytes and the kinetic of their death.

The pathological implication of these phenomena is a motivation for developing new approaches for a better understanding of the AT formation. Mathematical modeling can provide useful insights, in particular for identifying leading parameters. Noticeably, the mechanical feedback loop of adipogenesis stimulation is certainly a pivotal parameter that could control the ability of adipose tissue to expand through the recruitment of new adipocytes. We refer the reader to [164, 163] for attempts in this direction. Here, we shall present a different modeling of the AT development, including some differentiation processes and a velocity growth depending on the total surface, and investigate, theoretically and numerically, the main features of the adopted model.

3.1.1 Description of the homogeneous in space model

We think of the process as a compartment model with three populations of cells : mesenchymal, pre-adipocytes and adipocytes, the latter population being structured by the size of the cells. Let $t \mapsto m(t)$ and $t \mapsto p(t)$ stand for the number of mesenchymal, and pre-adipocytes, respectively ; in the first five sections, both quantities depend only on the time variable $t \geqslant 0$. Adipocytes are described by their radius distribution function $(t, r) \mapsto a(t, r)$: for given $0 \leqslant r_1 \leqslant r_2$, the integral $\int_{r_1}^{r_2} a(t, s)\,\mathrm{d}s$ gives the number of adipocytes with a radius r between r_1 and r_2, at time $t \geqslant 0$.

Mesenchymal and pre-adipocytes undergo proliferation and mortality. Furthermore, mesenchymal cells differentiate into pre-adipocytes, while pre-adipocytes differentiate into adipocytes. The mutation of pre-adipocytes gives rise to adipocytes with radius $r_\star \geqslant 0$, and $r_\star$ will be the minimal radius within the adipocytes population. Adipocytes can undergo mortality and dynamic change of their radius. Radius changes are modeled with a growth rate function $(t, r) \mapsto V(t, r)$. The expression of the growth rate function V will be determined later on, through volume considerations. As it will be detailed below, we assume the existence of a critical size $r_c > 0$, which stands for the maximal value of adipocyte radius.

The unknowns depend on the time variable $t \in [0, +\infty)$ and, for the adipocyte distribution, on the radius variable $r \in [r_\star, +\infty)$. The evolution of the population of mesenchymal cells, pre-adipocytes and adipocytes is governed by the following set of equations, defined on the domain $(t, r) \in [0, +\infty) \times [r_\star, +\infty)$

$$\begin{cases} \dfrac{\mathrm{d}m}{\mathrm{d}t}(t) = -\gamma m(t) + \alpha m(t) - \beta(\bar{r}(t))m(t), \\ \dfrac{\mathrm{d}p}{\mathrm{d}t}(t) = -\gamma' p(t) + \alpha' p(t) - \beta'(\bar{r}(t))p(t) + \beta(\bar{r}(t))m(t), \\ \dfrac{\partial a}{\partial t}(t, r) + \partial_r \left(Va\right)(t, r) = -\gamma'' a(t, r), \end{cases}$$

where all the parameters of the model are nonnegative and can be collected as follows :

α, α'	proliferation rates for m and p,
β, β'	differentiation rates for m and p, which depend on the mean radius of adipocytes $\bar{r}(t)$ at time t,
γ, γ', γ''	mortality rates for m, p and a,
r_m	radius of mesenchymal cells,
$r_\star$	emergence radius of adipocytes (minimal radius) and radius of pre-adipocytes,
r_c	maximal radius of adipocytes,
$V(t,r)$	growth rate of an adipocyte of radius r at time t.

Denoting by $\delta = \alpha - \gamma$ and $\delta' = \alpha' - \gamma'$, we obtain the following system :

$$\frac{\mathrm{d}m}{\mathrm{d}t}(t) = \delta m(t) - \beta(\bar{r}(t))m(t), \tag{3.1a}$$

$$\frac{\mathrm{d}p}{\mathrm{d}t}(t) = \delta' p(t) - \beta'(\bar{r}(t))p(t) + \beta(\bar{r}(t))m(t), \tag{3.1b}$$

$$\frac{\partial a}{\partial t}(t,r) + \partial_r \left(Va\right)(t,r) = -\gamma'' a(t,r), \tag{3.1c}$$

Dependency of the mutation rates on the mean radius. To keep feedback mechanisms description tractable, we assume that the differentiation rates β and β' are functions of the mean radius $\bar{r}(t)$ at time t. As said above, $\int_{r_\star}^{r_c} a(t,s)\,\mathrm{d}s$ represents the total number of adipocytes, at time t. The mean radius of adipocytes at time t is therefore equal to :

$$\bar{r}(t) = \frac{\displaystyle\int_{r_\star}^{r_c} s\ a(t,s)\,\mathrm{d}s}{\displaystyle\int_{r_\star}^{r_c} a(t,s)\,\mathrm{d}s} \tag{3.2}$$

and we also introduce for further purposes

$$S(t) = 4\pi \int_{r_\star}^{r_c} s^2\ a(t,s)\,\mathrm{d}s, \tag{3.3}$$

the total surface of the adipocytes at time t.

We define β and β' as functions of $\bar{r}$, typically with a sigmoid shape that reproduces threshold effects :

$$\beta(\bar{r}) = \beta_m + \frac{\beta_M - \beta_m}{1 + e^{-\frac{\bar{r} - r_\beta}{R_\beta}}} \quad \text{and} \quad \beta'(\bar{r}) = \beta'_m + \frac{\beta'_M - \beta'_m}{1 + e^{-\frac{\bar{r} - r_{\beta'}}{R_{\beta'}}}}$$

with all parameters positive and such that $\beta_M \geqslant \beta_m$, $\beta'_M \geqslant \beta'_m$. The image of β is $[\beta_m, \beta_M]$; the sigmoid β is "centered" on r_β and its slope at mid height is $\frac{\beta_M - \beta_m}{4R_\beta}$. The behaviour of β' relatively to its parameters is similar, see Figure 3.1 for a typical shape. In particular, from a mathematical point of view, β and β' are bounded Lipschitz-continuous functions.

Description of the growth rate. The dynamics of the radius of an adipocyte $t \to R(t)$ with respect to time can be approximated with the ODE

$$\frac{\mathrm{d}}{\mathrm{d}t}R(t) = V(t, R(t)),$$

where V is the growth rate. We assume that adipocytes capture all the excess of food, i.e. not used by the metabolism. Adipocytes gather the food through their membranes, thus the flux of food they receive is proportional to their surface. Given a radius $r_\star < R < r_c$ the flux of food is proportional to the ratio of the surface of the considered adipocyte over the total surface of all the adipocytes, that is

$$k \frac{R^2}{\displaystyle\int_{r_\star}^{r_c} s^2 a(t,s)\,\mathrm{d}s}$$

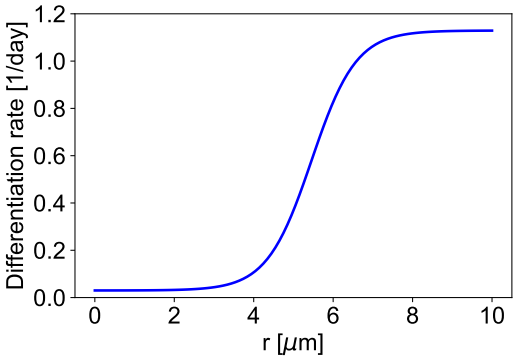

FIGURE 3.1 – Shape of β and β' as functions of the radius.

where $k > 0$ is the (excess of) available food. In the present paper, k is constant in time, but it could be relevant to consider it as evolving in time, for example with time periodic food input to mimic circadian cycle. Thus, in the time interval $[t, t + \mathrm{d}t]$, the volume variation of such an adipocyte with radius $R(t)$ is governed by

$$\mathscr{V}(t + \mathrm{d}t) = \mathscr{V}(t) + k \frac{R(t)^2}{\displaystyle\int_{r_\star}^{r_c} s^2 a(t,s)\,\mathrm{d}s} \times \mathrm{d}t.$$

Letting $\mathrm{d}t$ go to 0, we deduce that the volume obeys the ODE $\dfrac{\mathrm{d}\mathscr{V}}{\mathrm{d}t} = k \dfrac{R(t)^2}{\displaystyle\int_{r_\star}^{r_c} s^2 a(t,s)\,\mathrm{d}s}$. Since the volume $\mathscr{V}(t)$ is related to the radius $R(t)$ by $\mathscr{V}(t) = \dfrac{4}{3}\pi R(t)^3$, we end up with

$$\frac{\mathrm{d}\mathscr{V}}{\mathrm{d}t} = 4\pi R(t)^2 \frac{\mathrm{d}R}{\mathrm{d}t} = 4\pi R(t)^2 \times V(t, R(t)) = k \frac{R(t)^2}{\displaystyle\int_{r_\star}^{r_c} s^2 a(t,s)\,\mathrm{d}s}.$$

Consequently, we have

$$V(t,r) = \frac{k}{4\pi \displaystyle\int_{r_\star}^{r_c} s^2 a(t,s)\,\mathrm{d}s} = \frac{k}{S(t)}.$$

This relation holds as far as the radius is not too large. As already mentioned above, the size of the adipocytes is limited. There are several possibilities to model such a threshold, based either on phenomenological arguments, or on energetic considerations. In what follows, we make the equation as simple as possible, with the formula

$$V(t,r) = \frac{k}{S(t)} \mathbb{1}_{[r_\star, r_c)}(r) \tag{3.4}$$

which assumes that the growth rate vanishes outside the domain $r \in [r_\star, r_c]$. This simple definition will allow us to derive easily interesting formula for the stationary solutions of the model.

However, for the numerical simulations, we adopt the following regularized growth rate :

$$V(t,r) = \frac{k}{S(t)} \mathbb{1}_{[r_\star, r_c - \varepsilon)}(r) - \frac{r - r_c}{\varepsilon} \frac{k}{S(t)} \mathbb{1}_{[r_c - \varepsilon, r_c)}(r),$$

where $\varepsilon > 0$ is a small parameter.

Initial data and boundary conditions. The system is complemented by initial data

$$m(0) = m_0 \geqslant 0, \qquad p(0) = p_0 \geqslant 0, \tag{3.5a}$$

$$a(0,r) = a_0(r) \geqslant 0. \tag{3.5b}$$

Since $V(t, r_\star)$ is positive, we also need to prescribe the boundary condition for a when $r = r_\star$; this is where we take into account the differentiation of the pre-adipocytes into adipocytes :

$$V(t, r_\star)\ a(t, r_\star) = \beta'(\bar{r}(t))\ p(t). \tag{3.6}$$

For the largest adipocytes, the growth rate vanishes, and we simply assume that $V(t, r)\ a(t, r) = 0$ for $r > r_c$. It means that adipocytes beyond a certain size do not exist. Consistently, we also assume that the support of a_0 is included in $[r_\star, r_c]$.

The initial and boundary value problem under consideration is (3.1a), (3.1b), (3.1c), (3.2), (3.3), (3.4), (3.5a), (3.5b), Typical values for the parameters are collected in Table 3.2.

3.1.2 Definition of the solutions to system (3.1)-(3.6)

The definition (3.4) of the growth rate V raises some slight technical difficulties. Indeed, the equation for the adipocytes concentration $(t, r) \mapsto a(t, r)$ is a transport equation, which is classically understood by means of the characteristic curves associated with the growth rate $V(t, r)$. However, V, as given by (3.4), does not fullfil the regularity required to apply the Cauchy-Lipschitz theorem. Nevertheless, assuming that $S(t) \geqslant \varepsilon > 0$ for all $t \in [0, T)$, V satisfies the following one sided Lipschitz condition (OSLC) :

for all $r_1, r_2 \in [r_\star, +\infty)$, for all $0 \leqslant t \leqslant T < \infty$, $\big(V(t, r_1) - V(t, r_2)\big)(r_1 - r_2) \leqslant C(t)|r_1 - r_2|^2$ with $C \in L^1(0, T)$.

Hence, we can appeal to the generalized theory introduced by A. Filippov [78], see also [144] for an application to transport equations with discontinuous coefficients. It allows us to consider the family of continuous Filippov maps

$$X_t : ([0, t] \times \{r_\star\}) \cup (\{0\} \times [r_\star, +\infty)) \to [r_\star, +\infty),$$

satisfying $X_s(s, r_\star) = r_\star$ for all $s \in [0, t]$, $X_0(0, r) = r$ for all $r \in [r_\star, +\infty)$ and, for fixed $(s, r) \in (0, \infty) \times (r_\star, \infty)$, the function $t \mapsto X_t(s, r)$ is absolutely continuous on $[s, \infty)$ and satisfies the differential equation $\frac{\mathrm{d}}{\mathrm{d}t} X_t = V(t, X_t)$ for almost evert t with Cauchy datum $X_s(s, r) = r$. Owing to the OSLC, X_t is the unique flow of the differential equation for $t \geqslant s$.

In our particular case, the characteristic maps associated with a given S can be explicitly computed and are defined by :

$$X_t^S(0, r) = \min\left(r + \int_0^t \frac{k}{S(u)}\ \mathrm{d}u, r_c\right),\ t \geqslant 0, \quad X_t^S(s, r_\star) = \min\left(r_\star + \int_s^t \frac{k}{S(u)}\ \mathrm{d}u, r_c\right),\ t \geqslant s \geqslant 0. \tag{3.7}$$

Let a_0 be a positive finite measure supported on $[r_\star, r_c]$. We denote by $\mathcal{M} - w*$ the set of finite measures on $[r_\star, +\infty)$ endowed with the weak star topology.

We generalize Eq.(3.6) by replacing its right-hand side with a given positive continuous function $f \in \mathcal{C}^0(\mathbb{R}_+)$. In that context, we will call a solution to the problem (3.1c)-(3.5b)-(3.6) with initial condition, i.e.

$$\begin{cases} \partial_t a(t, r) + \partial_r(Va)(t, r) = -\gamma'' a(t, r), & t > 0, r > r_\star, \\ V(t, r_\star) a(t, r_\star) = f(t), & t > 0, \\ a(0, r) = a_0(r), & r > r_\star \end{cases} \tag{3.8}$$

any measure-valued function $a \in \mathcal{C}^0(\mathbb{R}_+; \mathcal{M} - w*)$ such that the following Duhamel formula holds : for all $\phi \in \mathcal{C}_b^0([r_\star, +\infty))$ and for all $t \in [0, T)$,

$$\int_{r_\star}^{+\infty} \phi(r)\ \mathrm{d}a_t(r) = \int_0^t e^{-\gamma''(t-s)} \phi\left(X_t^S(s, r_\star)\right) f(s)\ \mathrm{d}s + \int_{r_\star}^{+\infty} e^{-\gamma'' t} \phi\left(X_t^S(0, r)\right)\ \mathrm{d}a_0(r) \tag{3.9}$$

where $T = \inf\{t : S(t) = 0\}$.

Note that here, a_t denotes the measure a at time t and the condition $a \in C^0(\mathbb{R}_+; \mathcal{M} - w*)$ means that

$$\lim_{h \to 0} \int \phi(r)\ \mathrm{d}a_{t+h}(r) = \int \phi(r)\ \mathrm{d}a_t(r)$$

holds for any continuous and bounded trial function ϕ. In the following, we shall use the definition (3.9) with $f(t) = \beta'(\bar{r}(t))p(t)$. Moreover, we bear in mind that the problem is non linear, since the growth rate V depends on the total surface $S(t)$ of the adipocytes, see (3.3). It turns out that the OSLC on which the construction is based relies on the positivity of S, that we are going to discuss now, showing that the lifespan of solution is infinite (for positive times).

Bearing in mind the physical meaning of the unknown, the data f and a_0 are non negative, with, furthermore, $\mathrm{supp}(a_0) \subset [r_\star, r_c]$. Formula (3.9) then tells us that a_t is a non negative measure too. We also remark that the characteristics issued from $[r_\star, r_c]$ cannot exceed r_c (this is a consequence of the well-posedness of this Filippov-type Cauchy problem) and

$$\forall t \in [0,T),\ X_t^S\left(([0,t]\times\{r_\star\}) \cup (\{0\}\times[r_\star,+\infty))\right) \subset [r_\star, r_c].$$

Accordingly, the support of a_t remains in $[r_\star, r_c]$ for all $t \in [0,T)$. Finally, let us discuss formally that the model does not produce a shrinking of the surface, that would be an obstacle to the global existence of solutions. Since a_t is compactly supported, we can use (3.9) with $\phi(r) = 4\pi r^2$ to compute the surface as :

$$S(t) = 4\pi\left(e^{-\gamma'' t}\int_{r_\star}^{r_c}(X_t^S(0,r))^2\,\mathrm{d}a_0(r) + \int_0^t e^{-\gamma''(t-s)}(X_t^S(s,r_\star))^2 f(s)\,\mathrm{d}s\right). \tag{3.10}$$

This formula enables to bound from below the value of $S(t)$ as

$$\forall t\in[0,T),\qquad S(t) = 4\pi\int_{r_\star}^{+\infty} r^2\,\mathrm{d}a_t(r) = 4\pi\int_{r_\star}^{r_c} r^2\,\mathrm{d}a_t(r) \geqslant 4\pi r_\star^2 e^{-\gamma'' t}a_0([r_\star,r_c]).$$

The continuity of S, which comes from the continuity of $t \mapsto a_t$, enables to conclude that $T = +\infty$.

3.1.3 Outline of the article

In this article, a complete study of the model is proposed : in section 3.2, we begin with a computation of the stationary solutions of the model, followed by a proof of the existence and uniqueness of solutions in Section 3.3. The asymptotic in time behaviour of the system is described in Section 3.4 and some numerical simulations are displayed in Section 3.5. Finally, this model is extended by considering space heterogeneities through a coupling with a fluid environment and numerical simulations are presented in Section 3.6.

3.2 Stationary solutions

We will use the previous framework to exhibit stationary solutions of the system (3.1)-(3.6). Finding a stationary solution (m,p,a_0) is equivalent to finding a solution for the following system :

$$\begin{cases} (\delta - \beta(\bar{r}))\,m = 0 \\ (\delta' - \beta'(\bar{r}))\,p + \beta(\bar{r})m = 0 \\ Va(r_\star) = \beta'(\bar{r})\,p, \qquad \text{with } V = \dfrac{k}{S}, \\ \displaystyle\int_{r_\star}^{+\infty}\phi(r)\,\mathrm{d}a_0(r) = \int_0^t e^{-\gamma''(t-s)}\phi\left(X_t^S(s,r_\star)\right)\beta'(\bar{r})p\,\mathrm{d}s + \int_{r_\star}^{+\infty} e^{-\gamma'' t}\phi\left(X_t^S(0,r)\right)\,\mathrm{d}a_0(r) \end{cases} \tag{3.11}$$

for all $\phi \in \mathcal{C}_b^0([r_\star,+\infty))$ and for all $t \in [0,+\infty)$, with unknowns a_0 a positive finite measure supported on $[r_\star, r_c]$ and $m,p \in [0,+\infty)$. The last condition expresses the fact that $a_t = a_0$ for all $t \in [0,+\infty)$ where a is a solution in the sense given in the previous section.

Let (m,p,a_0) be a solution to (3.11) and $V = \frac{k}{S}$. The characteristics X_t^S are computed using the constant function $S = 4\pi\displaystyle\int_{r_\star}^{r_c} r^2 da_0(r)$ and are well defined since a_0 is positive, that is to say :

$$X_t^S(s,r_\star) = \min\left(r_\star + V(t-s), r_c\right) \qquad \text{and} \qquad X_t^S(0,r) = \min\left(r + Vt, r_c\right).$$

We can hence rewrite the last equation of system (3.11) at time $t = \frac{r_c - r_\star}{V}$ as

$$\int_{r_\star}^{r_c} \phi(r)\, \mathrm{d}a_0(r) = \frac{\beta'(\bar{r})p}{V} \int_{r_\star}^{r_c} e^{-\frac{\gamma''}{V}(u-r_\star)} \phi(u)\ \mathrm{d}u + e^{-\frac{\gamma''}{V}(r_c-r_\star)} \phi(r_c) a_0([r_\star, r_c]). \tag{3.12}$$

Using the equality $a(r_\star) = \frac{\beta'(\bar{r})p}{V}$, we deduce the form of a_0 as :

$$a_0 = a(r_\star) e^{-\frac{\gamma''}{V}(r-r_\star)} \mathbb{1}_{[r_\star, r_c]}\, \mathrm{d}r + \mu \delta_{r_c},$$

where μ can be determined from (3.12) through the relation :

$$\mu = \int_{r_\star}^{r_c} a(r_\star) e^{-\frac{\gamma''}{V}(r-r_\star)} e^{-\frac{\gamma''}{V}(r_c-r_\star)}\, \mathrm{d}r + \mu e^{-\frac{\gamma''}{V}(r_c-r_\star)}$$

and finally we find

$$\mu = \frac{V}{\gamma''} a(r_\star) e^{-\frac{\gamma''}{V}(r_c-r_\star)}.$$

Therefore the stationary solutions satisfy

$$\begin{cases} (\delta - \beta(\bar{r}))\, m = 0 \\ (\delta' - \beta'(\bar{r}))\, p + \beta(\bar{r}) m = 0 \\ V a(r_\star) = \beta'(\bar{r})\ p, \qquad \text{with } V = \dfrac{k}{S}, \\ a_0 = a(r_\star) e^{-\frac{\gamma''}{V}(r-r_\star)} \mathbb{1}_{[r_\star, r_c]}\, \mathrm{d}r + \dfrac{V}{\gamma''} a(r_\star) e^{-\frac{\gamma''}{V}(r_c-r_\star)} \delta_{r_c}, \end{cases} \tag{3.13}$$

with unknowns $p, m \in \mathbb{R}_+$, $a(r_\star) \in \mathbb{R}_+^*$.

Note that the expression for a_0 enables to compute $\bar{r}$ and S as functions of V, i.e. :

$$\bar{r} = \frac{\int_{r_\star}^{r_c} s\, \mathrm{d}a_0(s)}{\int_{r_\star}^{r_c} \mathrm{d}a_0(s)} = \frac{\gamma''}{V} \int_{r_\star}^{r_c} r e^{-\frac{\gamma''}{V}(r-r_\star)}\, \mathrm{d}r + r_c e^{-\frac{\gamma''}{V}(r_c-r_\star)} = r_\star + \frac{V}{\gamma''}(1 - e^{-\frac{\gamma''}{V}(r_c-r_\star)})$$

and

$$\begin{aligned} S &= 4\pi \int_{r_\star}^{r_c} s^2\, \mathrm{d}a_0(s) = 4\pi a(r_\star) \left(\int_{r_\star}^{r_c} r^2 e^{-\frac{\gamma''}{V}(r-r_\star)}\, \mathrm{d}r + r_c^2 \frac{V}{\gamma''} e^{-\frac{\gamma''}{V}(r_c-r_\star)} \right) \\ &= 4\pi a(r_\star) \left(\frac{V}{\gamma''} r_\star^2 - 2 \left(\frac{V}{\gamma''} \right)^2 \left(r_c e^{-\frac{\gamma''}{V}(r_c-r_\star)} - r_\star \right) + 2 \left(\frac{V}{\gamma''} \right)^3 \left(1 - e^{-\frac{\gamma''}{V}(r_c-r_\star)} \right) \right). \end{aligned} \tag{3.14}$$

Proposition 34. *System* (3.13) *has a non-zero solution if and only if one of the following two conditions hold :*

1. $\delta' \in \beta'\left((r_\star, r_c)\right)$,
2. $\delta \in \beta\left((r_\star, r_c)\right)$ *and* $\delta' - \beta'\left(\beta^{-1}(\delta)\right) < 0$.

Démonstration. We begin with noticing that p cannot be zero, since it would imply that $a(r_\star) = 0$ and therefore $a_0 = 0$.

Now, remark that the function Ψ such that $\bar{r} = \Psi(V)$ and defined by $\Psi : V \to r_\star + \frac{V}{\gamma''}(1 - e^{-\frac{\gamma''}{V}(r_c-r_\star)})$ is strictly increasing on $\mathbb{R}_+^*$ and satisfies $\lim_{V \to 0^+} \Psi(V) = r_\star$ and $\lim_{V \to +\infty} \Psi(V) = r_c$.

If $m = 0$, we should impose that $\delta' \in \beta'((r_\star, r_c))$. If $m \neq 0$, it implies that $\delta \in \beta((r_\star, r_c))$, namely $\delta = \beta(\bar{r})$ with $\bar{r}$ such that $\delta' - \beta'(\bar{r}) < 0$.

Therefore, if $\delta' \in \beta'((r_\star, r_c))$, we find a stationary solution defined by

$$\bar{r} = \beta'^{-1}(\delta'), \quad m = 0, \quad V = \Psi^{-1}(\bar{r}), \quad S = \frac{k}{V}.$$

From Eq.(3.14), we can deduce the value of $a(r_\star)$ knowing S and V, and therefore a_0 and $p = \dfrac{Va(r_\star)}{\beta'(\bar{r})}$.

Similarly, if $\delta \in \beta((r_\star, r_c))$ and $\delta' - \beta'\left(\beta^{-1}(\delta)\right) < 0$, then a solution is given by

$$\bar{r} = \beta^{-1}(\delta), \quad V = \Psi^{-1}(\bar{r}), \quad S = \frac{k}{V}, \quad a(r_\star) \text{ from Eq.(3.14)}, \quad p = \frac{Va(r_\star)}{\beta'(\bar{r})}, \quad m = \frac{-(\delta' - \beta'(\bar{r}))}{\beta(\bar{r})} p.$$

□

Remark : If exactly one condition is fulfilled, the stationary solution is unique. However, if both conditions are fulfilled, we may have two different values of $\bar{r}$ and thus two different stationary solutions.

3.3 Existence and uniqueness of unsteady solutions

Equations of system (3.1)-(3.6) are coupled altogether as follows : the ODE part of system (3.1), that is to say equations (3.1a) - (3.1b) is a simple linear ODE system, but which coefficients are defined through the mean radius function $\bar{r}$ of adipocytes, defined at Eq.(3.2). We therefore need to know function a to compute $\bar{r}$. Reciprocally, the transport part of system (3.1), that is to say equation (3.1c), depends on the total surface S of a through the velocity V defined at Eq. (3.4) and depends on function p solution to the ODE part, through the boundary condition (3.6).

In this section, we will prove the existence and uniqueness of solutions to system (3.1)-(3.6). To do so, we will proceed in three steps : first we prove, in Subsection 3.3.1, the existence and uniqueness of solutions to the ODE part (3.1a) - (3.1b)-(3.5a). Then, in Subsection 3.3.2, we prove the existence and uniqueness of solutions to the transport equation (3.1c)-(3.6)-(3.5b) for a given non negative flux by solving a fixed point equation. We also prove some stability property with respect to the flux that will be used later. Finally, in Subsection 3.3.3, we prove the existence and uniqueness of a solution to the general system thanks to a fixed-point theorem, coupling the results obtained at the foregoing subsections.

3.3.1 Some preliminary results on the solution of the ODE part (3.1a) - (3.1b)-(3.5a)

First we will give some existence and stability results on the solution of the ODE part (3.1a) - (3.1b) of system (3.1) with initial conditions (3.5a), assuming that the mean radius $\bar{r} \in \mathcal{C}^0([0,T],[r_\star, r_c])$ is given.

Since β and β' are bounded, the following function :

$$\begin{pmatrix} m \\ p \end{pmatrix} \mapsto \begin{pmatrix} \delta - \beta(\bar{r}(t)) & 0 \\ \beta(\bar{r}(t)) & \delta' - \beta'(\bar{r}(t)) \end{pmatrix} \begin{pmatrix} m \\ p \end{pmatrix}$$

is Lipschitz-continuous. We call L its Lipschitz modulus.

Therefore, the system satisfies the hypotheses of Cauchy-Lipschitz Theorem and we have the following bound :

$$\max(m(t), p(t)) \leqslant \max(m_0, p_0) \exp(Lt), \text{ for all } t \in [0,T]. \tag{3.15}$$

Moreover, we can prove the following stability property of the solution with respect to $\bar{r}$, where $p(\bar{r})$ denotes the solution p computed with the mean radius function $\bar{r}$: for all $\bar{r}_1, \bar{r}_2 \in \mathcal{C}^0([0,T],[r_\star, r_c])$,

$$|p(\bar{r}_1)(t) - p(\bar{r}_2)(t)| \leqslant C \max(m_0, p_0) \|\bar{r}_1 - \bar{r}_2\|_{L^1([0,t])} e^{2Lt}, \text{ for all } t \in [0,T]. \tag{3.16}$$

Indeed, let us denote by M the following Lipschitz-continuous function of Lipschitz modulus k :

$$M(r) = \begin{pmatrix} \delta' - \beta'(r) & \beta(r) \\ 0 & \delta - \beta(r) \end{pmatrix}.$$

We obtain the following inequality, using (3.15) :

$$\begin{aligned}
&\left\| \begin{pmatrix} m(\bar r_1)(t) - m(\bar r_2)(t) \\ p(\bar r_1)(t) - p(\bar r_2)(t) \end{pmatrix} \right\|_{\infty,\mathbb{R}^2} \\
&\quad \leqslant \int_0^t \left(k\,|\bar r_1(s) - \bar r_2(s)| \left\| \begin{pmatrix} m(\bar r_1)(s) \\ p(\bar r_1)(s) \end{pmatrix} \right\|_{\infty,\mathbb{R}^2} + \left\| M(\bar r_2(s)) \begin{pmatrix} m(\bar r_1)(s) - m(\bar r_2)(s) \\ p(\bar r_1)(s) - p(\bar r_2)(s) \end{pmatrix} \right\|_{\infty,\mathbb{R}^2} \right) \mathrm{d}s \\
&\quad \leqslant k \left\| \begin{pmatrix} m_0 \\ p_0 \end{pmatrix} \right\|_{\infty,\mathbb{R}^2} \|\bar r_1 - \bar r_2\|_{L^1([0,t])}\, e^{Lt} + \int_0^t L \left\| \begin{pmatrix} m(\bar r_1)(s) - m(\bar r_2)(s) \\ p(\bar r_1)(s) - p(\bar r_2)(s) \end{pmatrix} \right\|_{\infty,\mathbb{R}^2} \mathrm{d}s
\end{aligned}$$

and we conclude thanks to Grönwall's Lemma.

3.3.2 Solution to the transport equation (3.1c)-(3.6)-(3.5b) with a given non negative flux

In this section, the first theorem gives an existence and uniqueness result for the transport part (3.1c) of system (3.1), complemented with boundary condition (3.6) and initial condition (3.5b).

Remark that the velocity V, involved in the transport equation (3.8) and defined at Eq.(3.4), depends on the total surface S, which is computed thanks to the solution a of Eq. (3.8). We are therefore led to consider the following fixed-point problem, coming from the expression of the surface S as a function of the characteristic curves X_t^S, see Eq.(3.10) :

$$S(t) = 4\pi \left(e^{-\gamma'' t} \int_{r_\star}^{r_c} (X_t^S(0,r))^2 \,\mathrm{d}a_0(r) + \int_0^t e^{-\gamma''(t-s)} (X_t^S(s,r_\star))^2 f(s)\,\mathrm{d}s \right) \tag{3.17}$$

where

$$\begin{aligned}
X_t^S(0,r) &= \min\left(r + \int_0^t \frac{k}{S(u)}\,\mathrm{d}u, r_c \right), && t \geqslant 0, \\
X_t^S(s,r_\star) &= \min\left(r_\star + \int_0^t \frac{k}{S(u)}\,\mathrm{d}u - \int_0^s \frac{k}{S(u)}\,\mathrm{d}u, r_c \right), && t \geqslant s \geqslant 0.
\end{aligned}$$

It is easy to prove that solutions to Eq. (3.17) and solutions to Eq. (3.8) are the same, defining a by the following formula :

$$\int_{r_\star}^{r_c} \phi(r)\,\mathrm{d}a_t(r) = e^{-\gamma'' t} \int_{r_\star}^{r_c} \phi\left(X_t^S(0,r)\right)\,\mathrm{d}a_0(r) + \int_0^t e^{-\gamma''(t-s)} \phi\left(X_t^S(s,r_\star)\right) f(s)\,\mathrm{d}s,$$

for all $t \in [0,T]$ and for all $\phi \in \mathcal{C}_b^0([r_\star, r_c])$.

Now, let us prove the existence and uniqueness of solutions to system (3.8).

Theorem 35. *Let $T > 0$, $\gamma'' > 0$, $f \in \mathcal{C}^0([0,T];\mathbb{R}_+)$ and $a_0 \in \mathcal{M}$ a positive measure supported in $[r_\star, r_c]$. Then, system (3.8), with V defined at Eq. (3.4), has a unique solution.*

Démonstration. As explained before, it is enough to prove the existence and uniqueness of solutions to the fixed-point equation (3.17).

To do so, we define the following operator Γ on $\mathcal{C}^0([0,T],\mathbb{R}_+^*)$ by :

$$\Gamma(S)(t) = 4\pi \left(e^{-\gamma'' t} \int_{r_\star}^{r_c} (X_t^S(0,r))^2 \,\mathrm{d}a_0(r) + \int_0^t e^{-\gamma''(t-s)} (X_t^S(r,r_\star))^2 f(s)\,\mathrm{d}s \right), \; t \in [0,T]. \tag{3.18}$$

and we prove that Γ is a contraction.

We can prove easily that the range of Γ is $E = \mathcal{C}^0([0,T],[\varepsilon(T),+\infty))$, where $\varepsilon(T) = 4\pi e^{-\gamma'' T} r_\star^2 \int_{r_\star}^{r_c} \mathrm{d}a_0 > 0$ and, for any $\mu > 0$, we define the following norm on E :

$$\|f\|_E = \sup_{t\in[0,T]} |f(t)|\, e^{-\mu t}. \tag{3.19}$$

Then, the following inequality holds, for all $S_1, S_2 \in E$ and for all $t \in [0,T]$:

$$|\Gamma(S_1)(t) - \Gamma(S_2)(t)| \leqslant 8\pi r_c k \left(\int_{r_\star}^{r_c} \mathrm{d}a_0(r) + \|f\|_{L^1[0,t]} \right) \int_0^t \left| \frac{1}{S_1(s)} - \frac{1}{S_2(s)} \right| \mathrm{d}s,$$

which comes from the fact that

$$\left| \left(\min(r + \int_0^t \frac{k}{S_1(s)}\, \mathrm{d}s, r_c) \right)^2 - \left(\min(r + \int_0^t \frac{k}{S_2(s)}\, \mathrm{d}s, r_c) \right)^2 \right| \leqslant 2r_c k \int_0^t \left| \frac{1}{S_1(s)} - \frac{1}{S_2(s)} \right| \mathrm{d}s.$$

Indeed, for any $\lambda, \mu, \nu \in \mathbb{R}$, one has

$$|\min(\lambda,\nu)^2 - \min(\mu,\nu)^2| = |\min(\lambda,\nu) + \min(\mu,\nu)||\min(\lambda,\nu) - \min(\mu,\nu)| \leqslant 2\nu|\lambda - \mu|.$$

Since

$$\int_0^t \left| \frac{1}{S_1(s)} - \frac{1}{S_2(s)} \right| \mathrm{d}s \leqslant \frac{1}{\mu\varepsilon(t)^2} e^{\mu t} \|S_1 - S_2\|_E,$$

we obtain that

$$|\Gamma(S_1)(t) - \Gamma(S_2)(t)|\, e^{-\mu t} \leqslant 8\pi r_c k \left(\int_{r_\star}^{r_c} \mathrm{d}a_0(r) + \|f\|_{L^1[0,t]} \right) \frac{1}{\mu\varepsilon(t)^2} \|S_1 - S_2\|_E. \tag{3.20}$$

Thus, if we take μ large enough, the operator Γ is a contraction of the complete metric space $(E, \|.\|_E)$ and the Banach fixed point Theorem proves the existence and uniqueness of the solution to equation (3.17). □

We will denote by $S(f)$ the unique solution to equation (3.17), defined at Theorem 35, with the positive flux condition f. We prove now a stability result, that is to say an estimate of the quantity $|S(f_1)(t) - S(f_2)(t)|$ for $t \in [0,T]$.

Theorem 36. *Let $M \in \mathbb{R}^+$. We have the following estimate : there exists a continuous function $A_M \in \mathcal{C}^0([0,T])$ such that for all $t \in [0,T]$, for all $f_1, f_2 \in \mathcal{C}^0([0,T],[0,+\infty))$ such that $\|f_1\|_{L^1([0,T])} \leqslant M$,*

$$|S(f_1)(t) - S(f_2)(t)| \leqslant A_M(t) \|f_1 - f_2\|_{L^1([0,t])}.$$

Démonstration. We denote by Γ_1 (respectively Γ_2) the operator defined at Eq.(3.18) with the flux f_1 (respectively f_2). We decompose the difference $S(f_1) - S(f_2)$ as follows :

$$\begin{aligned} \|S(f_1) - S(f_2)\|_E &= \|\Gamma_1(S(f_1)) - \Gamma_2(S(f_2))\|_E \\ &\leqslant \|\Gamma_1(S(f_1)) - \Gamma_1(S(f_2))\|_E + \|\Gamma_1(S(f_2)) - \Gamma_2(S(f_2))\|_E. \end{aligned}$$

Using inequality (3.20), we can bound from above the first term of the right-hand side as follows :

$$\|\Gamma_1(S(f_1)) - \Gamma_1(S(f_2))\|_E \leqslant \frac{8\pi r_c k}{\mu\varepsilon(T)^2} \left(\int_{r_\star}^{r_c} \mathrm{d}a_0(r) + \|f_1\|_{L^1[0,T]} \right) \|S(f_1) - S(f_2)\|_E$$

and taking $\mu = \frac{16\pi r_c k}{\varepsilon(T)^2} \left(\int_{r_\star}^{r_c} \mathrm{d}a_0(r) + \|f_1\|_{L^1[0,T]} \right)$, we obtain $\|\Gamma_1(S(f_1)) - \Gamma_1(S(f_2))\|_E \leqslant \frac{1}{2} \|S(f_1) - S(f_2)\|_E$.
We now control the second term of the right-hand side $\|\Gamma_1(S(f_2)) - \Gamma_2(S(f_2))\|_E$, i.e. :

$$\|\Gamma_1(S(f_2)) - \Gamma_2(S(f_2))\|_E \leqslant \|\Gamma_1(S(f_2)) - \Gamma_2(S(f_2))\|_{L^\infty([0,T])} \leqslant 4\pi r_c^2 \|f_1 - f_2\|_{L^1([0,T])}$$

and therefore, using the value of μ and the definition (3.19) of the norm,

$$|S(f_2)(T) - S(f_1)(T)| \leqslant 8\pi r_c^2 \exp\left(T\frac{16\pi r_c k}{\varepsilon(T)^2}\left(\int_{r_\star}^{r_c} \mathrm{d}a_0(r) + M\right)\right) \|f_1 - f_2\|_{L^1([0,T])}.$$

For any $t \in [0,T]$, applying the previous inequality to the restriction of the solutions to $[0,t]$, we obtain

$$|S(f_2)(t) - S(f_1)(t)| \leqslant 8\pi r_c^2 \exp\left(t\frac{16\pi r_c k}{\varepsilon(t)^2}\left(\int_{r_\star}^{r_c} \mathrm{d}a_0(r) + M\right)\right) \|f_1 - f_2\|_{L^1([0,t])}.$$

□

3.3.3 Existence and uniqueness of solutions to system (3.1)-(3.6).

Now let us prove the following theorem, that states the existence and uniqueness for the full system (3.1)-(3.6), coupling the results of the previous two subsections.

Once again, this is equivalent to a fixed-point problem. Indeed, the resolution of the ODE part (3.1a) - (3.1b) requires the knowledge of the mean radius $\bar{r}$, which is computed from the solution a of the transport equation (3.1c). In turns, the boundary condition (3.6), which is necessary to compute a, involves the function p, solution of the ODE part.

More precisely, we consider a solution (m,p,a) to system (3.1)-(3.6). Knowing a, we can compute the function S thanks to formula (3.3) and therefore the characteristics X_t^S associated to system (3.1c)-(3.5b)-(3.6) thanks to formula (3.7).

We can consequently write $\bar{r}(t)$ under the form of a fixed point equation, using formula (3.2) and Eq.(3.9) with $f(t) = \beta(\bar{r}(t))p(t)$, that is to say

$$\bar{r}(t) = \frac{e^{-\gamma'' t}\int_{r_\star}^{r_c} X_t^S(0,r)\,\mathrm{d}a_0(r) + \int_0^t e^{-\gamma''(t-s)} X_t^S(s,r_\star)\beta(\bar{r}(s))p(s)\,\mathrm{d}s}{e^{-\gamma'' t}\int_{r_\star}^{r_c}\mathrm{d}a_0(r) + \int_0^t e^{-\gamma''(t-s)}\beta(\bar{r}(s))p(s)\,\mathrm{d}s}. \tag{3.21}$$

Reciprocally, if we find a function $\bar{r}$, solution to Eq.(3.21), we can then solve the ODE part (3.1a) - (3.1b)-(3.5a) of system (3.1) in order to obtain functions m and p, see Subsection 3.3.1. We can then deduce surface S from the fixed point equation (3.17) with $f(t) = \beta'(\bar{r}(t))\ p(t)$, that is to say, following the notation of Sec. 3.3.2, $S = S(\beta'(\bar{r})\ p)$. Solution a is finally given by Eq. (3.9).

We are therefore reduced to find a solution to the fixed point problem (3.21) with p solution to Eq. (3.1b) and $S = S(\beta'(\bar{r})\ p)$.

Now, let us prove the existence and uniqueness of solutions to system (3.1)-(3.6).

Theorem 37. *Let $m_0 \geqslant 0$, $p_0 \geqslant 0$, $a_0 \in \mathcal{M}$ with a_0 a positive measure supported in $[r_\star, r_c]$. Then, the system* (3.1)-(3.6) *has a unique solution $(m,p,a) \in \mathcal{C}^1([0,T],[0,+\infty))^2 \times \mathcal{C}^0([0,T],\mathcal{M}-w*)$.*

Démonstration. As explained before, we are reduced to find a solution to the fixed point problem (3.21) with p solution to Eq. (3.1b) and $S = S(\beta'(\bar{r})\ p)$. To do so, we define the following operator : $\Lambda : \mathcal{C}^0([0,T],[r_\star,r_c]) \to \mathcal{C}^0([0,T],[r_\star,r_c])$:

$$\Lambda(\bar{r})(t) = \frac{e^{-\gamma'' t}\int_{r_\star}^{r_c} X_t^S(0,r)\,\mathrm{d}a_0(r) + \int_0^t e^{-\gamma''(t-s)} X_t^S(s,r_\star)\beta(\bar{r}(s))p(s)\,\mathrm{d}s}{e^{-\gamma'' t}\int_{r_\star}^{r_c}\mathrm{d}a_0(r) + \int_0^t e^{-\gamma''(t-s)}\beta(\bar{r}(s))p(s)\,\mathrm{d}s} \text{ for all } t \in [0,T], \tag{3.22}$$

where $S = S(\beta'(\bar{r})\ p)$.

To prove the contraction of operator Λ, we will use the same idea and the same norm (3.19) than previously. We will also need the stability results demonstrated at subsections 3.3.1 and 3.3.2.

Let $F = \mathcal{C}^0([0,T],[r_\star,r_c])$. We will prove in the following that there exists $A > 0$ (which may depend on T) such that for all $\bar{r}_1, \bar{r}_2 \in F$ and for all $t \in [0,T]$,

$$|\Lambda(\bar{r}_1)(t) - \Lambda(\bar{r}_2)(t)| \leqslant A\int_0^t |\bar{r}_1(u) - \bar{r}_2(u)|\,\mathrm{d}u. \tag{3.23}$$

Therefore,

$$|\Lambda(\bar{r}_1)(t) - \Lambda(\bar{r}_2)(t)| \leqslant A \int_0^t \|\bar{r}_1 - \bar{r}_2\|_F \, e^{\mu u} \, \mathrm{d}u \leqslant \frac{A}{\mu} \|\bar{r}_1 - \bar{r}_2\|_F \, e^{\mu t}$$

and finally, if we take μ large enough, Λ is a contraction of the complete metric space $(F, \|.\|_F)$. Thus the Banach fixed-point theorem gives the existence and uniqueness of the solution to the fixed point equation (3.21).

Now let us prove inequality (3.23). Considering the definition (3.22) of operator Λ, it is sufficient to prove that the following three functions are Lipschitz-continuous and bounded with respect to $\bar{r}$ in $L^1([0,t])$:

1. $\bar{r} \mapsto e^{-\gamma'' t} \int_{r_\star}^{r_c} \mathrm{d}a_0(r) + \int_0^t e^{-\gamma''(t-s)} \beta(\bar{r}(s)) p(s) \, \mathrm{d}s$,
2. $\bar{r} \mapsto e^{-\gamma'' t} \int_{r_\star}^{r_c} X_t^S(0,r) \, \mathrm{d}a_0(r)$ where $S = S(\beta'(\bar{r}) \; p)$,
3. $\bar{r} \mapsto \int_0^t e^{-\gamma''(t-s)} X_t^S(s, r_\star) \beta(\bar{r}(s)) p(s) \, \mathrm{d}s$ where $S = S(\beta'(\bar{r}) \; p)$.

First, using the fact that β' is a bounded Lipschitz-continuous function, the bound (3.15) and the stability property (3.16) regarding the solution p of the ODE part (3.1b), it is straightforward to prove that for all $\bar{r}_1, \bar{r}_2 \in F$, for all $t \in [0,T]$,

$$\|\beta'(\bar{r}_1) p(\bar{r}_1) - \beta'(\bar{r}_2) p(\bar{r}_2)\|_{L^1([0,t])} \leqslant B \, \|\bar{r}_1 - \bar{r}_2\|_{L^1([0,t])} \, , \tag{3.24}$$

where $p(\bar{r})$ denotes the solution p of Eq. (3.1b) computed with the given mean radius function $\bar{r}$.

Function (1) : Function $\bar{r} \mapsto e^{-\gamma'' t} \int_{r_\star}^{r_c} \mathrm{d}a_0(r) + \int_0^t e^{-\gamma''(t-s)} \beta(\bar{r}(s)) p(s) \, \mathrm{d}s$ is therefore clearly bounded from below and above and Lipschitz-continuous.

Function (2) : Function $\bar{r} \mapsto e^{-\gamma'' t} \int_{r_\star}^{r_c} X_t^S(0,r) \, \mathrm{d}a_0(r)$ is bounded from above by $r_c \int_{r_\star}^{r_c} \mathrm{d}a_0(r)$.

Let $\bar{r}_1, \bar{r}_2 \in F$. Using the expression (3.7) of the characteristic curves, we obtain that

$$\begin{aligned} \left| X_t^{S(\beta'(\bar{r}_1) \; p_1)}(0,r) - X_t^{S(\beta'(\bar{r}_2) \; p_2)}(0,r) \right| &\leqslant \int_0^t \left| \frac{k}{S(\beta'(\bar{r}_1) p(\bar{r}_1))} - \frac{k}{S(\beta'(\bar{r}_2) p(\bar{r}_2))} \right| \mathrm{d}s \\ &\leqslant \frac{k}{\varepsilon(T)^2} \int_0^t |S(\beta'(\bar{r}_1) p(\bar{r}_1))(s) - S(\beta'(\bar{r}_2) p(\bar{r}_2))(s)| \; \mathrm{d}s. \end{aligned}$$

Since $\beta'(\bar{r}_1) p(\bar{r}_1)$ and $\beta'(\bar{r}_2) p(\bar{r}_2)$ are bounded, see the properties of β' and Eq. (3.15), we can use Theorem 36 and inequality (3.24) to obtain that

$$\begin{aligned} \left| X_t^{S(\beta'(\bar{r}_1) \; p_1)}(0,r) - X_t^{S(\beta'(\bar{r}_2) \; p_2)}(0,r) \right| &\leqslant \frac{k}{\varepsilon(T)^2} \int_0^t A_N(s) \, \|\beta'(\bar{r}_1) p(\bar{r}_1) - \beta'(\bar{r}_2) p(\bar{r}_2)\|_{L^1([0,s])} \; \mathrm{d}s \\ &\leqslant C \, \|\bar{r}_1 - \bar{r}_2\|_{L^1([0,t])} \, , \end{aligned}$$

which implies that function $\bar{r} \mapsto e^{-\gamma'' t} \int_{r_\star}^{r_c} X_t^S(0,r) \, \mathrm{d}a_0(r)$ is Lipschitz-continuous.

Function (3) : A similar proof enables to prove that function $\bar{r} \mapsto \int_0^t e^{-\gamma''(t-s)} X_t^S(s, r_\star) \beta(\bar{r}(s)) p(s) \, \mathrm{d}s$ is bounded from above and Lipschitz-continuous.

□

3.4 Asymptotic behaviour of the solutions in some simple degenerate cases

In this section, the behaviour of the solutions for large times is studied. We first prove that, under some conditions involving the growth rate and the differentiation rate, the number of mesenchymal cells (resp. of preadipocytes) goes either to zero or to infinity. In the case $\gamma'' \neq 0$, we prove that the mean radius converges towards the minimal radius as time goes to infinity. In the case $\gamma'' = 0$, we prove that the number of adipocytes converges towards a Dirac mass at r_c.

In some simple cases, we can therefore study the asymptotic behaviour of the solution, solving explicitly Eq. (3.1a) and (3.1b) as :

$$m(t) = m_0 \exp\left(\delta t - \int_0^t \beta\left(\bar{r}(s)\right)\, \mathrm{d}s\right),$$
$$p(t) = p_0 \exp\left(\delta' t - \int_0^t \beta'\left(\bar{r}(s)\right)\, \mathrm{d}s\right) + \int_0^t \exp\left(\delta(t-s) - \int_s^t \beta'\left(\bar{r}(u)\right)\, \mathrm{d}u\right) \beta\left(\bar{r}(s)\right) m(s)\, \mathrm{d}s.$$

For the proof of the asymptotic properties, we also introduce the zeroth and the first momentum of a_t, that is to say :

$$M_0(t) = \int_{r_\star}^{r_c} \mathrm{d}a_t(s), \qquad M_1(t) = \int_{r_\star}^{r_c} s\, \mathrm{d}a_t(s). \tag{3.25}$$

Note that $\bar{r}(t) = \dfrac{M_1(t)}{M_0(t)}$. We also have the following formula linking the zeroth and the first momenta of a :

$$M_0(t) = M_0(0)e^{-\gamma'' t} + \int_0^t e^{-\gamma''(t-s)} \beta'\left(\frac{M_1(s)}{M_0(s)}\right) p(s)\, \mathrm{d}s. \tag{3.26}$$

We have therefore the following proposition regarding the asymptotic behaviour of m and p :

Proposition 38. *Let $m_0 \geqslant 0$, $p_0 \geqslant 0$, $a_0 \in \mathcal{M} - w*$ with a_0 positive. We denote by m, p, a_t the solution given by Theorem 37. We have the following limits when $t \to +\infty$:*

1. *if $\delta - \beta(r_c) > 0$, then $m \to +\infty$,*
2. *if $\delta - \beta(r_\star) < 0$, then $m \to 0$,*
3. *if $m \to 0$ and if $\delta' - \beta'(r_\star) < 0$, then $p \to 0$,*
4. *if $m \to 0$ and if $\delta' - \beta'(r_c) > 0$, then $p \to +\infty$.*

Moreover, If $\delta - \beta(r_\star) < 0$ and $\delta' - \beta'(r_\star) < 0$, then there exist $C > 0$ and $\varepsilon > 0$ such that

$$p(t) \leqslant Ce^{-\varepsilon t},\ \forall t \in [0, +\infty). \tag{3.27}$$

Démonstration. First of all, as $r_\star \leqslant \bar{r}(s) \leqslant r_c$ for any $s \in [0, +\infty)$, we have the following inequality on m :

$$m_0 \exp((\delta - \beta(r_c))t) \leqslant m(t) \leqslant m_0 \exp((\delta - \beta(r_\star))t) \quad \forall t \in [0, +\infty), \tag{3.28}$$

which gives a limit for m in the two cases $\delta - \beta(r_c) > 0$ and $\delta - \beta(r_\star) < 0$.

In the same manner, when $m \to 0$, we can use the explicit expression to bound p as follows :

$$p_0 \exp((\delta' - \beta'(r_c))t) \leqslant p(t) \leqslant (p_0 + o(\exp(-\delta' + \beta'(r_\star))t)) \exp((\delta' - \beta'(r_\star))t),\ \forall t \in [0, +\infty).$$

Now, we denote by $\rho = -(\delta - \beta(r_\star))$ and $\rho' = -(\delta' - \beta'(r_\star))$ and we assume that $\rho > 0, \rho' > 0$. Thanks to (3.28), we obtain that $m(t) \leqslant m_0 e^{-\rho t}$, $\forall t \in [0, +\infty)$, and we use this bound in the formula for p, leading to :

$$p(t) \leqslant p_0 e^{-\rho' t} + \int_0^t e^{-\rho'(t-s)} \beta(r_c) m_0 e^{-\rho s}\, \mathrm{d}s$$

and therefore

$$p(t) \leqslant p_0 e^{-\rho t} + m_0 t e^{-\rho t}, \text{ if } \rho = \rho',$$
$$p(t) \leqslant p_0 e^{-\rho' t} + m_0 \frac{e^{-\rho t} - e^{-\rho' t}}{\rho' - \rho}, \text{ if } \rho \neq \rho'.$$

□

The previous proposition can be summarized in Table 3.1, where the couple in each cell represents $\left(\lim_{t\to+\infty} m, \lim_{t\to+\infty} p\right)$.

	$\delta - \beta(r_\star) < 0$	$\delta - \beta(r_c) > 0$
$\delta' - \beta'(r_\star) < 0$	$(0, 0)$	$(+\infty, ?)$
$\delta' - \beta'(r_c) > 0$	$(0, +\infty)$	$(+\infty, +\infty)$

TABLE 3.1 – Summary of the asymptotic behaviours of functions $t \to (m(t), p(t))$

3.4.1 Case $\gamma'' \neq 0$

In the case when $\gamma'' \neq 0$, we can make precise the result on the mean radius $\bar{r}$. More precisely, if the growth of p is exponential, which holds in particular if $\delta' - \beta'(r_c) > 0$, the total surface increases and the velocity decreases; meanwhile, the flux of mass in $r_\star$ increases and therefore a large proportion of the mass of adipocytes stays around $r_\star$.

Proposition 39. *We assume that $\gamma'' \neq 0$. We consider m, p, a_t the solution given by Theorem 37 and M_0 the zeroth momentum of a defined at Eq.(3.25). Then, we have the following limits when $t \to +\infty$:*

1. *if $p \to 0$, then $M_0 \to 0$,*
2. *if $p \to +\infty$, then $M_0 \to +\infty$.*

Moreover, if we assume that there exist $\varepsilon > 0$ and $C > 0$ such that for all $t \in [0, +\infty)$, $p(t) \geqslant Ce^{\varepsilon t}$, then $\lim_{t \to +\infty} \bar{r}(t) = r_\star$.

Démonstration. If $\gamma'' \neq 0$ and $p \to 0$ (resp. $p \to +\infty$) when $t \to +\infty$, we can use Eq.(3.26) to deduce that $M_0 \to 0$ (resp. $M_0 \to +\infty$).

Now, let us assume that $p(t) \geqslant Ce^{\varepsilon t}$, for all $t \in [0, +\infty)$. First we will prove that the surface increases exponentially, as follows :

$$S(t) \geqslant r_\star^2 M_0(t) \geqslant C r_\star^2 e^{-\gamma'' t} \int_0^t e^{\gamma'' s} \beta'(r_\star) e^{\varepsilon s} ds.$$

In particular, for t large enough, there exists $C > 0$ such that

$$S(t) \geqslant Ce^{\varepsilon t/2}$$

and therefore, since $r_\star < r_c$, we have for t large enough that :

$$\min(r_\star + \int_s^t \frac{k}{S(u)} \, \mathrm{d}u, r_c) = r_\star + \int_s^t \frac{k}{S(u)} \, \mathrm{d}u \in [r_\star, r_\star + Ke^{-\varepsilon t/2}]. \tag{3.29}$$

Now, from the expression of the mean radius (3.21) and of the characteristics (3.7), we get the following equivalent when $t \to +\infty$:

$$\bar{r}(t) \sim \frac{\displaystyle\int_0^t e^{\gamma'' s} \min(r_\star + \int_s^t \frac{k}{S(u)} \, \mathrm{d}u, r_c) \beta'(\bar{r}(s)) p(s) \, \mathrm{d}s}{\displaystyle\int_0^t e^{\gamma'' s} \beta'(\bar{r}(s)) p(s) \, \mathrm{d}s},$$

which leads to $\lim_{t \to +\infty} \bar{r}(t) = r_\star$ using Eq.(3.29).

□

3.4.2 Case $\gamma'' = 0$

Now, in this section, we consider the case $\gamma'' = 0$. The results on p and m of the previous section still hold but the results on M_0 are different. We prove that in the case when $\delta - \beta(r_\star) < 0$ and $\delta' - \beta'(r_\star) < 0$, the number of adipocytes converges towards a Dirac mass at r_c.

Proposition 40. *We assume that $\gamma'' = 0$, $\delta - \beta(r_\star) < 0$ and $\delta' - \beta'(r_\star) < 0$. We consider m, p, a_t the solution given by Theorem 37 and M_0 the zeroth momentum of a defined at Eq.*(3.25)*. Then, we have the following limits when $t \to +\infty$:*

$$\lim_{t\to+\infty} M_0(t) = M_0(0) + \int_0^{+\infty} \beta'(\bar{r}(s))p(s)\,\mathrm{d}s < +\infty$$

and

$$a_t \overset{*}{\rightharpoonup} \left(M_0(0) + \int_0^{+\infty} \beta'(\bar{r}(s))p(s)\,\mathrm{d}s \right) \delta_{r_c}.$$

Démonstration. The integrability of $\beta'(\bar{r}(s))p(s)$ comes from the exponential decay of p, see Eq. (3.27), and the limit for $M_0(t)$ when $t \to +\infty$ comes directly from the expression of M_0 at Eq.(3.26) with $\gamma'' = 0$.

Let us denote this limit by $M_{0,\infty} = M_0(0) + \int_0^{+\infty} \beta'(\bar{r}(s))p(s)\,\mathrm{d}s$. Since the total surface $S(t) \leqslant r_c^2 M_{0,\infty}$, we can deduce that S is bounded from above and therefore that $\int_0^{+\infty} \frac{k}{S(u)}\,\mathrm{d}u = +\infty$. Therefore, for t large enough, we can define $s_c(t)$ as the unique real such that

$$\int_{s_c(t)}^{t} \frac{k}{S(u)}\,\mathrm{d}u = r_c - r_\star.$$

Since S is bounded from above, we can deduce that $\lim_{t\to+\infty} s_c(t) = +\infty$.

Let $\phi \in \mathcal{C}^0([r_\star, r_c])$. For t large enough , Eq. (3.9) can be written as :

$$\int_{r_\star}^{r_c} \phi(r)\,\mathrm{d}a_t(r) = \phi(r_c)\int_{r_\star}^{r_c} \mathrm{d}a_0(r) + \phi(r_c)\int_0^{s_c(t)} \beta'(\bar{r}(s))p(s)\,\mathrm{d}s + \int_{s_c(t)}^{t} \phi(r_\star + \int_s^t \frac{k}{S(u)}\,\mathrm{d}u)\beta'(\bar{r}(s))p(s)\,\mathrm{d}s.$$

Moreover using

$$\left| \int_{s_c(t)}^{t} \phi(r_\star + \int_s^t \frac{k}{S(u)}\,\mathrm{d}u)\beta'(\bar{r}(s))p(s)\,\mathrm{d}s \right| \leqslant \|\phi\|_\infty \int_{s_c(t)}^{+\infty} \beta'(\bar{r}(s))p(s)\,\mathrm{d}s,$$

we can compute the limit and we get :

$$\lim_{t\to+\infty} \int_{r_\star}^{r_c} \phi(r)\,\mathrm{d}a_t(r) = M_{0,\infty}\phi(r_c),$$

which ends the demonstration. □

3.5 Numerical simulations

3.5.1 Numerical scheme

To find a numerical solution to the system of equations, we apply an explicit Euler scheme for the time approximation and an upwind scheme for the discretization of the transport-like equation of the adipocytes population.

We consider a grid with a uniform radius-step $\Delta r > 0$ (see Figure 3.2) and J intervals. The time step is denoted by Δt. The time step is not constant and it is updated at each iteration according to the Courant-Friedrichs-Lewy stability condition, that will be described later on. Nevertheless, for the sake of

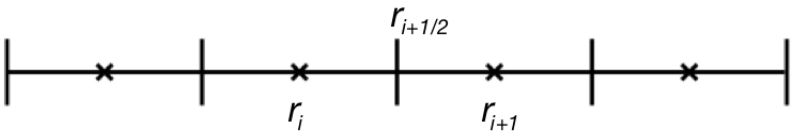

FIGURE 3.2 – Discretization of the interval. The variable a is computed in the middle of each interval, as well as the velocity.

simplicity, we denote it by Δt instead of Δt^n.
Let us denote by m^n, p^n the approximations of the solutions $m(t^n)$ and $p(t^n)$ at time t^n. Moreover, a_j^n stands for the approximation of $a(t^n, r_j)$ at time t^n and point r_j and $V^n_{j+1/2,j\in\{0,...,J\}}$ is the approximation of the velocity at time t^n at the cells boundaries.
Given the solutions $(m^n, p^n, a^n_{j\in\{1,...,J\}})$ and the velocity $V^n_{j+1/2,j\in\{0,...,J\}}$ at time t^n, the solution at time t^{n+1} is updated by

$$
\begin{aligned}
m^{n+1} &= m^n + \Delta t(\alpha(\bar r^n) - \gamma)m^n - \Delta t\beta(\bar r^n)m^n,\\
p^{n+1} &= p^n + \Delta t(\alpha'(\bar r^n) - \gamma')p^n + \Delta t\beta(\bar r^n)m^n - \Delta t\beta'(\bar r^n)p^n,\\
a_j^{n+1} &= a_j^n - \frac{\Delta t}{\Delta r}\left((V^n_{j+1/2})^+a_j^n - (V^n_{j+1/2})^-a^n_{j+1} - (V^n_{j-1/2})^+a^n_{j-1} + (V^n_{j-1/2})^-a_j^n\right) - \Delta t\gamma'' a_j^n, \qquad j\in\{1,...,J\},\\
V^n_{1/2}a_0^n &= \beta'(\bar r^n)p^n.
\end{aligned}
$$

Here above, for any real number V, $(V)^+$ and $(V)^-$ stand for the positive and negative parts of V : $(V)^+ = \max(V, 0)$ and $(V)^- = \max(-V, 0)$.

In this scheme, both integrals involved in the computation of $\bar r^n$ and the $V^n_{j+1/2,j\in\{0,...,J\}}$ are approximated via a centered rectangle formula (thus considering that the numerical approximation of a is piecewise constant in radius). We here decide to smooth out the velocity field by replacing the discontinuous one with the following Lipschitz-continuous one

$$V(t,r) = \frac{k}{S(t)}\mathbb{1}_{[r_\star, r_c-\varepsilon)}(r) - \frac{r-r_c}{\varepsilon}\frac{k}{S(t)}\mathbb{1}_{[r_c-\varepsilon, r_c)}(r),$$

where $\varepsilon > 0$ is a small parameter, which will be equal to $\varepsilon = 0.005r_c$ in the simulations.

Note that, in the case of a discontinuous velocity, such as (3.4), we would have used instead an upwind typed scheme, that would write (see [45, 46, 74]),

$$a_j^{n+1} = a_j^n - \frac{\Delta t}{\Delta r}\left((V_j^n)^+a_j^n - (V^n_{j+1})^-a^n_{j+1} - (V^n_{j-1})^+a^n_{j-1} + (V_j^n)^-a_j^n\right) - \Delta t\gamma'' a_j^n, \qquad j\in\{1,...,J\}.$$

Stability analysis : That the numerical unknowns remain non negative, as required by the modeling, imposes constraints on the time step.

Let us consider first the ODE part of the system. We are interested in situations where the parameters satisfy

$$\alpha - \gamma - \beta(r) < 0, \qquad \alpha' - \gamma' - \beta'(r) < 0 \qquad \forall r\in[r_\star, r_c].$$

Therefore, we expect the mesenchymal cells to decrease in time as well as the preadipocytes.

For the mesenchymal cells, the discrete relation casts as

$$m^{n+1} = \left(1 + \Delta t(\alpha - \gamma - \beta(\bar r^n))\right)m^n$$

Thus m^{n+1} remains non negative (if m^n is) as far as $1 + \Delta t(\alpha - \gamma - \beta(\bar r^n)) \geqslant 0$. A sufficient condition to satisfy this is that $\Delta t|\alpha - \gamma - \beta(r)| \leqslant 1$ for any r, thus the condition we keep is

$$\Delta t \leqslant \frac{1}{\max_{r\in[r_\star, r_c]}|\alpha - \gamma - \beta(r)|}.$$

In the same way we derive the condition for the preadipocytes equation. In the worst situation, m vanishes and the population of preadipocytes decreases with respect to time. Thus, p^{n+1} remains non negative provided

$$\Delta t < \frac{1}{\max_{r\in[r_\star,r_c]} |\alpha' - \gamma' - \beta'(r)|}.$$

Now let us consider the PDE in size space for the adipocytes. The upwind scheme is stable (in the linear case where the velocity field is given, see [45]) if the following Courant-Friedrichs-Lewy condition is satisfied :

$$\left|\frac{V^n \Delta t}{\Delta r}\right| \leqslant 1 \qquad \forall n,$$

where

$$V^n = \max_{j\in\{1,\dots,J\}} V_j^n.$$

Therefore, at each iteration the time step is updated in order to fulfill all three conditions identified so far.

3.5.2 Simulations

The parameters used in the simulations are given in Table 3.2, according to unpublished experimental data from C3M. A fit was performed with these data in order to calibrate the parameters ; a larger number of available data will be necessary to improve this calibration.

Value	Unit	Parameter or Indications
$\alpha = 0.1515$	1/day	proliferation rate for mesenchymal cells
$\alpha' = 0.0129$	1/day	proliferation rate for preadipocytes
$\beta(\bar{r}) = 0.0030 + \frac{0.1992}{1+e^{\frac{0.8550-\bar{r}}{0.0162}}}$	1/day	differentiation rate of mesenchymal cells in preadipocytes ($\bar{r}$ normalized, $\bar{r} \times 10$ is in microns)
$\beta'(\bar{r}) = 0.06043 - \frac{0.05965}{1+e^{\frac{\bar{r}-1.1125}{0.3640}}}$	1/day	differentiation rate of preadipocytes in adipocytes ($\bar{r}$ normalized, $\bar{r} \times 10$ is in microns)
$\gamma = 1.5\ 10^{-3}$	1/day	mortality rate for mesenchymal cells
$\gamma' = 1\ 10^{-5}$	1/day	mortality rate for preadipocytes
$\gamma'' = 1.653\ 10^{-6}$	1/day	mortality rate for adipocytes
$\bar{k} = 3.2875\ 10^{-9}$	mol/cell/day	available food per adipocytes with $k = \bar{k} \times$ ♯adipocytes
$r_m = 7.5$	μm	mesenchymal cells radius
$r_\star = 7.5$	μm	pre-adipocytes radius
$r_c = 50.64$	μm	maximal (critical) adipocytes radius

TABLE 3.2 – Values for parameters and variables used in the simulations.

Large time behaviour of the solutions to the model

The initial condition is defined as follows :

$$m_0 = 2.6793\,10^5 \qquad \text{[number of cells]}$$

$$p_0 = 7.6797\,10^3 \qquad \text{[number of cells]}$$

$$a_0(r) = \frac{0.0311}{\sqrt{2\pi\theta}} \exp\left(-\frac{r^2}{2\theta}\right)\ 10^8, \text{ with } \theta = 1.003 \qquad \text{[number of cells/}\mu\text{m]}$$

In this initial configuration, the adipocytes have a small radius. We study the behaviour of the solution in a large time scale, namely at the scale of a year ($t \in (0, 350)$ days).

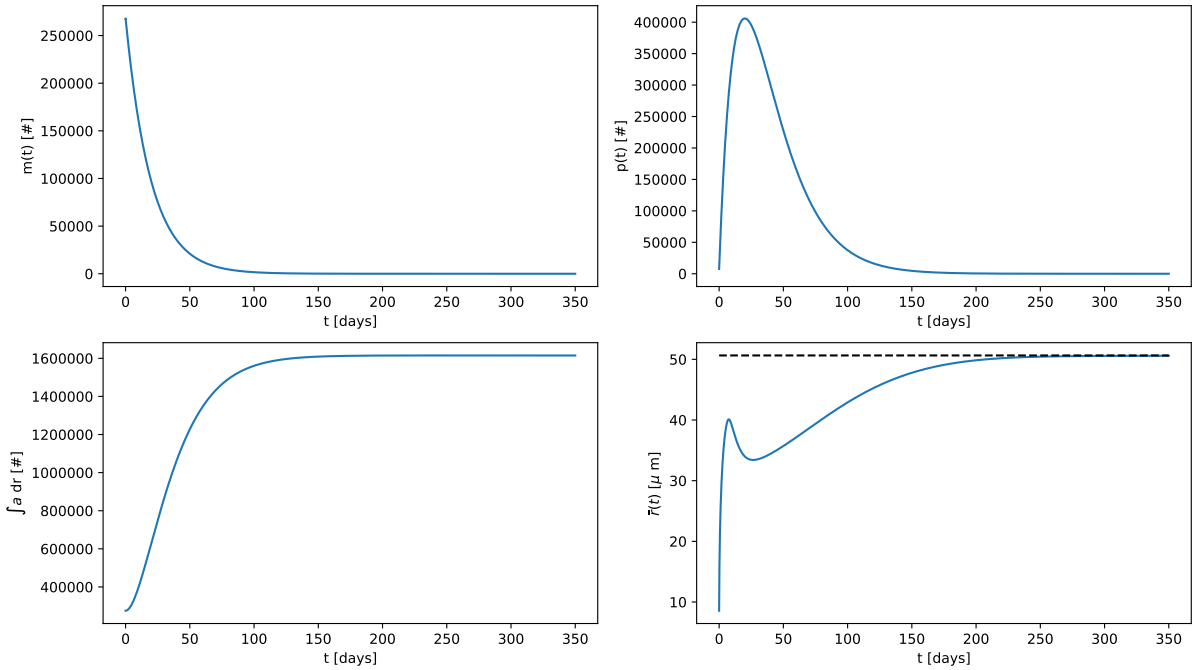

FIGURE 3.3 – Trend of the number of cells with respect to time : mesenchymal cells (*top left*), preadipocytes (*top right*), total number of adipocytes (*bottom left*) ; behaviour of the mean radius of adipocytes (*bottom right*).

Figure 3.3 shows the solution to the system of equations. Since we imposed that the proliferation rate is smaller than the sum of the differentiation and of the death rates, either the mesenchymal cells or the preadipocytes tend to zero for large time. At the beginning (first 40 days) the number of preadipocytes increases. This is due to the differentiation of the mesenchymal cells into preadipocytes. The number of adipocytes increases in time. Since we have set a very small death rate for the adipocytes ($\gamma'' \sim 10^{-6}$), the population reaches a plateau and the death of the adipocytes is not sensitive on this time scale of observation. We observe that the mean radius of the adipocytes grows rapidly at the beginning (first 10 days). Then, there is a drop due to the differentiation of preadipocytes into adipocytes : indeed, this process produces a large number of new adipocytes which have a radius equal to $r_\star$. Next, these small adipocytes grow until their radius reaches the critical value r_c.
The adipocytes growth can equally be observed in Figure 3.4. Initially, the adipocytes are small and they are subjected to a strong growth rate, since the growth rate is proportional to the inverse of the total surface of adipocytes. When the cells grow, the rate decreases because of an increasing of the surface of adipocytes. Figure 3.5 shows the distribution of adipocytes at the last time step. We observe the

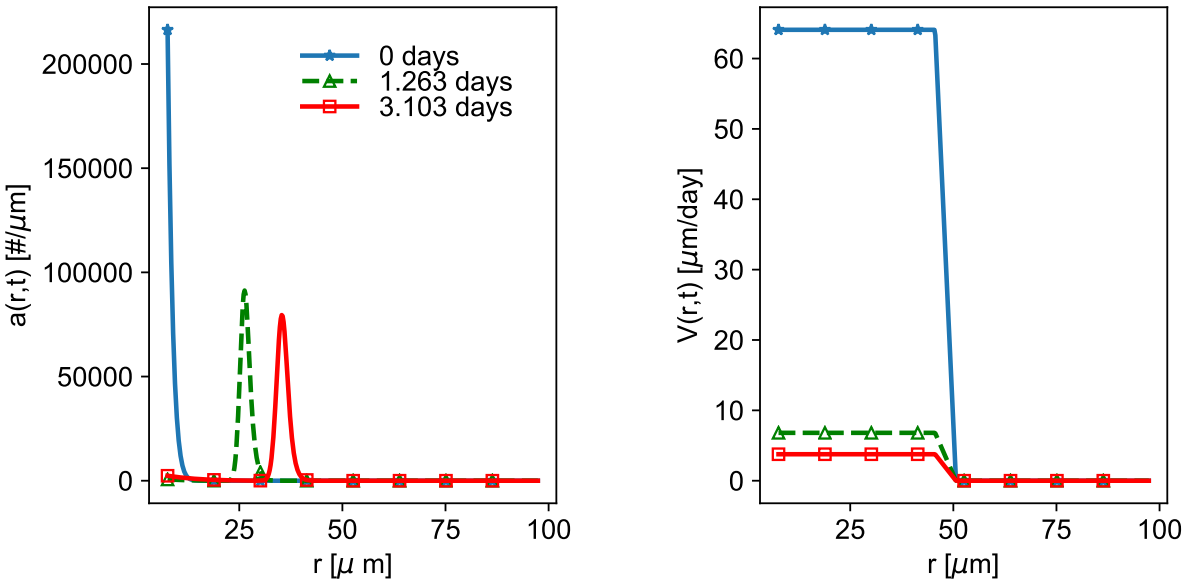

FIGURE 3.4 – Adipocytes distribution (*left*) and growth rate (*right*) with respect to the radius at three different time steps.

accumulation of the adipocytes population to the critical radius and the formation of the Dirac mass, according to the theoretical results.

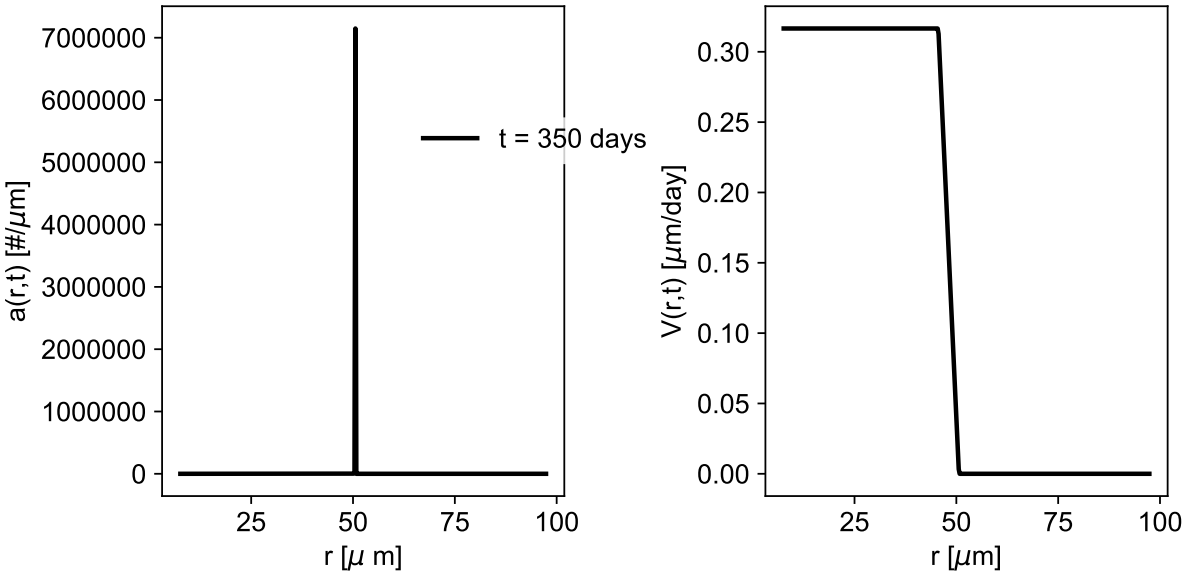

FIGURE 3.5 – Adipocytes distribution (*left*) and growth rate (*right*) with respect to the radius at the last time step.

Differentiation rates

We now observe the behaviour of the proliferations rates $\beta(\bar{r}(t))$ and $\beta'(\bar{r}(t))$. Figure 3.6 shows the dependency of the two functions with respect to the radius and to time (with parameters as given

in Table 3.2). Since the mean radius increases rapidly, also the differentiation rates reach rapidly the maximum value.

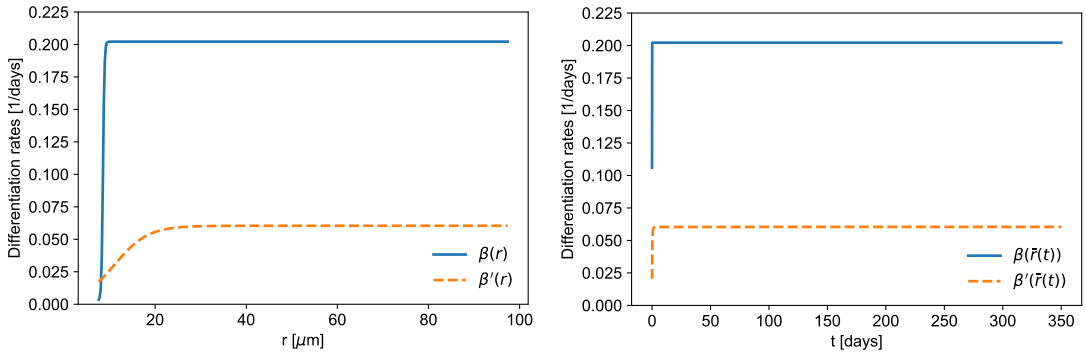

FIGURE 3.6 – Differentiation rates of the mesenchymal cells (blue continuous line) and the preadipocytes (orange dotted line) with respect to the radius (*left*) and to time (*right*).

The qualitative behaviour does not change significantly when working with constant differentiation rates (see Figure 3.7). It likely means that the quantities of interest remain in the low or high regions of the sigmoid in this example.

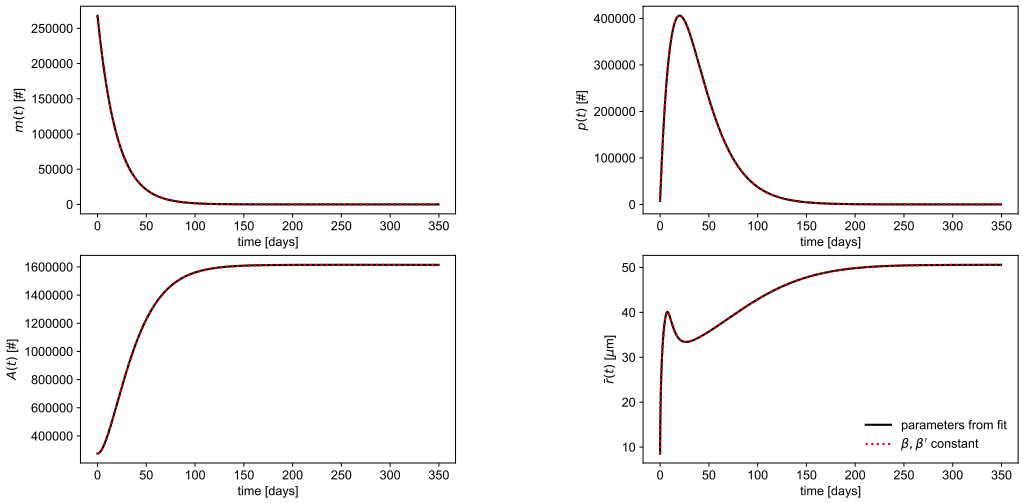

FIGURE 3.7 – Comparison between the cases when β and β' are sigmoid functions (black line) and constant (red dotted line).

However, changing the parameters of the the sigmoid functions β and β' can lead to different behaviours of the solutions. We consider three cases, detailed in Table 3.3 : we fix the slope of the sigmoid functions and we make the inflection points vary. Figure 3.8 shows the comparison of the populations dynamics in the different cases. The larger the inflection point of β', the more preadipocyte are generated, and therefore differentiate. In fact, since the differentiation rate is slower, they have time to duplicate. However, the dynamics of the adipocytes and of the mean radius in Figure 3.8 suggest that the parameters considered in Table 3.2 are in good agreement with the experimental data.

	$r_{\mathrm{ip},\beta}$	$r_{\mathrm{ip},\beta'}$
case 1	$0.5r_c$	$0.5r_c$
case 2	$0.5r_c$	r_c
case 3	$0.5r_c$	$0.7r_c$

TABLE 3.3 – Inflection points relative to β and β' in the different cases.

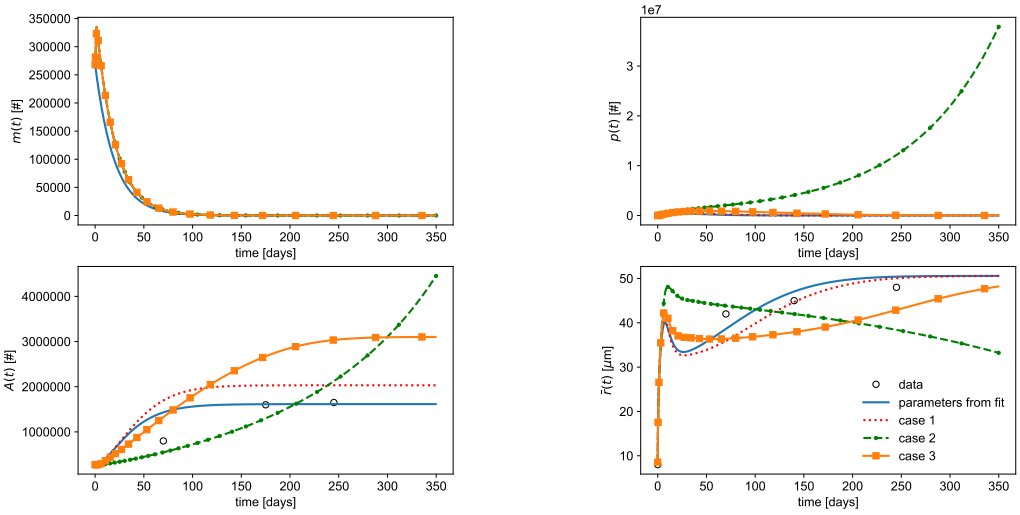

FIGURE 3.8 – Dynamics of the different cells (mesenchymal cells on the top left ; preadipocytes on the top right ; adipocytes on the bottom left) and of the mean radius of the adipocytes (bottom right) according to different shapes of the differentiation rates. The blue line refers to the parameters set in Table 3.2 and the black circles to the experimental data.

Comparison with experimental data

We now compare the models with the experimental data. We test the model structured in size (3.1) (referred to as 0D), and the models structured in both size and space, which will be detailed in the next sections : we refer to these models as 1D and 2D, depending on the space dimension used in the simulations. We observe in Figure 3.9 that the solutions to the 0D, the 1D and the 2D models have similar behaviour. Since the 0D model has been calibrated with the data, it is in good agreement with the experimental data.

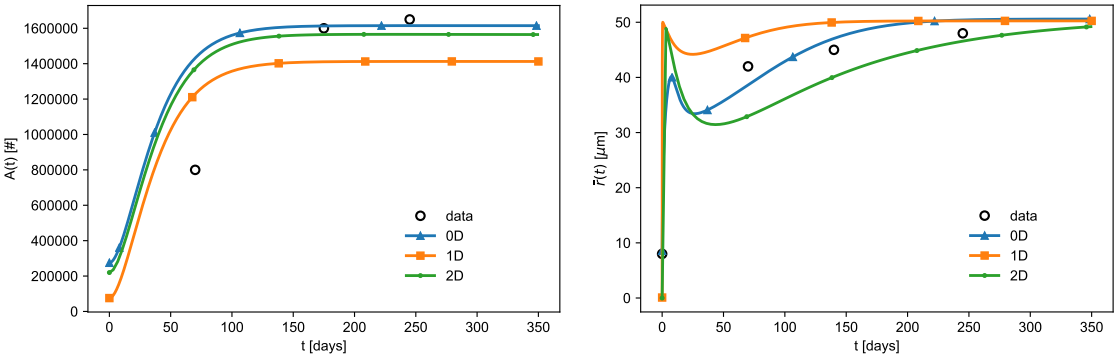

FIGURE 3.9 – Comparison of the models with the experimental data : adipocytes number (*left*) and mean radius (*right*).

3.6 Extension to a spatial model

3.6.1 Reinterpretation of the unknowns

We are now going to extend the previous model by incorporating a spatial dependence intended to describe inhomogeneities and displacement of the adipose tissue, following some ideas of mixture theory, see [4, 34, 68]. The functions $(t,x) \mapsto m(t,x)$, $(t,x) \mapsto p(t,x)$ now depend also on the space variable $x \in \Omega \subset \mathbb{R}^n$ ($n = 1$ or 2, and Ω is a bounded domain), and they are defined on $[0,\infty) \times \Omega$ with values in $[0,\infty)$. For the adipocytes, $(t,x,r) \mapsto a(t,x,r)$ is a function defined on $[0,\infty) \times \Omega \times [r_\star, +\infty)$ with values in $[0,\infty)$. We also introduce a new function $(t,x) \mapsto s(t,x)$ which is the volume fraction of the surrounding material (tissue) that is carrying the cells. The motion of all these species is driven by a velocity field $(t,x) \mapsto u(t,x)$.

In order to derive the model, let us go back to the mass balance relations. Given $r_2 > r_1 \geqslant r_\star$, the integral

$$\frac{4\pi}{3} \int_O \int_{r_1}^{r_2} a(t,x,r) r^3 \,\mathrm{d}r \,\mathrm{d}x,$$

gives the volume occupied in O at time t by the adipocytes with a radius $r \in (r_1, r_2)$. Accordingly,

$$\frac{4\pi}{3} \int_{r_\star}^{\infty} a(t,x,r) r^3 \,\mathrm{d}r$$

defines the volume fraction of the adipocytes, and the total volume of functional adipocytes at time t is given by

$$\mathbb{V}(t) = \frac{4}{3}\pi \int_\Omega \int_{r_\star}^{\infty} s^3 \; a(t,x,s) \,\mathrm{d}s \,\mathrm{d}x.$$

Schematically, we can split the volume of an adipocyte with radius $r \geqslant r_\star$ into two parts, see Fig. 3.10 : the center, with radius $r_\star$, is mainly made of water (volumetric mass density ρ_w), like the pre-adipocytes and mesenchymal cells, while the outer domain is made of lipids (volumetric mass density ρ_l). Therefore, the mass of such an adipocyte reads

$$\frac{4\pi}{3}\left(\rho_l(r^3 - r_\star^3) + \rho_w r_\star^3\right) = \frac{4\pi}{3}\rho_a(r) r^3$$

with

$$\rho_a(r) = \frac{\rho_l(r^3 - r_\star^3) + \rho_w r_\star^3}{r^3} \qquad \text{for } r \geqslant r_\star.$$

Accordingly, the mass density of the adipocytes is given by

$$M_a(t,x) = \frac{4\pi}{3} \int_{r_\star}^{\infty} \rho_a(r) a(t,x,r) r^3 \,\mathrm{d}r,$$

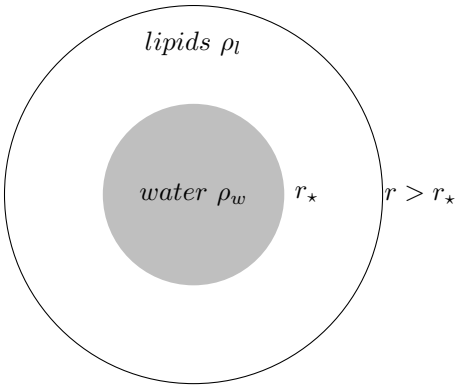

FIGURE 3.10 – Growing adipocyte.

and the total mass of adipocytes reads $\int_\Omega M_a(t,x)\,\mathrm{d}x$. The evolution of the mass density obeys

$$\partial_t M_a(t,x) = -\frac{4\pi}{3}\int_{r_\star}^{\infty} \gamma''\rho_a(r)a(t,x,r)r^3\,\mathrm{d}r + \frac{4\pi r_\star^3}{3}\rho_w\beta'(\bar r(t,x))p(t,x) + 4\pi\int_{r_\star}^{\infty}\rho_l V a(t,x,r)r^2\,\mathrm{d}r.$$

The last two terms describe two mechanisms of gain of mass : the transformation of pre-adipocytes into adipocytes with radius $r_\star$ and volumetric mass density ρ_w and the input of lipids from the surface of the existing adipocytes.

Similarly, the volume fractions of mesenchymal cells and pre-adipocytes are given by
— $\frac{4\pi}{3}r_m^3 m(t,x)$ for the mesenchymal cells,
— $\frac{4\pi}{3}r_\star^3 p(t,x)$ for the preadipocytes,
respectively, with r_m and $r_\star$ the typical radius of these cells. According to the biological data, we will use from now on that $r_m = r_\star$.

Given $O \subset \Omega$, the integrals $\int_O \frac{4\pi}{3}r_\star^3 m(t,x)\,\mathrm{d}x$ and $\int_O \frac{4\pi}{3}r_\star^3 p(t,x)\,\mathrm{d}x$ gives the volume occupied in O at time t by the mesenchymal cells and the preadipocytes, respectively.

The mass of each species is transported by a velocity field $(t,x) \in [0,\infty)\times\Omega \mapsto u(t,x) \in \mathbb{R}^n$, which amounts to say

$$\begin{cases} \dfrac{4\pi r_\star^3}{3}\rho_w\Big(\dfrac{\partial m}{\partial t} + \operatorname{div}_x(mu) - (\alpha-\gamma-\beta)m\Big) = 0, \\ \dfrac{4\pi r_\star^3}{3}\rho_w\Big(\dfrac{\partial p}{\partial t} + \operatorname{div}_x(pu) - (\alpha'-\gamma'-\beta')p - \beta m\Big) = 0, \\ \dfrac{\partial s}{\partial t} + \operatorname{div}_x(su) = 0. \end{cases} \tag{3.30}$$

For the adipocytes, we get

$$\partial_t(\rho_a r^3 a) + \nabla_x\cdot(\rho_a r^3 u a) + \rho_a r^3\partial_r(Va) = -\gamma''\rho_a r^3 a$$

which can also be written in the conservative form

$$\partial_t(\rho_a r^3 a) + \nabla_x\cdot(\rho_a r^3 u a) + \partial_r\left(\rho_a r^3 V a\right) - 3\rho_l r^2(Va) = -\gamma''\rho_a r^3 a \tag{3.31}$$

In fact, we can get rid of the densities in all these equations, and (3.31) can be simplified as :

$$\partial_t a + \nabla_x\cdot(ua) + \partial_r(Va) = -\gamma'' a. \tag{3.32}$$

Beyond the transport by the velocity u, the modeling also uses a pressure field, hereafter denoted $(t,x) \mapsto \mathrm{q}(t,x)$; we shall assume that the parameters β and β' are now functions of both $\bar r$ and this quantity q. It incorporates another source of space inhomogeneities. We assume that β, β' are non decreasing with respect to q. The pressure acts as a mechanical constraint that limits the expansion of

the adipocytes : the weaker the pressure, the easier the transformation of mesenchymal cells and pre-adipocytes to pre-adipocytes and adipocytes, respectively.

Let us now discuss the equations for the pair (u, q). The following constraint on the volume fractions holds, (using that the radius of pre-adipocytes and of mesenchymal cells coincides with the radius $r_\star$ of the smallest adipocytes)

$$s(t,x) + \frac{4\pi}{3}\left(r_\star^3 m(t,x) + r_\star^3 p(t,x) + \int_{r_\star}^{+\infty} r^3 a(t,x,r)\,\mathrm{d}r\right) = 1, \tag{3.33}$$

for a. e. $x \in \Omega$, $t \geqslant 0$. Therefore, adding the equations in (3.30) and (3.32), we find

$$\mathrm{div}_x u = \frac{4\pi}{3}\left(r_\star^3(\alpha-\gamma)m + r_\star^3\left(\alpha'-\gamma'-\beta'\right)p - \int_{r_\star}^{\infty} r^3 \partial_r\left(Va\right)\,\mathrm{d}r\right).$$

Using the same boundary condition as (3.6), we obtain

$$\mathrm{div}_x u = \frac{4\pi}{3}\left(r_\star^3(\alpha-\gamma)m + r_\star^3\left(\alpha'-\gamma'\right)p + 3\int_{r_\star}^{\infty} r^2 Va\,\mathrm{d}r\right). \tag{3.34}$$

Again, we observe that the last term can be integrated by parts to make two contributions appear, the former from the passage of pre-adipocytes to adipocytes with size $r_\star$, the latter due to surface fluxes of lipids. This constraint is related to the pressure q, which may be seen as the corresponding Lagrange multiplier.

Next, we use Darcy's equation :

$$u(t,x) = -K(x)\nabla_x \mathrm{q}(t,x) \text{ in } \Omega, \tag{3.35}$$

which have different frames of application [36, 107]. In (3.35), $x \mapsto K(x)$ takes values in the set of symmetric positive matrices. With (3.35) we are directly led to an equation for q, by using equation (3.34)

$$\begin{aligned} -\mathrm{div}_x(K(x)\nabla_x \mathrm{q}) &= \mathrm{div}_x u \\ &= \frac{4\pi}{3}\Big(r_\star^3(\alpha-\gamma)m + r_\star^3\left(\alpha'-\gamma'\right)p + 3\int_{r_\star}^{\infty} r^2 Va\,\mathrm{d}r\Big). \end{aligned}$$

We complement the whole system with initial conditions :

$$\begin{aligned} &m(0,x) = m_0(x), p(0,x) = p_0(x), s(0,x) = s_0(x), a(0,x,r) = a_0(x,r), \\ &u(0,x) = u_0(x) \end{aligned}$$

satisfying constraint (3.33).

Finally, we need to impose boundary conditions. For $r = r_\star$, we make use of the same birth condition as in the homogeneous case

$$V(t,r_\star)\ a(t,x,r_\star) = \beta'\left(\bar{r}(t,x),\ \mathrm{q}(t,x)\right)p(t,x).$$

On $\partial\Omega$, we shall find boundary conditions. For example, we can use

— for cells, the no-incoming-flux condition :

$$\text{if } u\cdot n < 0, \text{ then } a = p = m = 0 \text{ and } s = 1$$

where n stands for the unit outward normal vector on $\partial\Omega$, we also set

$$\mathrm{q} = 0 \text{ on } \partial\Omega.$$

— or the wall conditions.

These boundary conditions have to be compatible with condition (3.34).

3.6.2 Description of the numerical discretization

In order to discretize the system of equations, we apply the finite volume method. First, we find the spatial velocity u solving the Darcy's law. We formulate the Darcy's equation as a Laplace problem :

$$\begin{cases} -\mathrm{div}(K\nabla \mathrm{q}) = \mathrm{div}u, & \text{in } \Omega, \\ \mathrm{q} = 0, & \text{on } \partial\Omega, \end{cases} \tag{3.36}$$

From (3.36) we compute the pressure q. Then, we find the velocity $\mathbf{u}$ thanks to

$$u = -K\nabla q, \qquad \text{in } \Omega.$$

Applying the finite volume method, we obtain the following discretization on each element $\mathcal{K}_i$ of the domain.

$$\begin{aligned} -\int_{\mathcal{K}_i} \mathrm{div}(K\nabla \mathrm{q})\mathrm{d}x &= \int_{\mathcal{K}_i} \mathrm{div}(u)\mathrm{d}x \\ -[K\nabla \mathrm{q}\cdot n]_{\partial\mathcal{K}_i} &= \int_{\mathcal{K}_i} \mathrm{div}(u)\mathrm{d}x \end{aligned}$$

Finally, we apply an explicit upwind scheme in order to solve the system of hyperbolic equations. Regarding the adipocytes, we use a "directional" splitting and solve the transport equation either in space or with respect to the radius dimension applying the finite volume upwind scheme.

3.6.3 Numerical simulations for the spatial case

In one dimension, we consider an interval $(0, L)$ where $L = 1$ cm, therefore $x \in \Omega = (0, 0.01)$. We discretize the interval in $J = 300$ subintervals with a homogeneous spatial step Δx. Moreover, we have to consider the "radius" dimension of the adipocytes. To approximate their growth, we consider the radius of the adipocytes r to be in the interval $I_r = (r_\star, R)$, and we set $R = 90\mu$m. We divide I_r into 100 homogeneous intervals of size Δr. Then, we solve the problem that has one dimension with respect to the mesenchymal cells m and the preadipocytes p and two dimensions with respect to the adipocytes a.

Parameters setting and initial conditions

The parameters used for the simulations are the ones introduced in Table 3.2.
Regarding the initial condition, we consider the three populations to be distributed as gaussians centered in different points of Ω with various standard deviations (with respect to space and radius), namely

$$\begin{aligned} m_0(x) &= \frac{m_0}{\sqrt{2\theta^2L^2\pi}} \exp\left(-\frac{(x-x_m)^2}{2\theta^2L^2}\right), \\ p_0(x) &= \frac{p_0}{\sqrt{2\theta^2L^2\pi}} \exp\left(-\frac{(x-x_p)^2}{2\theta^2L^2}\right), \\ a_0(x,r) &= \left(\bar{a}_0 + \frac{a_0}{\sqrt{2\pi\theta_r}\sqrt{\theta_a^2L^2\pi}} \exp\left(-\frac{r^2}{2\theta_r}\right) \exp\left(-\frac{(x-x_a)^2}{\theta_a^2L^2}\right)\right) \mathbb{1}_{r<r_c}. \end{aligned}$$

For the numerical simulations, we take the following values for the standard variations : $\theta = 0.1$, $\theta_r = 0.1$, $\theta_a = 0.8$.

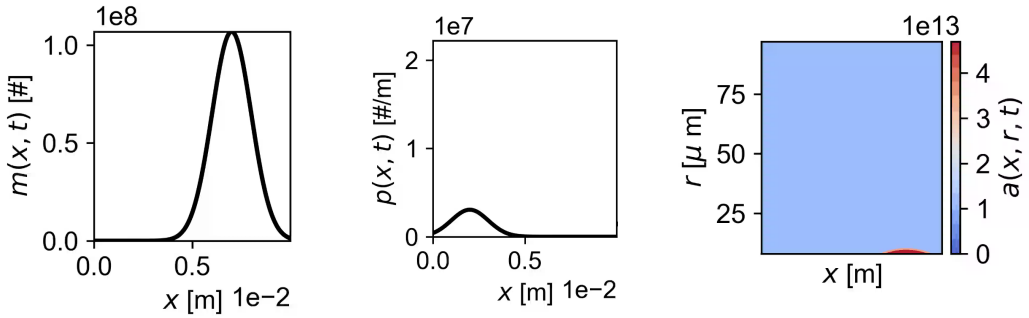

FIGURE 3.11 – Initial conditions for m (*left*), p (*center*) and a (*right*) relative to the 1D spatial model. The figure on the right represents the distribution of a in each point of the space x and with a radius r.

Figure 3.11 shows the initial conditions of the three unknowns. At the beginning we consider the highest number of adipocytes to have the minimal radius $r_\star$. However, since the growth rate is proportional to the inverse of the surface of adipocytes in each spatial point, we consider minimum number of cells $\bar{a}_0$ in each spatial point.

Simulations

We study the behaviour of the populations and of the mean radius first looking at a small time scale. In particular, we focus on the growth of the initial adipocytes. Figure 3.12 shows the adipocyte dynamic in the first day. We observe a slow growth of cells at the center of the initial gaussian, where the total surface of the cells is the highest. If we move from this point, the total surface of the cells decreases and consequently the radius of the cells increases faster. In Figure 3.13 we observe the global growth of adipocytes at different time steps. Like with the the space homogeneous equations, we observe a high growth rate at the beginning, leading to a fast growth of the adipocytes at the initial configuration.

Since the spatial velocity is very small, we do not observe a displacement of the different cells in the interval. The spatial dependency indeed introduces two different timescales relative to the growth of adipocytes and to the spatial displacement.

We observe on numerical simulations, see Fig.3.13, that dealing with the space dependent framework favors the apparition of bimodal size-distributions, that have been recorded in experiments, see [164, 163]. We were unable to reproduce such bimodal shape with the space homogeneous model. It is likely that such distributions correspond only to transient states of the model ; nevertheless they can be relevant on the time scale of observation. Going further in this direction requires a better knowledge of the parameters of the model and deserves a thorough investigation.

3.7 Conclusion

This work aims at setting up the basis of a multi-species model for adipose tissue growth, with the aim of improving our understanding of obesity. Our model is based on detailed behaviours and interactions of adipose tissue cells. It accounts for the adipocyte maturation, starting from mesenchymal cells differentiating into pre-adipocytes, which in turn differentiate into adipocytes whose sizes grow with food supply. The core of our model is the coupled regulation of cell differentiation and proliferation using phenomenological laws with sigmoid shapes that depend on the mean size of adipocytes.

The model in its non-spatial version is able to reproduce with reasonable precision experimental data after a fitting process, indicating that the main biological phenomena are probably accounted for in our model hypotheses. The time dynamics of the adipocyte radii exhibits an interesting early overshoot that cannot be seen in the data because of its sampling. The overshoot is easily explained by the model dynamics and its existence could be investigated in future experimental work. A shift in early adipocyte numbers is also observed, probably because of the difficult choice of an initial condition in the absence of a more detailed set of data.

The spatial model also keeps a reasonable agreement with the data, at least in order of magnitude and allows to exhibit a well known behaviour for adipocyte distribution : a bimodal distribution of adipocytes in space [164, 163]. This last result can be seen as a first step for validation of our model and makes it very promising. The fact that we do not observe spatial displacements of the cells needs more investigations and we can consider the mechanical properties of adipose tissues described in [143] to improve the spatial description in our model.

The next step is now to gather more complete data sets from experimental studies and to reach a proper validation. Once validated, such a model could prove invaluable to identify and quantify the biological mechanisms involved in adipose tissue growth and to understand potential dysfunctions linked to obesity.

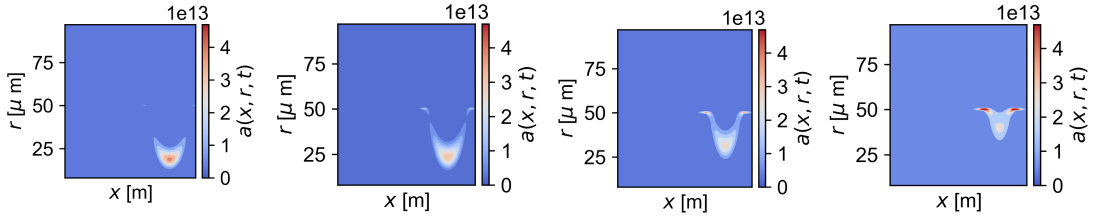

(a) $t = 0.1$ days (b) $t = 0.2$ days (c) $t = 0.5$ days (d) $t = 1$ day

FIGURE 3.12 – Adipocytes distribution with respect to space and radius at different time steps.

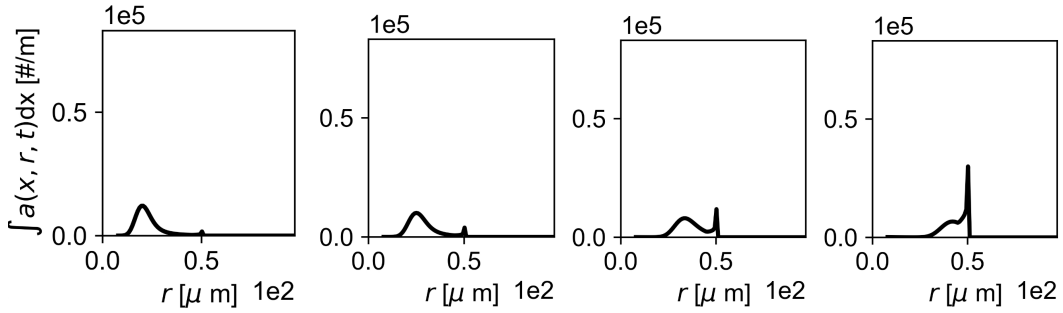

(a) $t = 0.1$ days (b) $t = 0.2$ days (c) $t = 0.5$ days (d) $t = 1$ day

FIGURE 3.13 – Adipocytes distribution with respect to the radius at different time steps.

Chapitre 4

Étude de l'apparition de cycles anormaux dans des lignées de levures

---

Ce chapitre porte sur un travail très exploratoire, réalisé en collaboration avec Marie Doumic, Teresa Teixeira et Zhou Xu, qui fait suite à la mise en évidence dans [180] d'un phénotype de *Saccharomyces cerevisiae* jusque là inconnu. On essaie donc de tirer des informations des données obtenues par nos collègues biologistes. On y étudie notamment la loi d'apparition du premier cycle anormalement long et les successions de tels cycles. Un article présentant nos résultats est en cours d'écriture et sera soumis pour publication cette année.

Introduction

The renewal of tissues in organisms is ensured by cell proliferation. Controlled proliferation is the result of the interaction of many complex mechanisms, that ensure that cells proliferate only when they should. However, these mechanisms can be subverted, resulting in an uncontrolled proliferation, which is the hallmark of cancer [96]. To understand how these sophisticated mechanisms can be flawed, one can study model organisms, such as yeasts, which are a good compromise between convenience to obtain a large amount of data, knowledge and technology relative to these organisms and similarity with the human cells behaviour.
Chromosomes are deoxyribonucleic acid (DNA) molecules that contain the genetic material of an organism. The cell proliferation goes through the replication of the chromosomes, which is ensured by the DNA polymerases. These enzymes are unable to replicate the DNA all the way to the end of the chromosome, because their activities are directional and they need a primer on which to add new deoxyribonucleotides. As a consequence, the terminal sequences of the chromosomes are shortened at each duplication. To prevent coding DNA from not being replicated, noncoding DNA caps each bound of the chromosomes. These regions of repetitive nucleotide sequences are called telomeres. A reverse transcription polymerase [5], called telomerase, has the ability to elongate them [18]. This enzyme is active mostly in cells that are fated to divide very often, such as stem cells or white blood cells. Thus, as divisions come one after another, the telomeres are subject to two antagonistic mechanisms : shortening and elongation, resulting in a dynamic equilibrium.
The lack of telomerase induces the shortening of telomeres and causes replicative senescence, a mechanism that prevents cells to undergo uncontrolled proliferation. In [180], the authors repressed the expression of telomerase, enabling the investigation of the telomeres shortening, and identified two different routes to replicative senescence. The model organism was *Saccharomyces cerevisiae* yeast mutant. They tracked the duration of the cell cycle yeast cells in each lineages, and classified them into two groups. The li-

neages that composed the first group, called type A, displayed cell cycles of normal duration before going through a sharp, irreversible transition to senescence. This behaviour is consistent with gradual telomere attrition [99, 98, 132]. This subpopulation of the lineages of yeast is the subject of [19] and [73], in which stochastics models were proposed to model the telomeres dynamics both in the presence and absence of telomerase. The accuracy of these models were confirmed by numerical simulations. In contrast, lineages belonging to the second group experience earlier, reversible arrests and are yet to be modeled.
Our goal in the present work is to revisit and systematically analyse the results obtained in [180], in order to get more insights on the possible mechanisms underlying this route to senescence. A first concern is to find other classifications to distinguish between type A and type B cells, in order to strenghten the previous results. An immediately related question is to assess the robustness of these potential classifications. The second step consists in studying the behaviour of the type B lineages : can we provide a law for the appearance of the early arrests ? How different are these arrests from the senescence ? Are the senescence of the type A and type B lineages comparable ?
In section 4.1, we summarize the work of [180] and investigate the robustness of the clusterings the authors proposed in it. Section 4.2 contains the main contribution of the present work. We identified three periods in the lineages. The first goes from the begining of the lineage to the appearance of the first long cycle. We present different attempts to predict the onset of the first arrest. The second period runs from the first arrest to the cycle preceeding the senescent phase. Finally, the last phase is made up of the senescence of the lineage, for lineages which experience it.

4.1 Recall and extension of the previous results

One of the major findings in [180] was to prove the existence of two different phenotypes in *Saccharomyces cerevisiae*. To achieve this, the authors separated the lineages in two groups, with three different clustering methods. This ensures that a core phenomenon is captured by their classification.
In the first part, we present the data available. In the second part, we explain the methodology of classification used by the authors in [180], and apply it to our (richer) dataset. The last part is devoted to the investigations on the robustness of the classification with respect to the value of the threshold, where we emphasize this critical matter.

4.1.1 Presentation of the data

In [180], the authors used a microfluidic device to track individual lineages and measure the duration of single cell cycles. A picture was taken every ten minutes to check if the cell followed has divided since the last picture. The resulting data are represented in Figures 4.1, 4.2 and 4.3. Each line represents a single lineage, and each rectangle represents a cycle. The time scale is given in minutes by the colorbar on the right side of the plot.

Wild type lineages and definition of a long cycle

The lineages with active telomerase, called *wild type* lineages, are represented in Figure 4.1. They display remarkably stable cell cycle durations as generations go on, although an accident might occur from time to time. To illustrate this property, we depicted on the top of Figure 4.4 the median duration and the most central 50% of the cycle duration for each generation. Another way to see this phenomenon is to plot the cumulative frequency of different generations, which we do in Figure 4.4, bottom, where 5^{th}, 25^{th} and 45^{th} are represented. We emphasize the fact that in this part of the experiment, there is no particular 'generation 0', in contrast with the second part explained below.
In [180], a cycle was considered as long if it lasts longer than $\mu + 3\sigma$, where μ is the total mean duration of the *wild type* cell cycles and σ their standard deviation. After censoring the first and two last cycles for experimental reasons, we obtain the value $9 + 3 * 3 = 18$. We discuss this definition in subsection 4.1.3.

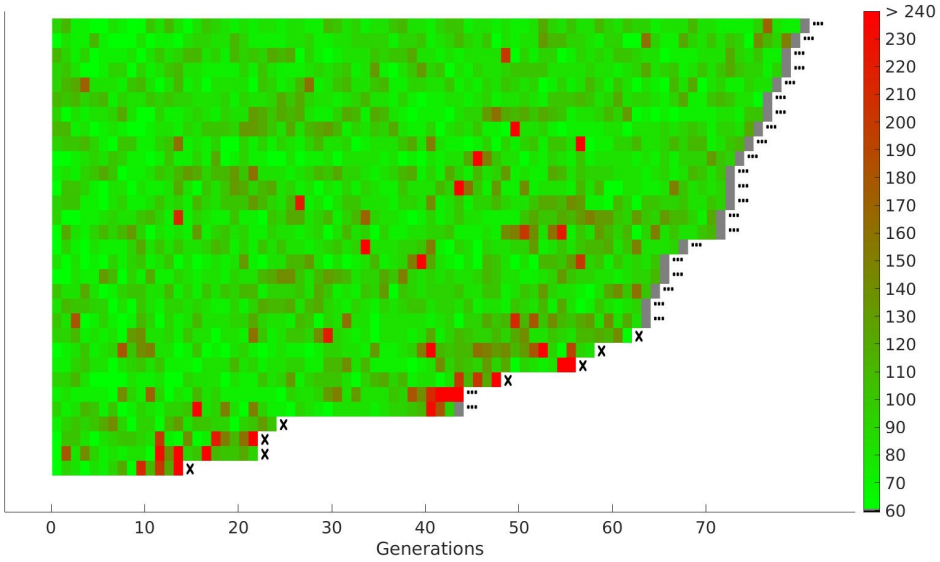

FIGURE 4.1 – The 31 *wild type* lineages. Each horizontal line represents a single lineage, and each segment is a cell cycle. The ellipsis (...) at the end of a lineage indicates that the cell was still alive at the end of the experiment and a cross that it was not. Cell-cycle duration is indicated by the color bar. A grey segment indicates that the cell cycle was not complete at the end of the experiment. A black segment indicates cycles longer than 360 minutes.

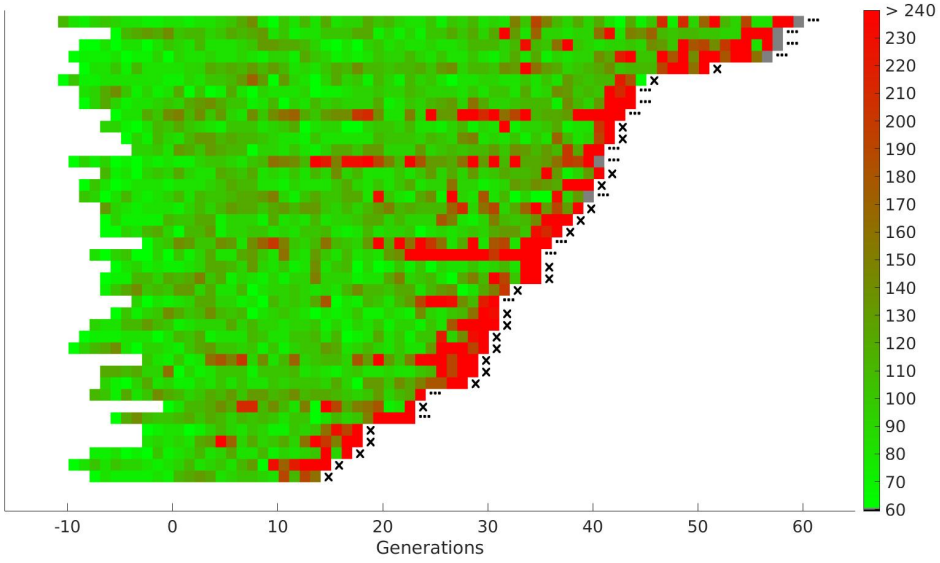

FIGURE 4.2 – The initial 40 telomerase negative lineages. The convention is the same than used in Figure 4.1, except gereration 0 corresponds to the moment when the doxicycline was added.

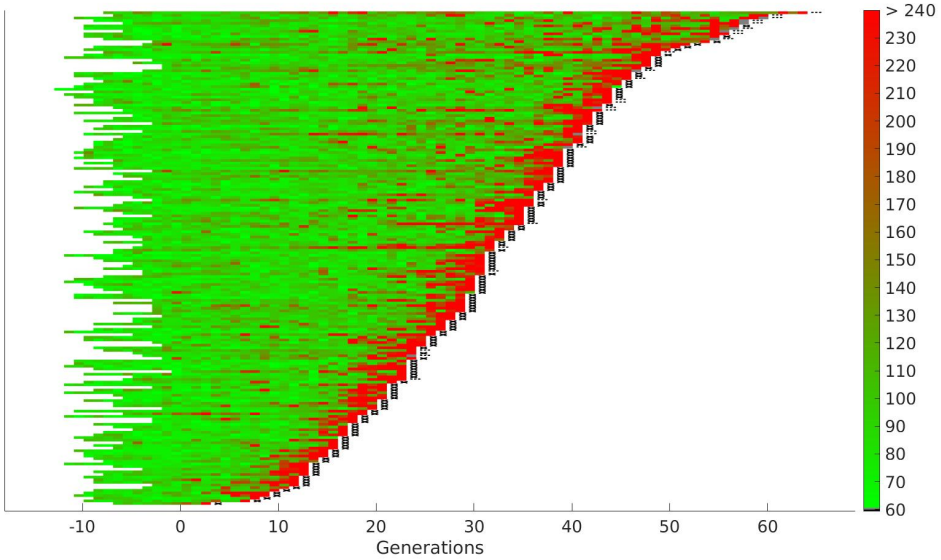

FIGURE 4.3 – The 187 telomerase negative lineages. The convention is the same than used in Figure 4.2.

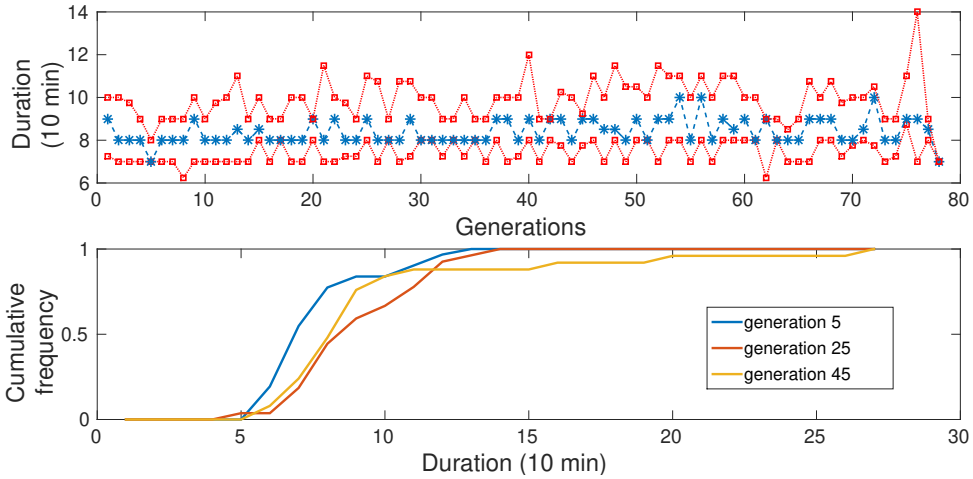

FIGURE 4.4 – Evolution of the duration of the cycles as generations go on for the *wild type* lineages. Top : quartiles of the duration of each generation. Blue : median duration. Red : upper and lower bounds of the second and third quartiles, respectively. Bottom : for a given generation, one can compute the frequency of the duration of the cycles, for all lineages. We display the cumulative frequencies of the duration of the cycles of generations 5, 25 and 45.

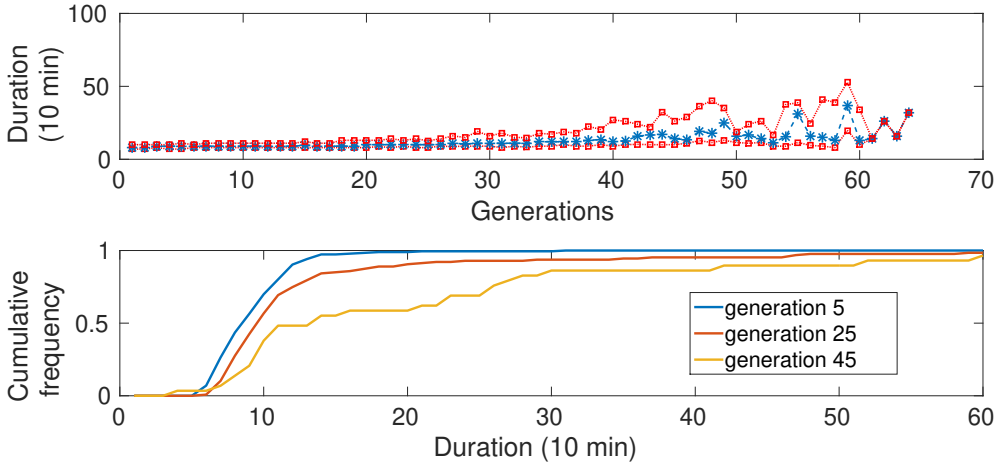

FIGURE 4.5 – Evolution of the duration of the cycles as generations go on for telomerase negative lineages. We display the same informations than in Figure 4.4. One can see that later generations tend to be made up with longer cycles.

Telomerase negative lineages

Studying the mechanism of telomere shortening requires to repress the expression of telomerase. To achieve this, doxycycline was added in the microfluidics device at a certain time in the experiment, thus marking the first generation with a nonfunctional telomere elongation mechanism in each lineage. In [180], the authors worked on 40 lineages, resulting in Figure 4.2. We now have a richer dataset, that counts 187 lineages, displayed in Figure 4.3.
In contrast with the *wild type* lineages, we observe in this case a more heterogeneous distribution of the durations of the cell cycles, with a significant amount of long cycles. As depicted in Figure 4.5, on top, the duration of the cell cycles increases significantly as the divisions go on. This indicates that the repression of telomerase induces the appearance of a significant amount of long cycles. Unlike the consistency depicted in Figure 4.4 on bottom, the estimates of the cumulative frequency of telomerase negative lineages display a slower rise to 1, see Figure 4.5, bottom.

4.1.2 Classification of the lineages in two categories

In [180], the authors classified the telomerase negative lineages into two groups. The first group, called type A, is composed by lineages which behaviour is consistent with gradual telomere attrition [99, 98, 132]. In contrast, lineages belonging to the second group, called type B, experience earlier, reversible arrests.
In the first part of this subsection, we explain precisely the main classification used in [180]. In the following part, we show that the definition we take for senescence, slightly different from the one used in that article, produces a similar classification in type A/type B on the 40 lineages, which suggests that applying it to our richer data still catch the core phenomenon of the existence of two different phenotypes. Finally, in the last part, we investigate the rate of extinction of each group.

The method using the number of long cycles before senescence

The first step of the classification is to split the cycles into two groups, short and long. The method used was mentionned in subsubsection 4.1.1.
The second step is to demarcate a senescence phase. In [180], it was taken as the gathering of long cycles at the end of a lineage, with potentially one short cycle inside, to take into account the randomness inherent to living organisms. We take a slightly different definition of 'senescent lineage' in the present work. To be considered as senescent, a lineage shall fulfil two conditions. First, it has to be terminated

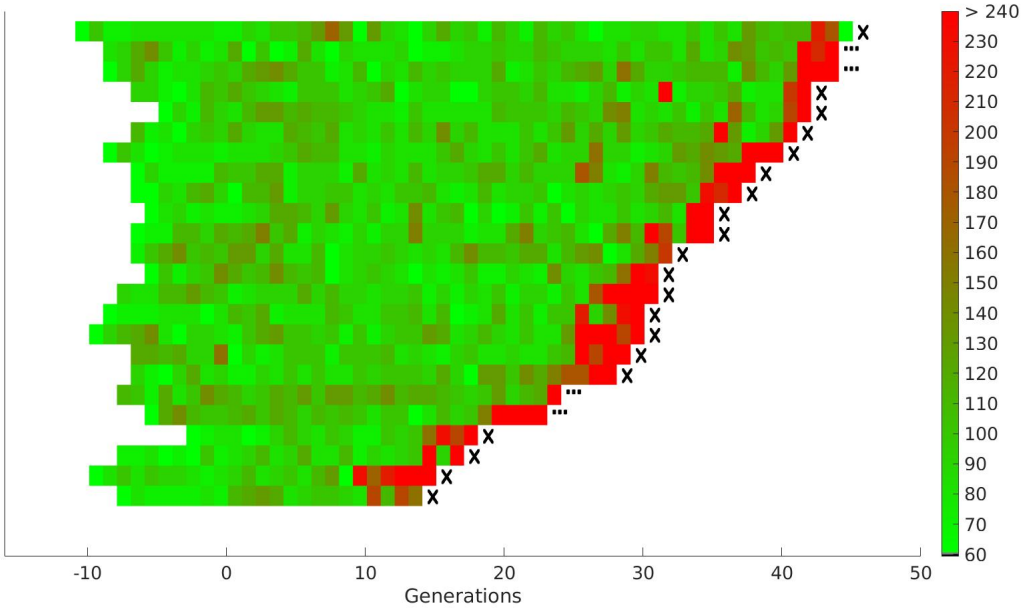

FIGURE 4.6 – the 24 telomerase negative lineages of type A from [180]. The convention is the same than used in Figure 4.7. It appears clearly that this groupe is made of lineages whose long cycles are concentrated at the end.

at the end of the experiment (denoted by a cross at the right of the lineages in Figure 4.3 and similar ones), *i.e.* the last representative of a lineage was not able to divide anymore. Second, the ultimate cycle of the lineage must be long, otherwise it might just be an accidental death. The senescent phase is then defined as the consecutive long cycles that are located at the very end of a lineage.
Finally, the lineages are classified according to the number of long cycles that occur before the senescence phase. The type A group is constituted of lineages that count 0 or 1 long cycle before this phase, and are consistent with regular shortening of the telomeres. The type B group is made up of the other lineages. The clustering obtained in [180] is depicted on Figure 4.6 for the type A group and on Figure 4.7 fro the type B.
In the present work, we first apply the method based on the number of long cycles before senescence to the 40 telomerase-negative lineages, except we determine the senescence with our definition instead of the one used in [180]. On Figure 4.8, we represent the group called type A obtained through our method and on Figure 4.9 for the type B group. The visual similarity with Figures 4.6 and 4.7 suggests that our procedure does not miss the phenomenon that was highlighted in [180], which makes us confident to apply it to the richer dataset and capture it in this situation too. Our groups are made up of 17 and 16 lineages, which means that some lineages were sorted neither in the type A group nor the type B group. This is a consequence of our classification method, as detailed below.
This results to Figure 4.10 for the type A and Figure 4.11 for the type B. Additionaly, we obtained 56% of type A lineages, which is close to the proportion given in [180], namely 60%.

Duration in generations of the lineages

The ability of the type B to escape arrests suggests that the lineages sorted in this group tend to count more generations from the addition of doxycycline to the end of the lineage. So we depicted on Figure 4.12 the percentage of the lineages present from generation 0 that are still alive at each generation. It happens that this representation is not very informative. As expected, the type B lineages start to extinguish slightly later than the type A lineages. It happens that lineages of both groupe extinguish with the same

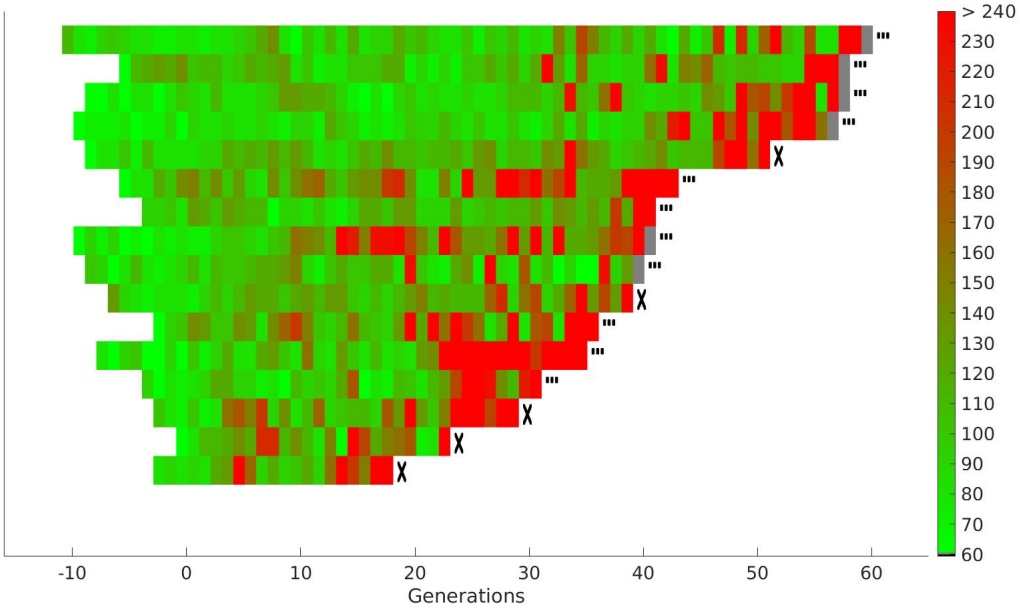

FIGURE 4.7 – the 16 telomerase negative lineages of type B from [180]. The convention is the same than used in Figure 4.7. Unlike the behaviour depicted in Figure 4.2, for this group the long cycles are more scattered throughout the lineages.

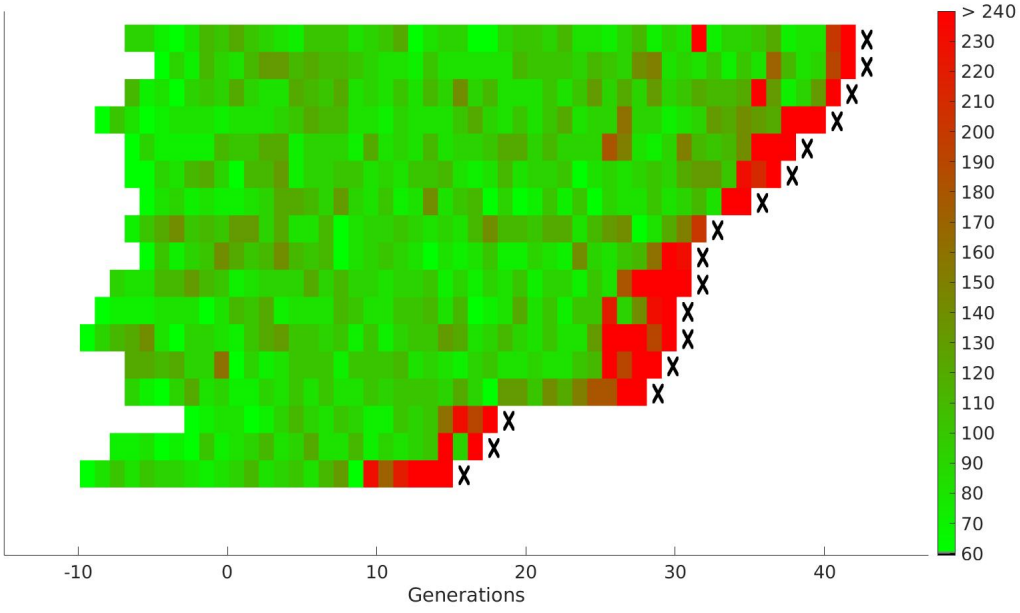

FIGURE 4.8 – the 17 telomerase negative lineages of type A obtained with our method. The convention is the same than used in Figure 4.7. It appears clearly that this groupe is made of lineages whose long cycles are concentrated at the end.

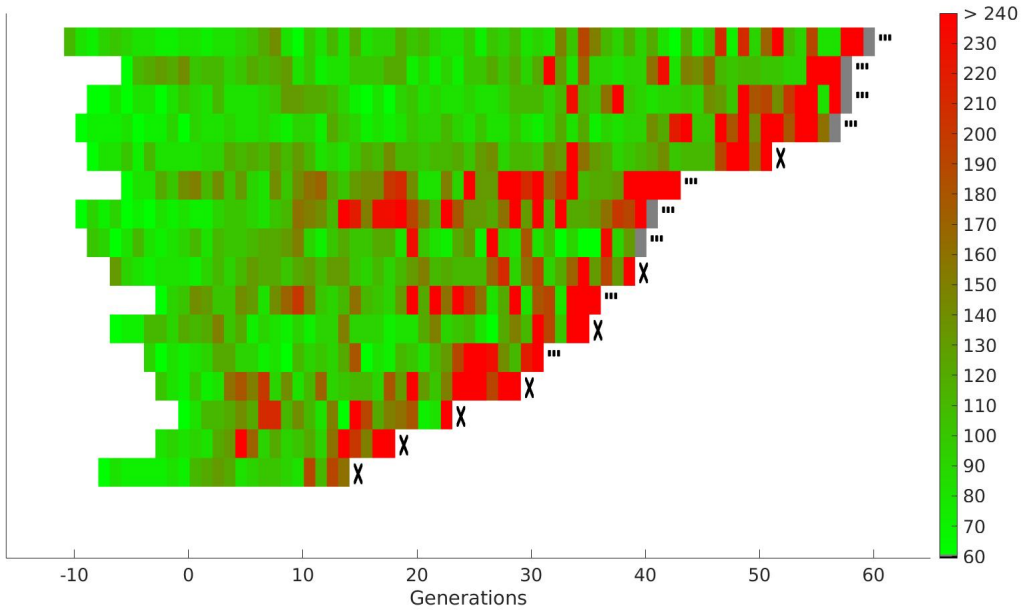

FIGURE 4.9 – the 16 telomerase negative lineages of type B obtained with our method. The convention is the same than used in Figure 4.7. Unlike the behaviour depicted in Figure 4.2, for this group the long cycles are more scattered.

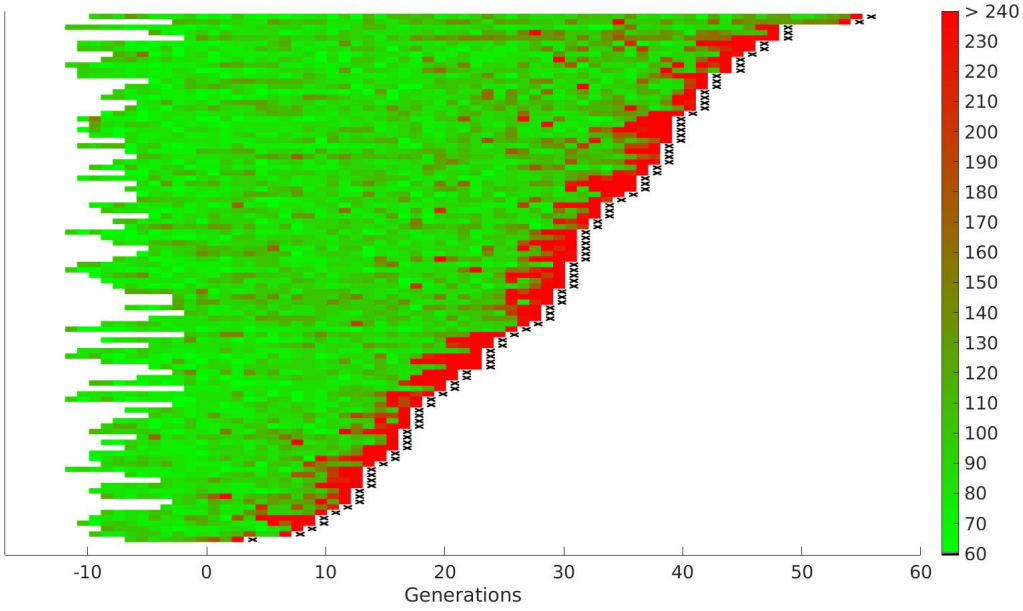

FIGURE 4.10 – Telomerase negative lineages of type A. The convention is the same than used in Figure 4.7. It appears clearly that this groupe is made of lineages whose long cycles are concentrated at the end.

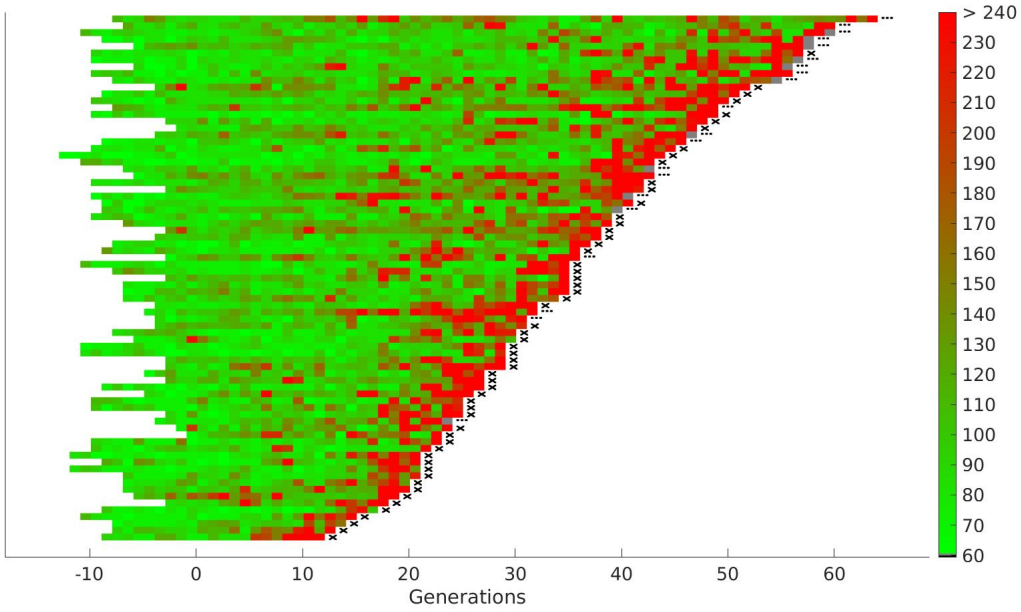

FIGURE 4.11 – Telomerase negative lineages of type B. The convention is the same than used in Figure 4.3. Unlike the behaviour depicted in Figure 4.7, for this group the long cycles are more scattered.

rate. Thus, this study does not provide a fresh way to discriminate type A and type B lineages.

4.1.3 Robustness of the classification

In [180], the definition chosen to tell apart short and long cycles was $\mu + 3\sigma$ of the *wild type*. We investigate in this subsection the robustness of the results with respect to the definition, which is partly arbitrary. First, we calculate the proportion of type A in the population with different methods of clustering that managed to create two groups for a fixed value of the threshold, but this time for a wide range of values. We finish this subsection by explaining how the type A/type B classification combined with our definition of the senescence phase can lead to exclude some lineages of our study.

Number of long cycles before the senescence phase

To assert robustness of the classification number of long cycles before senescence, we repeat the whole procedure for different values of the threshold. The result is depicted on Figure 4.13 and show no plateau, which would have indicated a local stability of the classification, and thus pointed a particular value for the threshold to consider. The shape of this figure is easy to interprete. For small values of the threshold, almost every cycle is classified as long, so almost all lineages ending by a death is considered as senescent. As a consequence, a significant number of lineages are then composed only of the senescence phace, so only a few number of them can have more than one long cycle before this phase. This tendency is reversed as the value of the threshold increases. For high values, very few cycles are long, so it is unlikely for a lineage to have two or more long cycles before its senescence.

Limits of the type A/type B classification : unclassifiable lineages

The procedure to classify the lineages based on the number of long cycles before the senescence phase can lead to censor some data. The first step in this classification consists in determining the senescence phase, but the definition of this phase that we take implies that some lineages, partly depending on the value of the threshold, might not fulfill the two conditions (see section 4.1.2). When a lineage is not

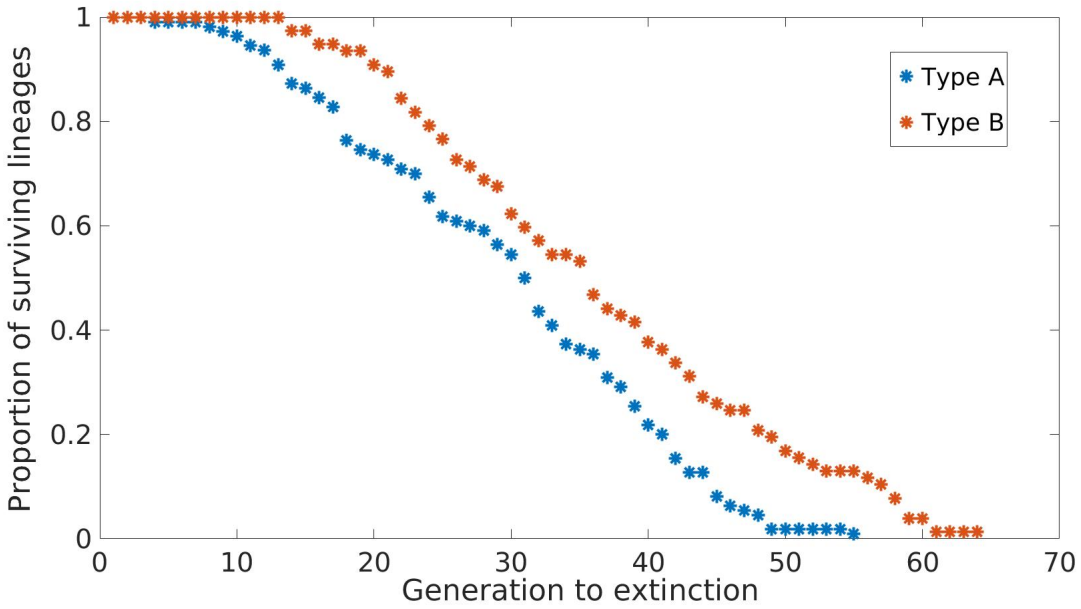

FIGURE 4.12 – Proportion of surviving lineages as the generations go on. Type A and type B lineages appears to extinguish at the same rate.

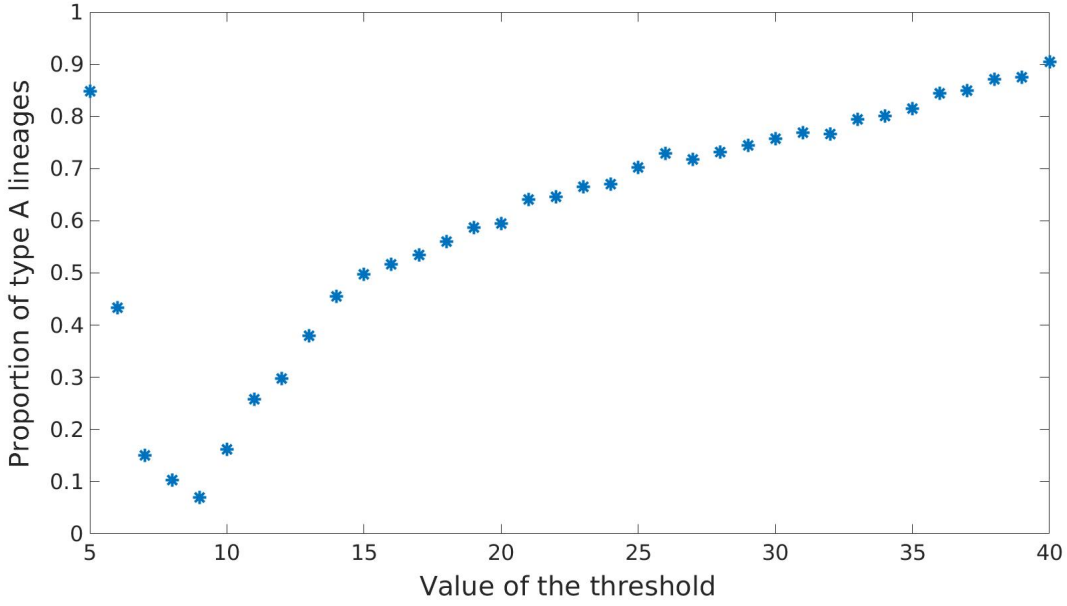

FIGURE 4.13 – Proportion of type A lineages in the population as a function of the value of the threshold.

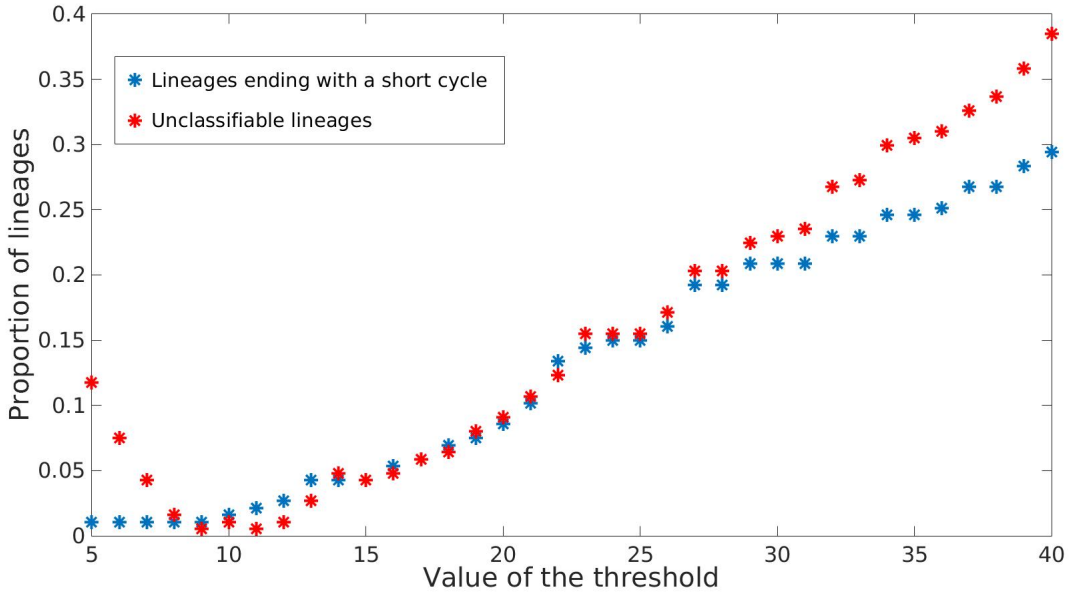

FIGURE 4.14 – Influence of the value of the threshold on our interpretation of the data. Blue : proportion of cells ending with a short cycle, thus interpreted as an 'accidental death', with respect to the value of the threshold defining a long cycle. Red : proportion of lineages that can be classified neither as type A nor as type B.

senescent, it can either come from ending by a short cycle or not being terminated at the end of the experiment.
In the first case, it is hardly possible to attribute this death to senescence, thus we shall interprete this termination as an 'accidental death'. The amount of lineages for which we interprete their death as accidental is straightforwardly related to the value of the threshold. If the lineage counts at least two long cycles, we can anyway classify it as a type B, but if not, it is impossible to conclude. Indeed, if the lineage had not encountered death otherwise than through senescence, it might either have been a type A or type B, depending on what could have happened until senescence. The second case is impacted by the value of the threshold in a similar manner. If the lineage is not terminated at the end of the experiment, both type A or type B behaviour could have been observed if it had lasted longer. Again, if the lineage already experienced long cycles twice or more, then we know for sure that it is a type B.
The proportion of accidental death and unclassifiable lineages are depicted on Figure 4.14. These exclusions weaken our dataset by decreasing the number of lineages available for statistical tests, and their number increases as the value of the threshold increases, so only careful considerations shall result in an increase of the value of the threshold considered.
In conclusion, even though the type A/type B classification surely reveals a core phenomenon, the absence of a region for the value of the threshold for which the two groups would remain roughly unchanged is not entirely satisfying. That is why in the sequel we will avoid to make this *a priori* clustering, but still bearing in mind that a gradient between these two routes to senescence does exist.

4.2 Identification and study of three periods in a lineage

The behaviour observed in type A lineages was studied in [19] and [73]. In these articles, the number of generations before the onset of senescence and the mechanisms leading to it was modeled by two stochastic models, and then confirmed by numerical simulations. In the present study, we aim at understanding the dynamics of appearance of precocious long cycles. In particular, we want to comprehend the onset of the

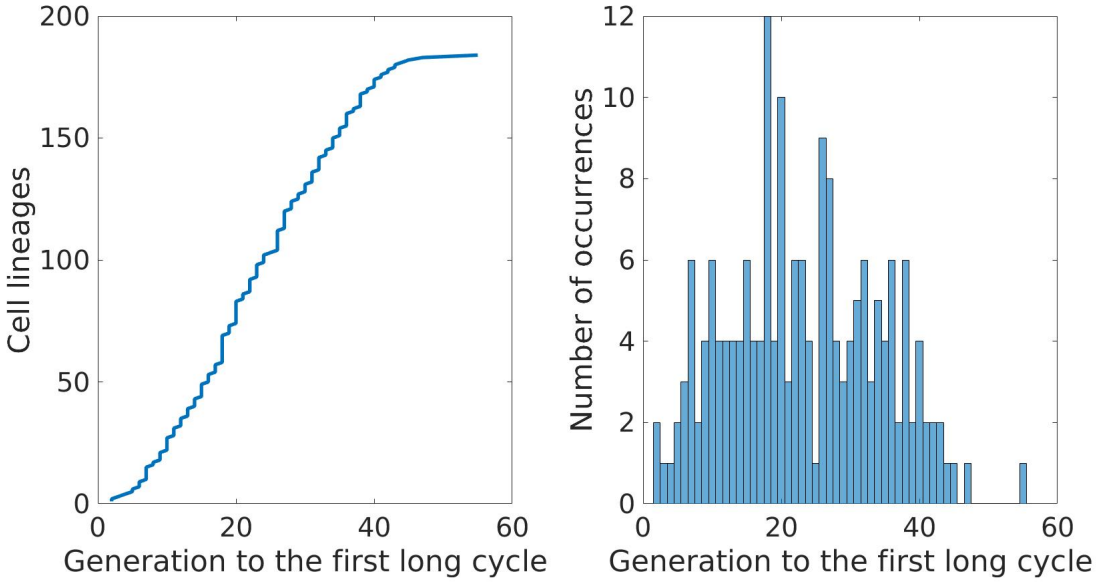

FIGURE 4.15 – Experimental data used in this section. We reccorded the generation of onset of the first long cycle in each lineage. Left : first long cycle for each lineage. Right : distribution of the number of divisions before the onset of the first long cycle.

first long cycle of a lineage, which is the topic of the first subsection. Long cycles are easily interpreted as the cell taking time to deal with an internal difficulty. It can happen that a cell fails to solve the problem and divide anyway, leaving its daughters settling it, a phenomenon know as adaptation to DNA damage [171, 97, 40, 39]. Thus, we studied the distribution of the number of successive long cycles between two short ones, in the second part. We conclude this section by highlighting crucial differences between senescence and the precocious long cycles.

4.2.1 First period : from the begining to the first long cycle

To understand the causes of the first arrest, we are especially interested in modeling the law of its appearance. The very first hypothesis we tested is a geometric law. Next, we tried to adapt the models suited for the onset of senescence. In the third part, we propose a model in which experiencing or not a long cycle for a yeast at a given generation is considered as a Bernoulli experiment, with a parameter depending on this generation. Finally, we propose a model that proves able to predict the onset of the first long cycle.
There are two ways to present the data here. On one hand, we can represent them by one point per lineage, with on the $x-$axis the number of generations from generation 0 to the onset of the first long cycle and on the $y-$axis the label of the lineage. In this view, the data are sorted by increasing number of divisions before the first long cycle. On the other hand, we can draw the corresponding histogram. Both representations are depicted on Figure 4.15. The threshold used is $\mu + 3\sigma = 18.1$ units of the *wild type* lineages.

Geometric law

When a long cycle occurs, it is likely that the yeast has a biomolecular problem during its duplication. This can easily be interpreted as a 'failure', while the short cycles are ordinary success. Denoting j the index of the first arrest, it occurs after a succession of $j-1$ normal cycles. If the probability of observing a short cell cycle at each division is constant, this setting is modeled by a geometric distribution. However,

the distribution depicted on Figure 4.15 right, suggests that it is not the case, which is confirmed by a χ^2 goodness of fit test, and this robustly with respect to the value of the threshold.

Adaptation of the previous models

In [19] and [73] two variants of a telomeres shortening model were studied numerically. In [19], the authors tested the relative importance of the second shortest telomere with respect to the shortest to signal senescence, and found that only the latter matters. To obtain this result, the authors minimized an error function on two parameters a and $L_{\min}$. In their work, a linear combination $L_1 + aL_2$ of the two shortest telomeres triggers the senescence when this quantity is smaller than a certain length $L_{\min}$. For each of the 24 lineages, the generation of onset of the senescence predicted by this model is recorded and an error $e(a, L_{\min})$ is computed. The minimal error was found with the couple $a = 0$ and $L_{\min} = 19$. Simulations with this couple of parameters were then found consistent with the experimental data. The 32 telomeres of *Saccharomyces cerevisiae* were considered as independent. The continuation proposed in [73] coupled the telomeres in twos.
We formulate the hypothesis that this model can be adapted to the prediction of the onset of the first long cycle. We adapt the tools used in the two former articles We want to minimize the error

$$e(a, L_{\min}) = \sqrt{\frac{\sum_{l=1}^{N}\sum_{i=1}^{K}\left(g_i^l - G_i\right)^2}{N\sum_{i=1}^{K} G_i^2}},$$

where N is the number of simulations (typically $n = 500$), for the l^{th} simulation, $g_1^l, \cdots, g_K^l$ are the K simulated data, in increasing order, and $G_1, \cdots, G_K$ are the experimental data, sorted in the same fashion. The model used to produce the simulation is the one from [73].
Consistently with the findings of [19], the parameter a that minimizes the error is always 0. However, the $L_{\min}$ found is 41, which is not surprising since the onset of the very first long cycle for the whole population of lineages is expected to occur earlier than the replicative senescence for the type A lineages from [180]. As was done in [19], we then simulated a thousand time the K lineages and sorted the predicted generations in increasing order. For each lineage, we represent the earliest and latest generation predicted by the simulations in red dots, resulting in two red dotted lines, se Figure 4.16, left. It is clear that this model is not suited for such prediction, the generations of onset of the first long cycle of the experimental data are too heterogeneous for its predictions.
Afterwards, we investigated the possibility that this model could be suited for the subgroup of lineages for which the first long cycle is also the beginning of senescence. We call this subpopulation of the type A lineages 'type A+'. The result is depicted on Figure 4.16, right. The predictions are slightly better than for the whole population, yet stil do not display enough heterogeneity.

A Bernoulli experiment with parameter that is a function of the index of the cycle

Let us denote $p(j)$ the proportion of lineages that have not had their first long cycle until cycle $j-1$ and have it at the j^{th} cycle. Of course, $0 \leqslant p(j) \leqslant 1$, for all integer $j \geqslant 1$. A lineage might extinguish without showing any long cycle. In this case, we exclude it from the dataset at the generation of its disappearance. If the onset of the first long cycle was given by a geometric law, then $p(j)$ would be approximately constant (see Figure 4.17, where $p(j)$ are computed from simulated data given by a geometric law and depicted with blue stars, to be compared with the true parameter $p = 0.043$, blue line). In contrast, taking 18.1 as the value for the threshold short/long, the $p(j)$ computed from the experimental data suggest, at least for the generations such that there are a sufficient number of lineages still in the pool, that an exponential curve would best fit the data, as depicted in Figure 4.17. This reinforces the idea that a geometric law is not suited to describe the generation of onset of the first long cycle.
In this setting, for a lineage to have its first long cycle at cycle k, it has to not have experienced a long cycle during the first $k-1$ cycles. Let X be the random variable describing the index at which the first

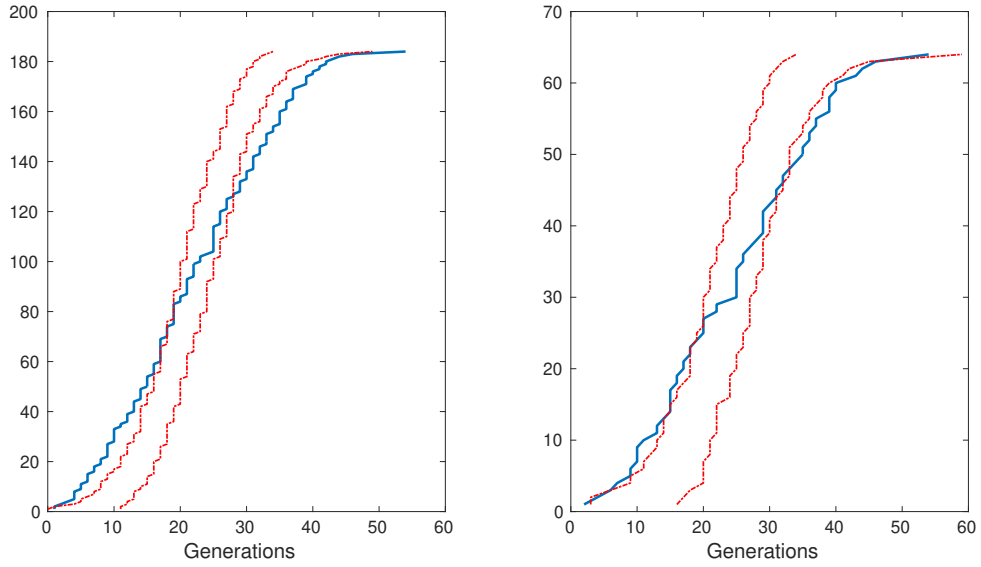

FIGURE 4.16 – Adaptation of the shorter telomere model for the onset of the first arrest. Left : all lineages that have a short cycle are used as experimental data, with threshold = 18.1. Right : subpopulation of lineages for which the first arrest corresponds to the beginning of senescence, with threshold = 18.

long cycle occurs. Then for every positive integer k, one has

$$\mathbb{P}(X = k) = p(k) \prod_{j=1}^{k-1} (1 - p(j)) \,. \tag{4.1}$$

The experimental data from Figure 4.17 (red stars) suggest that the function p shows an exponential growth. Thus to ensure that $0 \leqslant p(j) \leqslant 1$ hold for every integer, we choose to fit the data with a sigmoid function, namely

$$p : j \mapsto \frac{1}{1 + e^{-\frac{j-a}{b}}}. \tag{4.2}$$

The corresponding curve is depicted in Figure 4.18, and the resulting predictions for the onset of the first long cycle (left), along with the probability mass distribution of the random variable X (right, red crosses) are shown in Figure 4.19.
We must emphasize that even if Figure 4.19 suggests a good adequacy with experimental data, the model proposed is actually unsatisfactory for two reasons. First, it is not mechanistically-driven, so an accurate prediction would be hardly informative about biological processes. Second, it relies on two variables, which leads to the risk of overfitting the data.

A two parameters, mechanistic model

A direct adaptation of the shorter telomere model suggested a lack of heterogeneity to predict the onset first long cycle/senescence for the so-called type A+. Thus, we could add some in order to make it work for the richer data nowat hand. A straightforward way to do it was to include stochasticity to the threshold at which senescence is signaled. The idea was to had a step before what corresponds to telomerase repression, in which a $L_{\min}$ was randomly drawn the each individual lineage. The first probability law that came in our mind was a gaussian distribution. To avoid negative values for the L_{min} (which could actually be considered, see [1]), we truncated the probability density and renormaliszed it. Then, for each couple (μ, σ), we computed the associated error, to obtain Figure 4.20, left. The minimum is reached with $\mu = 36.7, \sigma = 39$. On Figure 4.20 right, is depicted the associated probability density.

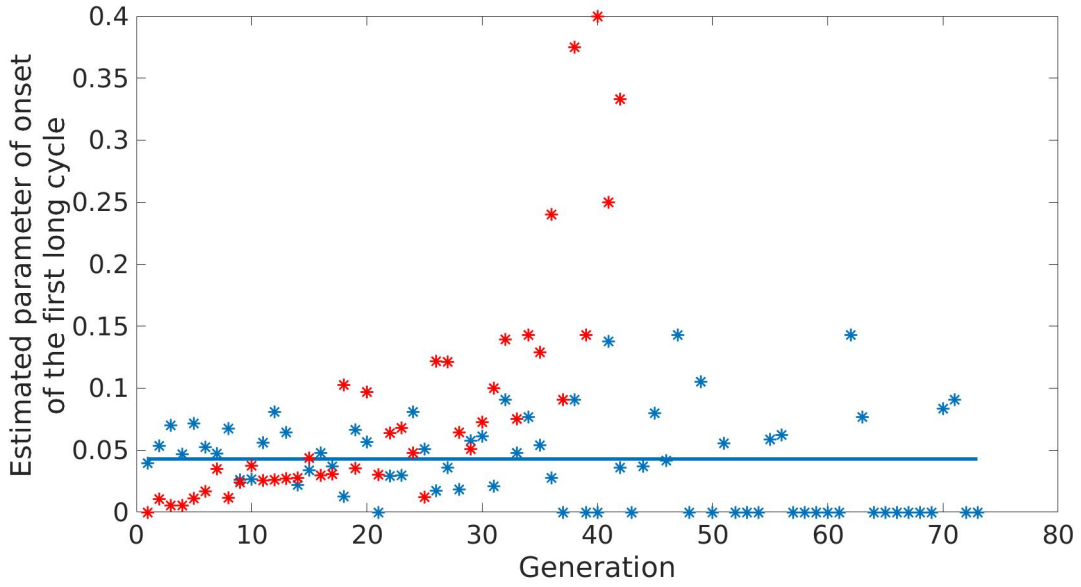

FIGURE 4.17 – Probability of onset of the first long cycle at a given generation. We used the whole population as experimental data. Red : probability estimated from the experimental data. Blue stars : simulated data of a geometric law with a parameter obtained from experimental data using a maximum likelihood estimation. Blue line : the value of this estimated paramater.

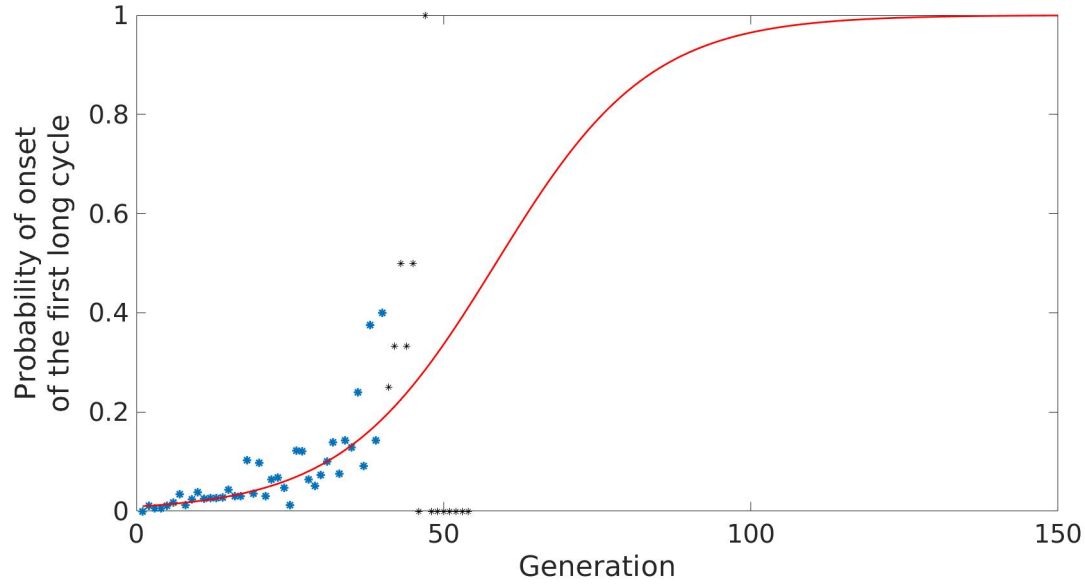

FIGURE 4.18 – Modeling of the probability of onset of the first long cycle at each generation. We used the whole population as experimental data. Stars : probability estimated from the experimental data. Blue : the data used to fit the sigmoid. Black : unused data (when less than 15 lineages have not experienced a long cycle yet). Red line : sigmoidal fit with $a = 61.25$ and $b = 13.47$ and 95% confidence intervals $(58.22, 64.29)$ and $(12.04, 14.89)$, respectively.

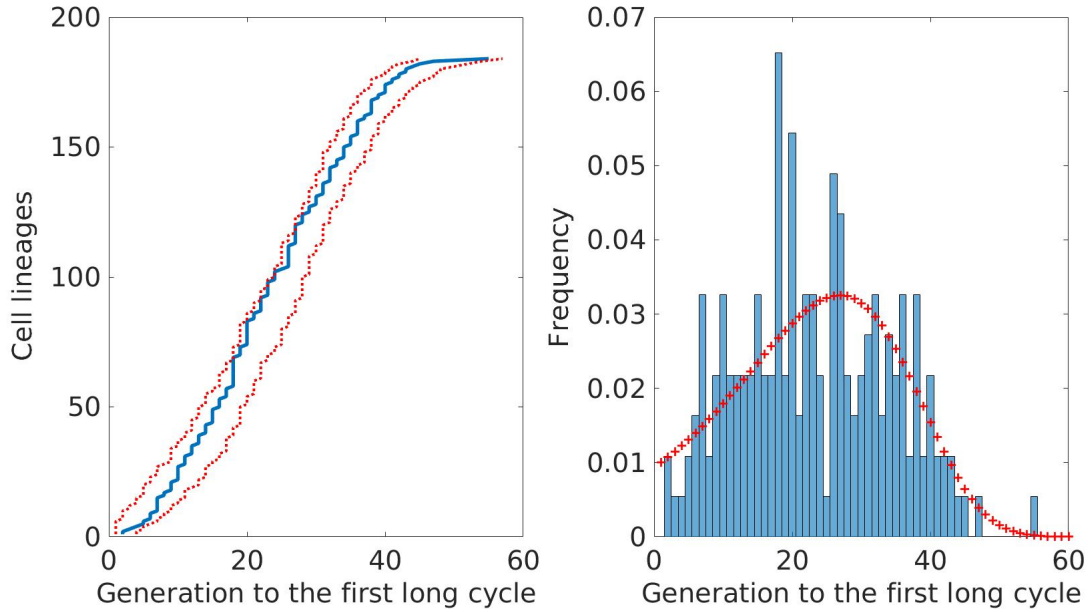

FIGURE 4.19 – Predictions of the model with a probability of onset of the first long cycle fitted with a sigmoid curve. We used the whole population as experimental data. Left : lineages representation. Blue line : experimental data. Red dots : envelope of the 1000 simulations. Right : histogram representation. Red crosses : probabilities obtained from the model.

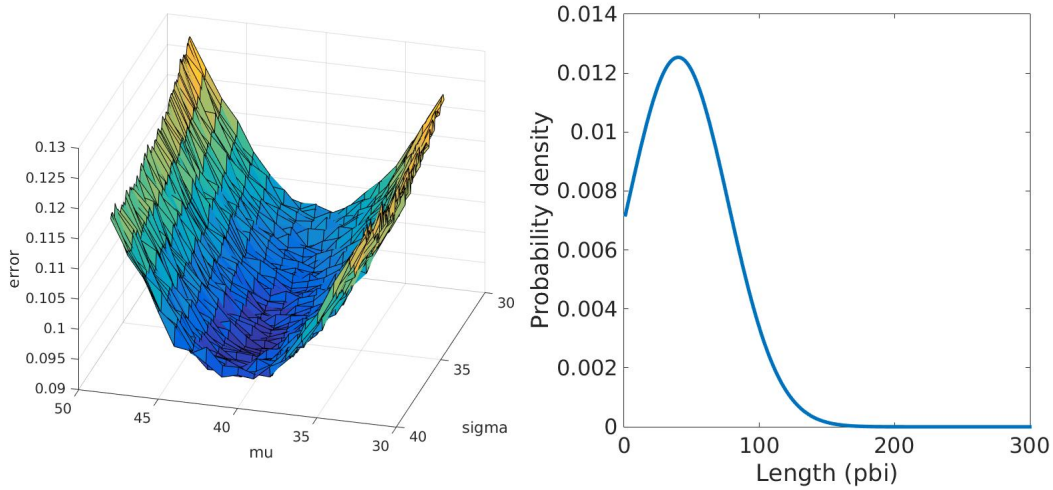

FIGURE 4.20 – Minimization of the error functionnal. Left : the error, as function of μ and σ. The minimum is reached at $\mu = 36.7, \sigma = 39$ and is 0.0922 for $N = 500$ simulations. Right : the probability distribution of L_{min} computed from the previous parameters, using a truncated gaussian probability density function.

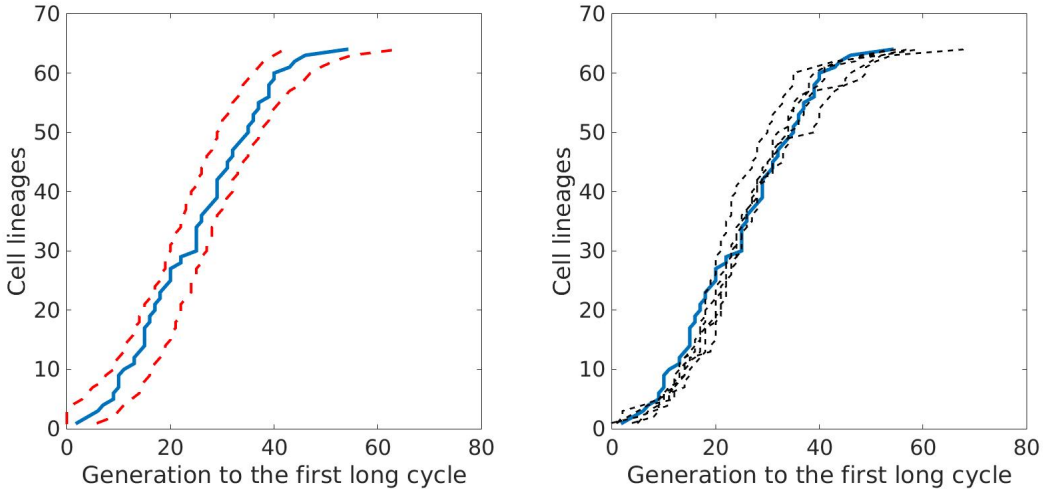

FIGURE 4.21 – Fit of first long cycle onset timings. Lineages of the so-called type A+ group were used as experimental data (blue line). Left : 1000 simulations were carried out. For each lineage, the central 95% quantile is depicted between the two red dotted lines. Right : representative set of 5 simulations of 63 onsets of first long cycle in independent lineages (black dotted lines, $\mu = 36.7, \sigma = 39$) compared to the experimental first long cycle onset timings (blue line).

The present model with this couple of parameters proves able to predict such onset, see Figure **??**. The blue line represent the experimental data used, namely the generation of onset of the first long cycle for the 148 lineages that experienced it. The dotted red lines are the bounds of the central 95% quantile for each lineage for 1000 simulations. The dotted black lines represent 5 typical simulations, compared to the experimental data. The accuracy of the prediction lead us to apply this model to the whole population. The resulting predictions are made with $\mu = 49, \sigma = 35.5$. These simulations, depicted on Figure 4.22, suggest that there exist different lengths used as checkpoints that can trigger an arrest.

4.2.2 Second period : from the first long cycle to the senescence

Regardless of the phenotype of a given lineage, the onset of the first long cycle is a significant event. We might easily conjecture that it has an impact on the cell that can affect its internal mechanisms. The first hypothesis that we investigate is how dependant is the number of divisions from the first long cycle to the second on the number of divisions from the addition of doxycycline to the appearance of the first long cycle. Then if there is not evidence to reject the hypothesis of independence, we test if a geometric law would be suited to predict this number of generations. These hypotheses are tested in the first part. When a cell cycle lasts much longer than the usual duration, *i.e.* when it lasts longer than the value of the threshold we consider, we interprete this event as the cell having trouble to divide and taking its time to 'fix a problem' at the molecular level. If it does not manage to repair itself, the problem is potentially passed on to its daughter cell through mitosis. If the probability of remission is constant at each step, then the distribution of the number of generations in a sequence of long cycles is modeled by a geometric law. This hypothesis is the subject of the second part. Finally, we investigate the hypothesis of geometrical distribution for the short cycles of this period, in the same spirit of the second subsubsection. The biological interpertation for this hypothesis is that after the yeast encountered its first problem and solved it, some kind of switch of functioning might occurs, resulting in a constant probability at each step to experience another long cycle.

The second long cycle

Successfully modeling the number of divisions between the two first long cycles could provide useful informations about the causes of the long cell cycles and whether the fact of having experienced a long

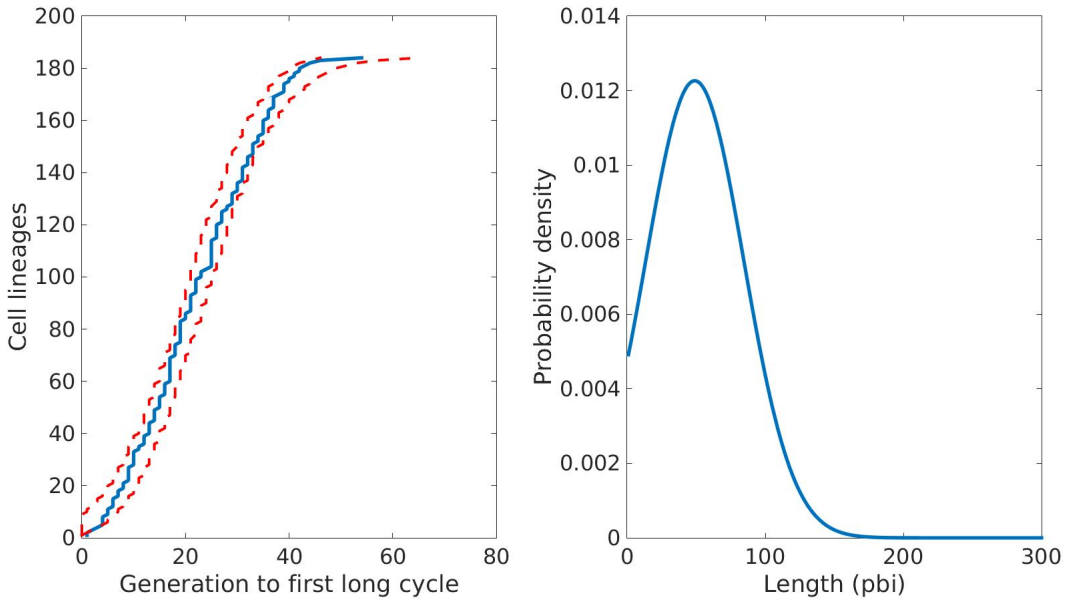

FIGURE 4.22 – Fit of first long cycle onset timings. Lineages of the so-called type A+ group were used as experimental data (blue line). Left : 1000 simulations were carried out. For each lineage, the central 95% quantile is depicted between the two red dotted lines. Right : the probability distribution of L_{min} computed from the previous parameters, using a truncated gaussian probability density function with $\mu = 49, \sigma = 35.5$.

cell cycle increases the chances of other problems. Data are represented on Figure 4.23 in two different ways.
First, we investigate how the number of generations before the onset of the first long cycle influences the number of divisions before another long cycle is observed. To do so, we perform a χ^2 independence test, for different values of the threshold, and found that the generation of onset of the first long cycle does not influence the number of divisions that will occur before observing the second long cycle.
Next, we try the hypothesis of geometric distribution to model the number of divisions between the two first long cycles. A χ^2 goodness of fit test rejects it, for each value tested. The main reason is the over-representation of the value 1 in the dataset. Regarding the distribution depicted in Figure 4.23 right, it appears that after a yeast experiences its first long cycle, if the second long cycle is not amongst the three following generations, it is likely that the problem previously encountered is fixed.

Geometric distribution of the sequences of long cycles

In the previous subsection, we saw that the number of divisions between the two first long cycle is not modeled by a geometric distribution, for excess of 1 in the dataset. In contrast, it happens that the succession of long cycles before a return to normal, called a *sequence* of long cycles, is well described by a geometric law. This fact has a straightforward interpretation : after encountering a molecular problem, a cell can take its time to try to solve this problem. It is possible that it does not manage to do it. In this case, the cell can divide anyway, letting one of its daughters solve the problem. Thus, at each step, the cell has a certain constant probability to 'repair itself'.
Additionally, the description with a geometric law is robust with respect to the threshold. Indeed, for each value of the threshold from which a cell cycle is considered as long, we perform a χ^2 goodness of fit test, which rejects the hypothesis of geometric distribution for a clear range of values of the threshold, and does not for threshold in $[14, 33]$. The result is depicted on Figure 4.24, top. This suggests that a reasonable value for the threshold between short and long cycles could be 14 units, *i.e.* 140 minutes, since

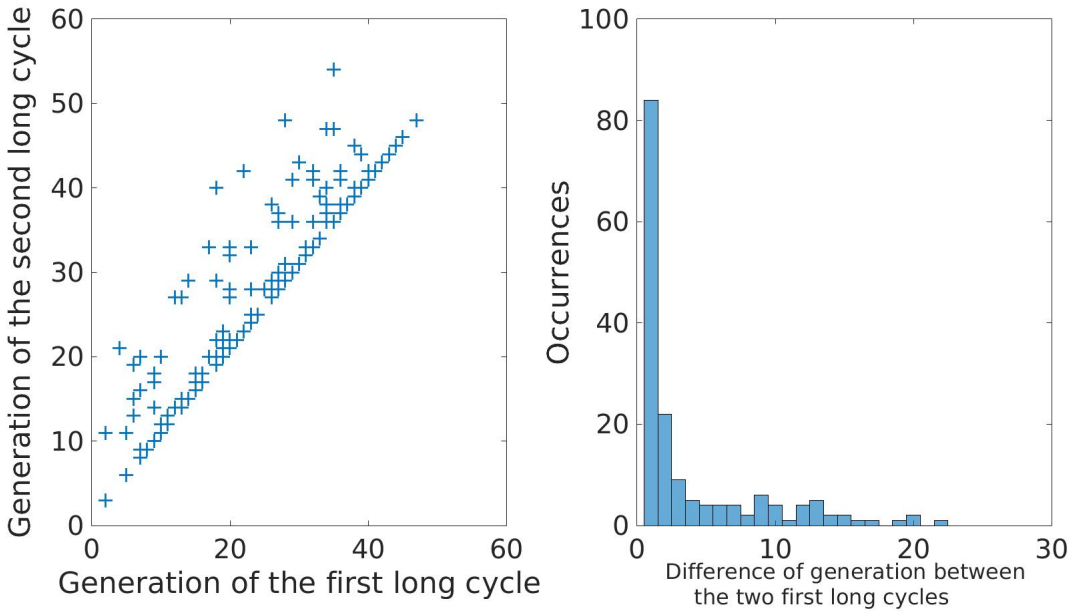

FIGURE 4.23 – Study of the onset of the second long cycle. Left : scatter plot of the data. On the abscissa is represented the generation of the first long cycle, and on the ordinate is the generation of the second long cycle. Right : histogram plot of the number of divisions between the first and second long cycle.

this phenomenom of geometric distribution of the number of generations in a sequence of long cycles (senescence excluded) is captured.

4.2.3 Third period : senescence

In some occasions, a cell can recover from a sequence of long cycles. When it does not and dies during the experiment, we call this special sequence of long cycles the senescence phase. If a long cycle is a significant event for a lineage, the senescence phase is then a particular target for investigation. The main question we address in this subsection is how different this specific sequence is to the other sequences of long cycles.
In the first part, we adapt the model with extra heterogeneity we used for the onset of the first long cycle in section 4.2.1.0 to predict the onset senescence. The second part is dedicated to the investigation of the number of generations that make up the senescence phase. The last part continues this comparison using the durations of long cycles, in particular the ones of the ultimate long cycle of the sequences.

Onset of senescence

In section 4.2.1.0 we adapted the shorter telomere model to predict the onset of the first arrest. One can also use the new richer data as an input to this model to predict the onset of senescence. We proceeded as before, and obtained an error depicted on Figure 4.25, left. The minimum is reached with $\mu =, \sigma =$. On Figure 4.25 right, is depicted the associated probability density. The present model with this couple of parameters proves able to predict such onset, see Figure 4.26. The blue line represent the experimental data used, namely the generation of onset of senescence for the 148 lineages that experienced it. The dotted red lines are the bounds of the central 95% quantile for each lineage for 1000 simulations. The dotted black lines represent 5 typical simulations, compared to the experimental data. The fact that this model, for different couples of parameters, is able to predict both the onset of the first arrest and the onset of senesence should makes us very carefull. Indeed, since two parameters are estimated, there a risk of overfitting. This could be addressed in a future work.

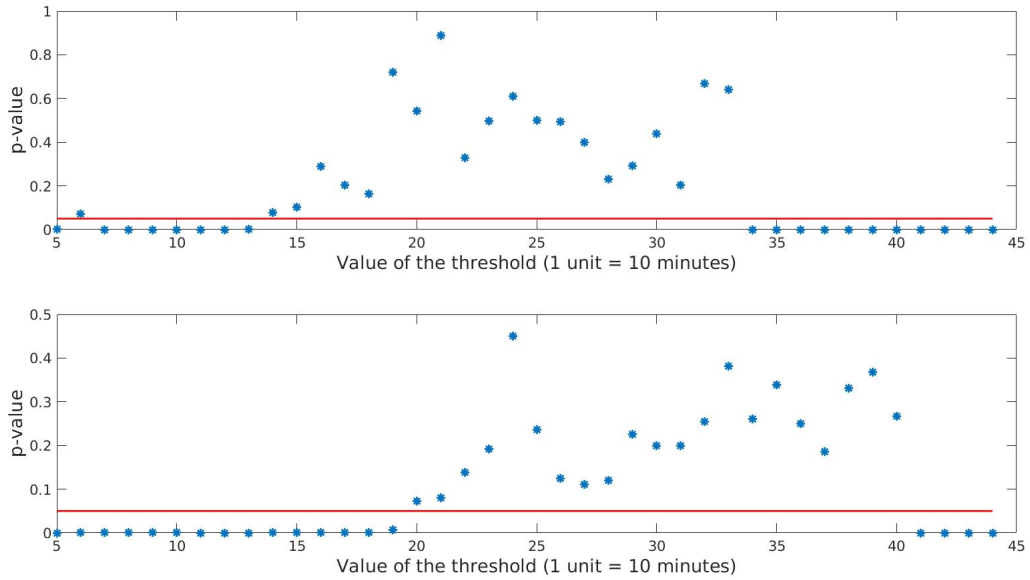

FIGURE 4.24 – Study of the robustness of the geometric law, with respect to the value of the threshold short/long. Blue stars : $p-$value given by the χ^2 test at each value of the threshold. Red line : threshold 0.05 of rejection of the test. Top : the experimental data used are the sequences of long cycles that occur before the onset of senescence. In this case, a geometric law corresponds to a constant probability of repairing at each step. Bottom : the experimental data used are the sequences of long cycles that are the senescence in the lineages. In this case, a geometric law corresponds to a constant probability of extinguishing at each step.

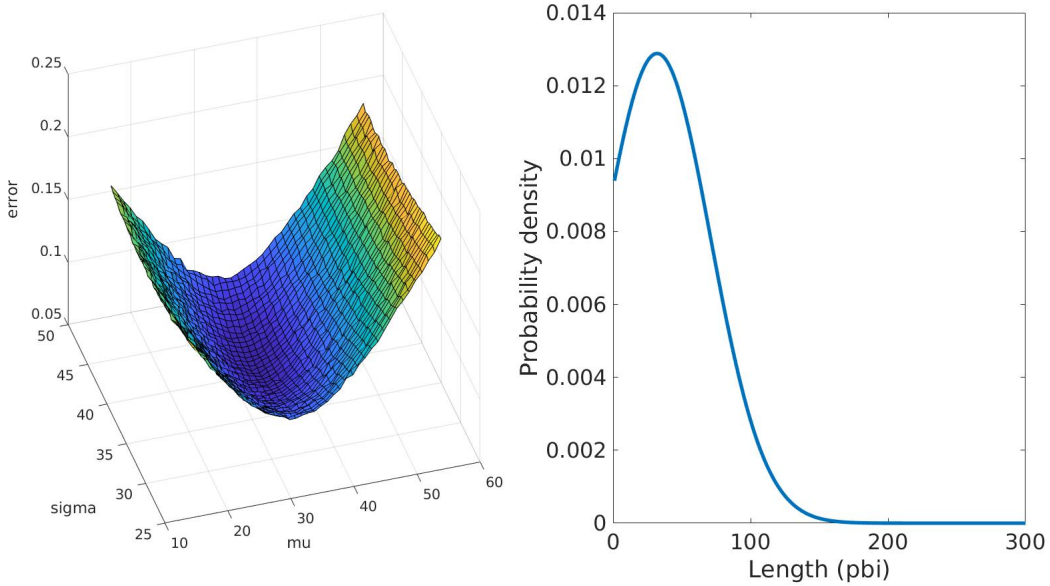

FIGURE 4.25 – Minimization of the error functionnal. Left : the error, as function of μ and σ. The minimum is reached at $\mu =, \sigma =$ and is 0.0666. Right : the probability distribution of L_{min} computed from the previous parameters, using a truncated gaussian probability density function.

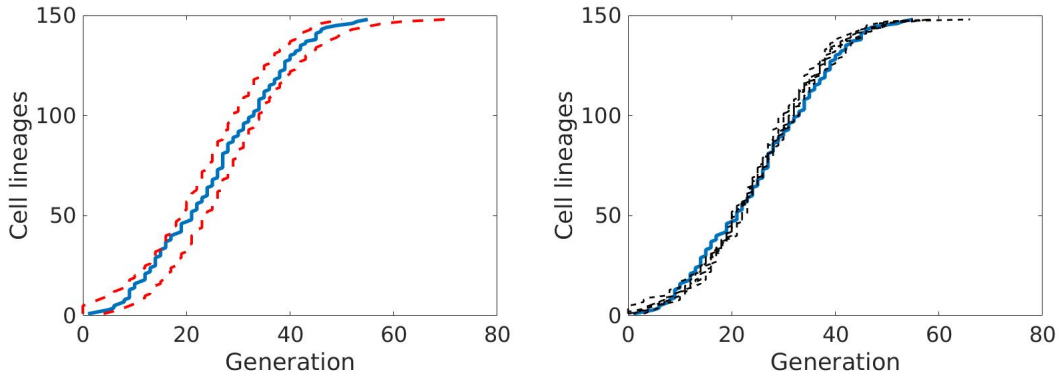

FIGURE 4.26 – Fit of senescence onset timings. All lineages experiencing senescence (according to the method describbed in section 4.1.2) were used as experimental data (blue line). Left : 1000 simulations were carried out. For each lineage, the central 95% quantile is depicted between the two red dotted lines. Right : representative set of 5 simulations of 184 senescence timings in independent lineages (black dotted lines, $\mu = 33, \sigma = 37.5$) compared to the experimental senescence onset timings (blue line).

Study of the number of generations in senescence phase

The time of onset of the senescence was extensively studied in [19] and [73]. However, the number of generations from the beginning of this phase to the end of the lineage has yet to be investigated.
First, we formulate the hypothesis that the number of generations in the senescence phase depends on the generation of onset of this phase. To test this hypothesis, we perform an independence χ^2 test, that rejected it for every reasonable value of the threshold.
As for the previous sequences of long cyles, we test the hypothesis of geometric distribution of the number of generations in the senescence. The hypothesis of geometric distribution is not rejected if the value of the threshold is included in $[20, 40]$. This suggests that for the senescence, some different mechanisms are at work and are not during precocious sequences of long cycles.

The ultimate cycle of the senescence phase is atypical

We now investigate what happens when a cell dies through senescence. To that end, we represent in Figure 4.27 boxplots of the duration of the different cycles. On the left, we compare the durations of the last cycles of the sequences of long cycles, and found that the last cycle of the senescence is significatively longer than that of the other sequences, as shown in Figure 4.27, left. Such difference holds when we compare the durations of the last cycle of the senescence phase to the other cycles of the senescence, see 4.27, center. In contrast, we found no particular difference in the durations of the cycles that made up the other sequences of long cycles, as depicted in Figure 4.27, right.

4.3 Conclusion and future work

In this work, we have studied recent data of yeast single-lineages. In the first part, we assessed the robustness of the sorting proposed in [180] and found that even though two different phenotypes were undoubtedly revealed, we might need deeper data analysis and different criterion to tell apart separate behaviours. These criterions we try to establish in Section 4.2. The unsuccessfull modeling of the onset of the first long cycles nevertheless provided useful information for a future model. The inadequacy with a geometric law suggests that this onset does not rely solely on a succession of heads or tails. In contrast, the robustness of the hypothesis of geometric distribution for the number of generations that made up the sequences of long cycles that occur before the senescence suggests that when a yeast experiences such a cycle, it has the ability to pass down the problem to its daughters, resulting in a constant probability of repairing at each generation.Finally, the critical difference between the senescence and the other sequences

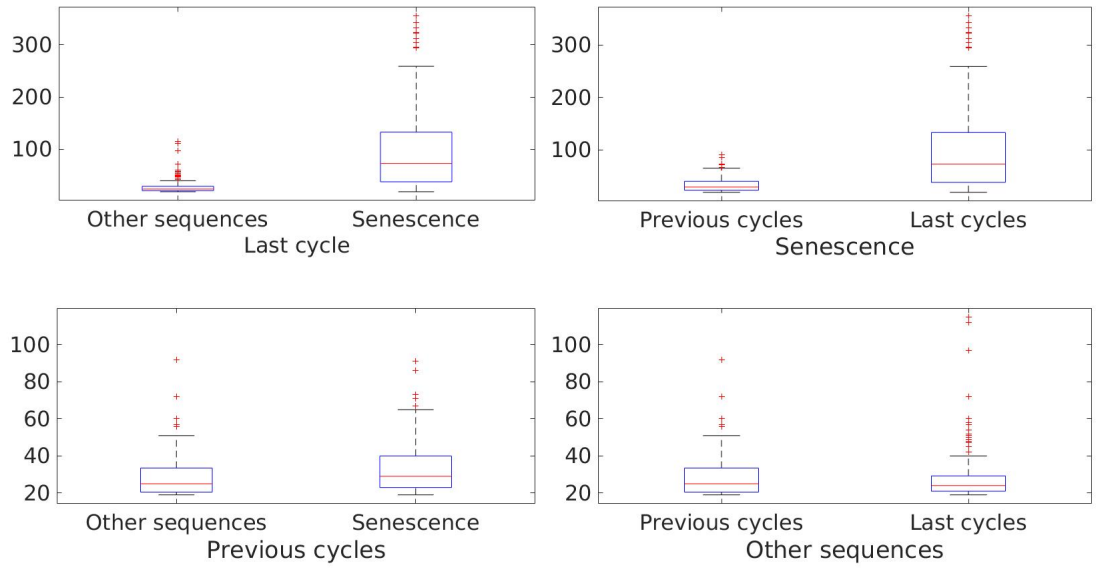

FIGURE 4.27 – Comparisons of durations of the cycles in different sequences of long cycles. Top left : durations of the last cycle of the senescence in senescent lineages compared with the last cycle of the other sequences of long cycles. Top right : comparison of the durations of the cycles of the senescence. Botom left : comparison of the non terminal cycles in senescence and precocious sequences of long cycles. Botom right : comparison of the durations of the cycles of the other sequences of long cycles. Red line : median. Blue box : the 25th and 75th percentiles, respectively. Black dotted line : data ouside the the 25th and 75th percentiles that are not considered as outliers. Black dotted lines : separates first, second and third cycles of the sequences

.

of long cycles shown in section 4.2.3, namely the number of generations in it not being dictated by a geometric law, at least for reasonable values of the threshold short/long, and the very last cycle of senescence tending to be way longer that any other long cycles, confirms that particular mechanisms are at work during senescence and not before. Future models will have to take these differences into account. Possible continuations are numerous. The model we used both in sections 4.2.3 and 4.2.1.0, based on the one proposed in [73] works well enough to predict both the onset of the first arrest and the onset of senesence should makes us very carefull. Indeed, since two parameters are estimated, there a risk of overfitting. This could be addressed in a future work. One can think of a model in which telomeres would not be homogeneous anymore, but could have individually a specific length at which senescence is signaled. More generally, a long-term goal is to develop an age and telomere length-structured population model able to account for the generation time distribution up to senescence.

Bibliographie

[1] P. Abdallah, P. Luciano, K. W. Runge, M. Lisby, V. Géli, E. Gilson, and M. T. Teixeira. A two-step model for senescence triggered by a single critically short telomere. *Nature Cell Biology*, 11(8) :988–993, jul 2009.

[2] M. Adimy, A. Chekroun, and T.-M. Touaoula. Age-structured and delay differential-difference model of hematopoietic stem cell dynamics. *Discrete and Continuous Dynamical Systems - Series B*, 20(9) :2765–2791, sep 2015.

[3] A. Amir. Cell size regulation in bacteria. *Physical Review Letters*, 112(208102), 2014.

[4] S. Astanin and L. Preziosi. *Multiphase models of tumor growth*, pages 223–253. Model. Simul. Sci. Eng. Technol. Birkhauser, 2008.

[5] C. Autexier and N. F. Lue. The structure and function of telomerase reverse transcriptase. *Annual Review of Biochemistry*, 75(1) :493–517, jun 2006.

[6] H. B. Regularity of formation of dust in self-similar fragmentations. *Annales de l ?Institut Henri Poincare (B) Probability and Statistics*, 40(4) :411–438, aug 2004.

[7] N. Bacaër. *Histoires de mathématiques et de populations*. Cassini, 2009.

[8] A. Ballesta, Q. Zhou, X. Zhang, H. Lv, and J. M. Gallo. Multiscale design of cell-type–specific pharmacokinetic/pharmacodynamic models for personalized medicine : Application to temozolomide in brain tumors. *CPT Pharmacometrics Syst. Pharmacol.*, 3(4) :e112, apr 2014.

[9] V. Bansaye, B. Cloez, and P. Gabriel. Ergodic behavior of non-conservative semigroups via generalized doeblin's conditions.

[10] V. Bansaye, B. Cloez, P. Gabriel, and A. Marguet. A non-conservative Harris' ergodic theorem.

[11] D. Barbolosi, A. Benabdallah, S. Benzekry, J. Ciccolini, C. Faivre, F. Hubert, F. Verga, and B. You. A mathematical model for growing metastases on oncologists's service. In *Computational Surgery and Dual Training*, pages 331–338. Springer New York, nov 2013.

[12] D. Barbolosi, A. Benabdallah, F. Hubert, and F. Verga. Mathematical and numerical analysis for a model of growing metastatic tumors. *Mathematical Biosciences*, 218(1) :1–14, mar 2009.

[13] G. I. Bell and E. C. Anderson. Cell growth and division : I. A Mathematical Model with Applications to Cell Volume Distributions in Mammalian Suspension Cultures. *Biophysical Journal*, 7(4) :329 – 351, 1967.

[14] E. Bernard, M. Doumic, and P. Gabriel. Cyclic asymptotic behaviour of a population reproducing by fission into two equal parts. *Kinetic and Related Models*, Sept. 2019.

[15] D. Berry, Y. Jiang, and J. Graff. Emerging roles of adipose progenitor cells in tissue development, homeostasis, expansion and thermogenesis. *Trends Endocrinol. Metab.*, 27(8) :574–585, 2016.

[16] J. Bertoin and A. R. Watson. Probabilistic aspects of critical growth-fragmentation equations. *Advances in Applied Probability*, 48(A) :37–61, jul 2016.

[17] F. Billy, J. Clairambaultt, O. Fercoq, S. Gaubertt, T. Lepoutre, T. Ouillon, and S. Saito. Synchronisation and control of proliferation in cycling cell population models with age structure. *Mathematics and Computers in Simulation*, 96 :66–94, feb 2014.

[18] E. H. Blackburn and K. Collins. Telomerase : An RNP enzyme synthesizes DNA. *Cold Spring Harbor Perspectives in Biology*, 3(5) :a003558–a003558, jul 2010.

[19] T. Bourgeron, Z. Xu, M. Doumic, and M. T. Teixeira. The asymmetry of telomere replication contributes to replicative senescence heterogeneity. *Scientific Reports*, 5(1), oct 2015.

[20] H. Brezis. *Functional Analysis, Sobolev Spaces and Partial Differential Equations*. Springer New York, 2010.

[21] F. Bubba, B. Perthame, C. Pouchol, and M. Schmidtchen. Hele-shaw limit for a system of two reaction-(cross-)diffusion equations for living tissues.

[22] F. Bubba, C. Pouchol, N. Ferrand, G. Vidal, L. Almeida, B. Perthame, and M. Sabbah. A chemotaxis-based explanation of spheroid formation in 3d cultures of breast cancer cells.

[23] M. J. Cáceres, J. A. Cañizo, and S. Mischler. Rate of convergence to an asymptotic profile for the self-similar fragmentation and growth-fragmentation equations. *Journal de Mathématiques Pures et Appliquées*, 96(4) :334–362, oct 2011.

[24] R. T. Calado and N. S. Young. Telomere diseases. *New England Journal of Medicine*, 361(24) :2353–2365, dec 2009.

[25] V. Calvez, J. Carrillo, and F. Hoffmann. Equilibria of homogeneous functionals in the fair-competition regime. *Nonlinear Analysis*, 159 :85–128, aug 2017.

[26] V. Calvez, N. Lenuzza, M. Doumic, J.-P. Deslys, F. Mouthon, and B. Perthame. Prion dynamics with size dependency–strain phenomena. *Journal of Biological Dynamics*, 4(1) :28–42, jan 2010.

[27] M. Campos, I. V. Surovtsev, S. Kato, A. Paintdakhi, B. Beltran, S. E. Ebmeier, and C. Jacobs-Wagner. A constant size extension drives bacterial cell size homeostasis. *Cell*, 159(6) :1433–1446, dec 2014.

[28] C. Carrère. Optimization of an in vitro chemotherapy to avoid resistant tumours. *Journal of Theoretical Biology*, 413 :24–33, jan 2017.

[29] J. Carrillo, R. Colombo, P. Gwiazda, and A. Ulikowska. Structured populations, cell growth and measure valued balance laws. *Journal of Differential Equations*, 252(4) :3245–3277, feb 2012.

[30] J. A. Carrillo, B. Perthame, D. Salort, and D. Smets. Qualitative properties of solutions for the noisy integrate and fire model in computational neuroscience. *Nonlinearity*, 28(9) :3365–3388, aug 2015.

[31] J. Chevallier, M. J. Cáceres, M. Doumic, and P. Reynaud-Bouret. Microscopic approach of a time elapsed neural model. *Mathematical Models and Methods in Applied Sciences*, 25(14) :2669–2719, dec 2015.

[32] M. Chyba, J.-M. Coron, P. Gabriel, A. Jacquemard, G. Patterson, G. Picot, and P. Shang. Optimal geometric control applied to the protein misfolding cyclic amplification process. *Acta Applicandae Mathematicae*, 135(1) :145–173, jun 2014.

[33] J. Clairambault, S. Gaubert, and T. Lepoutre. Circadian rhythm and cell population growth. *Mathematical and Computer Modelling*, 53(7-8) :1558–1567, apr 2011.

[34] F. Clarelli, C. Di Russo, R. Natalini, and M. Ribot. A fluid dynamcis model of the growth of phototrophic biofilms. *J. Math. Biol.*, 66(7) :1387–1408, 2013.

[35] F. Clément, F. Robin, and R. Yvinec. Analysis and calibration of a linear model for structured cell populations with unidirectional motion : Application to the morphogenesis of ovarian follicles. *SIAM Journal on Applied Mathematics*, 79(1) :207–229, jan 2019.

[36] R. Clément, B. Mauroy, and A. Cornelissen. Tissue growth pressure drives early blood flow in the chicken yolk sac. *Developmental Dynamics*, 246(8), 2017.

[37] C. Colijn and M. C. Mackey. A mathematical model of hematopoiesis—i. periodic chronic myelogenous leukemia. *Journal of Theoretical Biology*, 237(2) :117–132, nov 2005.

[38] J.-M. Coron, P. Gabriel, and P. Shang. Optimization of an amplification protocol for misfolded proteins by using relaxed control. *Journal of Mathematical Biology*, 70(1-2) :289–327, feb 2014.

[39] H. Coutelier and Z. Xu. Adaptation in replicative senescence : a risky business. *Current Genetics*, jan 2019.

[40] H. Coutelier, Z. Xu, M. C. Morisse, M. Lhuillier-Akakpo, S. Pelet, G. Charvin, K. Dubrana, and M. T. Teixeira. Adaptation to DNA damage checkpoint in senescent telomerase-negative cells promotes genome instability. *Genes & Development*, 32(23-24) :1499–1513, nov 2018.

[41] C. M. Dafermos. Generalized characteristics in hyperbolic systems of conservation laws. *Archive for Rational Mechanics and Analysis*, 107(2) :127–155, 1989.

[42] B. de Pagter. Irreducible compact operators. *Math. Z.*, 192(1) :149–153, Mar 1986.

[43] A. M. de Roos. Numerical methods for structured population models : The escalator boxcar train. *Numerical Methods for Partial Differential Equations*, 4(3) :173–195, 1988.

[44] T. Debiec, M. Doumic, P. Gwiazda, and E. Wiedemann. Relative entropy method for measure solutions of the growth-fragmentation equation. *SIAM Journal on Mathematical Analysis*, 50(6) :5811–5824, jan 2018.

[45] F. Delarue, F. Lagoutière, and N. Vauchelet. Analysis of finite volume upwind scheme for transport equation with discontinuous coefficients. *J. Math. Pures Appliquées*, 918-951(108), 2017.

[46] F. Delarue, F. Lagoutière, and N. Vauchelet. Convergence analysis of upwind type schemes for the aggregation equation with pointy potential. *preprint hal-01591602*, 2018.

[47] L. Desvillettes, T. Lepoutre, A. Moussa, and A. Trescases. On the entropic structure of reaction-cross diffusion systems. *Communications in Partial Differential Equations*, 40(9) :1705–1747, jun 2015.

[48] A. Devys, T. Goudon, and P. Lafitte. A model describing the growth and the size distribution of multiple metastatic tumors. *Discrete and Continuous Dynamical Systems - Series B*, 12(4) :731–767, aug 2009.

[49] O. Diekmann, H. Heesterbeek, and T. Britton. *Mathematical Tools for Understanding Infectious Disease Dynamics (Princeton Series in Theoretical and Computational Biology)*. Princeton University Press, 2012.

[50] O. Diekmann and J. A. P. Heesterbeek. *Mathematical Epidemiology of Infectious Diseases : Model Building, Analysis and Interpretation*. Wiley, 2000.

[51] O. Diekmann, H. Heijmans, and H. Thieme. On the stability of the cell size distribution. *Journal of Mathematical Biology*, 19 :227–248, 1984.

[52] O. Diekmann and J. Metz, editors. *The Dynamics of Physiologically Structured Populations*. Springer, 1986.

[53] R. J. DiPerna. Measure-valued solutions to conservation laws. *Archive for Rational Mechanics and Analysis*, 88(3) :223–270, 1985.

[54] R. J. DiPerna and A. J. Majda. Oscillations and concentrations in weak solutions of the incompressible fluid equations. *Communications in Mathematical Physics*, 108(4) :667–689, dec 1987.

[55] D. Discher, P. Janmey, and Y. L. Wang. Tissue cells feel and respond to the stiffness of their substrate. *Science*, 310(5751) :1139–1143, 2005.

[56] M. Doumic. Analysis of a Population Model Structured by the Cells Molecular Content. *Math. Model. Nat. Phenom.*, 2(3) :121–152, 2007.

[57] M. Doumic and P. Gabriel. Eigenelements of a General Aggregation-Fragmentation Model. *Mathematical Models and Methods in Applied Sciences*, 20(5) :757–783, May 2010.

[58] M. Doumic, T. Goudon, and T. Lepoutre. Scaling limit of a discrete prion dynamics model. *Communications in Mathematical Sciences*, 7(4) :839–865, 2009.

[59] M. Doumic, M. Hoffmann, N. Krell, and L. Robert. Statistical estimation of a growth-fragmentation model observed on a genealogical tree. *Bernoulli*, 21 :1760–1799, 2015. 46 pages, 4 figures.

[60] M. Doumic, M. Hoffmann, P. Reynaud-Bouret, and V. Rivoirard. Nonparametric estimation of the division rate of a size-structured population. *SIAM Journal on Numerical Analysis*, 50(2) :925–950, jan 2012.

[61] M. Doumic, A. Marciniak-Czochra, B. Perthame, and J. P. Zubelli. A structured population model of cell differentiation. *SIAM Journal on Applied Mathematics*, 71(6) :1918–1940, jan 2011.

[62] M. Doumic and B. van Brunt. Explicit solution and fine asymptotics for a critical growth-fragmentation equation. *ESAIM : Proceedings and Surveys*, 62 :30–42, 2018.

[63] Y. Du. *Order structure and topological methods in nonlinear partial differential equations. Vol. 1. Maximum principles and applications.* Series in Partial Differential Equations and Applications. World Scientific Publishing Co. Pte. Ltd., Hackensack, NJ, 2006. Maximum principles and applications.

[64] G. Dumont and P. Gabriel. The mean-field equation of a leaky integrate-and-fire neural network : measure solutions and steady states.

[65] N. Echenim, F. Clément, and M. Sorine. A multiscale model for the selection control of ovulatory follicles. In *Biology and Control Theory : Current Challenges*, pages 45–52. Springer Berlin Heidelberg.

[66] N. Echenim, D. Monniaux, M. Sorine, and F. Clément. Multi-scale modeling of the follicle selection process in the ovary. *Mathematical Biosciences*, 198(1) :57–79, nov 2005.

[67] M. Efendiev, B. Brunt, A. A. Zaidi, and T. H. Shah. Asymmetric cell division with stochastic growth rate. Dedicated to the memory of the late Spartak Agamirzayev. *Mathematical Methods in the Applied Sciences*, 41(17) :8059–8069, sep 2018.

[68] T. El Bouti, T. Goudon, S. Labarthe, B. Laroche, B. Polizzi, A. Rachah, M. Ribot, and R. Tesson. A mixture model for the dynamic of the gut mucus layer. *ESAIM : ProcS,*, 55 :111–130, 2016.

[69] M. Escobedo. On the non existence of non negative solutions to a critical growth-fragmentation equation.

[70] M. Escobedo and M. Doumic. Time asymptotics for a critical case in fragmentation and growth-fragmentation equations. *Kinetic and Related Models*, 9(2) :251–297, mar 2016.

[71] M. Escobedo, S. Mischler, and B. Perthame. Gelation in coagulation and fragmentation models. *Communications in Mathematical Physics*, 231(1) :157–188, aug 2002.

[72] M. Escobedo, S. Mischler, and M. Rodriguez Ricard. On self-similarity and stationary problem for fragmentation and coagulation models. *Annales de l'I.H.P. Analyse non linéaire*, 22(1) :99–125, 2005.

[73] S. Eugène, T. Bourgeron, and Z. Xu. Effects of initial telomere length distribution on senescence onset and heterogeneity. *Journal of Theoretical Biology*, 413 :58–65, jan 2017.

[74] B. Fabrèges, H. Hivert, K. Lebalc'h, S. Martel, F. Delarue, F. Lagoutière, and N. Vauchelet. Numerical schemes for the aggregation equation with pointy potentials. *To appear in the proceedings of CEMRACS 2017*, 2019.

[75] J. Z. Farkas, P. Gwiazda, and A. Marciniak-Czochra. Asymptotic behaviour of a structured population model on a space of measures.

[76] P. Feijoo, D. Dominguez, L. Tusell, and A. Genesca. Telomere-dependent genomic integrity : Evolution of the fusion-bridge-breakage cycle concept. *Current Pharmaceutical Design*, 20(41) :6375–6385, oct 2014.

[77] P. A. Ferrari, A. Galves, I. Grigorescu, and E. Löcherbach. Phase transition for infinite systems of spiking neurons. *Journal of Statistical Physics*, 172(6) :1564–1575, jul 2018.

[78] A. F. Filippov. *Differential Equations with Discontinuous Righthand Sides.* Springer Netherlands, 1988.

[79] P. Gabriel, , and H. M. and. Steady distribution of the incremental model for bacteria proliferation. *Networks & Heterogeneous Media*, 14(1) :149–171, 2019.

[80] P. Gabriel. Global stability for the prion equation with general incidence. *Mathematical Biosciences and Engineering*, 12(4) :789–801, apr 2015.

[81] P. Gabriel. Measure solutions to the conservative renewal equation. *ESAIM : Proceedings and Surveys*, 62 :68–78, 2018.

[82] P. Gabriel, S. P. Garbett, V. Quaranta, D. R. Tyson, and G. F. Webb. The contribution of age structure to cell population responses to targeted therapeutics. *Journal of Theoretical Biology*, 311 :19–27, oct 2012.

[83] A. Galves, E. Löcherbach, C. Pouzat, and E. Presutti. A system of interacting neurons with short term plasticity.

[84] M. E. Gilpin. Do hares eat lynx ? *The American Naturalist*, 107(957) :727–730, sep 1973.

[85] S. Girel, C. Arpin, J. Marvel, O. Gandrillon, and F. Crauste. Model-based assessment of the role of uneven partitioning of molecular content on heterogeneity and regulation of differentiation in CD8 t-cell immune responses. *Frontiers in Immunology*, 10, feb 2019.

[86] A. Goldenshluger and O. Lepski. Bandwidth selection in kernel density estimation : Oracle inequalities and adaptive minimax optimality. *The Annals of Statistics*, 39(3) :1608–1632, jun 2011.

[87] A. Goldenshluger and O. Lepski. Uniform bounds for norms of sums of independent random functions. *The Annals of Probability*, 39(6) :2318–2384, nov 2011.

[88] C. W. Greider and E. H. Blackburn. Identification of a specific telomere terminal transferase activity in tetrahymena extracts. *Cell*, 43 :405–413, Dec. 1985.

[89] P. Gwiazda, T. Lorenz, and A. Marciniak-Czochra. A nonlinear structured population model : Lipschitz continuity of measure-valued solutions with respect to model ingredients. *Journal of Differential Equations*, 248(11) :2703–2735, jun 2010.

[90] P. Gwiazda and A. Marciniak-Czochra. Structured population equations in metric spaces. *Journal of Hyperbolic Differential Equations*, 07(04) :733–773, dec 2010.

[91] P. Gwiazda and E. Wiedemann. Generalized entropy method for the renewal equation with measure data. *Oberwolfach Preprints ;2016*, pages 07–, 2016.

[92] B. Haas. Asymptotic behavior of solutions of the fragmentation equation with shattering : An approach via self-similar markov processes. *The Annals of Applied Probability*, 20(2) :382–429, apr 2010.

[93] K. P. Hadeler and H. I. Freedman. Predator-prey populations with parasitic infection. *Journal of Mathematical Biology*, 27(6) :609–631, nov 1989.

[94] A. J. Hall and G. C. Wake. A functional differential equation arising in modelling of cell growth. *The Journal of the Australian Mathematical Society. Series B. Applied Mathematics*, 30(04) :424, apr 1989.

[95] A. J. Hall, G. C. Wake, and P. W. Gandar. Steady size distributions for cells in one-dimensional plant tissues. *J. Math. Biol.*, 30(2) :101–123, Nov 1991.

[96] D. Hanahan and R. A. Weinberg. The hallmarks of cancer. *Cell*, 100(1) :57–70, jan 2000.

[97] J. C. Harrison and J. E. Haber. Surviving the breakup : The DNA damage checkpoint. *Annual Review of Genetics*, 40(1) :209–235, dec 2006.

[98] L. Hayflick. The limited in vitro lifetime of human diploid cell strains. *Experimental Cell Research*, 37(3) :614–636, mar 1965.

[99] L. Hayflick and P. Moorhead. The serial cultivation of human diploid cell strains. *Experimental Cell Research*, 25(3) :585–621, dec 1961.

[100] M. T. Hemann, M. A. Strong, L.-Y. Hao, and C. W. Greider. The shortest telomere, not average telomere length, is critical for cell viability and chromosome stability. *Cell*, 107(1) :67–77, oct 2001.

[101] U. Herbach, A. Bonnaffoux, T. Espinasse, and O. Gandrillon. Inferring gene regulatory networks from single-cell data : a mechanistic approach. *BMC Systems Biology*, 11(1), nov 2017.

[102] P. Ilmonen, A. Kotrschal, and D. J. Penn. Telomere attrition due to infection. *PLoS ONE*, 3(5) :e2143, may 2008.

[103] K. Iwata, K. Kawazaki, and N. Shigesada. A dynamical model for the growth and size distribution of multiple metastatic tumors. *Journal of Theoretical Biology*, 203(2) :177–186, mar 2000.

[104] G. Jankowiak, D. Peurichard, A. Reversat, C. Schmeiser, and M. Sixt. Modelling adhesion-independent cell migration.

[105] W. O. Kermack and A. G. McKendrick. A contribution to the mathematical theory of epidemics. *Proceedings of the Royal Society A : Mathematical, Physical and Engineering Sciences*, 115(772) :700–721, aug 1927.

[106] W. O. Kermack and A. G. McKendrick. Contributions to the mathematical theory of epidemics—II. the problem of endemicity. *Bulletin of Mathematical Biology*, 53(1-2) :57–87, mar 1932.

[107] J. King and S. Franks. *Mathematical Modelling of Nutrient-limited Tissue Growth*, volume 154 of *International Series of Numerical Mathematics*, pages 273–282. Birkhauser, 2007.

[108] B. Laroche and A. Perasso. Threshold behaviour of a SI epidemiological model with two structuring variables. *Journal of Evolution Equations*, 16(2) :293–315, nov 2015.

[109] P. Laurençot and B. Perthame. Exponential decay for the growth-fragmentation/cell-division equation. *Communications in Mathematical Sciences*, 7(2) :503–510, 2009.

[110] M. Lerch. Sur un point de la théorie des fonctions génératrices d'Abel. *Acta Math.*, 27 :339–352, 1903.

[111] P. H. Leslie. On the use of matrices in certain population mathematics. In *Mathematical Demography*, pages 227–238. Springer Berlin Heidelberg, 1945.

[112] P. H. Leslie. Some further notes on the use of matrices in population mathematics. *Biometrika*, 35(3-4) :213–245, 1948.

[113] F. Lévi, A. Okyar, S. Dulong, P. F. Innominato, and J. Clairambault. Circadian timing in cancer treatments. *Annual Review of Pharmacology and Toxicology*, 50(1) :377–421, feb 2010.

[114] A. Lorz, B. Perthame, and C. Taing. Dirac concentrations in a chemostat model of adaptive evolution. *Chinese Annals of Mathematics, Series B*, 38(2) :513–538, mar 2017.

[115] P. Magal and C. McCluskey. Two-group infection age model including an application to nosocomial infection. *SIAM Journal on Applied Mathematics*, 73(2) :1058–1095, jan 2013.

[116] P. Magal, C. McCluskey, and G. Webb. Lyapunov functional and global asymptotic stability for an infection-age model. *Applicable Analysis*, 89(7) :1109–1140, jul 2010.

[117] A. G. McKendrick. Applications of mathematics to medical problems. *Proceedings of the Edinburgh Mathematical Society*, 44 :98, feb 1925.

[118] P. Michel. Existence of a solution to the cell division eigenproblem. *Mathematical Models and Methods in Applied Sciences*, 16(supp01) :1125–1153, jul 2006.

[119] P. Michel, S. Mischler, and B. Perthame. General entropy equations for structured population models and scattering. *C. R., Math., Acad. Sci. Paris*, 338(9) :697 – 702, 2004.

[120] P. Michel, S. Mischler, and B. Perthame. General relative entropy inequality : an illustration on growth models. *J. Math. Pures Appl. (9)*, 84(9) :1235 – 1260, 2005.

[121] I. Miller, J. Ashton-Chess, H. Spolders, V. Fert, J. Ferrara, W. Kroll, J. Askaa, P. Larcier, P. F. Terry, A. Bruinvels, and A. Huriez. Market access challenges in the EU for high medical value diagnostic tests. *Personalized Medicine*, 8(2) :137–148, mar 2011.

[122] S. Mirrahimi and B. Perthame. Asymptotic analysis of a selection model with space. *Journal de Mathématiques Pures et Appliquées*, 104(6) :1108–1118, dec 2015.

[123] S. Mischler, B. Perthame, and L. Ryzhik. Stability in a Nonlinear Population Maturation Model. *Mathematical Models and Methods in Applied Sciences*, 12(12) :1751–1772, dec 2002.

[124] S. Mischler and J. Scher. Spectral analysis of semigroups and growth-fragmentation equations. *Ann. Inst. Henri Poincaré, Anal. Non Linéaire*, 33(3) :849–898, 2016.

[125] J. D. Murray, editor. *Mathematical Biology*. Springer New York, 2004.

[126] T. N. Nguyen, J. Clairambault, T. Jaffredo, B. Perthame, and D. Salort. Adaptive dynamics of hematopoietic stem cells and their supporting stroma : A model and mathematical analysis. working paper or preprint, Dec. 2018.

[127] S. Nordmann, B. Perthame, and C. Taing. Dynamics of concentration in a population model structured by age and a phenotypical trait. *Acta Applicandae Mathematicae*, 155(1) :197–225, dec 2017.

[128] A. Nouri, , and C. S. and. Aggregated steady states of a kinetic model for chemotaxis. *Kinetic & Related Models*, 10(1) :313–327, 2017.

[129] T. Nyström. Conditional senescence in bacteria : death of the immortals. *Molecular Microbiology*, 48(1) :17–23, mar 2003.

[130] A. Olivier. How does variability in cells aging and growth rates influence the malthus parameter ? *Kinetic and Related Models*, 10(2) :481–512, June 2017.

[131] A. Olivier and C. Pouchol. Combination of direct methods and homotopy in numerical optimal control : Application to the optimization of chemotherapy in cancer. *Journal of Optimization Theory and Applications*, dec 2018.

[132] A. Olovnikov. A theory of marginotomy. *Journal of Theoretical Biology*, 41(1) :181–190, sep 1973.

[133] W. H. organization. Obesity and overweight, 2018.

[134] K. Pakdaman, B. Perthame, and D. Salort. Dynamics of a structured neuron population. working paper or preprint, Feb. 2009.

[135] K. Pakdaman, B. Perthame, and D. Salort. Adaptation and fatigue model for neuron networks and large time asymptotics in a nonlinear fragmentation equation. *The Journal of Mathematical Neuroscience*, 4(1) :14, 2014.

[136] A. Perasso and B. Laroche. Well-posedness of an epidemiological problem described by an evolution PDE. *ESAIM : Proceedings*, 25 :29–43, 2008.

[137] A. Perasso and U. Razafison. Asymptotic behavior and numerical simulations for an infection load-structured epidemiological model : Application to the transmission of prion pathologies. *SIAM Journal on Applied Mathematics*, 74(5) :1571–1597, jan 2014.

[138] A. Perasso and Q. Richard. Implication of age-structure on the dynamics of Lotka Volterra equations. *Differential and Integral Equations. An International Journal for Theory & Applications*, 32(1-2) :91–120, 2019.

[139] B. Perthame. *Transport Equations in Biology.* Basel : Birkhäuser, 2007.

[140] B. Perthame. Some mathematical aspects of tumor growth and therapy. In *ICM 2014 - International Congress of Mathematicians*, Seoul, South Korea, Aug. 2014.

[141] B. Perthame and L. Ryzhik. Exponential decay for the fragmentation or cell-division equation. *Journal of Differential Equations*, 210(1) :155–177, mar 2005.

[142] B. Perthame, M. Tang, and N. Vauchelet. Traveling wave solution of the hele-shaw model of tumor growth with nutrient.

[143] D. Peurichard, F. Delebecque, A. Lorsignol, C. Barreau, J. Rouquette, X. Descombes, L. Casteilla, and P. Degond. Simple mechanical cues could explain adipose tissue morphology. *Journal of Theoretical Biology*, 429 :61 – 81, 2017.

[144] F. Poupaud and M. Rascle. Measure solutions to the linear multi-dimensional transport equation with non-smooth coefficients. *Communications in Partial Differential Equations*, 22(1-2) :225–267, jan 1997.

[145] S. Prigent, A. Ballesta, F. Charles, N. Lenuzza, P. Gabriel, L. M. Tine, H. Rezaei, and M. Doumic. An efficient kinetic model for assemblies of amyloid fibrils and its application to polyglutamine aggregation. *PLoS ONE*, 7(11) :e43273, nov 2012.

[146] S. Prigent, H. Haffaf, H. Banks, M. Hoffmann, H. Rezaei, and M. Doumic. Size Distribution of Amyloid Fibrils. Mathematical Models and Experimental Data. *International Journal of Pure and Apllied Mathematics*, 93(6), jun 2014.

[147] R. Reddel. Telomere maintenance mechanisms in cancer : Clinical implications. *Current Pharmaceutical Design*, 20(41) :6361–6374, oct 2014.

[148] J. D. F. Richard L. Burden. *Numerical Analysis*. Boston, MA : PWS Publishing Company ; London : ITP International Thomson Publishing, 5th ed. edition, 1993.

[149] L. Robert, M. Hoffmann, N. Krell, S. Aymerich, J. Robert, and M. Doumic. Division in escherichia coliis triggered by a size-sensing rather than a timing mechanism. *BMC Biology*, 12(1) :17, Feb 2014.

[150] M. Rotenberg. Transport theory for growing cell populations. *Journal of Theoretical Biology*, 103(2) :181–199, jul 1983.

[151] Rudin. *Analyse réelle et complexe : Cours et exercices*. Dunod, 1998.

[152] S. Saker. Oscillation and global attractivity in hematopoiesis model with delay time. *Applied Mathematics and Computation*, 136(2-3) :241–250, mar 2003.

[153] J. T. Sauls, D. Li, and S. Jun. Adder and a coarse-grained approach to cell size homeostasis in bacteria. *Current Opinion in Cell Biology*, 38 :38 – 44, 2016. Cell architecture.

[154] H. H. Schaefer. *Banach Lattices and Positive Operators*. Springer, 1974.

[155] N. Sfakianakis, D. Peurichard, A. Brunk, and C. Schmeiser. Modelling cell-cell collision and adhesion with the filament based lamellipodium model. *BIOMATH*, 7(2) :1811097, nov 2018.

[156] F. Sharpe and A. Lotka. L. a problem in age-distribution. *The London, Edinburgh, and Dublin Philosophical Magazine and Journal of Science*, 21(124) :435–438, apr 1911.

[157] W. Shen, L. Liu, and S. Zeng. Senescence and cancer. *Cancer Translational Medicine*, 4(3) :70, 2018.

[158] N. Shoham and A. Gefen. Mechanotransduction in adipocytes. *J. Biomech.*, 45(1) :1–8, 2012.

[159] P. Shoham, N. an d Girshovitz, R. Katzengold, N. T. Shaked, D. Benayahu, and A. Gefen. Adipocyte stiffness increases with accumulation of lipid droplets. *Biophys. J.*, 106(6) :1421–1431, 2014.

[160] J. W. Sinko and W. Streifer. A new model for age-size structure of a population. *Ecology*, 48(6) :910–918, 1967.

[161] I. Soifer, L. Robert, and A. Amir. Single-cell analysis of growth in budding yeast and bacteria reveals a common size regulation strategy. *Current Biology*, 26(3) :356–361, feb 2016.

[162] J. Soudet, P. Jolivet, and M. T. Teixeira. Elucidation of the DNA end-replication problem in saccharomyces cerevisiae. *Molecular Cell*, 53(6) :954–964, mar 2014.

[163] H. Soula, A. Géloën, and C. Soulage. Model of adipose tissue cellularity dynamics during food restriction. *Journal of Theoretical Biology*, 364 :189–196, jan 2015.

[164] H. Soula, H. Julienne, C. Soulage, and A. Géloën. Modelling adipocytes size distribution. *Journal of Theoretical Biology*, 332 :89–95, sep 2013.

[165] T. Stiehl and A. Marciniak-Czochra. Stem cell self-renewal in regeneration and cancer : Insights from mathematical modeling. *Current Opinion in Systems Biology*, 5 :112–120, oct 2017.

[166] J. Swift, I. L. Ivanovska, A. Buxboim, T. Harada, P. C. Dingal, J. Pinter, J. D. Pajerowski, K. R. Spinler, J. W. Shin, M. Tewari, F. Rehfeldt, D. W. Speicher, and D. E. Discher. Nuclear lamin-A scales with tissue stiffness and enhances matrix-directed differentiation. *Science*, 341(6149) :1240104, 2013.

[167] S. Taheri-Araghi, S. Bradde, J. T. Sauls, N. S. Hill, P. A. Levin, J. Paulsson, M. Vergassola, and S. Jun. Cell-Size Control and Homeostasis in Bacteria. *Current Biology*, 25(3) :385 – 391, 2015.

[168] J. T. Tanner. The stability and the intrinsic growth rates of prey and predator populations. *Ecology*, 56(4) :855–867, jul 1975.

[169] M. T. Teixeira, M. Arneric, P. Sperisen, and J. Lingner. Telomere length homeostasis is achieved via a switch between telomerase- extendible and -nonextendible states. *Cell*, 117 :323–335, Apr. 2004.

[170] H. R. Thieme and C. Castillo-Chavez. How may infection-age-dependent infectivity affect the dynamics of HIV/AIDS ? *SIAM Journal on Applied Mathematics*, 53(5) :1447–1479, oct 1993.

[171] D. P. Toczyski, D. J. Galgoczy, and L. H. Hartwell. Cdc5 and ckii control adaptation to the yeast dna damage checkpoint. *Cell*, 90 :1097–1106, Sept. 1997.

[172] L. Villain, D. Commenges, C. Pasin, M. Prague, and R. Thiébaut. Adaptive protocols based on predictions from a mechanistic model of the effect of IL7 on CD4 counts. *Statistics in Medicine*, 38(2) :221–235, sep 2018.

[173] W. J. Voorn and L. J. H. Koppes. Skew or third moment of bacterial generation times. *Archives of Microbiology*, 169(1) :43–51, dec 1997.

[174] Q. Wang, Y. Zhan, N. L. Pedersen, F. Fang, and S. Hägg. Telomere length and all-cause mortality : A meta-analysis. *Ageing Research Reviews*, 48 :11–20, dec 2018.

[175] J. D. Watson. Origin of concatemeric t7 dna. *Nature : New biology*, 239 :197–201, Oct. 1972.

[176] G. Webb. *Theory of Nonlinear Age-Dependent Population Dynamics (Chapman & Hall Pure and Applied Mathematics)*. CRC Press, 1985.

[177] G. F. Webb. Dynamics of populations structured by internal variables. *Mathematische Zeitschrift*, 189(3) :319–335, sep 1985.

[178] G. F. Webb. An operator-theoretic formulation of asynchronous exponential growth. *Transactions of the American Mathematical Society*, 303(2) :751–751, feb 1987.

[179] Z. Xu, K. D. Duc, D. Holcman, and M. T. Teixeira. The length of the shortest telomere as the major determinant of the onset of replicative senescence. *Genetics*, 194(4) :847–857, jun 2013.

[180] Z. Xu, E. Fallet, C. Paoletti, S. Fehrmann, G. Charvin, and M. T. Teixeira. Two routes to senescence revealed by real-time analysis of telomerase-negative single lineages. *Nature Communications*, 6(1), jul 2015.

[181] A. A. Zaidi, B. V. Brunt, and G. C. Wake. Solutions to an advanced functional partial differential equation of the pantograph type : Figure 1. *Proceedings of the Royal Society A : Mathematical, Physical and Engineering Science*, 471(2179) :20140947, July 2015.

Résumé

Dans cette thèse, nous nous intéressons à l'étude de dynamiques cellulaires, tant au niveau de l'analyse mathématique d'un modèle établi que de la modélisation et l'analyse de données. Les deux premiers chapitres s'intéressent à des équations de type croissance-fragmentation avec vitesse de croissance linéaire. Nous nous intéressons en premier lieu au récent modèle dit incrémental, décrivant une population bactérienne. Nous prouvons l'existence et l'unicité de la solution du problème aux valeurs propres dans un espace de Lebesgue à poids. Ensuite, nous étudions le comportement asymptotique de solutions mesures de l'équation de croissance-fragmentation dans le cas mitose égale. Une solution est alors exprimée sous la forme d'un semigroupe agissant sur une condition initiale. Nous étendons à ce cadre un phénomène connu de dynamique oscillante en temps long, qui se traduit ici par une convergence faible de la solution vers une famille périodique de mesures. Le troisième chapitre porte sur les dynamiques conjointes entre cellules mésenchymateuses, préadipocytes et adipocytes. Nous proposons un modèle non linéaire dans lequel la vitesse de croissant dépend de la taille moyenne de ces dernières et l'analysons par des approches à la fois analytiques et numériques. Dans le dernier chapitre, nous effectuons une analyse statistique de données expérimentales de lignées individuelles de levures. Nous mettons notamment en évidence l'existence de phénomènes distincts entre les arrêts précoces et la sénescence réplicative. Nous proposons enfin un raffinement d'un modèle existant, maintenant apte à décrire la génération d'entrée en sénescence pour l'ensemble des lignées.

Mots-clés: populations structurées ; croissance-fragmentation ; solutions mesures ; comportement asymptotique ; modélisation ; analyse de données.

Abstract

In this dissertation, we are interested in the study of some dynamics in molecular biology, making use of mathematical analysis of established models, modelling and data analysis. The first two chapters focus on growth-fragmentation equations with linear growth rate. We are first interested in the recent so-called incremental model, describing a bacterial population. We prove the existence and uniqueness of the solution of the eigenproblem in a weighted Lebesgue space. Then we study the asymptotic behaviour of measures solutions of the growth-fragmentation equation in the equal mitosis case. A solution is then expressed as a semigroup acting on an initial condition. We extend to this framework a known phenomenon of long time oscillating dynamics, which results here in a weak convergence of the solution towards a periodic family of measures. The third chapter deals with the joint dynamics between mesenchymal, pre-adipocyte and adipocyte cells. We propose a non-linear model in which the growth rate depends on the average size of the latter and analyze it using both analytical and numerical approaches. In the last chapter, we carry out a statistical analysis of experimental data from individual yeast lines. In particular, we highlight the existence of distinct phenomena between early arrests and replicative senescence. Finally, we propose a refinement of an existing model, now able to describe the generation of onset of senescence for all the lineages.

Keywords: structured populations ; growth-fragmentation ; measure solutions ; asymptotic behaviour ; modeling ; data analysis.